The Fallout of Single Glazing under Radiant Heat Exposure

by

Daniel Liang Wei WONG

Supervised by

Dr. Michael Spearpoint

And

Dr. Kai-Yuan Li

A research project report submitted in partial fulfilment of the requirements for the degree of Master of Engineering in Fire Engineering

Department of Civil and Natural Resources Engineering

University of Canterbury

Christchurch, New Zealand

2011

ABSTRACT

Glass fallout in windows has the potential to alter the ventilation condition and the behaviour of the fire in a compartment. Therefore, it is of an interest to fire modellers to be able to simulate the behaviour of glass windows in fires. Most research work has dealt with the fracture of glass windows in fires while some work studied the glass fallout behaviour in the general sense.

This research investigated the fallout behaviour of 4 mm and 6 mm thick single glazed glass exposed to a radiant heat source. Only ordinary float type glass was studied in this research. The fallout behaviour of glass was quantified in a probabilistic manner based on the fallout results from the experiments. Standard rubber beadings and non-standard beadings made of kaowool fibres were used to glaze the glass samples in this research.

A total of 117 experiments were carried out in this research. The radiant heat fluxes which the glass samples were exposed to ranged from 13 kW/m^2 to 58 kW/m^2. In some experiments, the temperature at various points on the glass and thermal strains were measured. Radiant heat flux measurements were also taken during the experiments. The time to glass fracture and amount of fallout were recorded in every experiment.

The four-point bending test was carried out on 24 glass specimens to determine the fracture strength and modulus of elasticity for the glass panes used in this research. The mean fracture strength and modulus of elasticity were 64 MPa ± 15 MPa and 76.5 ± 4.0 MPa respectively.

The simple lumped heat capacity method was used to predict the time to glass fracture in each experiment. Generally, the times to glass fracture recorded in the experiments were within the predicted times to glass fracture in 60% of the experiments.

The distribution of temperature differences at fracture was predicted using the fracture criterion suggested by Keski-Rahkonen (1988). The range of predicted temperature differences at glass fracture was compared with the temperature differences obtained from the experiments. The mean temperature difference at glass fracture ranged from 90 °C to 98 °C while the predicted temperature differences were between 55 °C to 129 °C. Generally, the actual temperature differences were within range of predicted temperature differences in 60% of the experiments.

The measured thermal strains at glass fracture were between 239 μstrain to 697 μstrain.

The type of glazing beading was concluded not to have affected the glass fallout behaviour. It was found that a window with a thinner glass pane is more likely to fallout compared with a window with

a thicker glass pane when exposed the same level of heat flux.

The fallout behaviour of glass was quantified with an exponential distribution function and a glass fallout prediction model for 4 mm and 6 mm thick glass was produced from the experimental results.

ACKNOWLEDGEMENTS

This research project would not have been possible without the assistance of several individuals. I would like to acknowledge the assistance of my supervisors, Dr Michael Spearspoint and Dr Kai-Yuan Li for their guidance and valuable feedbacks during the course of this research.

I would also like to extend my gratitude to Grant Dunlop for his technical advice and management of the material procurement for the research. I would like to thank Bob Wilsea-Smith for his technical service in setting up my experimental rig and assisting me with the experiments.

I would also like to acknowledge the assistance of Alan Poynter for carrying out the four-point bending test in the Structural Lab and Peter Coursey for his assistance in setting up the recording instruments for the strain gauges.

I wish to thank my parents for the motivational support they have provided me during my three years at the university.

Finally, I would also like to acknowledge the financial assistance granted to me by BRANZ through the FRST programme and the continuing support of the New Zealand Fire Service to the Fire Engineering programme.

TABLE OF CONTENTS

LIST OF FIGURES

LIST OF TABLES

NOMENCLATURE

Symbol	Description
a	Distance between two points of load application (m)
A	Surface area of glass (m^2)
b	Width of the glass specimen (m)
Bi	Biot number
c	Distance between two specimen supports (m)
c_p	Specific heat of capacity (J/kg.K)
E	Modulus of elasticity (GPa)
g	Geometry factor
h	Convective heat transfer coefficient ($W/m^2.K$)
h_{max}	Maximum convective heat transfer coefficient ($W/m^2.K$)
h_{min}	Minimum convective heat transfer coefficient ($W/m^2.K$)
H	Half-width of exposed glass dimension (m)
k	Thermal conductivity (W/m.K)
L_c	Characteristic length (m)
m	Mass of glass (kg)
m_v	Weibull distribution parameter
M	Bending moment (kN.m)
P	Breaking load (N)
P_f	Probability of failure

$P_{fallout}$	Probability of glass fallout
$\dot{q}''_{crit}$	Critical heat flux (kW/m^2)
$\dot{q}''$	Applied heat flux (kW/m^2)
s	Shading width (m)
t	Time (seconds)
t_{crack}	Time to first crack or fracture (seconds)
t_1	Time after first crack or fracture (seconds)
T_c	Glass temperature at centre of glass pane (°C or K)
T_e	Glass temperature at edge of glass pane (°C or K)
T_{glass}	Glass temperature (°C or K)
T_{shade}	Shaded glass edge temperature (°C or K)
T_u	Upper layer temperature in a compartment (°C or K)
T_0	Initial temperature of glass (°C or K)
T_∞	Heated ambient temperature (°C or K)
$\overline{T}$	Average temperature across the glass thickness (°C or K)
Z	Section modulus (m^3)

Greek	Description
β	Linear thermal expansion coefficient (/°C or /K)
δ	Glass thickness (m)

Δ	Deflection of glass specimen (m)
$\Delta T1$	Local exposed edge temperature difference (°C or K)
$\Delta T2$	Local exposed centre temperature difference (°C or K)
$\Delta T3$	Local bulk temperature difference (°C or K)
ρ	Density (kg/m^3)
σ_b	Breaking strength of glass (MPa)
σ_f	Fracture strength of glass (MPa)
σ_y	Tensile strength of glass (MPa)
σ_0	Scale factor (MPa)
σ_u	Lowest strength for a sample size (MPa)

1 INTRODUCTION

1.1 Research Background

When a fire breaks out in a compartment, the fire will transient from a growth phase to a fully developed phase. One factor which will influence the development of the fire is the air supply.

The ventilation in a compartment may be limited during a fire unless there is adequate number of open vents to allow air from outside the compartment to enter and sustain the fire until it reaches the fully developed phase. The open vents may exist in the form of doors or windows that are open. Open vents can still be created from closed windows if the glass panes in the windows fracture and fall out after being exposed to a fire. The open vents will also provide a path for hot gases to exit the compartment, thus reducing the average temperature in the compartment.

Keski-Rahkonen (1988) discussed that for regular soda glass, the time to first crack and the total destruction of the glass pane can be assumed to be the same for many purposes. The experimental work carried out by Harada et al. (2000) with 3 mm thick float glass showed that generally, small pieces of glass will fallout at the same time as the initial crack while in some tests, large pieces of glass fell out successively after the first crack. The progressive fallout behaviour of single glazing was also observed in the experimental work carried out by Shields et al. (2001 and 2002). The fallout behaviour of glazing in windows is of interest to fire modellers as the dynamics of the fire can change dramatically depending on the ventilation condition.

Pope et al. (2006) mentioned that many of the previous studies on glass breakage had too small data sets for a meaningful statistical analysis but these studies are likely to reveal the probabilistic nature of glass breakage. Many of the previous work mainly address the window fracture behaviour instead of the fallout behaviour of the glass windows which is the reason behind the creation of the open vents.

1.2 Research Objectives

The purpose of this research was to investigate the likelihood that different proportions of single glazed glass fall out when exposed to constant and uniform radiant heat. An experimental approach was used for this research. The experimental work involved exposing a number of glass samples to a radiant heat source to enable the fallout behaviour of the single glazing to be quantified in a probabilistic manner.

In this research, ordinary float glass type glazing was used. Two glass thicknesses were investigated as these thicknesses are commonly used in the industry. While the window industry may be moving into the realms of double and triple glazing, the understanding of fallout behaviour for single glazing is still lacking. Therefore, this research was carried out with the intention to provide a method to describe the behaviour of single glazing.

1.3 Definitions

The following terms are used throughout this report.

Break/Breakage

These terms are found in the literature review chapter. The meaning of the terms vary between glass fracture and glass fallout throughout the literatures reviewed although both the fracture and fallout terms have very different meaning in terms of the state of the glass. However, it is acknowledged that these terms are used to refer to both glass fracture and fallout in the literatures.

Beading

A compressible packing used to provide a seal around the glass pane in a window.

Bifurcation

Crack that is divided into two separate branches.

Fallout

This term is used to describe the state of the glass whereby the glass has cracked and separated into pieces that are no longer attached on the plane of the glass.

Fracture

This term refers to the state of the glass which has cracked.

Frame

A structure typically constructed of wood or aluminium for the purpose of holding the glass pane.

Pane

A single piece of glass cut to size for glazing.

Shaded

This term is used to describe a thermocouple or glass element that is fitted inside the window frame.

Uncovered

This term is used to describe a thermocouple that is bare and one that has no shielding medium applied onto the thermocouple.

Exposed face

Face of window and glass that are directly exposed to the fire.

Unexposed face

Face of window and glass that are not directly exposed to the fire.

Sample/specimen

A thing that is taken from a group.

Breaking strength/fracture strength/tensile strength

The terms breaking strength, fracture strength and tensile strength refer to the ability of the glass to carry the load imposed on the glass prior to cracking.

Window

A frame enclosing a glass pane. The different basic components that make up a window in this research are shown in Figure 1-1.

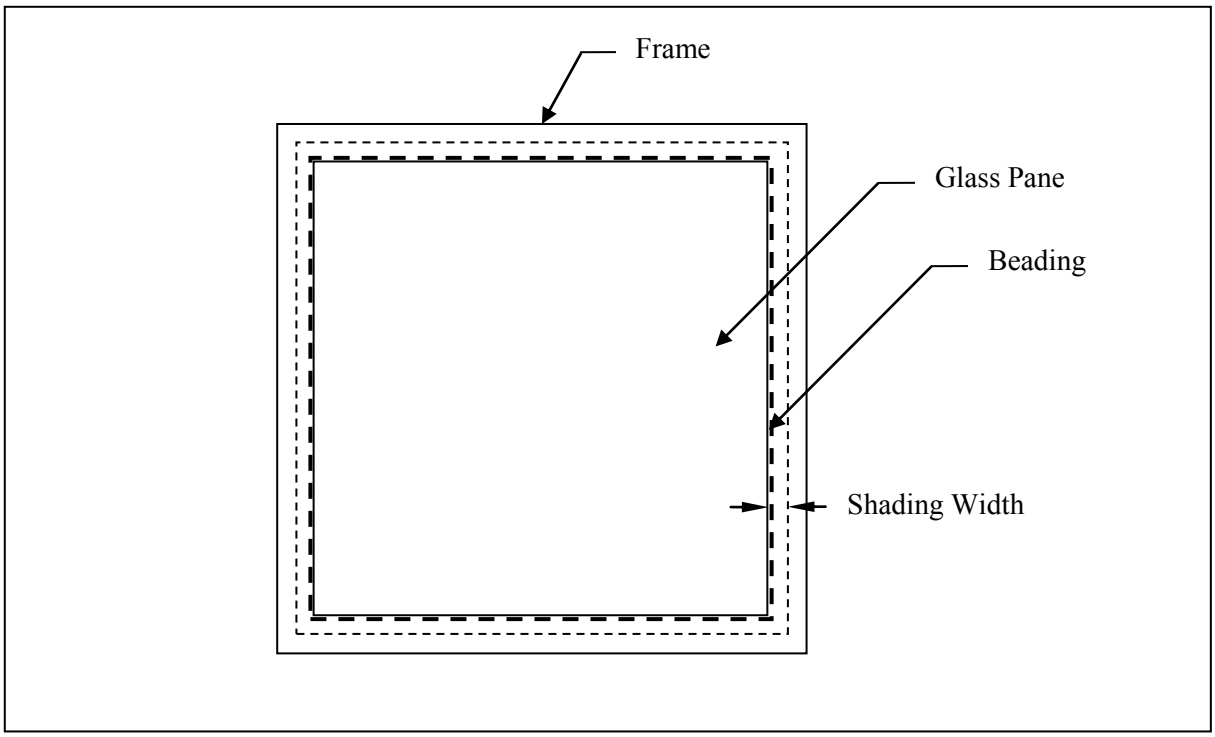

Figure 1-1: Components of a Simple Window

1.4 Outline of Research Report

This report is divided into further chapters that cover the different parts of the research.

Chapter 2: Literature Review summarises the various work that were carried out to investigate the fracture and fallout behaviour of glass in fires. In this section, the analytical and experimental work of various researches and findings are presented. Computer modelling tools and simulation studies regarding this subject are also discussed in this section.

Chapter 3: Experimental Methodology outlines the experimental setup and step-by-step procedures to carry out the experiments. A brief discussion about the data reduction of the outputs from the thermocouples, heat flux gauge, strain gauges and amount of glass fallout are included in this chapter.

Chapter 4: Experimental Results and Discussions presents the results from the experiments and analytical results from the data reduction. Typical results are discussed in this section to provide an overview of the results.

Chapter 5: Glass Fallout Prediction Model explains the model to predict the glass fallout based on the results of the experiments. The basis for the model and proposed procedure to use this model are also

presented in this section.

Chapter 6: Conclusions contains the summary of findings from this research.

Chapter 7: Recommendations aims to provide recommendations for future research.

Chapter 8: References lists all the references that were used to facilitate this research.

2 LITERATURE REVIEW

2.1 Philosophy

2.1.1 Emmons (1986)

In the first fire safety science symposium, Emmons in his paper “The Needed Fire Science” acknowledged the need to investigate the glass window breaking subject and according to the paper, this subject is of importance to the growth of the fire. According to Emmons, the only study into glass breakage at that time was carried out by two Harvard seniors for their senior project where 6” x 7” window glass plates were subjected to a radiant heat source.

2.1.2 Keski-Rahkonen (1988)

Keski-Rahkonen presented a mathematical model to calculate the thermal field in a long-strip glass window pane heated by thermal radiation, except on narrow strips along edges built in the frame. Keski-Rahkonen discussed the several mechanisms which could break a framed glass pane when heated by thermal radiation.

The first mechanism is a steep thermal gradient created across the thickness of the pane. The deep gradient from the rapid heating crates thermal stresses which could break the glass pane. However, Keski-Rahkonen remarked that such breaking is uncommon in fires.

The second mechanism is a thermal gradient over the thickness of the glass pane that causes the pane to deform. Window frames which are usually strong will keep the edges of the pane in the same plane. The boundary condition of the glass could be between that of a simply supported or built-in edge. These types of boundary conditions bend the pane and induce stresses which are greatest close to the corners of the panes. The stresses could become high in very small panes but the larger panes are flexible that breaking of the glass seems improbable.

The third mechanism involves non-uniform heating of the glass pane which induces thermal stresses and tension develops at locations where temperature is lower than average. Since glass is a brittle material, cracks will start at locations with high tensile stress. This occurs along the rim of the pane which goes into the frame, screening radiation and acting as a heat sink on the edge of the pane. Keshi-Rahkoken commented that this is the first mechanism to cause the window panes to crack in fires.

Keski-Rahkonen derived an equation to quantified the maximum tensile stress in the glass pane which is given as,

$$\sigma_y = \beta\left(T_{glass} - T_o\right)E \tag{1}$$

Keski-Rahkoken derived a temperature difference 80 °C using Equation (1) where the soda glass would crack by taking a maximum tensile stress of 50 MPa, linear thermal expansion of 8.1 x 10^{-6} /K and modulus of elasticity of 80 GPa.

2.1.3 Pagni (1988)

Pagni suggested a simple strain equation based on Hooke's Law to define the criterion for glass cracking which is similar to the equation presented by Keski-Rahkonen (1988). The equation is given as,

$$\sigma_y = \beta E \Delta T \tag{2}$$

Pagni mentioned that pressure difference across a heated window is sufficient to remove the glass within milliseconds after the glass has cracked.

Pagni determined that a temperature difference of 58 °C is required to cause glass to crack from Equation (2) using a tensile stress of 47 MPa, modulus of elasticity of 78 GPa and a coefficient of linear thermal expansion of 9.2 x 10^{-6} /°C.

2.1.4 Pagni and Joshi (1991a and 1994a)

Pagni and Joshi (1991a) discussed the heat transfer theory between the compartment fire and the glass temperature and provided a model based on the Laplace transform on time to relate the stress field to the temperature field.

Pagni and Joshi (1991a) suggested a geometry factor, g to be included in the fraction criterion and the equation is given as,

$$\sigma_b = g\frac{\left(\overline{T} - T_i\right)}{E\beta} \tag{3}$$

where

$$g = 1 + \frac{s}{H} \tag{3a}$$

for a step temperature profile

Or

$$g = \frac{2}{\left[\tanh\left(\frac{s}{\delta}\right) + \ln\left[\frac{\cosh\left(\frac{H}{\delta}\right)}{\cosh\left(\frac{s}{\delta}\right)}\right]\frac{\delta}{(s+H)}\right]} \tag{3b}$$

for a hyperbolic tangent temperature profile

The terms in Equations 3a and 3b is explained in Figure 2-1.

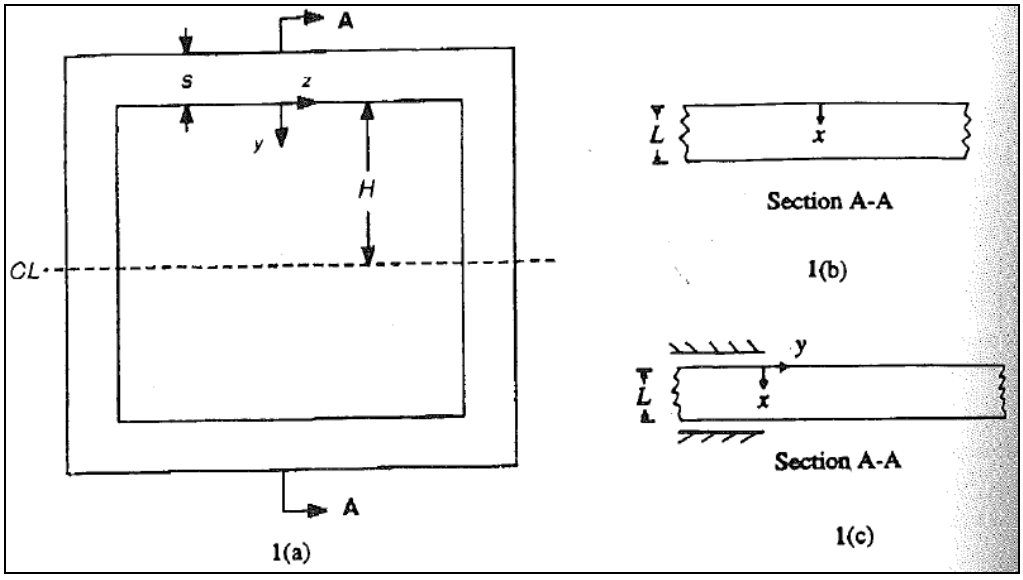

Figure 2-1: Window Geometry (Pagni and Joshi, 1991a)

Joshi and Pagni (1994a) carried on from their previous work (Pagni and Joshi, 1991a) and did more detailed work with the model.

2.1.5 Brabraukas (2006)

Brabraukas summarised the experimental work carried out by various researchers into glass breakage. The discussion provided an overview and findings of the researchers.

2.2 Glass Breaking Models

2.2.1 Pagni and Joshi (1991b)

Pagni and Joshi developed a computer program called BREAK1 to determine the response of glass windows when exposed to a compartment fire and calculates the time for the glass to break. The program is based on the numerical procedure for heat transfer discussed in Pagni and Joshi (1991a) and fracture criterion in Pagni (1988).

2.2.2 Sincaglia and Barnett (1997)

Sincaglia and Barnett developed a one-dimensional heat transfer and glass pane fracture model for zone-type computer fire codes. The heat transfer model uses the numerical method to solve for temperature distribution within the glass pane. The distribution of temperatures across the thickness of the glass is averaged and compared with the maximum allowable temperature difference. If the average glass temperature exceeds the maximum allowable temperature difference, then the glass window fractures and a vent opening is created. The time to fracture is taken as the time required for the glass to reach the maximum allowable temperature difference when exposed to heat.

2.2.3 Parry (2002)

Parry developed a glass fracture model using the heat transfer model developed by Sincaglia et al. (1997) and fracture criterion by Pagni and Joshi (1991a) to be incorporated into a two-zone model called BRANZFire (Wade, 2000). The user inputs required for the glass fracture model in BRANZFire are shown in Figure 2-2. The glass fracture model was also developed as a spreadsheet. Parry compared the predicted fracture time results between the glass fracture model and BREAK1 created by Joshi and Pagni (1991a) and according to Parry, the results showed close agreement although Parry reported that BREAK1 consistently predicted a slightly earlier fracture time. Parry reasoned that the differences in the modelling the radiative heat transfer contributed to the

earlier fracture time predicted by BREAK1.

Parry also compared the predicted fracture time results from the glass breaking model with the fracture time results from the experiments carried out by Skelly et al. (1991) and the results from both the glass fracture model prediction and experiments are close in comparison. Parry also commented that although Skelly et al.(1991) presented a gas temperature history for the compartment fire, the predicted gas temperature by BRANZFire showed that the gas temperature was much lower than the measured gas temperature in the experiment. Parry deduced that the gas layer temperature histories given by Skelly et al. (1991) may be in error.

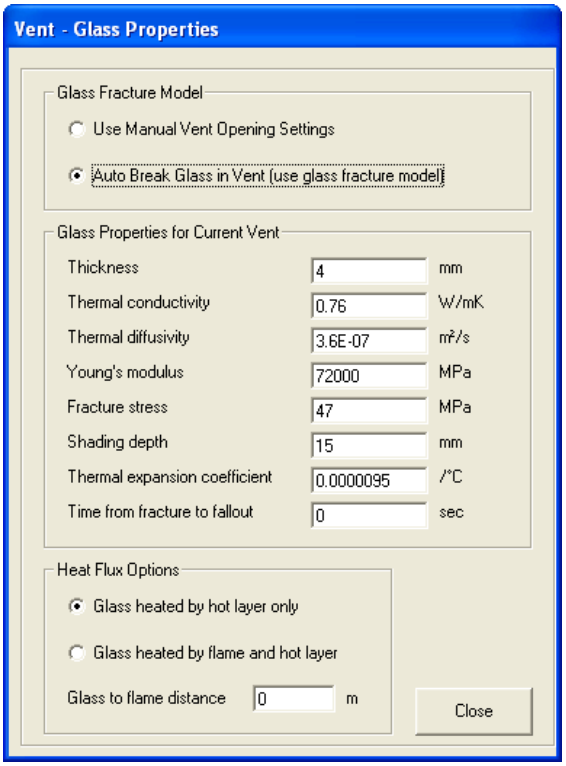

Figure 2-2: User dialog box of glass fracture model for vent creation in BRANZFire

2.3 Experimental Studies

2.3.1 Skelly et al. (1991)

Skelly et al. carried out a series of experiments using a 150 cm x 120 cm x 100 cm compartment. The experimental setup is shown in Figure 2-3 and Figure 2-4. The experiments were carried out with 0.24 cm thick x 28 cm x 50 cm soda ash glass windows which were mounted in a 36 cm x 56 cm

aluminium frame that was fitted on one side of the compartment. A protected edge of 2.5 cm wide was maintained around the perimeter of the pane. The glass was cut by hand with a scribe and the edges were not ground.

Four different sizes of aluminium trays filled with liquid hexane were used in the experiments to simulate the fires. A total of 17 experiments were carried out in the form of 11 edge-protected and 6 edge-unprotected experiments. In all of the experiments, it was reported that the entire pane of glass was fully submerged in the hot gas layer of the fire within the first 10 seconds.

There were 10 cases where catastrophic window failures were reported out the total 11 experiments carried out for the edge-protected window experiments while no glass breakage was reported for the remaining one experiment. Hietaniemi (2005) commented that the phrase "catastrophic window failure" is likely to suggest substantial glass fallout. Partial collapse of the window was reported in all 10 cases.

Skelly et al. indicated that the edge temperature of the glass must be predicted to obtain accurate predictions of the breakage time. Skelly et al. also remarked that although conservative predictions of breakage time can be made if the edge heating was ignored, in situations where there is a slow growing fire, this edge temperature may be of importance. In the experiments carried out with the edge-protected windows, the cracks were reported to have initiated at the edge of the glass and propagated rapidly such that all breakage was complete in less than one second.

In the edge-unprotected experiments, it was reported that the average glass temperature during fracture was 197 °C ± 15 °C. Skelly et al. reported that the crack patterns produced in the edge-unprotected experiments were very similar to the crack patterns produced in the edge-protected experiments although multiple bifurcations and individual cracks were not present in the edge-unprotected experiments. All the cracks in the edge-unprotected experiments were also initiated at the edges of the glass. Where partial collapse was reported in each of the 10 experiments with the edge-unprotected windows, all of the edge-unprotected windows held and remained firmly in the frame even when cracking had occurred.

Skelly et al. also carried out tests to determine the material properties of the glass used in the experiments. The linear thermal expansion coefficient, β was determined with a Netzsch Dilatometer. Two samples were measured and each had a linear thermal expansion coefficient of 9.5×10^{-6} /°C. The modulus of elasticity, E for the glass and tensile strength σ_y, were measured on a universal testing machine. Skelly et al. explained that tensile loads were applied to "dog-bone" shaped glass samples until breaking point to obtain the tensile strength of the glass samples. The "dog-bone" shaped

samples were 3 cm wide at the ends and necked down to 1.5 cm in the middle and were cut from a glass sheet. The tensile strength of the glass was calculated as the load at breaking point divided by the cross-sectional area of the sample where the break occurred. Skelly et al. reported that the "dog-bone" samples had more edge imperfections than the glass panes due to the difficulty in cutting the glass samples. Due to this reason, the highest tensile strength of any test was found to be 47 MPa.

The modulus of elasticity for the glass was obtained from the stress-strain diagram that was produced for each test sample. The strain was measured using a strain gauge fixed to the samples. The results of the stress-strain diagrams were used to calculate an average modulus of elasticity of 70 GPa ± 10 %.

Using the fracture criterion proposed by Keski-Rahkonen (1988) and materials properties of the glass obtained from the various tests, an average temperature difference at cracking of 70 °C was obtained.

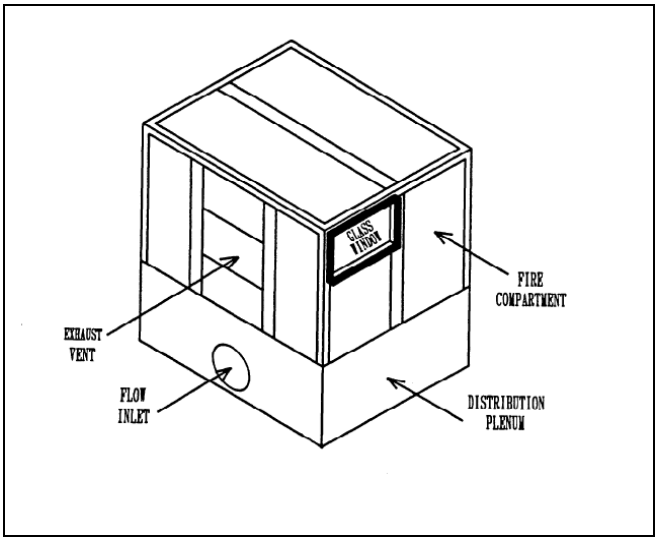

Figure 2-3: Schematic of the compartment used for the window break experiments (Skelly et al., 1991)

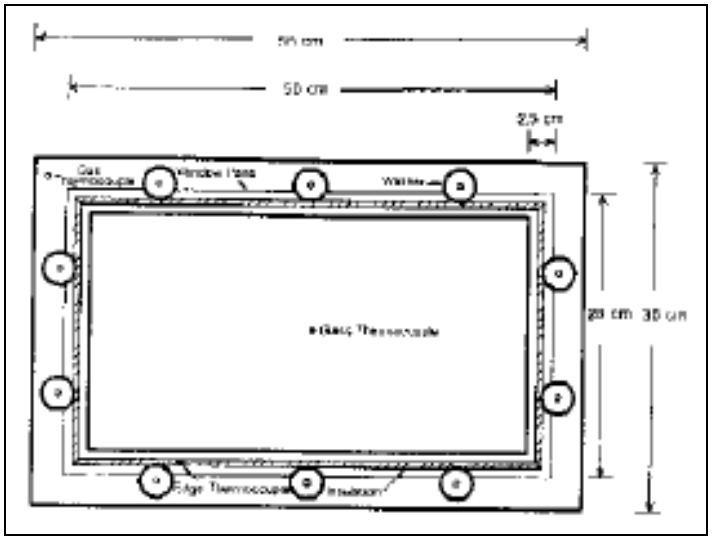

Figure 2-4: Schematic of window installation including thermocouples placement (Skelly et al., 1991)

2.3.2 Mowrer (1997)

Mowrer carried out a number of small and large scale experiments to investigate the performance of different window assembles, glazing materials and protective treatments under imposed radiant heat fluxes ranging from 2 kW/m^2 to 18 kW/m^2. The window assemblies include wood, vinyl and vinyl-clad wood frames. The glazing materials include single and double glazing, tempered glass and a heat-resistant ceramic glass. The protective treatments include insect screens, vinyl film sun shades and aluminium foil.

In the small-scale experiments, 61 experiments were carried out in a gas-fired radiant heat exposure apparatus under imposed radiant heat fluxes ranging from approximately 2 kW/m^2 to 16 kW/m^2. Single glass panes with dimensions of 230 mm wide and 340 mm high with a shielded perimeter of 13 mm wide around the edges of the glass were used.

In the large-scale experiment, 19 experiments were carried out using commercially available residential window assemblies were consisted of single and double glazed windows with frames made of wood, vinyl and vinyl-covered wood.

Mowrer mentioned that at lower heat fluxes of approximately 3.3 kW/m^2 the assemblies did not fail while at higher heat fluxes in the range of 4 kW/m^2 to 5 kW/m^2, the single glazed windows always failed. The term "fail" was not clearly defined by Mowrer. However, Mowrer stated that ***"Once the glass begins to fail, a bifurcating fracture pattern typically develops, with cracks propagating from the perimeter of the glass in to the field".*** This would suggest that the term "fail" used by Mowrer is

referring to glass fracture. Mowrer concluded that for exposed glass with the edges shielded in a frame, fracture will initiate at the edges.

2.3.3 Tanaka et al. (1998)

Tanaka et al. as cited by Pintea et al. (2008) described the probabilistically based results from a glass breakage experiment carried out by the Building Research Institute (BRI) of Japan. The experiment was carried out in a large-scale fire compartment as shown in Figure 2-5. The walls consisted of 200 mm thick normal concrete with a thermal conductivity of 0.8 W/m.K and specific heat capacity of 840 J/kg.K. Three of the four walls of the compartment were fitted with 2.0 m high glass windows with a sill height of 1.0 m while the remaining wall was fitted with 0.5 m high windows with a sill height of 0.5 m. The windows where made up of single glazed 3 mm thick glass.

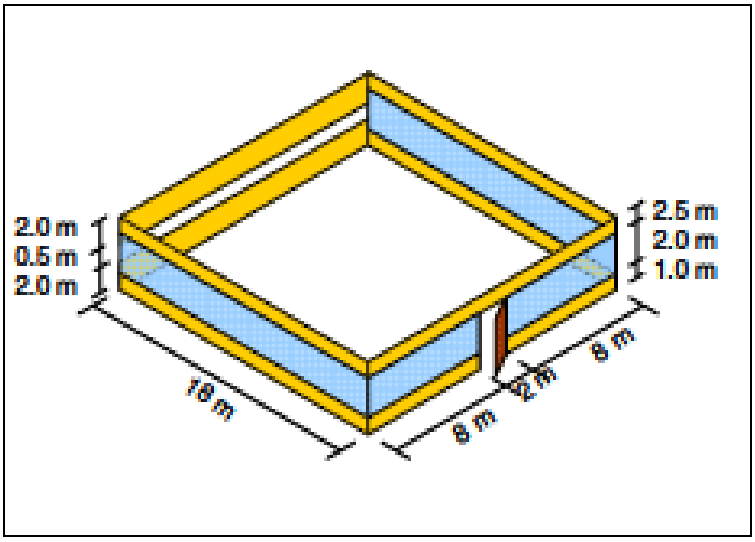

Figure 2-5: Fire compartment (Tanaka et al., 1998 as cited by Pintea et al., 2008)

At a temperature of 300 °C, 30% of the windows were reported to be broken while at a temperature of 500 °C, all windows were reported to be broken. A cumulative probability distribution curve for the glass fallout as a function of temperature rise above ambient was plotted and a Gaussian distribution curve was fitted to the plots as shown in Figure 2-6. The paper did not mention whether the temperature mentioned at breakage is the gas or glass temperature. The meaning of breakage in the paper does not clearly indicated whether fracture or fallout is being referred to. The type of glass that

was used in the experiment was not reported by Pintea et al. (2008).

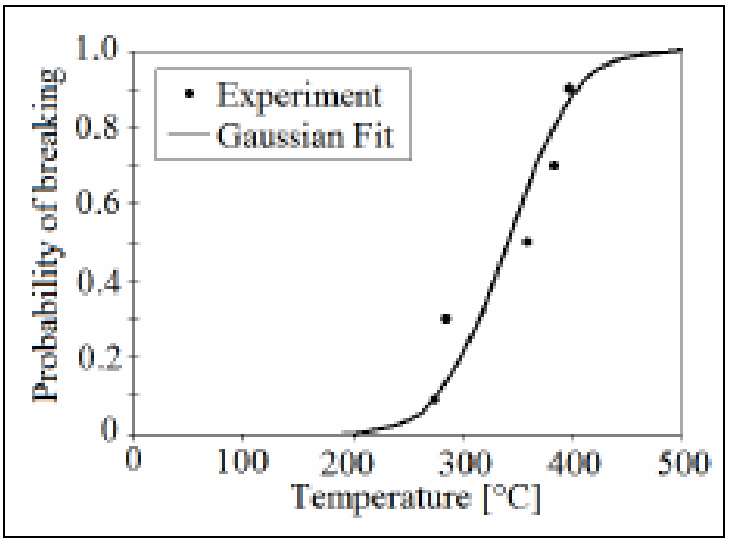

Figure 2-6: Distribution of glass breaking temperatures (Tanaka et al., 1998 as cited by Pintea et al., 2008)

2.3.4 Harada et al. (2000)

Harada et al. exposed 25 specimens of 3 mm float glass and 25 specimens of 3 mm wired glass to radiant heat in a study to investigate glass cracking and fallout. A vertical propane burner was used to generate the radiant heat. The experiment was set up as shown in Figure 2-7.

The experiments were carried out with and without lateral restraints. In the experiments with lateral restraints, the perimeter edges of glass was restrained while in the experiments without lateral restraints, only the top and bottom edges of the glass were restraint. Harada et al. compared the time to fracture using the lumped heat capacity model given by,

$$t_{crack} = \frac{\left(\frac{c_p \rho \delta}{2h}\right)}{\log_e\left(\frac{\dot{q}''}{\dot{q}'' - \dot{q}''_{crit}}\right)} \tag{4}$$

Harada et al. commented that the predicted times to fracture are in reasonable agreement with the times to fracture from the experiments.

In the experiments involving the float glass, the imposed heat fluxes range between 2.85 kW/m^2 to 9.6 kW/m^2 while in the experiments involving the wired glass, the imposed heat fluxes range between 2.7 kW/m^2 to 9.7 kW/m^2.

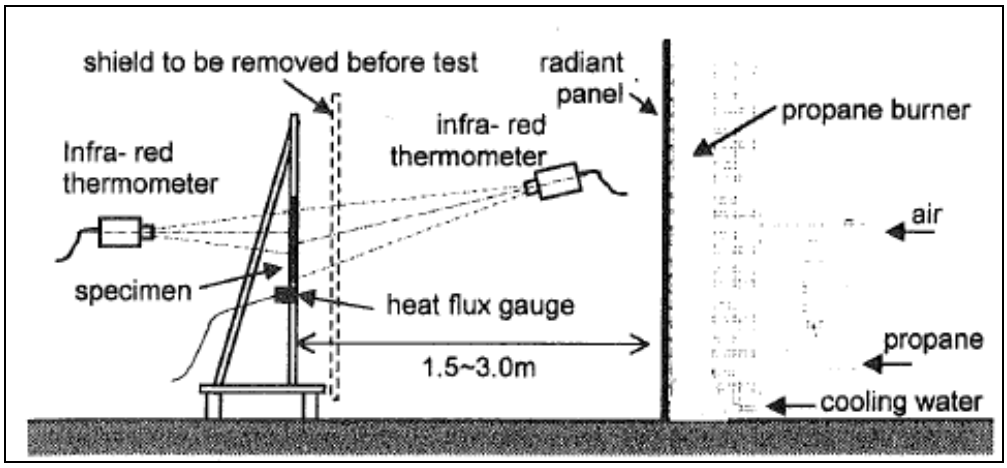

Figure 2-7: Experimental apparatus (Harada et al., 2000)

Glass fallout was reported in the experiments involving the float glass while no glass fallout occurred in the experiments involving the wired glass as the embedded wires held the glass together even after the cracks had developed. Harada et al. reported glass fallout between 0.3 % to 24 % for the range of imposed heat fluxes and no glass fracture when the glass specimens were exposed to a heat flux lower than 5 kW/m^2.

Harada et al. concluded that glass cracking is the triggering mechanism for glass fallout but sometimes fallout does not occur. The different types of glass restraint used in the research generally did not affect the glass cracking but the restraint appeared to have affected the glass fallout behaviour.

2.3.5 Shields et al. (2001 and 2002)

Shields et al. carried out 19 and 14 experiments under enclosed fire conditions to study the performance of single glazing under varying heat fluxes and hot gas layers for fires located at the corner and centre of an enclosure respectively. The enclosure measured 3.6 m x 2.4 m x 2.4 m with a 0.4 m wide x 2.0 m high opening on one wall. The enclosure was constructed and instrumented to the standard of an ISO 9075 room. The experimental setup is shown in Figure 2-8. The size of the fire in

each experiment varied between 187.5 kW to 1023.4 kW measured using the fuel mass loss rate method. A glazing assembly consisting three float glass panes of 6 mm thickness was incorporated into one of the enclosure walls during each experiment. Two windows in the assembly were 845 mm x 845 mm while one was 1897 mm in height and 845 mm in width.

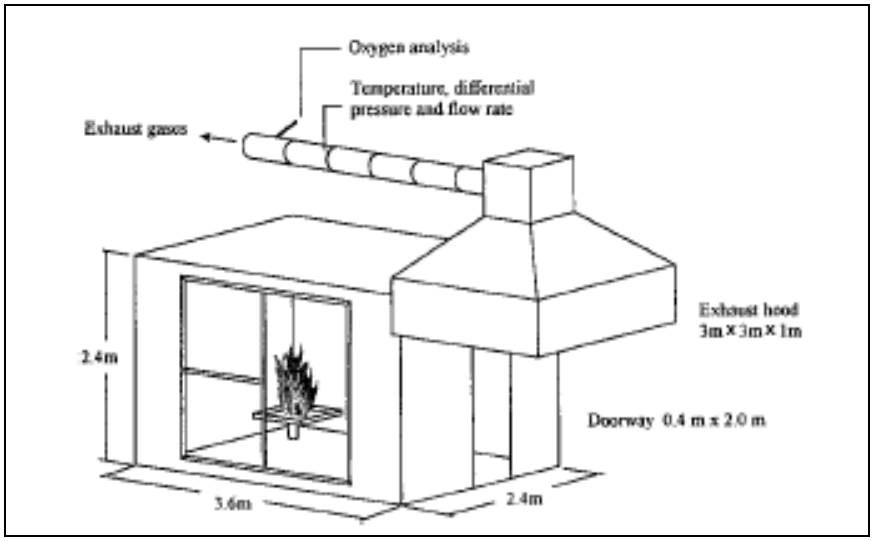

Figure 2-8: Schematic diagram of fire enclosure with large scale calorimeter (Shields, 2001)

Generally, as the size of pan fire increased, the extent of loss of integrity of the windows increased. The research reported that major loss of integrity occurred when bifurcations joined up to form closures. Shields reported that the temperature difference at first cracking was approximately 110 °C and the glass surface temperatures at failure were in the region of 447 °C. A lower limit of 3 kW/m^2 was reported below which glass would be crack.

2.4 Glass Breakage Simulation Studies

2.4.1 Pope et al. (2002)

Pope et al. developed a Gaussian glass breakage model to be used within a computational fluid dynamics fire model called the Fire Dynamic Simulator Version 4 (McGrattan, 2005). The Greater London Authority (GLA) building was used for the case study using the model. The actual triple glazing on the external façade of the building was replaced with single glazing in the FDS model. The Gaussian glass breakage model consisted of two parts, namely the heat transfer and Gaussian

distribution of glass breaking temperatures.

Pope et al. made use of different methods taken to study glass breakage. The four methods are as follow,

- The obstructions (glass) were ignored to simulate the condition where the ventilation is open at the start and throughout the simulation.
- The obstructions (glass) were removed with the activation of heat detectors which is the method used in the obstruction removal in FDS4.
- The obstructions (glass) were modelled based on a one dimensional solid heat transfer, and an absolute breaking temperature was assigned to the obstructions.
- The obstructions (glass) were modelled based on a one dimensional solid heat transfer but an average breaking temperature with a standard deviation based on a Gaussian distribution to generate a different breaking temperature for each obstruction.

Pope et al. concluded that the gas temperature profile within the compartment was changed significantly with the inclusion of the Gaussian glass breakage model after carrying out similar simulations using the first three methods suggested.

2.4.2 Kang (2009)

Kang discussed the development of a model to predict the window glass breakage and fallout in a field model called the Fire Dynamic Simulator Version 4 (McGrattan, 2006). Several modifications and functions were added as part of the glass breakage and fallout algorithm. The additions were as follow,

- A model boundary object which allows the user to specify each individual window pane and provide geometric information of the window was included to represent the window glass.
- The use of default material setting or specific thermal physical properties for each window such as the modulus of elasticity, glass failure stress, decay length (or radiation absorption coefficient), specific heat capacity, thermal conductivity and density.
- The glass breakage was defined as a function of rise in temperature. In the simulation, the glass temperature was averaged across the pane over the front and back side of the glass and

the difference between the average temperature and the ambient temperature was compared to the rise in temperature criterion to determine the occurrence of glass breakage. The rise in temperature was also used to determine the time of subsequent glass breakages.

- The number and location of each glass breakage was tracked during the simulation. With each glass breakage, the solid cell with the maximum temperature was identified and removed which resulted in a small opening which was used to approximate leakage due to glass fracture.
- When the number of breakages exceeds a user set threshold, the entire glass was removed.
- Information regarding the average temperature history, occurrence of breakage and fallout were saved into a file.

Kang compared the results from the model against the compartment fire experiments carried out by Shields et al. (2001 and 2002). The heat release rates from the experiments were used as input parameters in the field model. The criterion for fallout was set at three breakages. Kang found that there was generally good agreement between both the results.

2.5 Material Properties of Glass

Pagni and Joshi (1991a) provided information on material properties of glass, breaking strains and temperature increases shown in Table 2-1.

Table 2-1: Material properties of glass (Reproduced from Pagni and Joshi, 1991a)

$\beta \times 10^6$ (/K)	σ_f (MPa)	E (GPa)	Strain (%)	ΔT (K)
9.5	47	70	0.07	70
9.2	20 – 50	72	0.03 – 0.07	30 – 75
8.5	55 – 138	72.4	0.08 – 0.19	90 – 220
9.0	35 - 70	70	0.05 – 0.10	55 - 110

3 EXPERIMENTAL METHODOLOGY

3.1 Scope of Experimental Work

This experimental work investigated the fallout behaviour of glass in fires. A series of experiments involving glass samples exposed to radiant heat were carried out. The radiant heat was generated using a 350 kW burner with pre-defined distances between the centre of the burner and the glass samples. During each experiment, temperature, heat flux and strain measurements as well as the amount of glass fallout were taken to quantify the behaviour of the heated glass with time.

A number of tests using the four-point bending test were also performed to determine the fracture strength and modulus of elasticity for the glass panes used in this research. These mechanical properties were used to predict the time to glass fracture.

3.2 Four-Point Bending Test

The four-point bending test was used to obtain the necessary data to derive the fracture strength and modulus of elasticity of the glass used in this research. This testing method was adopted based on the work carried out by Joshi and Pagni (1994b). Joshi and Pagni (1994b) used the four-point bending test to obtain a distribution of breaking strengths for 59 glass specimens. Joshi and Pagni (1994b) commented that a uniaxial tensile test, which is typically used to determine the tensile strength of materials, is not suitable to be performed on glass due to its brittle nature, and failure may occur at the end of the sample. The shape of the sample used in the uniaxial tensile test was shaped like a “dog bone”. However, it should be noted that the setup and procedure used to conduct the four-point bending test in this research were not based on any known standards due the unavailability of suitable equipment. At best, the results produced will be crude estimates and caution is advised when using these estimates for any purposes.

The specimens used in the experiment by Joshi and Pagni (1994b) were 178 mm long x 25.4 mm wide x 2.5 mm thick. However, the specimen dimensions in this research varied from the specimen dimensions used by Joshi and Pagni (1994b), as the Instron Universal Testing Machine shown in Figure 3-1 was not able to accommodate the specimen of such dimensions as used by Joshi and Pagni (1994b). The 24 glass test specimens tested in this research had a nominal length of 210 mm and width of 30 mm. Specimens with nominal thicknesses of 4 mm and 6 mm were tested. The test specimens were manually cut using a pen type glass cutter from

525 mm x 525 mm glass panes. Three test specimens were cut from each glass pane. The specimens are shown in Figure 3-2. A digital vernier calliper was used to measure the actual width and thickness of each test specimen. The actual width and thickness are tabulated in Appendix I.

Figure 3-1: Instron Universal Testing Machine

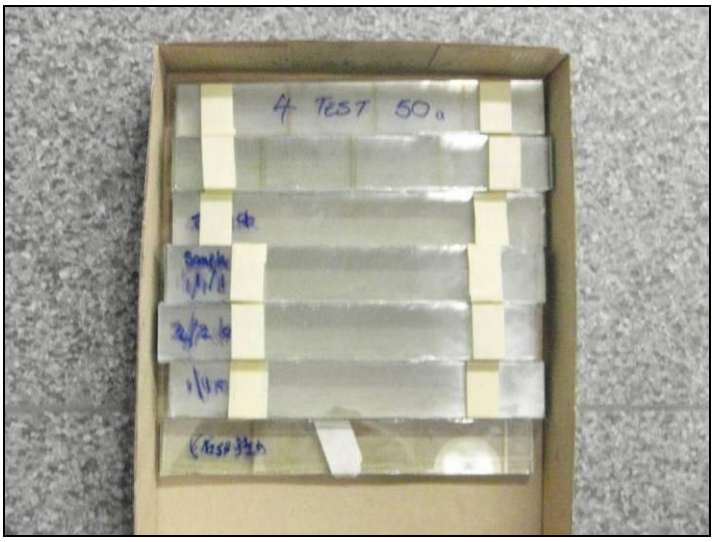

Figure 3-2: Glass specimens for bending test

The rate of loading was defined by the deflection rate which was set at 0.5 mm/min. The loading arrangement is shown in Figure 3-3. The loading fixture on the testing machine was fitted with counter-weight springs as shown in Figure 3-4 to prevent the fixture from pre-loading the test specimens.

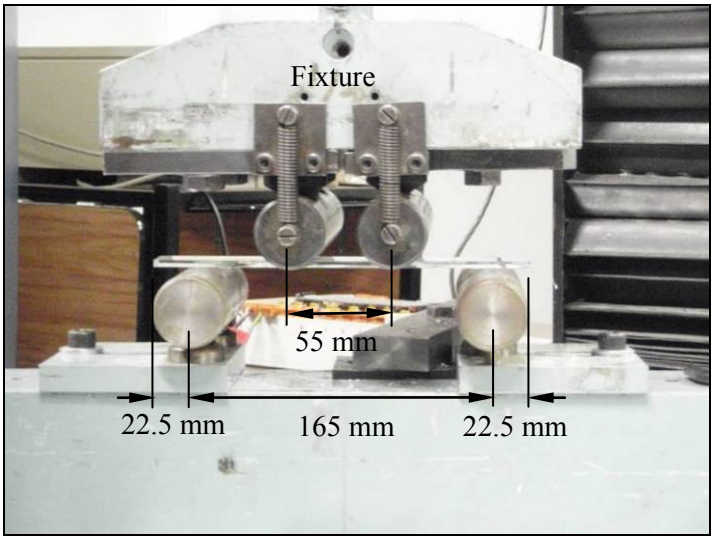

Figure 3-3: Glass bending test setup

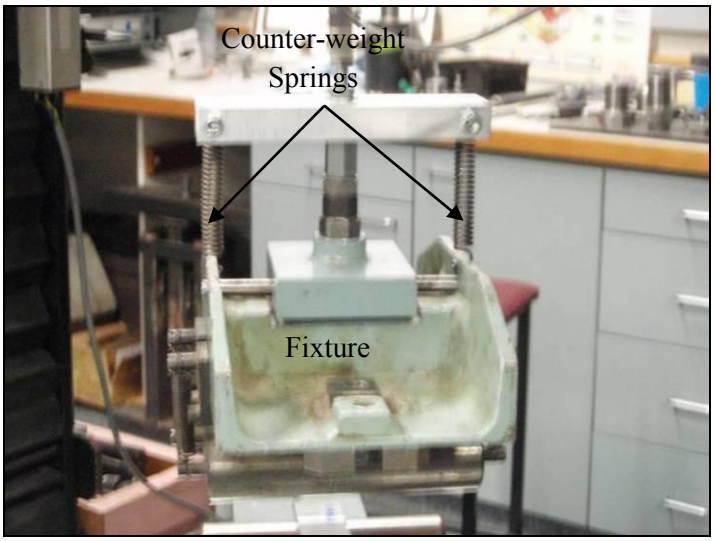

Figure 3-4: Location of counter-weight springs on fixture

3.3 Test Facility for Glass Fallout Experiments

The experimental work was conducted in the Special Purpose Fire Engineering Lab at the University of Canterbury, New Zealand. The make-up air for the burner fire was provided through louvers and a double leaf door to the fire lab. A layout of the fire engineering lab is shown in Figure 3-5. There is a calorimeter hood in the fire engineering lab where combustible products were collected when required.

The experiments were viewed from either a separate control room or the main entrance area. Two video cameras were used to record each experiment. The video cameras were positioned in the main entrance area and control room respectively.

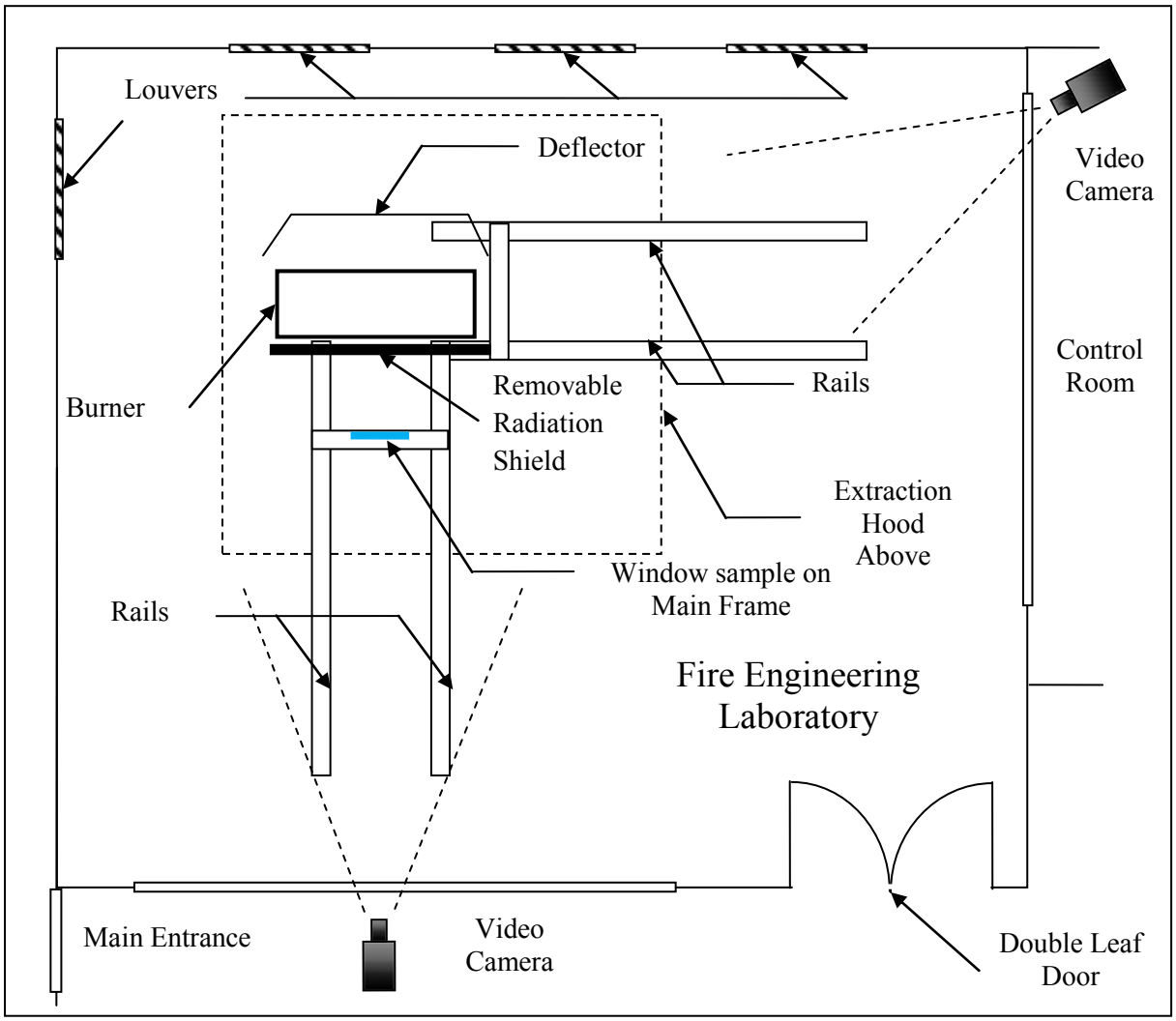

Figure 3-5: Equipment setup in the Special Purpose Fire Engineering Laboratory

3.4 Radiant Heat Source

The heat release rate of the burner fire was controlled via two parallel mass flow controllers or with a larger capacity single mass flow controller. Each controller was electrically connected to a mass flow controller power supply/readout unit, which allowed a set-point to be specified corresponding to a percentage of the maximum flow through the valve.

A 300 mm (width) x 900 mm (length) gas burner was used in this research. The gas burner was also the largest burner that was available in the fire engineering lab. The orientation of the burner was such that its length was parallel to the plane of the glass sample.

Initially, the fuel source for the burner was a gas fuel mix containing 64% butane and 36% propane. However, this proportion of fuel mix limited the number of experiments to a maximum three per day. While the experiments were being carried out using this fuel mix proportion, the fuel tanks froze after three or four experiments which resulted in a gradual drop in the heat release rate so a constant heat release rate was not achievable. A decision was made to change the gas mix to a mix that had higher propane proportion. The new fuel mix contained between 80% - 90% propane and 20% - 10% butane as this was the proportion that the supplier was able to guarantee. The use of the 80% - 90% propane/20% -10% butane fuel mix enabled the heat release rate to be maintained at a constant rate in each experiment.

The burner was filled up close to the brim with 19 mm fired clay balls as shown in Figure 3-6 to diffuse the fuel gas across the top surface of the burner and to ensure that the base of the flame was at the top surface of the burner.

A deflector made of stainless steel which is shown with the burner in Figure 3-6 was placed on the opposite side of the glass sample with the burner in between to increase the radiation from the burner fire. The deflector was initially located 550 mm measured from the centre of the burner to the face of the deflector. However, during the course of the experiments when the gas fuel mixture was changed from 64% butane/36% propane to 80% - 90% propane/20% - 10% butane, the measured radiation output was reduced. The deflector was moved closer to the burner and the ranges of radiation output from the initial fuel mixture of 64% butane/36% propane were restored.

Figure 3-6: Gas burner filled with clay balls and deflector

The size of the burner fire was defined by its heat release rate. The heat release rate of the burner fire was determined during the start of the research and towards the completion of the research. The measurement of heat release rate was done only twice because the heat release rate was not an important parameter to determine the amount of glass fallout. The two measurements were made to enable the size of the burner fire to be defined and also ensured that the heat release rate was consistent in each experiment.

3.5 Radiant Heat Flux Distribution Tests

The fire from the burner imposed a varying degree of heat fluxes at each point on the surface of the glass sample depending on the exposure time and the distance between the centre of the burner and the surface of the glass specimen. Therefore, it was important to ensure that the position of the glass sample would have benefited from the optimum distribution of the radiant heat from the burner fire so that the heat flux distribution was uniform across the glass samples. The position of the heat flux measurement points was 10 mm from the perimeter of the expose area of the window with exception to the centre measurement point (Point 5).

In the distribution test, the radiant heat flux measurements were taken at ten positions. The points were numbered from 1 to 10. Point 10 was the position of the heat flux gauge during every glass fallout experiment. The measurement points and labels are shown in Figure 3-7. The 530 mm x 530 mm dummy sample was cut out from a larger size 10 mm thick kaowool fibreboard.

The dummy sample was fitted into the window frame and nine holes were drilled to enable the heat flux gauge to be positioned on the dummy sample.

The radiant heat flux distribution test was carried out at two distances measured from the centre of the gas burner to the face of dummy sample. The two distances were 250 mm and 500 mm.

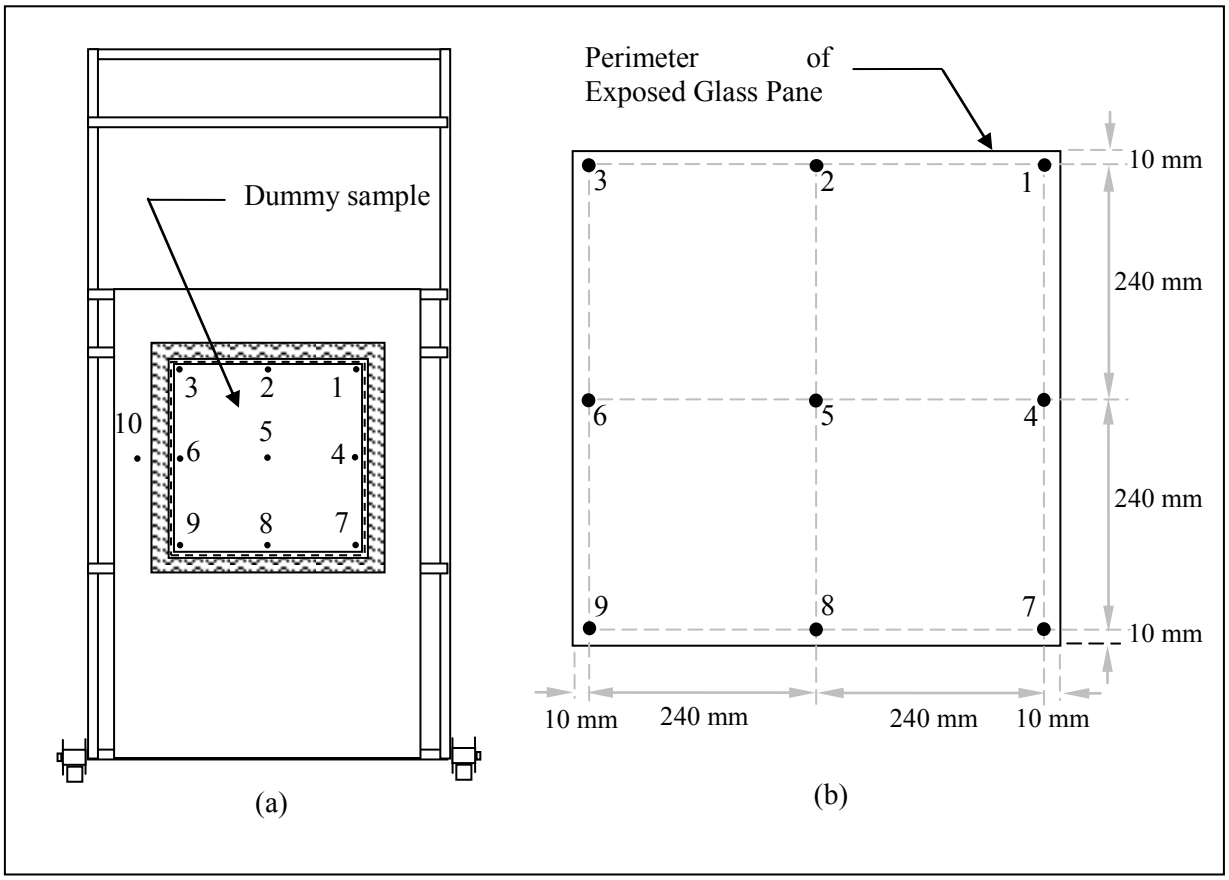

Figure 3-7: Radiant heat flux measurement points (face shown is exposed to radiant heat)

3.6 Experimental Setup

3.6.1 General

The experiment setup, which consisted of the main frame holding the window frame with the glass sample, radiation shield which separated the glass sample from the fire prior to each experiment, gas burner and spark igniter, is shown in Figure 3-8.

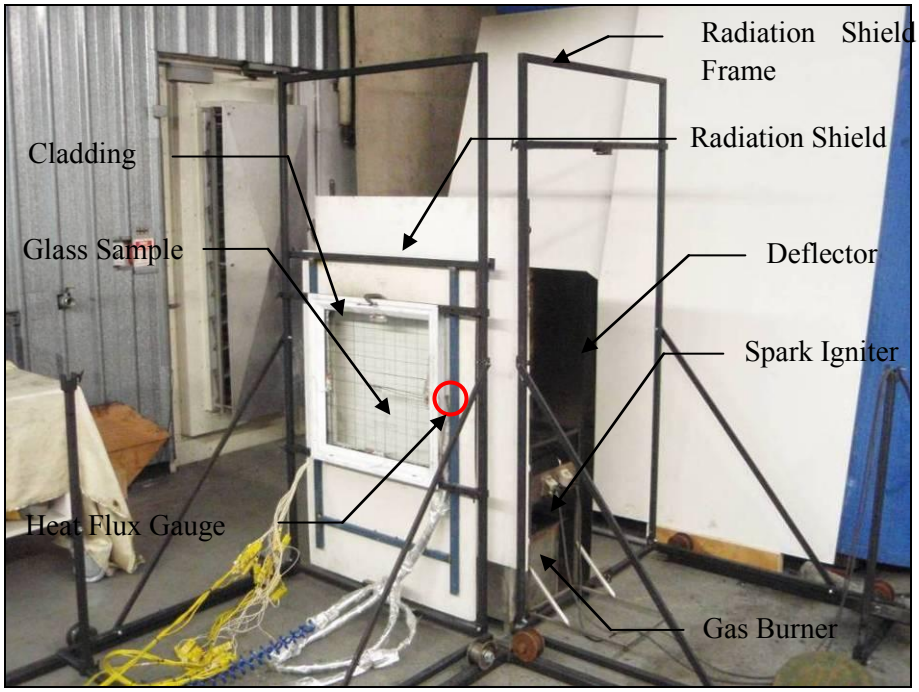

Figure 3-8: Experiment setup

3.6.2 Main Frame and Radiation Shield Frame

Two trolley frames were used in this research. Each trolley frame measured approximately 950 mm (width) by 1850 mm (height) and sat on two 40 mm x 40 mm steel square hollow section (SHS) rails. The trolley frames were referred to as the main frame and radiation shield frame. The trolley frames were made with 25 mm x 25 mm SHS sections that were welded together. Intermediate adjustable sections in the form of 25 mm x 25 mm SHS sections were used within the frame for stability. The adjustable sections were also used to hold in place the window frame fitted with the glass sample on the main frame.

In a burning compartment, only one face of the window is typically exposed to the heat from the fire. In order to simulate this condition for the glass sample, a 12 mm thick calcium silicate board was fitted to the main frame to insulate the other face of the glass sample from the direct exposure of the radiant heat.

3.6.3 Glass Samples

The glass samples used in the experiments were ordinary float glass (also known as soda glass) panes with thicknesses of 4 mm and 6 mm. The size of each glass pane was 525 mm x 525 mm. The glass panes were cut by the supplier and the edges were ordered as clean cut which meant that the edges were not polished. The area of the glass sample exposed to the radiant heat was 500 mm x 500 mm.

As the length of the available gas burner was 900 mm, the size of the glass panes was limited to 525 mm x 525 mm. A gas burner of this dimension was able to generate a fire with its flame boundary much greater than the size of exposed glass which provided a reasonably uniform distributed heat flux across the surface of the glass.

Glass panes with cracks were not used in the experiments. However, glass with minor defects like small chips and uneven edges were still used in the experiments. This was to simulate the condition where glass panes are manually cut on site to fit inside the window frames.

Grids of 50 mm x 50 mm were drawn on the surface of each glass sample using a permanent pen marker to allow the amount of fallout in the glass to be estimated. The grids were drawn on the face of the glass which was not facing the fire as direct exposure to the radiant heat will cause the marking to evaporate quickly.

The procedure to glaze the glass with rubber beading into the aluminium frame was as follows,

1. The window edge fins on the window frame were removed.
2. The glass pane was positioned into the window frame so that the offset of the glass perimeter from the sides of the window frame were equal. This was done by using a glass sucker shown in Figure 3-9a for easy handling.
3. The fins were snapped back into the window frame.
4. The glass edge was sprayed with a cleaning solution. The cleaning solution acts as a lubricant in order to make the glazing with rubber beading easier.
5. The glazing was carried out along each of the edge of the unshaded glass. The rubber beading was cut to the length equivalent to the one edge of the exposed glass. The rubber beading was pushed at one end into the gap between the glass and the edge fin using the pointed end of the glazing roller shown in Figure 3-9b. The remaining length of the rubber beading was rolled with the roller into the gap while the other end was finished off by pushing the remainder into

the gap using the glazing roller. This step was repeated on the other edges.

In the case of the kaowool beading, no lubrication was required and the kaowool beading was push into the gap using the glazing tool.

(a) Glass sucker

(b) Glazing roller

Figure 3-9: Glazing tools (Photos from www.alufix.co.nz)

3.6.4 Window Frames

The glass window frames that were used in this research were made of aluminium. The aluminium window frames were used because aluminium frames are not combustible and therefore reusable for subsequent experiments. Aluminium frames are able to withstand high temperatures without distortion. The aluminium window frames were proprietary “Vantage” designed profile windows. Figure 3-10 shows the specification label on one of the aluminium window frames. Four aluminium window frames were ordered for this research.

Figure 3-10: Specification label on aluminium window frame

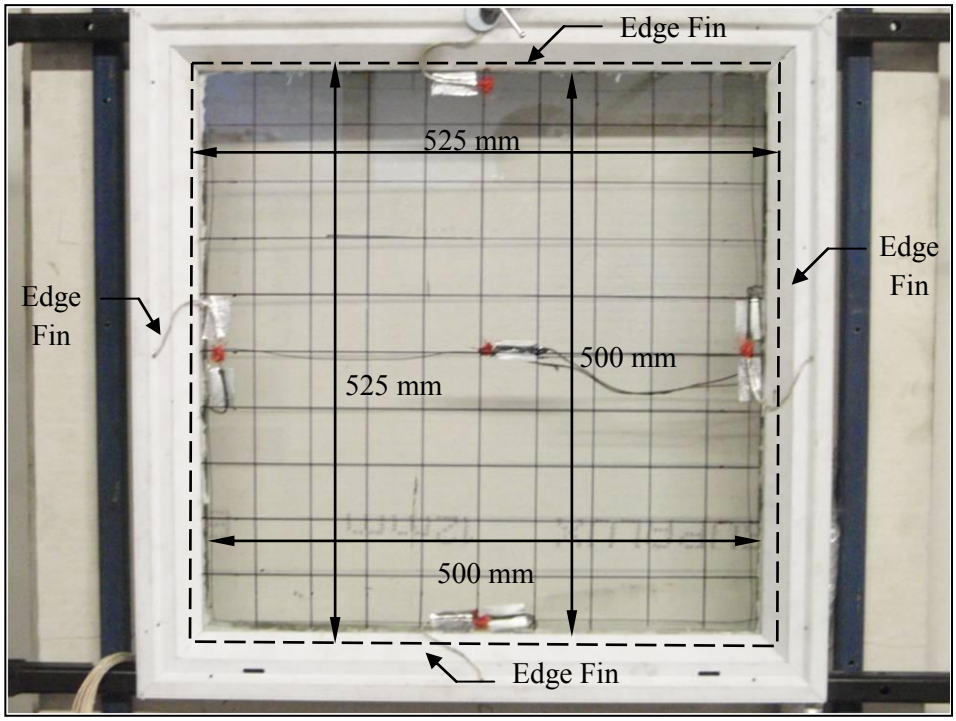

Figure 3-11: Aluminium frame and glass with 50 mm x 50 mm grids

Each glass sample as glazed in the aluminium window frame as shown in Figure 3-11. The aluminium window frames were delivered with 4 mm glass panes already glazed in the frames. The edge fins shown in Figure 3-12 were removed from the window frame prior to any re-glazing work. The groves in the frame for the glazing beading are shown in Figure 3-13.

The glass panes were held in place using rubber beading which is typical of aluminium window frames with single glazing. Trial experiments were carried out with these four windows without any measuring instruments to study the feasibility of the experimental setup.

The four trial experiments showed that the rubber beading would ignite and melt during the heating stage of the experiment. The ignited rubber beading then charred and formed a hard solid that stuck to the edges of the glass panes and the aluminium window frame. The solid char residue which stuck onto the groves of the aluminium window frame where the rubber beading was positioned made the cleaning process for the subsequent re-glazing task difficult.

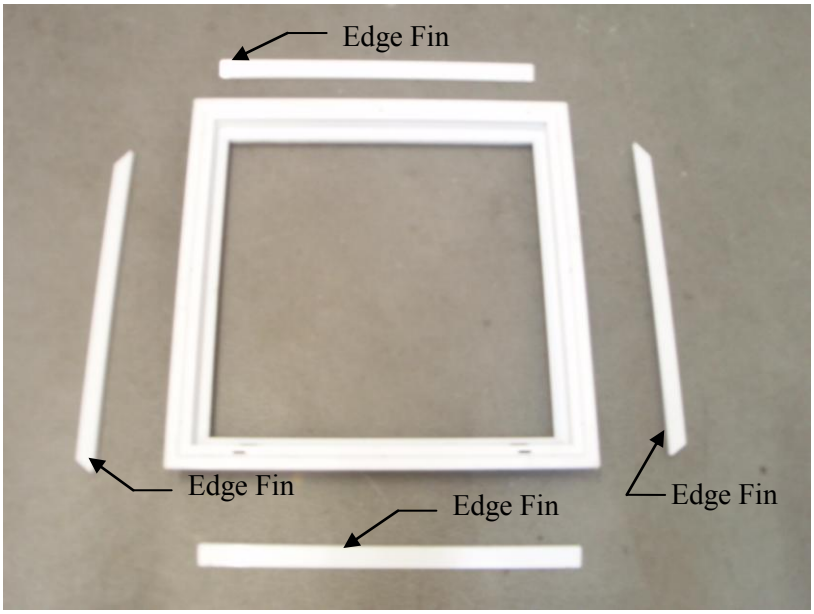

Figure 3-12: Edge fins removed from window frame

In order to facilitate the cleaning of the rubber beading char residue in the groves of the aluminium window frames, aluminium foil strips were fit into the groves and the surrounding area of the aluminium window frame where the rubber beading will be positioned. The aluminium foil strips prevented the rubber beading char residue from sticking onto the aluminium window frames by acting as a separating medium. The aluminium foil strips were replaced when the strips were damaged during the removal of the rubber beading char residue.

Table 3-1 which is reproduced from NZS 4223.1:2008 lists the minimum glazing dimensions for the glazing materials with the terms shown in Figure 3-14. The minimum dimensions in Table 3-1 for the

4 mm and 6 mm thick glass samples were compared with the actual dimensions of the window frames. The actual dimensions were found to have met the minimum dimensions in the table.

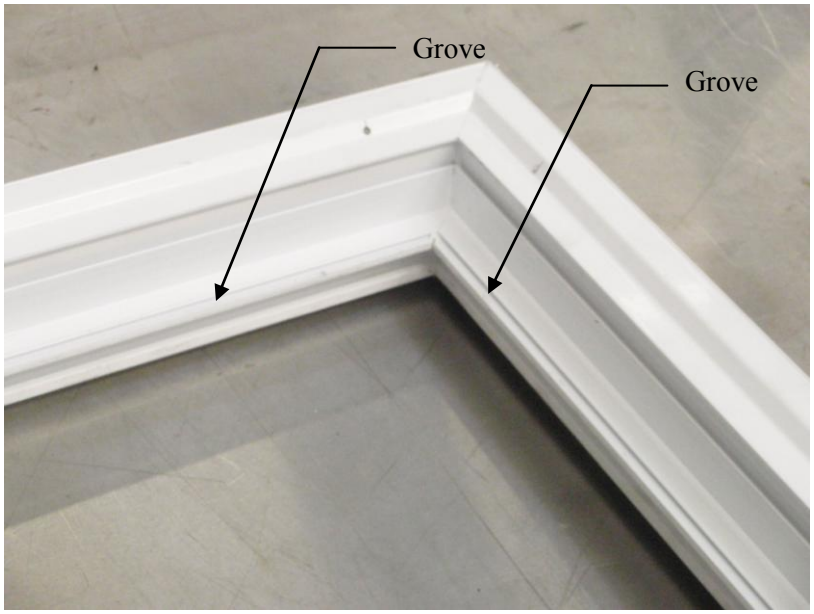

Figure 3-13: Corner of window frame showing groves for beading

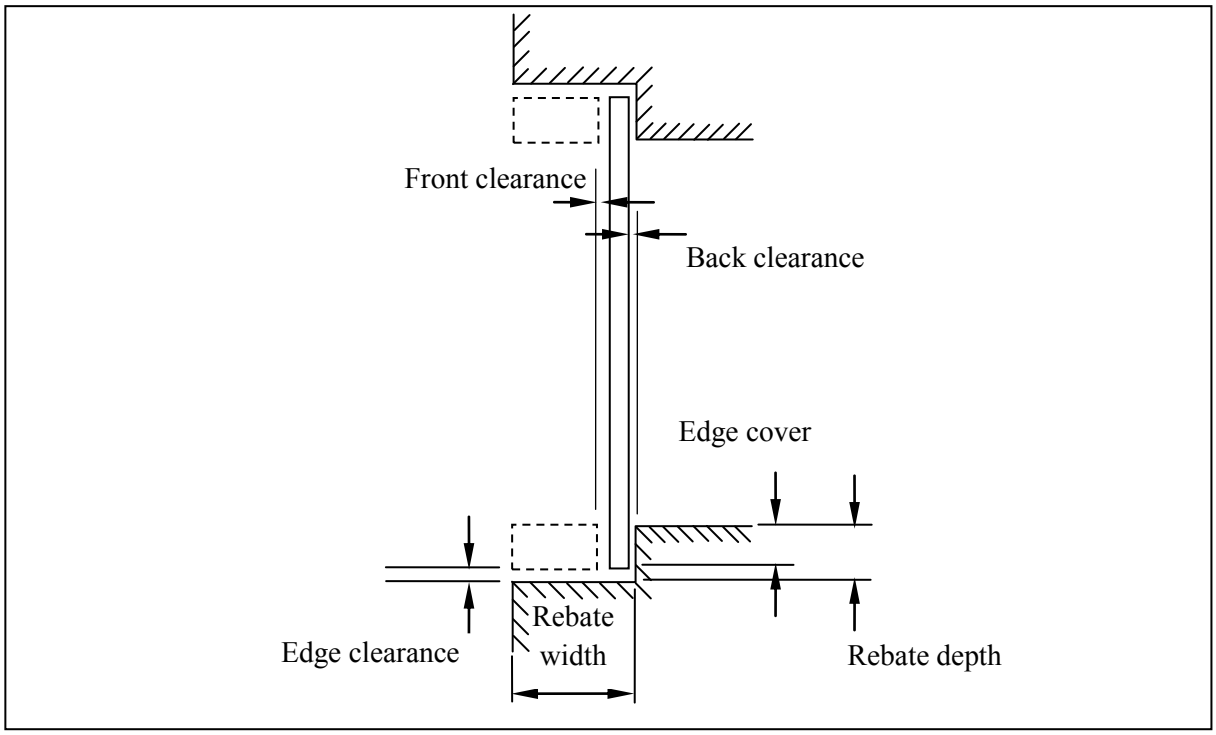

Figure 3-14: Sizes and rebates (adapted from Figure 1 in NZS 4223.1:2008)

Strips of kaowool in aluminium foil shown in Figure 3-15 were fitted onto the exposed face of each aluminium window frame which surrounds the exposed glass pane in order to minimise the rise in temperature of the glass inside the window frame. This was carried out to increase the temperature difference between the glass exposed to the radiant heat and glass shaded from the radiant heat to induce the more cracks in the glass samples.

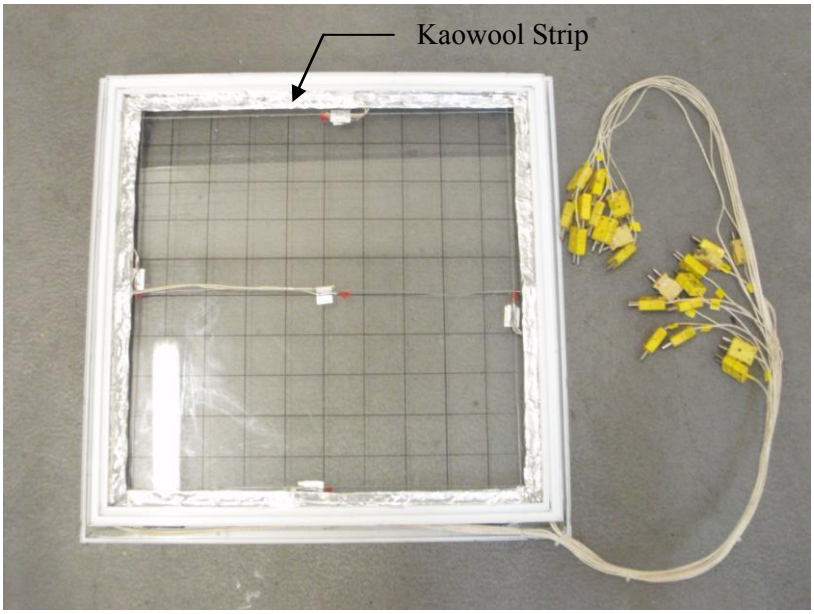

Figure 3-15: Kaowool strips on exposed face of window frame with glass sample

Table 3-1: Minimum glazing dimensions for glazing materials (reproduced from Table 5 in NZS 4223.1:2008)

Nominal thickness	Front and back clearance			Edge clearance	Edge cover	Rebate depth
	Type (a)[1]	Type (b)[2]	Type (c)[3]			
(millimetres)						
3 ($\leq$ 0.1 m^2)	2	-	-	2	4	6
3 (> 0.1 m^2)	2	-	-	2	6	8
3	-	2	1	3	6	9
4	2	-	-	2	6	8
4	-	2	1	3	6	9
5	2	2	2	4	6	10
6	2	2	2	4	6	10
8	-	3	2	5	8	13
10	-	3	2	5	8	13
12	-	3	2	6	9	15
15	-	5	4	8	10	18
19	-	5	4	10	12	22
25	-	5	4	10	15	25

NOTE –

1. Type (a) applies to putties or glazing compounds containing linseed oil.
2. Type (b) applies to elastomeric sealants and preformed strip materials.
3. Type (c) applies to glazing seals held in position by pressure.
4. The dimensions are the minimum necessary for the structural integrity of the glass only but do not apply to insulating glass units (refer to AS/NZS 4666).
5. For non-standard glass thicknesses the nearest values of nominal thickness, shall be used.
6. Timber and PVC frames may not require the specified front and back and clearances provided the waterproofing performance requirements are met.

3.6.5 Beading

Rubber and kaowool type beadings were used to glaze the glass panes onto the aluminium frames. The rubber beadings consisted of standard beadings which are typically used for glazing purpose. The beading is specific to the thickness of the glass pane so two beading sizes were used to glaze the 4 mm and 6 mm thick glass panes. However, the kaowool beading which was kaowool cable rope was not a standard beading used in window glazing. The rope consisted of three pre-twisted strands twisted together. The rope was used to glazed the 4 mm thick glass panes while the strand form the kaowool beading for the 6 mm thick glass panes.

3.6.6 Variations of Experiment

The experiments carried out consisted of either 4 mm or 6 mm thick glass samples glazed with either kaowool or rubber beading. Some of the glass samples had thermocouples attached. The summary of the glass samples variations is shown in Table 3-2. Gas temperature at different points on the glass sample was measured in all of the experiments.

Table 3-2: Summary of characteristics of glass samples

Sample Characteristic	Type of Beading	Glass Thermocouples
1	Rubber	Attached
2	Kaowool	Attached
3	Rubber	Not attached
4	Kaowool	Not attached

3.6.7 Heat Release Rate Measurement

The heat release rate of the burner was determined using the oxygen depletion method. Combustion products (i.e. oxygen, carbon dioxide and carbon monoxide) were measured using the calorimeter and the readings were converted into the heat release rate.

3.6.8 Temperature Measurement

The gas and glass temperatures were measured using Type K, 24 gauge thermocouples. The thermocouples were made by welding two wires insulated by the yellow and red sheathing of the thermocouples wire.

The arrangement of the thermocouples and strain gauges is shown in Figure 3-16 and Figure 3-17. The thermocouple wires were attached to each glass sample with aluminium or reflective adhesive tapes that were not combustible while the thermocouples were attached to the glass surface using high temperature resistant sealant.

The glass thermocouples in the window frame on the unexposed face were not applied with the sealants and were left exposed while touching the glass. Since the glass thermocouples in the window frame were not directly exposed to the fire, it was deemed unnecessary to shield the thermocouples with sealants. The application of sealant on these thermocouples was also difficult due to the position of the thermocouples in the window frame.

The thermocouple readings were recorded in the unit °C. The thermocouples were labelled from TC01 to TC021 for identification in the UDL. Thermocouples labelled TC01, TC06, TC11, TC16 and TC21 were used to measure the gas temperature at various points on the glass sample. Thermocouples labelled TC02, TC07, TC12, TC17 and TC22 were used to measure the temperature of the glass on the exposed face. Thermocouples labelled TC03, TC08, TC13 and TC18 were used to measure temperature of the shaded glass on the exposed face. Thermocouples labelled TC04, TC09, TC14 and TC19 were used to measure the temperature of the shaded glass on the unexposed glass. Thermocouples labelled TC05, TC10, TC15 and TC20 were used to measure the temperature of the glass on the unexposed side.

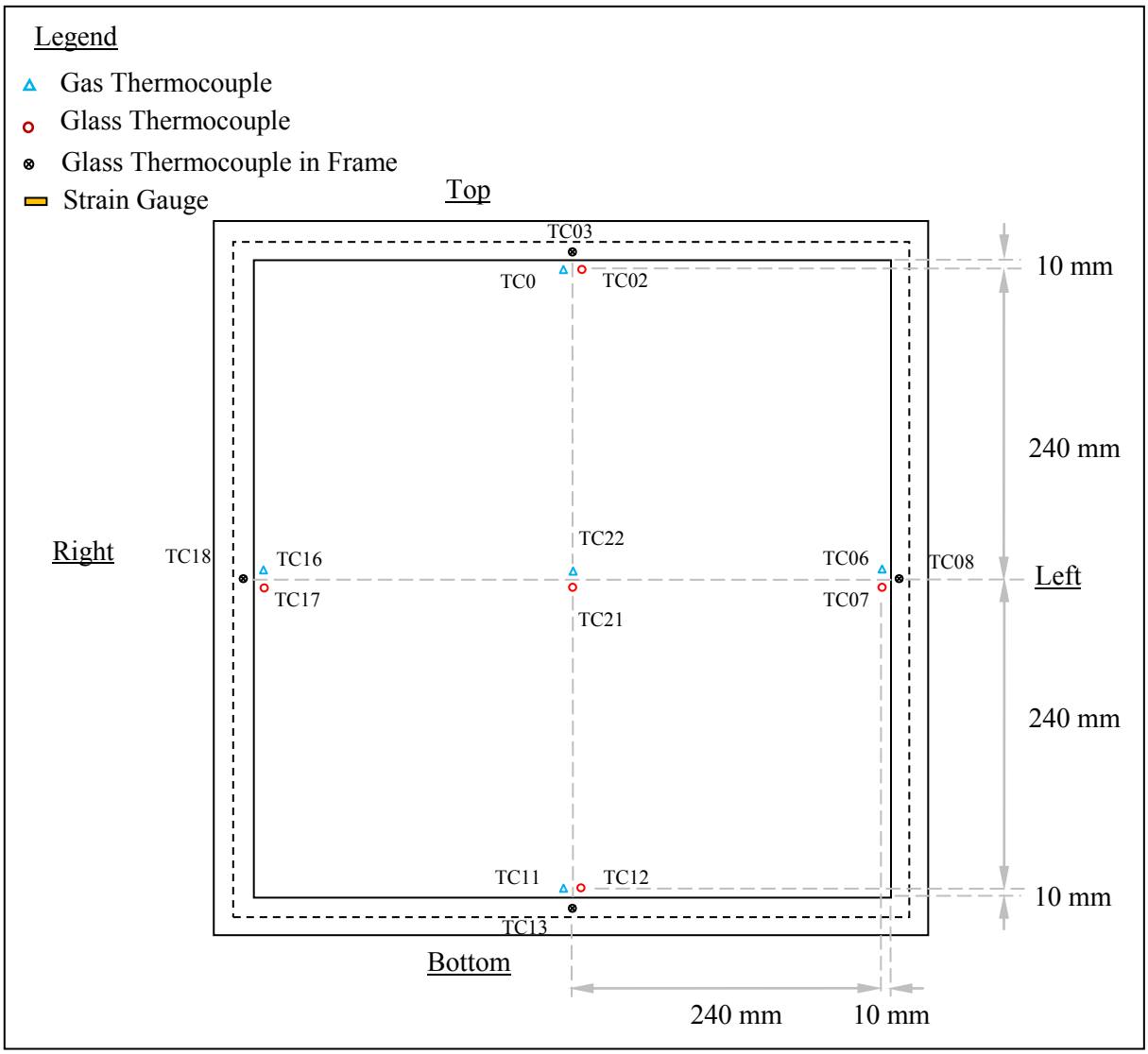

Figure 3-16: Location of thermocouples on exposed face

During the early stage of the research, the Vital Red RTV sealant was used to shield the thermocouples from the fire. However, the sealant was not easy to apply and on some occasions, the sealant ignited during an experiment. The Vital Red RTV sealant was replaced with the HOLDFAST® Firecement HT sealant which has a higher temperature resistant than the Vital Red RTV. The sealants are shown in Figure 3-18. The thermocouples which were used to measure the temperatures of the gas were attached to the aluminium window frames using steel wires, which were strung through holes drilled into the window frames.

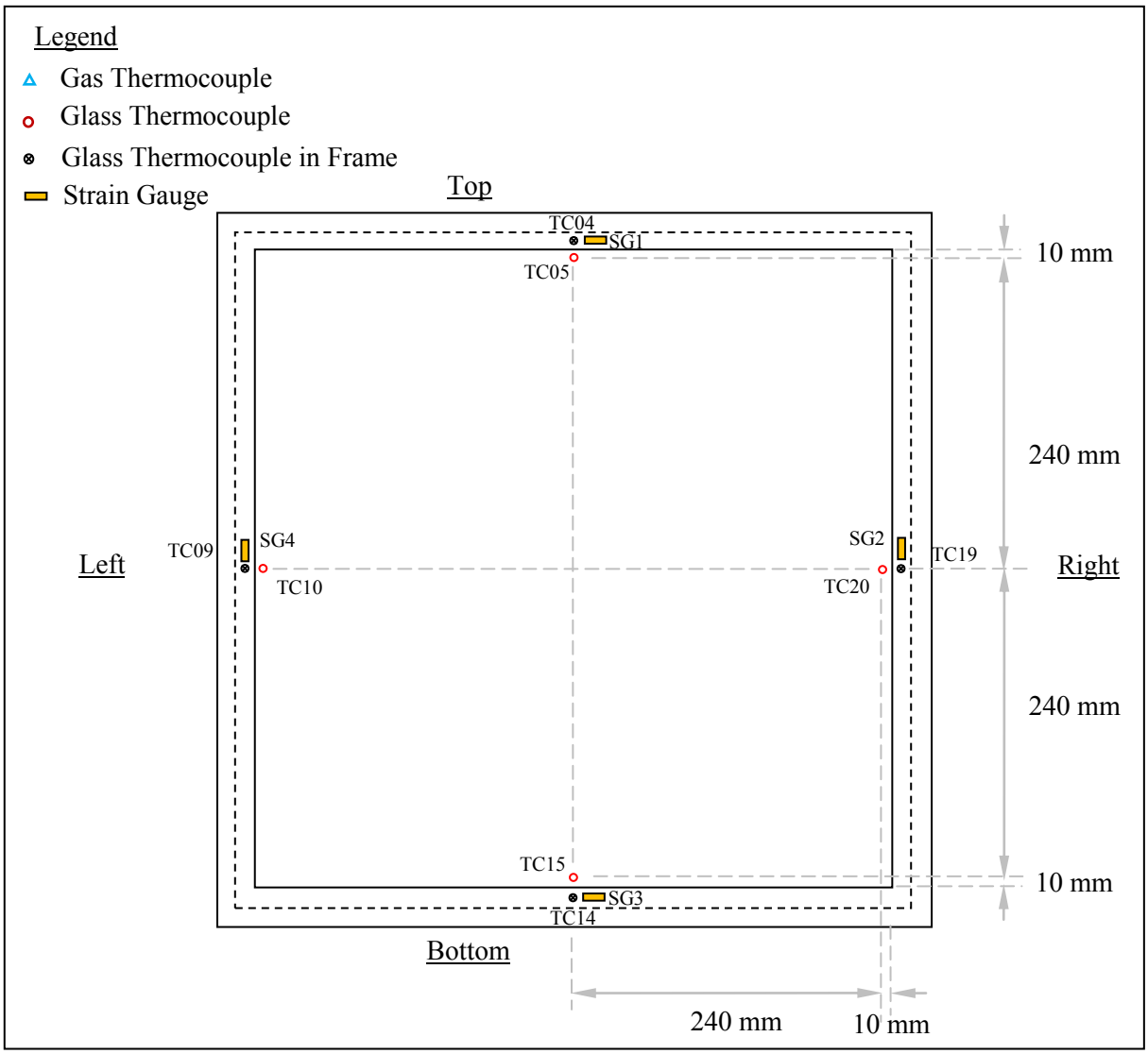

Figure 3-17: Location of thermocouples and strain gauges on unexposed face

Figure 3-18: HOLDFAST® Firecement HT and Vital Red RTV sealants

3.6.9 Thermal Strain Measurement

The thermal strains in the glass samples were measured with general purpose strain gauges. The strain gauges were TML FLA-5-11 strain gauges. A typical TML FLA-5-11 strain gauge is shown in Figure 3-19. The stain gauges were ordered with a 1.5 m lead wire attached to each strain gauge. The operating temperature for the strain gauges of this model ranged from -20 °C to 80 °C. According to the strain gauge technical specification sheet, the strain gauges are able to measure up to a maximum strain limit of 5%. The strain gauges were attached to the unexposed shaded face close to the edge of the glass.

The surface of the glass sample, where the stain gauges would be attached, was first cleaned with acetone. A drop of acrylic glue was then applied onto the back surface of the strain gauge. The strain gauge was then pressed gently onto the glass surface and held down using the transparent sheet provided for a minimum 15 seconds to allow the glue to cure. The two wires attached to each strain gauge were separated and the Vital Red RTV sealant is applied onto the wires to prevent any contact between the two wires and also to keep the wires in position.

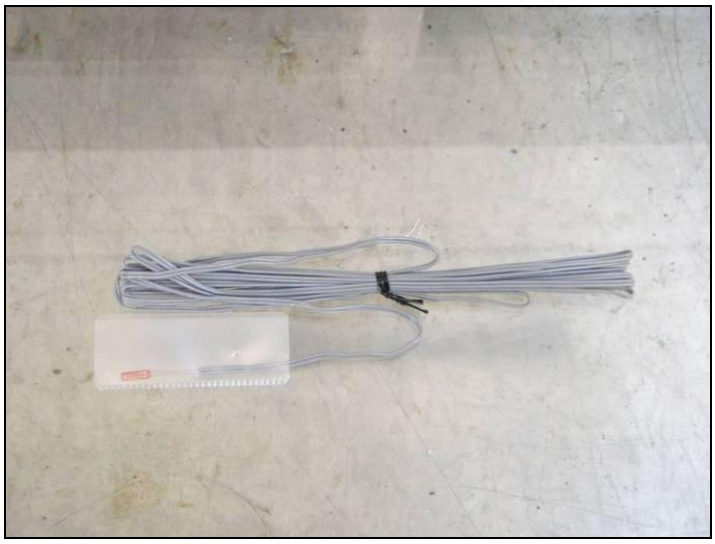

Figure 3-19: TML FLA-5-11 strain gauge with lead wires

The strain gauge readings were recorded in the unit microstrain (μstrain). The strain gauges were attached at the unexposed face on the edges of the glass sample. There were 10 experiment samples which were attached with strain gauges. The strain gauges were arranged as shown in Figure 3-17.

3.6.10 Radiant Heat Flux Measurement

A single heat flux gauge was used to measure the radiant heat flux imposed on the glass during the experiments. The heat flux gauge was mounted on one side of the main frame as shown in Figure 3-20. The position of the heat flux gauge was chosen as it was not ideal for the heat flux gauge to extend beyond the boundary of the aluminium window frame which could affect the heat transfer from the fire to the glass sample.

The heat flux gauge used was a Schmidt-Boelter type gauge. The heat flux gauge was constantly cooled by running water supplied through flexible hoses connected to the two hollow rods connected to the heat flux gauge. The heat flux gauge has a range of 0 – 100 kW/m^2. The Schmidt-Boelter type gauge measures the total heat flux from a fire source. However, given the close proximity between the heat flux gauge and the fire, the contribution of the convective heat flux from the fire will be negligible.

The output for the heat flux gauge was recorded in mV. A conversion factor of 5.376 kW/m^2 per mV obtained from the heat flux gauge calibration sheet was used to convert the heat flux gauge reading

from mV to kW/m^2.

Due to the turbulent nature of the burner fire, a steady state radiant heat flux measurement was not possible and "noise" was present in all of the measured radiant heat flux profiles. In order to report the radiant heat flux profiles in a meaningful way for analysis and reporting purposes, each radiant heat flux profile was reduced to a value which reflected the average reading of the profile.

For the experimental results, the first 10 seconds of data after a glass sample was exposed to radiant heat and last 20 seconds of data before the burner was turned off were discarded. For the radiant heat flux distribution test results, the first 10 seconds of data after the heat flux gauge was exposed to radiant heat was discarded and heat flux data up to 240 seconds was taken for analysis since logging was terminated while the heat flux gauge was still exposed to the radiant heat and therefore the logged data did not have a heat flux decay stage.

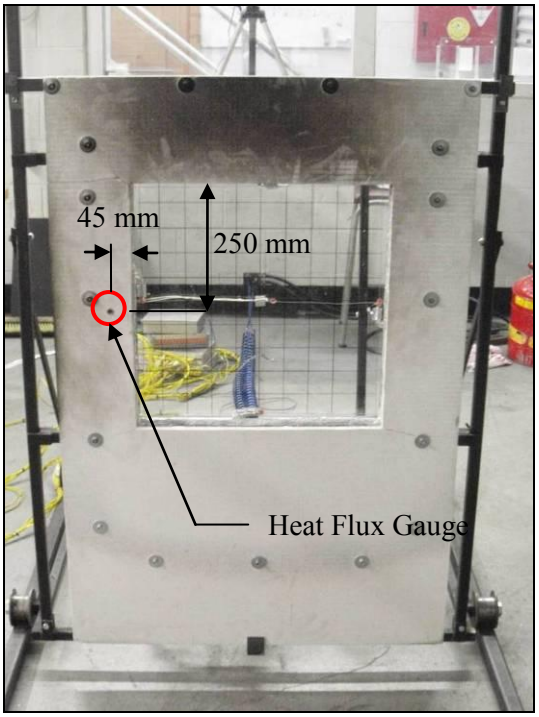

Figure 3-20: Location of heat flux gauge on main Frame

3.6.11 Visual Recording and Capture Equipment

The visual recording of the experiments were carried out using two Canon XM2 digital video camcorders placed at two locations behind the protective glass windows outside the fire laboratory.

Each camera was mounted on a steel frame and visual recording was made for each experiment. The video recordings were captured on miniDV cassette tapes which were uploaded into the hard disk of a DVD player and the recordings were downloaded onto DVDs. A digital camera was used to take photos during each experiment.

3.7 Flame Impingement

Flame impingement occurs due to the pressure differences around the flame. Flame impingement on the surface of the glass sample was undesirable in the experiments as the flame when attached onto the glass surface will heat up the glass at localised areas only and prevents the development of a uniform heat flux across the surface of the glass

The introduction of a deflector on the opposite side of the glass sample across the gas burner induced the flame to move away from the glass sample. Figure 3-21 and Figure 3-22 show the location of the deflectors at 550 mm and 380 mm away from the centre of the burner.

Figure 3-21: Deflector at 550 mm from centre of burner (Photo showing experiment with sample 4 Test 7 in progress)

Figure 3-22: Deflector at 380 mm from centre of burner (Photo showing experiment with sample 6 Test 51 in progress)

When the deflector was 550 mm away from the centre of the gas burner, the flame was relatively steady with intermittent impingement to the glass sample which was acceptable. Due to the change in the fuel mix, the deflector was moved closer to the burner to maintain a relatively similar range of radiant heat fluxes. With the new arrangement, the flame impinged onto the deflector due to the close proximity to the deflector compared with the glass sample which prevented the flame from impinging on the glass samples permanently.

3.8 Universal Data Logger (UDL)

An "in-house" data logging software called the UDL was used to record the thermocouple, radiant heat flux gauge and strain gauge measurements and the readings were stored as .csv files. A .csv file was set up through the UDL for each experiment.

3.9 Experimental Procedure

Each glass fallout experiment was carried as follows,

- At time = 0 seconds, the UDL data logger was activated.
- At time = 30 seconds, the video cameras were turned on.

- At time = 60 seconds, the burner was turned on. In the experiments, the burner was turned on a few seconds earlier as it took a few seconds for the gas in the pipeline to reach the gas burner.
- At time = 90 seconds, the radiation shield was removed thereby exposing the glass sample to the fire.
- At time = 720 seconds, the burner was turned off.
- At time = 1020 seconds, the video cameras were turned off.

In addition, the time to glass fracture was recorded during each experiment. Any fallout between the initial fracture and the time the cameras were operating was noted. Throughout the experiments, the glass samples were exposed to the fire for approximately 630 seconds. The 630 seconds exposure time was chosen based on the four trial experiments carried out prior to the start of the glass fallout experiments. During the trial experiments, glass fallout (if any) ceased after approximately 5 minutes after the glass samples were exposed to the fire so the 630 seconds exposure time. An allowance which is approximately equal to the 5 minutes is included in the experiments. If a major fallout occurred during an experiment where no further fallout and cracking was deemed possible, the experiment was terminated.

The 300 seconds cooling period was arbitrarily chosen to allow the main frame and window frame to cool down prior to changing over to a new experiment and allow any combustible products to be extracted from the fire engineering lab.

3.10 Data Reduction

The .csv files that were saved using UDL were converted into .txt files for analysis. A visual basic macro was written in Microsoft Excel 2007 to transfer the data from the .txt into spreadsheet template that was created to process the data recorded and present the data in a graphical format.

An academic version of @Risk version 5.5 from Palisade was used with Microsoft Excel 2007 to fit distribution curves and analyse the data from the experiments.

4 EXPERIMENTAL RESULTS AND DISCUSSIONS

4.1 General

The results from the glass fallout experiments and four-point bending test are presented and discussed in this section. Due to the large number of glass fallout experiments carried out, only a selected few which are representative of the many others are discussed. The full sets of results for the glass fallout experiments are available in the Appendices section. The experiments with samples 4 Test 4, 6 Test 2 and 6 Test 51 did not form part of this research and therefore, the results were not presented and discussed.

The number of experiments conducted is as follows:

a. A total of 24 experiments were carried out using the 4 mm thick glass samples glazed with rubber beading involving 9 experiments with thermocouples attached and 15 experiments without thermocouples attached.

b. A total of 18 experiments were carried out using the 6 mm thick glass samples glazed with rubber beading involving 8 experiments with thermocouples attached and 10 experiments without thermocouples attached.

c. A total of 39 experiments were carried out using 4 mm thick glass samples glazed with kaowool beading involving 12 experiments with thermocouples attached and 27 experiments without thermocouples attached.

d. A total of 36 experiments were carried out using 6 mm thick glass samples glazed with kaowool beading involving 7 experiments with thermocouples attached and 29 experiments without thermocouples attached.

4.2 Mechanical Properties of Glass

Figure 4-1 shows the typical load – deflection plot for each of the 4 mm and 6 mm thick specimens obtained from the four-point bending test. At the start of each bending test, the deflection of the glass specimen was zero as there was no load applied onto the glass specimen. Load was applied onto the glass specimen at a deflection rate of 0.5 mm/min until the glass specimen fractured, which is shown as a sudden drop in the applied load for the plots in Figure 4-1. Prior to failure of each glass specimen, the increase in applied load and deflection was proportional. This behaviour is typical for an elastic material. So it was deduced that glass behaves elastically up to failure.

It is observed from Figure 4-1 that during the initial phase of the each test when load was applied onto the glass specimen, the slope of the plot was less steep compared with the slope towards the end of each test. This situation was caused by the rollers of the fixture attempting to correct the unevenness of the glass specimen.

In view of this situation, the plots in Figure 4-1 were corrected by ignoring these portions of the plots so only the later portions of the plots were considered to be the true results of the bending tests. The corrected plots are shown in Figure 4-2. The starting point of each plot where the true result was deemed to begin was shifted to the origin of the plot. The breaking load (P), glass thickness (δ), width (b), fracture strength (σ_f) and modulus of elasticity (E) of each specimen are tabulated in Appendix I.

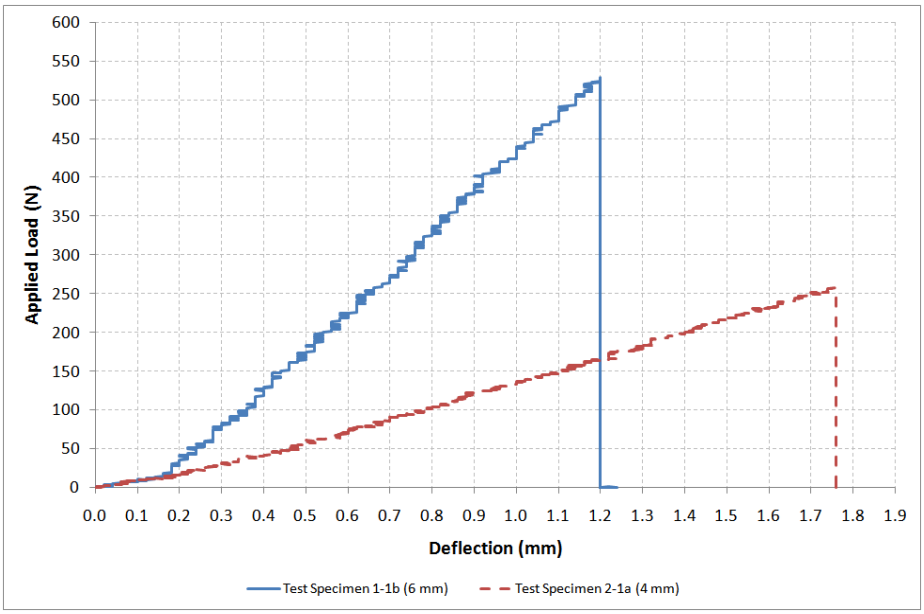

Figure 4-1: Load – deflection plots for 4 mm and 6 mm thick glass samples

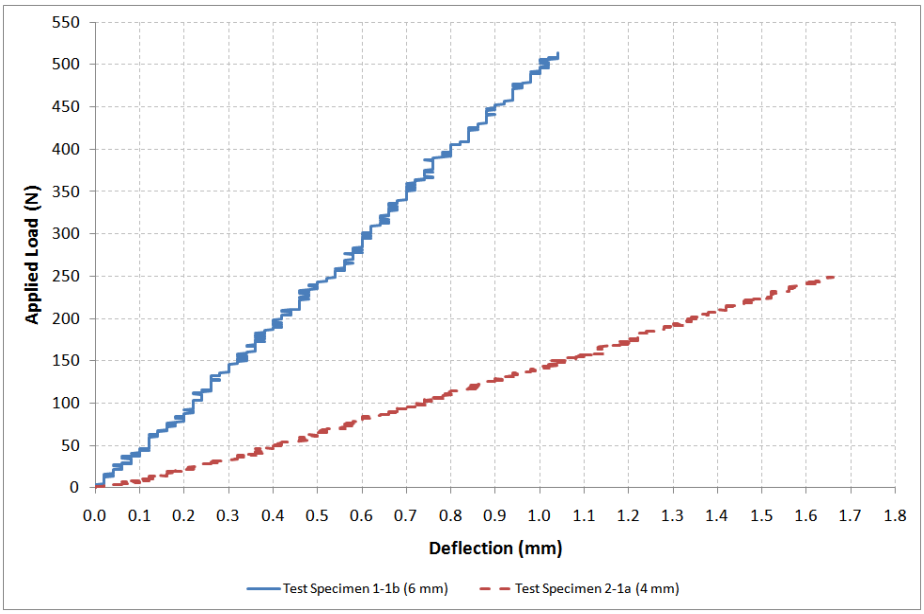

Figure 4-2: Corrected load-deflection plots for 4 mm and 6 mm thick glass samples

4.2.1 Fracture Strength

The fracture strength was determined using the equation,

$$\sigma_f = \frac{3P(c-a)}{2b\delta^2} \tag{5}$$

The derivation of Equation (5) can be found in Appendix J. The parameters a and c in Equation (5) are 55 mm and 165 mm respectively as shown in Figure 3-3.

The s the glass fracture strength was found to have the characteristic of a 3-parameter Weibull distribution. The cumulative frequency distribution of a 3-parameter Weibull distribution is given by,

$$P_f = 1 - \exp\left[\left(\frac{\sigma_f - \sigma_u}{\sigma_0}\right)^{m_v}\right] \tag{6}$$

where $\sigma_f \geq \sigma_u$ and $P_f = 0$ when $\sigma_f < \sigma_u$

Based on the 3-parameter Weibull distribution curve fit using Palisade @Risk, σ_u = 39.5 MPa, σ_0 = 28.9 MPa and m_v = 2.56 as shown in Figure 4-3.

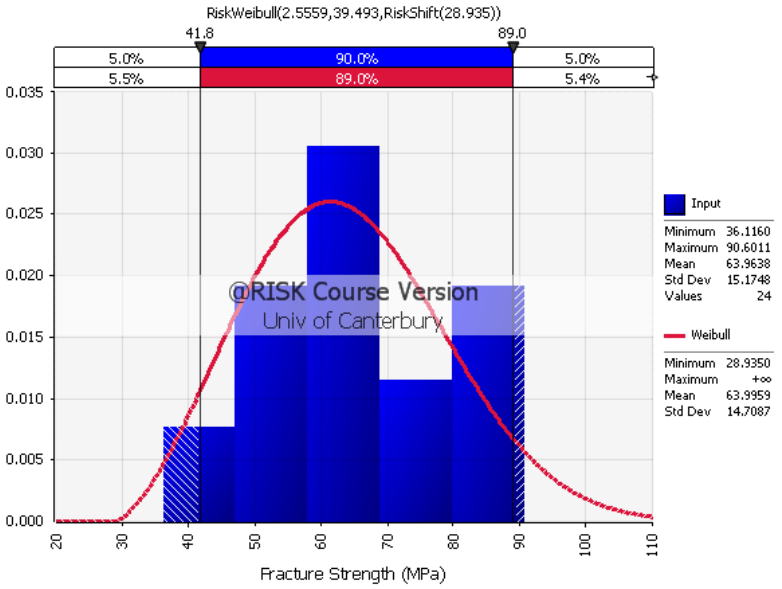

Figure 4-3: Distribution of fracture strength data for glass test specimens obtained from four-point bending test

Based on Figure 4-3, the mean breaking strength of the glass population is 64 MPa ± 15 MPa. The fracture strength ranges from 36.1 MPa to 90.6 MPa. The mean fracture strength obtained in this research is within the ranges of fracture strength reported by Pagni and Joshi (1991a) shown in Table 2-1. The fracture strength distribution from this research also established the wide variability of the glass fracture strength as reported in Pagni and Joshi (1991a).

4.2.2 Modulus of Elasticity

The modulus of elasticity of the glass was determined using the deflection equation given in Mikhelson (2004) for a four-point bending load arrangement.

The equation is given as,

$$\Delta = \frac{P(c-a)}{48EI}\left[3c^2 - 4\left(\frac{c-a}{2}\right)^2\right] \qquad (7)$$

Rearranging Equation (7),

$$E = \frac{P(c-a)}{48\Delta I}\left[3c^2 - 4\left(\frac{c-a}{2}\right)^2\right] \tag{8}$$

The distribution of the modulus of elasticity data derived from the four-point bending test is shown in Figure 4-4. The data is fitted with a normal distribution curve with a mean of 76.5 GPa and a standard deviation of 4.0 GPa. The modulus of elasticity ranges from 64.5 GPa to 82.4 GPa. The mean modulus of the elasticity obtained from this research is higher than the values reported by Pagni and Joshi (1991a) in Table 2-1.

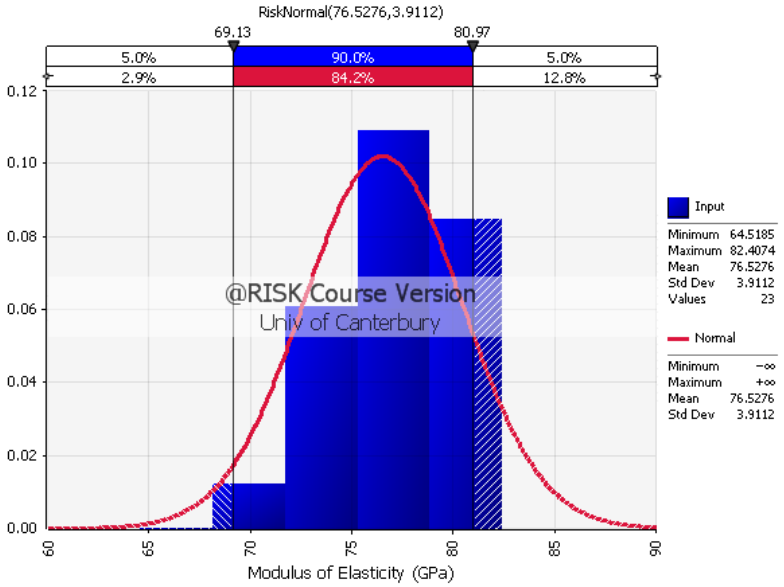

Figure 4-4: Distribution of modulus of elasticity data of glass test samples obtained from four-point bending test

4.3 Heat Release Rate

Figure 4-5 shows the raw and 60 second moving average heat release rate curves for the burner fire using the oxygen depletion method. The heat release rate of the burner fire from the figure is approximately 350 kW. The fire size was kept to 350 kW after taking into consideration the possible number of experiments likely to be carried out daily and the allowable burning time before the gas tanks froze.

A baseline data of 180 seconds was collected at the start of the heat release rate measurement and another 180 seconds worth of data was also collected once the burner was turned off. This is a standard procedure that was adopted by the fire engineering lab in logging the heat release rate data for a burner fire.

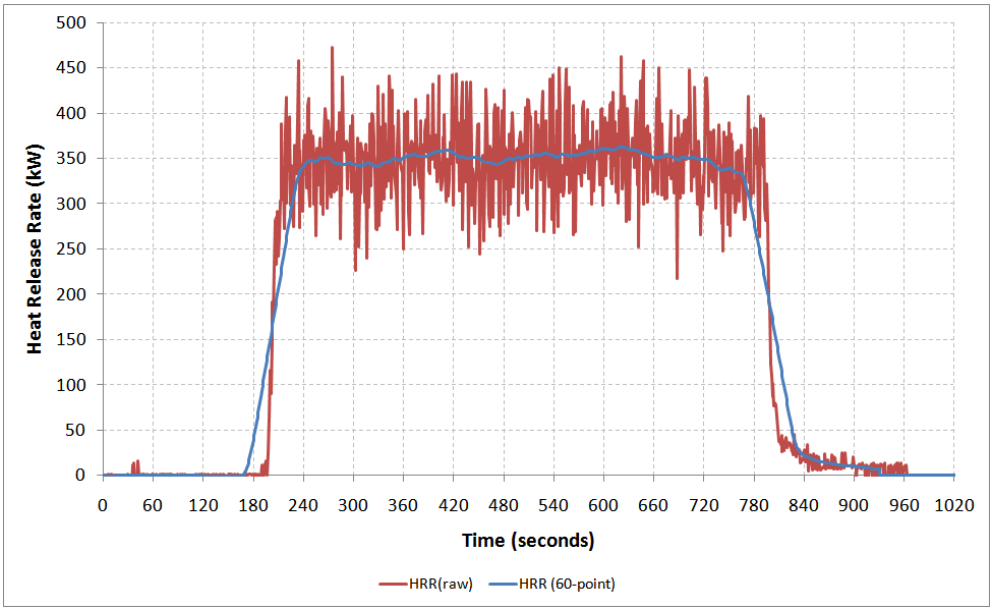

Figure 4-5: Heat release rate profiles for gas burner fire with 80% – 90% propane/ 20% - 10% butane fuel mix (Raw and 60 second moving average plotted)

4.4 Radiant Heat Flux

Figure 4-6 to Figure 4-9 show some typical distribution of radiant heat flux data from the radiant heat flux distribution tests and glass fallout experiments. The data are based on the radiant heat flux profiles recorded using the heat flux gauge. The radiant heat flux data can be fitted with a normal distribution which indicates that the radiant heat flux profiles recorded by the heat flux gauge can be defined with an average value.

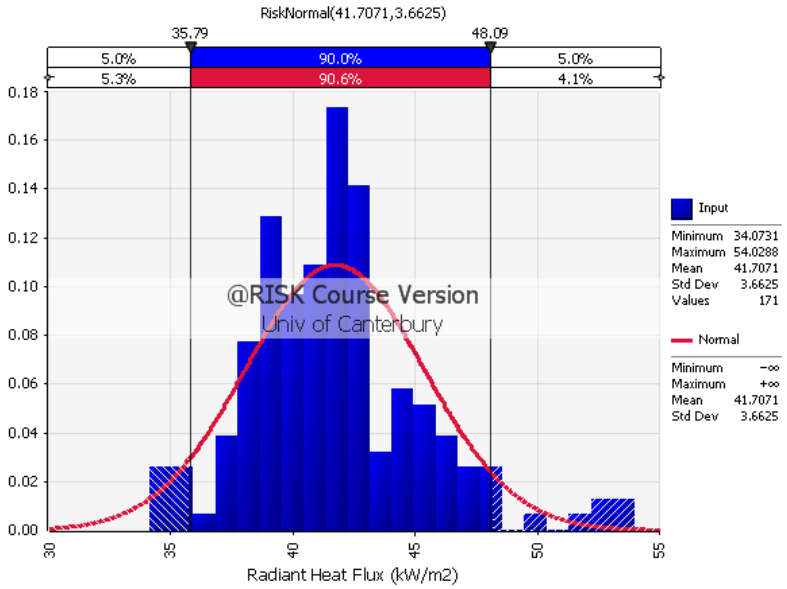

Figure 4-6: Distribution of radiant heat flux data at Point 5 for radiant heat flux distribution test at 250 mm from burner

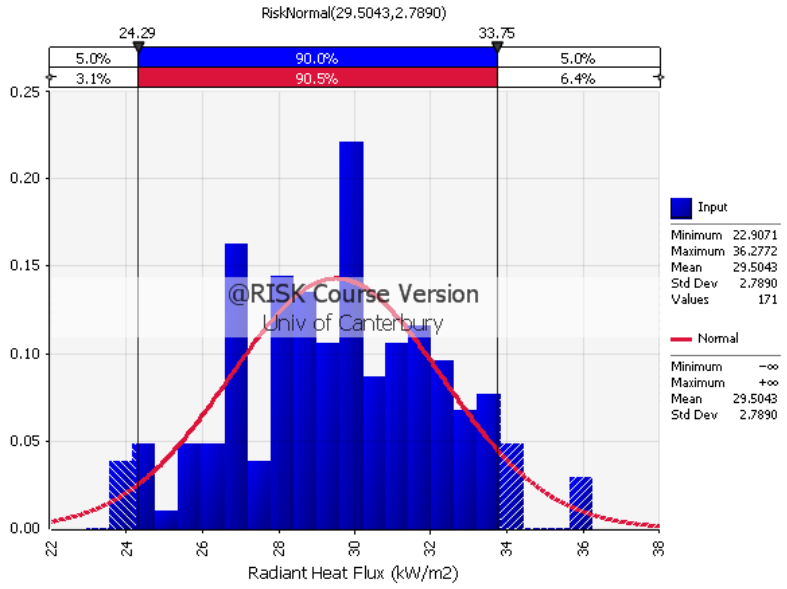

Figure 4-7: Distribution of radiant heat flux data at Point 5 for radiant heat flux distribution test at 500 mm from burner

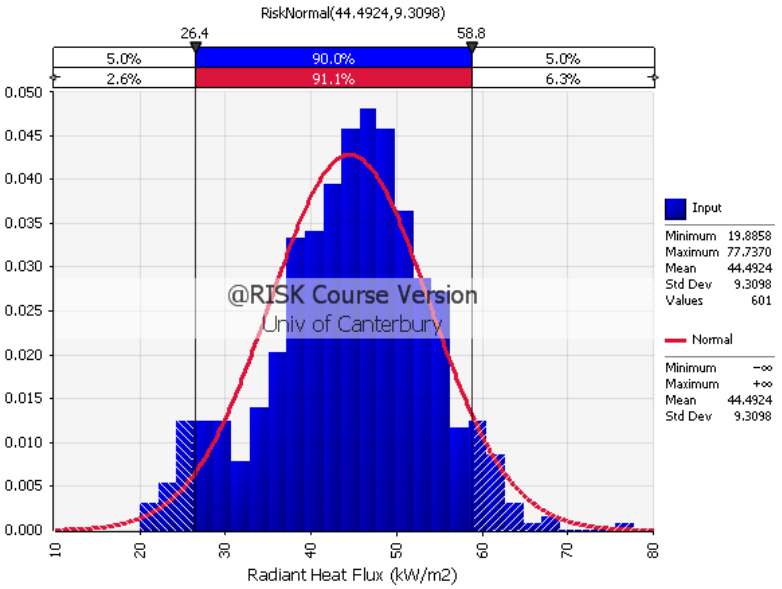

Figure 4-8: Distribution of radiant heat flux data at Point 10 for experiment with sample 4 Test 1

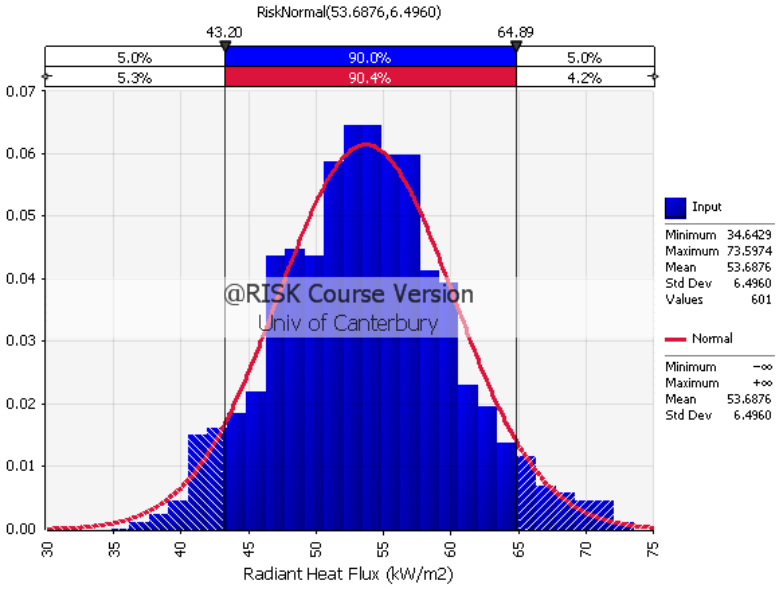

Figure 4-9: Distribution of radiant heat flux data at Point 10 for experiment with sample 6 Test 56

4.4.1 Radiant Heat Flux from Distribution Tests

Figure 4-10 shows the radiant heat flux profiles for the radiant heat flux distribution test at 250 mm from the burner. There is a 60 second baseline included in the radiant heat flux data collection. The 60 second baseline was chosen to reflect the same baseline during each experiment when the heat flux gauge at

Point 10 was exposed to the fire. Each profile was reduced to a single average value and summarised in Table 4-1. The table shows that the radiant heat flux intensities are different at the nine measuring points. Therefore, the radiant heat flux distribution across the glass sample was not truly uniform which was expected given the turbulent nature of the flame. The radiant heat flux distribution on the face of the dummy sample is shown in Figure 4-11.

The mean radiant heat flux from the nine readings at 250 mm from the burner is 36.5 kW/m^2. When compared with the radiant heat flux at Point 10 which is 46.4 kW/m^2, there is a 9.9 kW/m^2 difference between the two readings. This was expected as the positions of the heat flux gauge within the perimeter of the glass sample is relatively further away from the fire compared with the heat flux gauge position during the experiments.

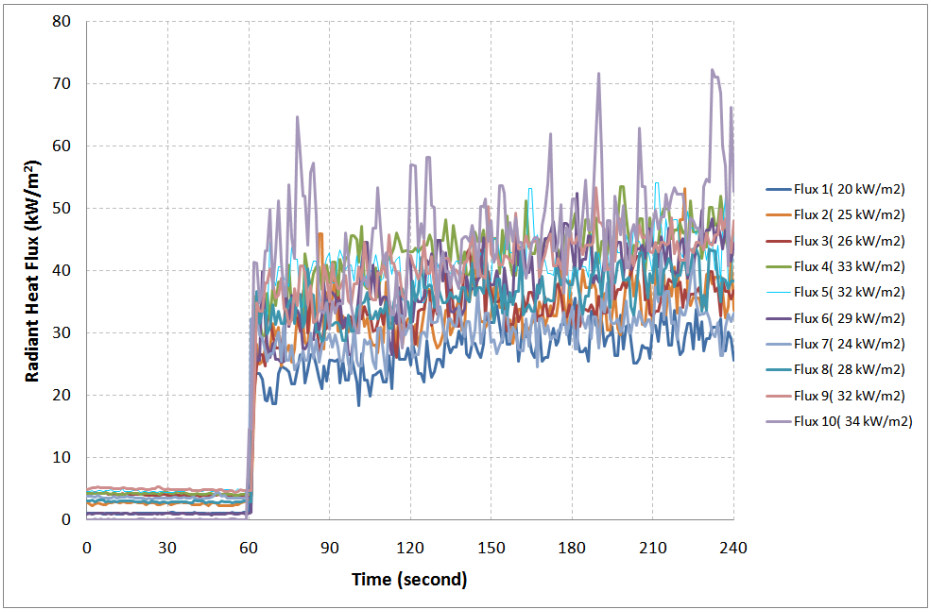

Figure 4-10: Radiant heat flux profiles from heat flux distribution test at 250 mm from burner (Radiant heat flux in bracket)

Table 4-1: Radiant heat flux at various points for distribution test at 250 mm from burner

Location of Heat Flux Gauge	Radiant Heat Flux (kW/m^2)
1	27.4
2	33.8

Table 4-1 **(con't)**

Location of Heat Flux Gauge	Radiant Heat Flux (kW/m^2)
3	34.6
4	43.5
5	41.7
6	39.0
7	30.5
8	36.4
9	41.5
10	46.4

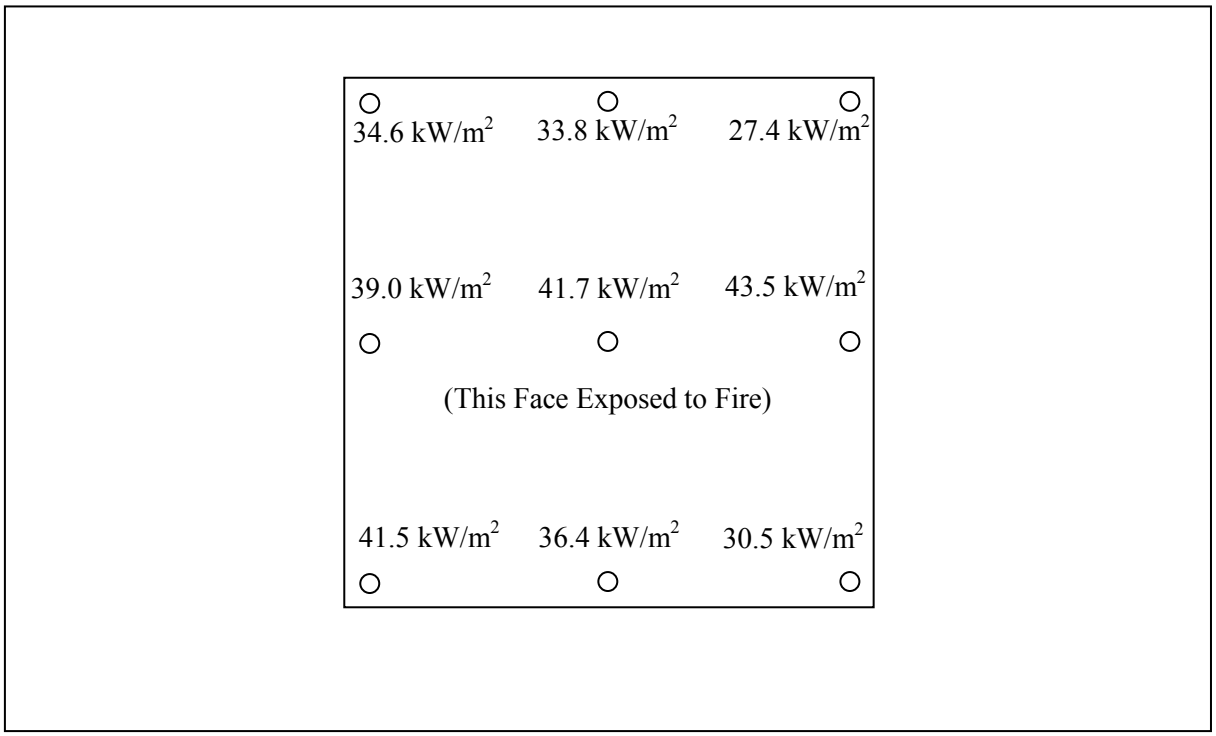

Figure 4-11: Distribution of radiant heat flux data at various points on the dummy sample at 250 mm from centre of burner

Figure 4-12 shows the radiant heat flux profiles at 500 mm from the burner. The mean radiant heat flux from the nine readings at 500 mm from the burner is 27.4 kW/m^2. The radiant heat flux distribution on the dummy sample is shown in Figure 4-13. The radiant heat flux at Point 10 during the experiment is 32.9 kW/m^2. This means that there is a 5.5 kW/m^2 difference between the two readings.

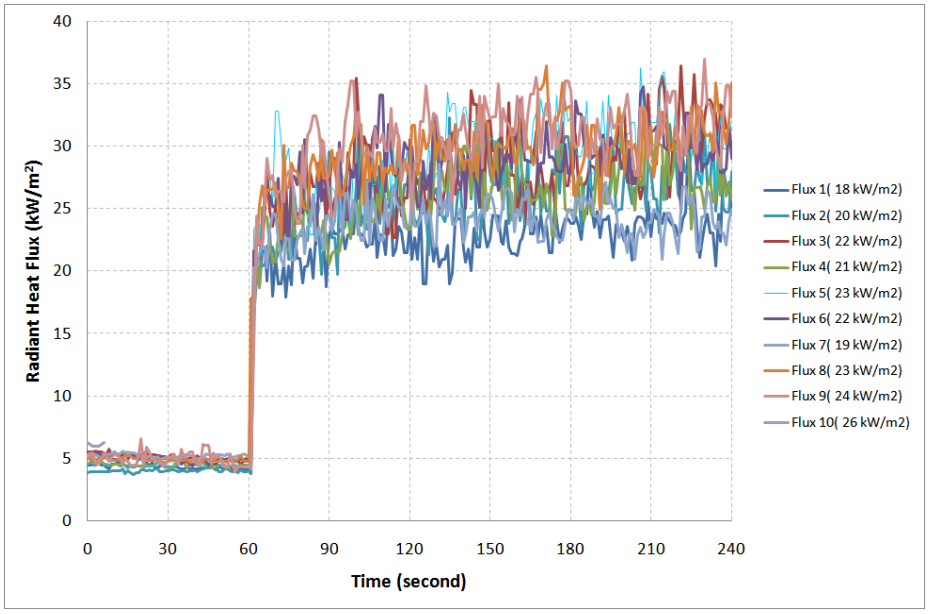

Figure 4-12: Radiant heat flux profiles from heat flux distribution test at 500 mm from burner

Table 4-2: Radiant heat flux at various points for distribution test at 500 mm from burner

Location of Heat Flux Gauge	Radiant Heat Flux (kW/m^2)
1	22.9
2	26.0
3	28.4
4	26.3
5	29.5
6	28.8
7	24.1

Table 4-2 **(con't)**

Location of Heat Flux Gauge	Radiant Heat Flux (kW/m^2)
8	29.8
9	30.9
10	32.9

Initially, 33 experiments were carried out with the glass samples positioned at 300 mm from the burner. The radiant heat flux difference between Point 10 and the glass sample was estimated by linear interpolating the radiant heat flux differences at 250 mm and 500 mm. The linear interpolation gave a radiant heat flux difference of 9.0 kW/m^2 between the experiments and distribution test.

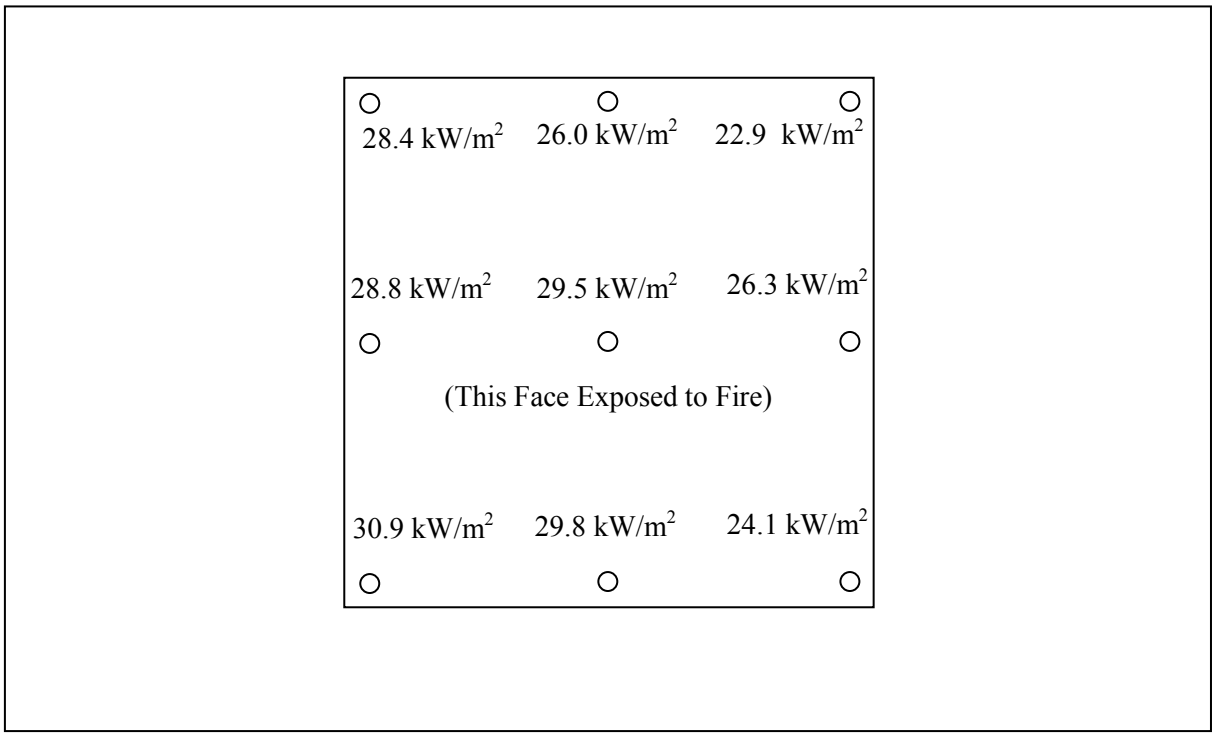

Figure 4-13: Distribution of radiant heat flux data at various points on the dummy sample at 500 mm from centre of burner

As the error between the radiant heat flux differences is in the order of 10%, it was deemed acceptable to reduce the radiant heat flux in each experiment by 9.9 kW/m^2. The reduced radiant heat fluxes are now known as actual radiant heat fluxes.

4.4.2 Radiant Heat Flux from Experiments

Figure 4-14 and Figure 4-15 show the radiant heat flux profile from experiments with samples 4 Test 1 and 6 Test 56 respectively. The two experiments represent the first and the last experiment samples subjected to radiant heat in this research.

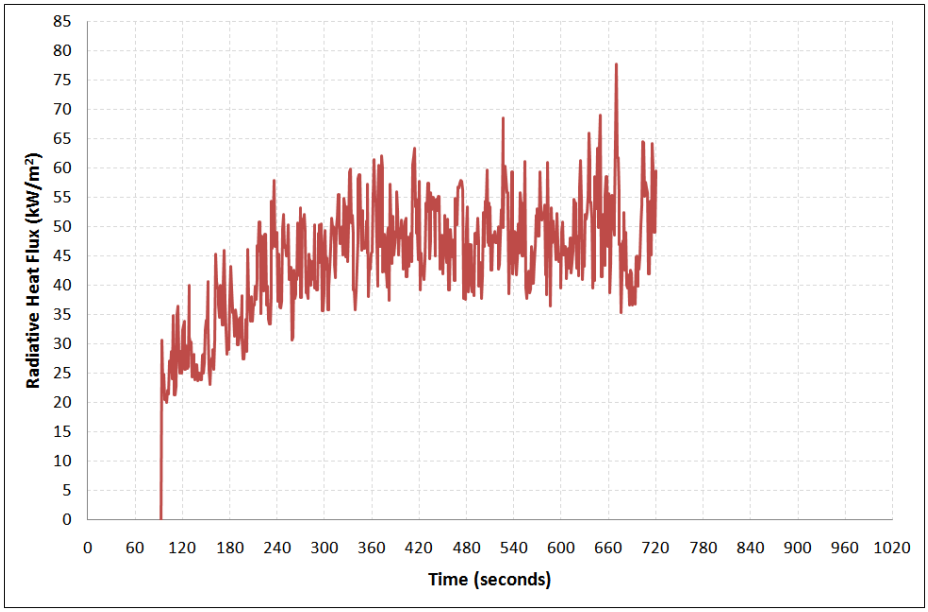

Figure 4-14: Radiant heat flux profile measured at Point 10 from experiment with sample 4 Test 1 (Cooling stage data not available)

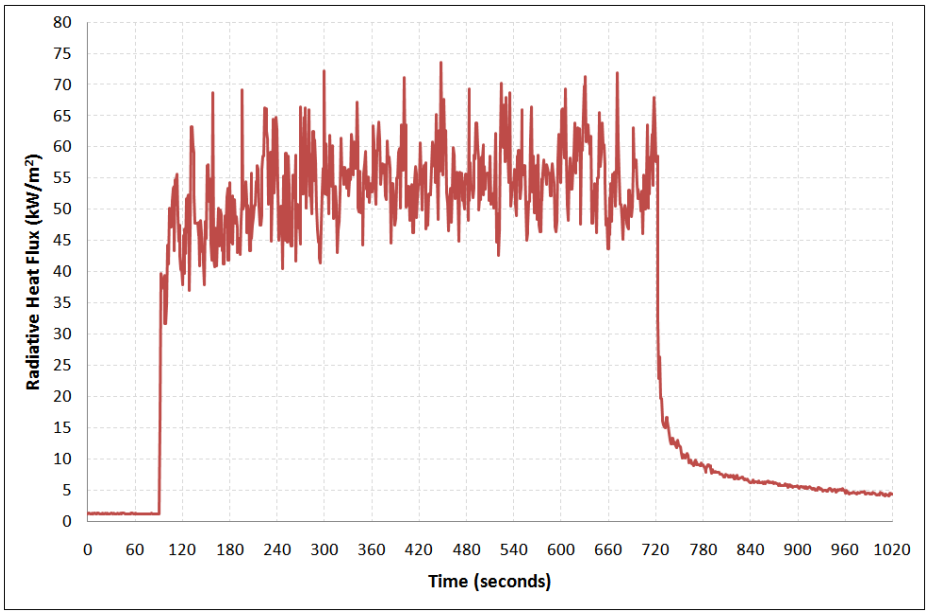

Figure 4-15: Radiant heat flux profile measured at Point 10 from experiment with sample 6 Test 56

The distribution of actual radiant heat fluxes for all the experiments is shown in Figure 4-16 which has the characteristic of a 3-parameter Weibull distribution. The actual radiant heat fluxes from the burner fire were between 13 kW/m^{2}and 58 kW/m^2. The average actual radiant heat flux is 40.2 kW/m^2 with a standard deviation of 7.4 kW/m^2. It is observed from Figure 4-16 that a majority of the experiment samples was subjected to actual heat fluxes ranging from 43 kW/m^2 to 47 kW/m^2.

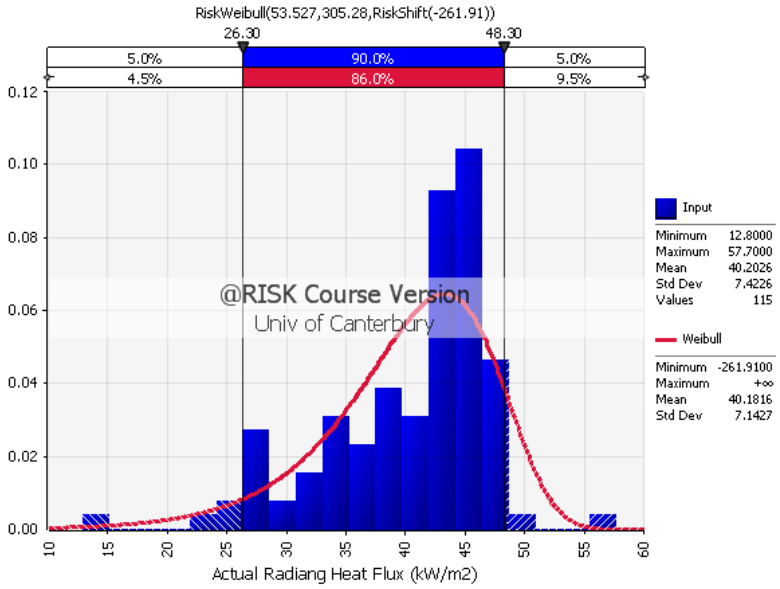

Figure 4-16: Distribution of actual radiant heat flux data for all experiments

4.5 Experimental Observations

4.5.1 General

All the glass samples fractured after being exposed to the burner fire in the experiments. Generally, fracture initiated from the edge of the glass and started propagating at an angle away from the edge. The cracks then bifurcated towards the other edges of the glass.

In the experiments with the glass samples glazed with rubber beading, the rubber beading started to smoulder and ignited at a gas reading of approximately 200 °C. The localised burning then spread towards the ends of the rubber beading. The burning of the rubber beading was limited to the edge where the burning of the rubber beading initiated. It was observed that once the rubber beading has cooled, the rubber beading formed a solid char residue that adhered to the glass panes and aluminium frame. The solid residue made the re-glazing task difficult, so in order to facilitate the removal of the char residue, the tested glass samples were removed immediately after each experiment. The cooling stage in each experiment allowed the residue to exist in a semi-solid state which allowed for easier removal.

In the experiments involving glass samples glazed with kaowool beading, the kaowool beading did not ignite and change from its original solid state.

The glass sample was observed to have stopped cracking approximately half-way into each experiment. The fallout behaviour was not observed in every experiment. Some cracked glass pieces remained in place within the frame after the experiments. Generally, fallout occurred when the bifurcating cracks joined together to form a closure although in some experiments the glass stayed in place even after the closure was formed. This situation was more apparent in 6 mm thick glass samples.

4.6 Time-Temperature History Curves

4.6.1 Glass Sample with Rubber Beading

Figure 4-17, Figure 4-18 and Figure 4-19 show the gas and glass temperature profiles from the experiment with sample 4 Test 2.

The glass sample from this experiment was glazed with rubber beading and had thermocouples attached. Figure 4-17, Figure 4-18 and Figure 4-19 show a steady state temperature profile prior to 90 seconds. After 90 seconds, the temperature profiles in Figure 4-17, Figure 4-18 and Figure 4-19 rose as the radiation shield was removed at 90 seconds which exposed the glass sample to the fire.

The rise in temperature continued until 720 seconds when the burner was turned off and the glass sample was left to cool for another 600 seconds before the experiment was terminated. The rise in temperature of the unshaded glass was slower than the rise in temperature of the gas while the shaded glass temperature rose much slower compared with the temperature of the unshaded glass. This scenario was also observed for the unexposed face of the glass.

Generally, the temperatures of the exposed face of the unshaded glass were higher than the temperatures of unexposed face of the unshaded glass. The difference between the temperatures of the shaded glass on the exposed face and unexposed face was small compared with the temperature differences between the unshaded glass on the exposed and unexposed face.

In Figure 4-17 and Figure 4-18, there was a sudden rise in temperature for thermocouples TC16 and TC17. The sudden rise was attributed to the ignition of the rubber beading. Thermocouple TC16 recorded more sudden rises compared with TC17. This situation occurred because TC16 was bare while TC17 was protected with a sealant, so TC16 was more sensitive to any temperature fluctuations. The sudden rise in temperature is considered a localised effect since the thermocouple was measuring the temperature at that particular point when the rubber is burning and the reading does not represent the temperature along the edge of the glass sample. Therefore, the thermocouple readings when the sudden rise in temperature occurred were ignored in the analysis.

The gas temperatures started to decay once the burner was turned off. The temperatures of the unshaded glass also started to decay albeit at a slower rate compared with the gas temperatures. The temperatures of the unshaded glass continued to increase after the burner was turned off but started to decay shortly after in a gradual manner compared with the temperatures of the unshaded glass.

There were more fluctuations in the gas thermocouple readings compared with the glass thermocouple readings due to the erratic behaviour of the fire. In some readings, the gas thermocouple readings were lower than the glass thermocouple readings. This may be due to the air circulation around the thermocouples as air was being drawn towards the fire and may have cooled the thermocouples as heat was constantly being lost.

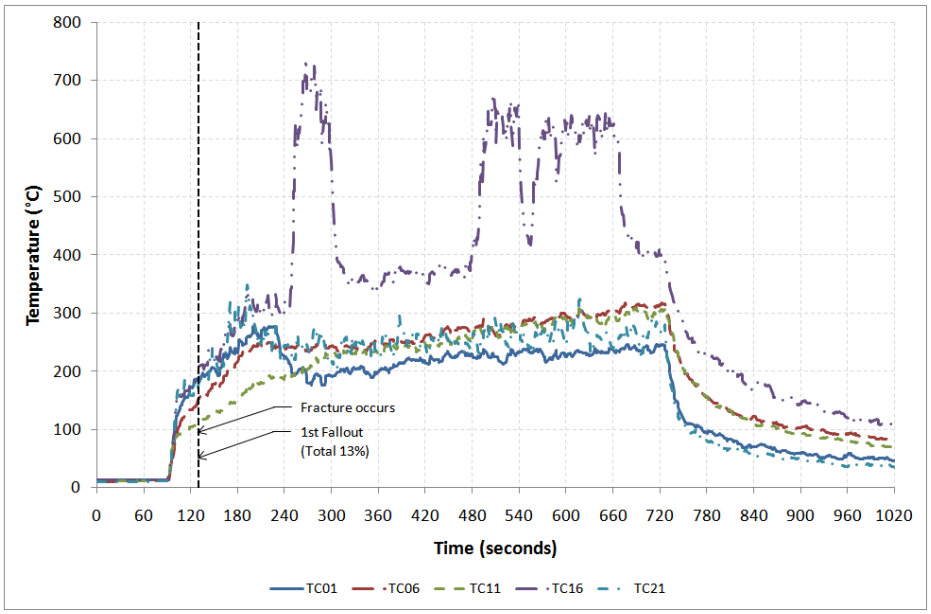

Figure 4-17: Gas temperature profiles for experiment with sample 4 Test 2

The maximum glass temperature recorded was 435 °C from thermocouple TC12 ignoring the sudden rise of temperature due to the burning of the rubber beading. The thermocouple TC08 in this experiment did not work so there were no data from this thermocouple.

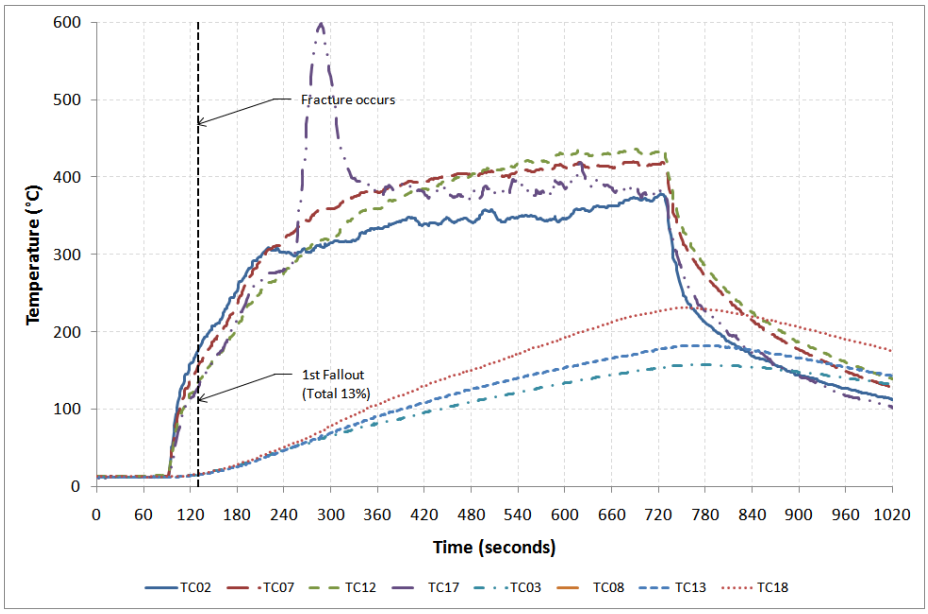

Figure 4-18: Glass temperature profiles at exposed face for experiment with sample 4 Test 2

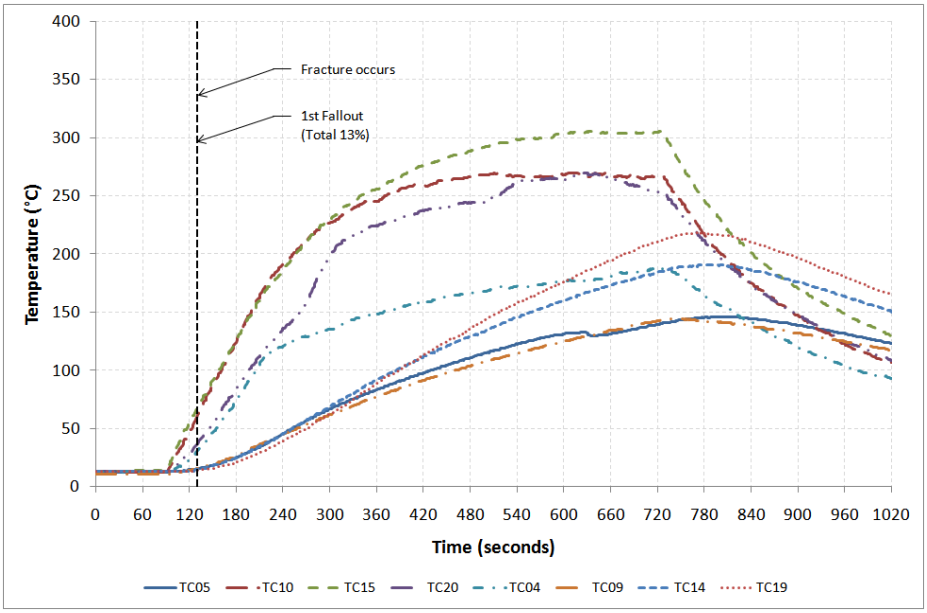

Figure 4-19: Glass temperature profiles at unexposed face for experiment with sample 4 Test 2

4.6.2 Glass Sample with Kaowool Beading

The temperature profiles of the gas and glass for the sample glazed with kaowool beading are shown in Figure 4-20, Figure 4-21 and Figure 4-22. The maximum glass temperature recorded was 364 °C from thermocouple TC02. The development of the temperature profiles during the experiment was similar to the development of the temperature profiles for the experiment using the sample glazed with rubber beading.

The only difference observed was that there was no sudden rise in temperatures due to the ignition of the rubber beading. As shown in Figure 4-20 for thermocouple TC11, there were occasions where the thermocouples might not be working properly. The data collected from these thermocouples were usually ignored in the analysis. These “spoiled” readings were obvious from the temperature profiles.

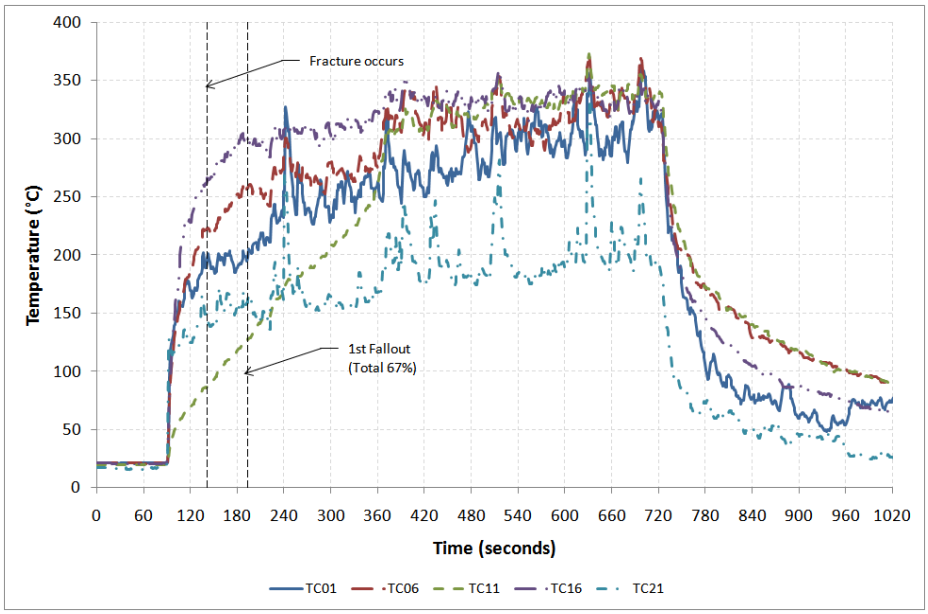

Figure 4-20: Gas temperature profiles for experiment with sample 4 Test 37

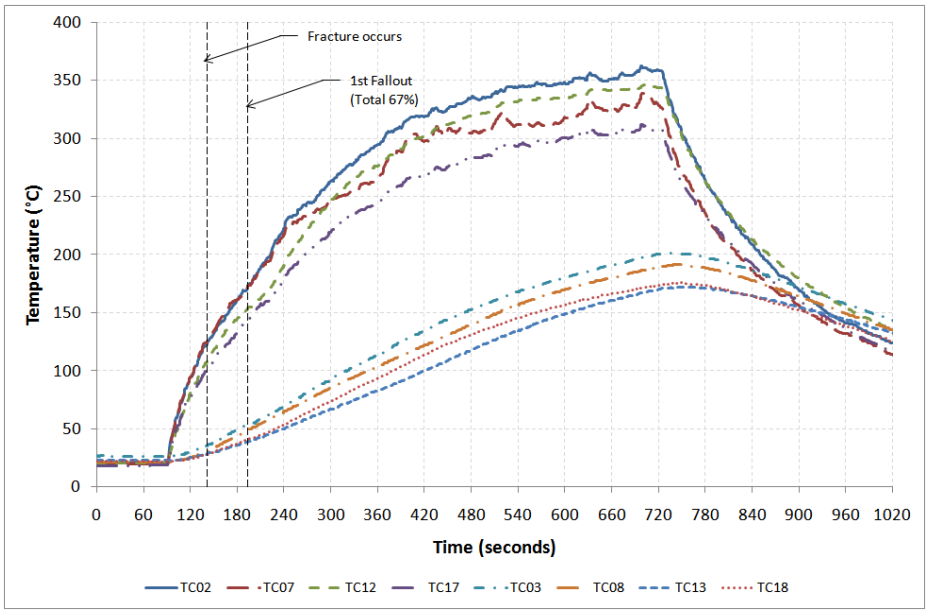

Figure 4-21: Glass temperature profiles at exposed face for experiment with sample 4 Test 37

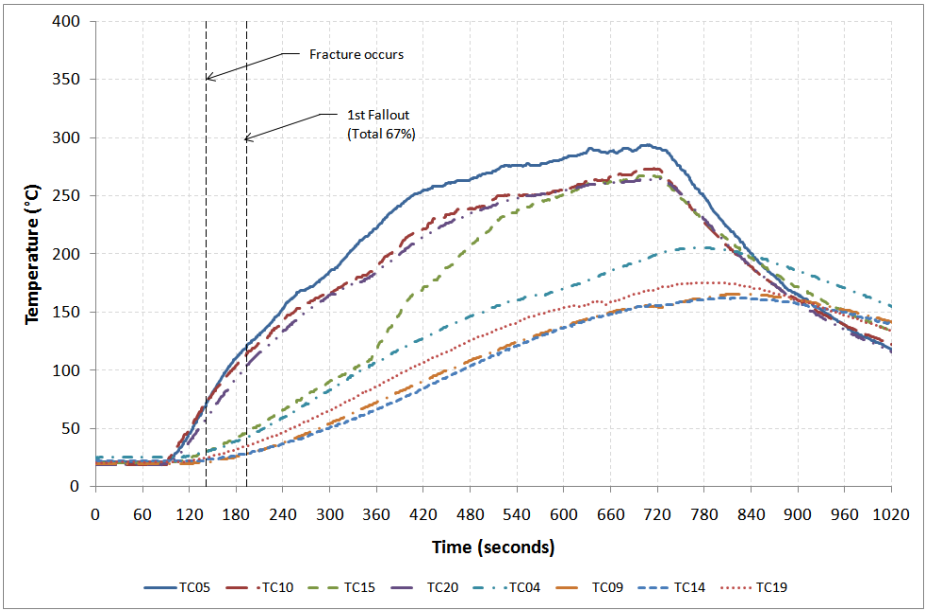

Figure 4-22: Glass temperature profiles at exposed face for experiment with sample 4 Test 37

4.7 Temperature Differences at Fracture and Fallout

In this research, three types of temperature differences were derived based on the work by Shields et al. (2001). The temperature differences are ΔT1 which is local exposed edge temperature difference, ΔT2 which is the local exposed centre temperature difference and ΔT3 which is the local bulk temperature difference. Each temperature difference was obtained by using the temperature readings as shown in Figure 4-23.

The temperature profiles from two experiments were plotted and discussed in this report. The temperature difference profiles for the remaining experiments were not provided in this report due to the space required to accommodate the plots.

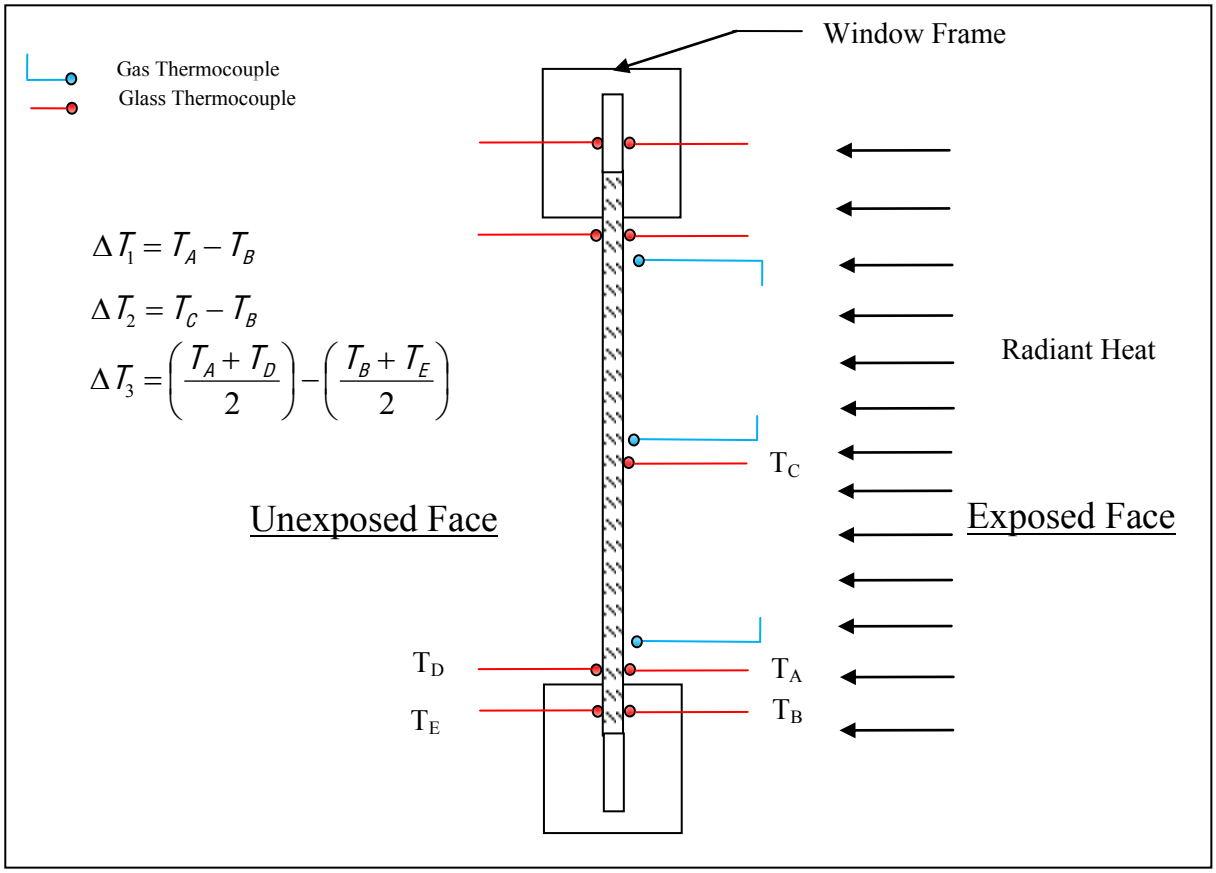

Figure 4-23: Simplified single glazing framing arrangement

Figure 4-24, Figure 4-25 and Figure 4-26 show the temperature difference profiles of ΔT1, ΔT2 and ΔT3 for the experiment with sample 4 Test 2. Each of the figures shows three plots instead of four since thermocouple TC08 which was on the left side of the sample facing the fire did not work and there were no data obtained from this thermocouple. At fracture time of 130 seconds, the maximum temperature differences ΔT1, ΔT2 and ΔT3 were 159 °C, 165 °C and 145 °C respectively. Approximately 13% of the exposed glass sample area fell out at 1 seconds after the glass has fractured. No further fallout was recorded during the experiment. The maximum temperature difference obtained from the profiles for temperature differences ΔT1, ΔT2 and ΔT3 were 280 °C, 312 °C and 360 °C respectively.

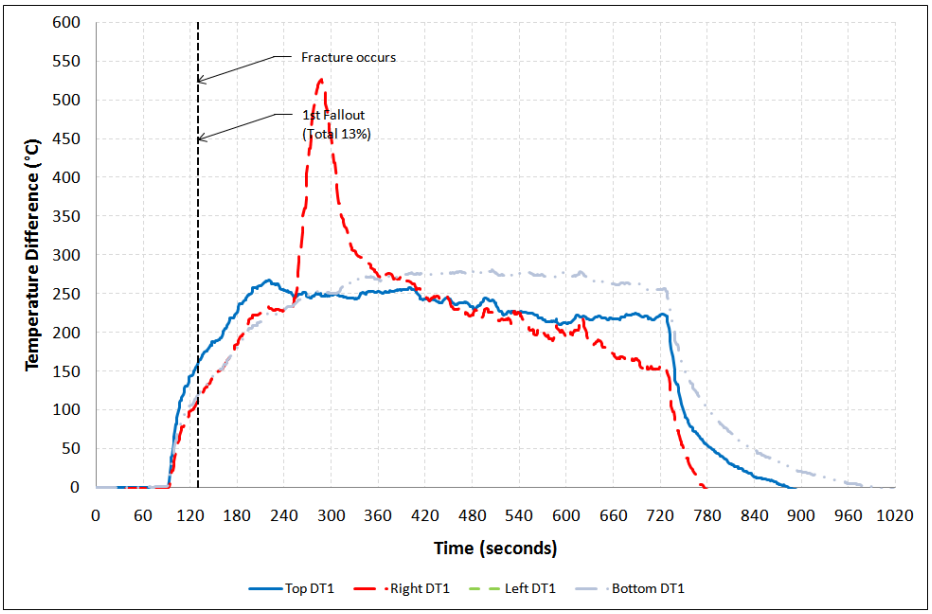

Figure 4-24: Temperature differences ΔT1 for experiment with sample 4 Test 2

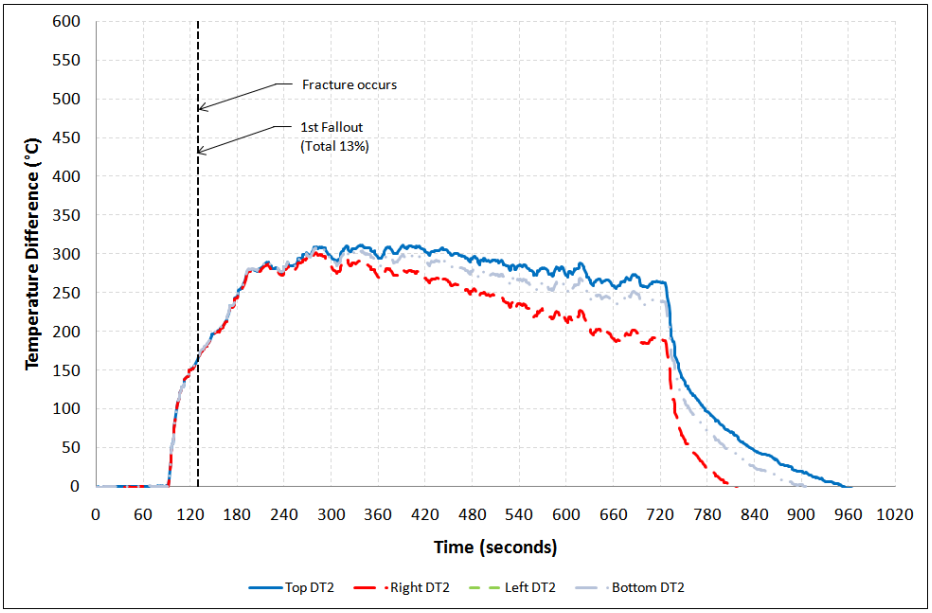

Figure 4-25: Temperature differences ΔT2 for experiment with sample 4 Test 2

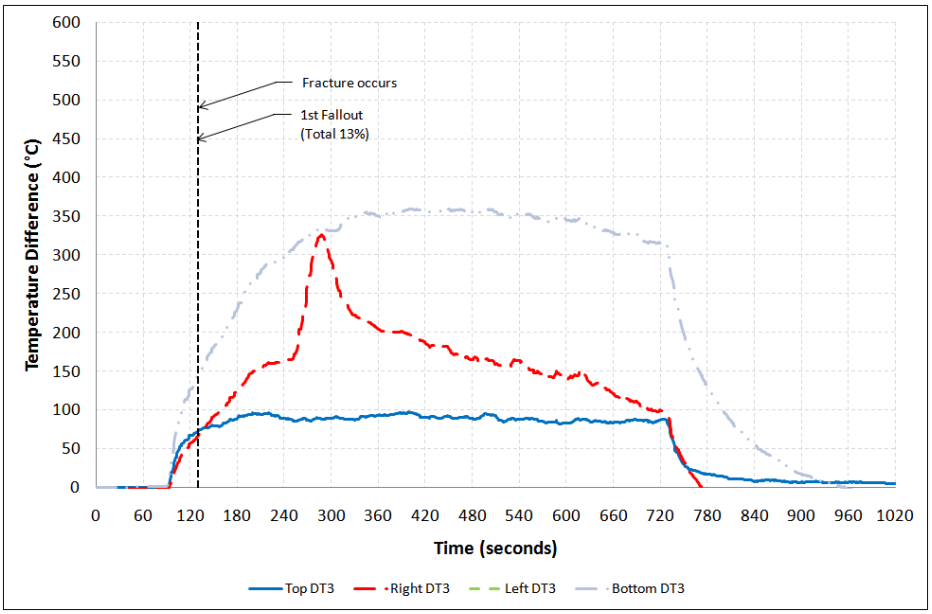

Figure 4-26: Temperature differences ΔT3 for experiment with sample 4 Test 2

Figure 4-27, Figure 4-28 and Figure 4-29 show the temperature difference profiles of ΔT1, ΔT2 and ΔT3 for the experiment with sample 4 Test 37. At fracture time of 149 seconds, the maximum temperature differences ΔT1, ΔT2 and ΔT3 are 100 °C, 131 °C and 79 °C respectively. At 193 seconds, 67% of the exposed glass sample area fell out. No further fallout was recorded during the heating stage of the experiment. The maximum temperature difference obtained from the profiles for temperature differences ΔT1 and ΔT3 were 206 °C and 159 °C respectively. The maximum temperature difference ΔT2 in the experiment was the same as the temperature difference at fracture since the piece of glass that fell out had the glass thermocouple which the data would be used to determine ΔT2 was attached to the piece of glass that fell out.

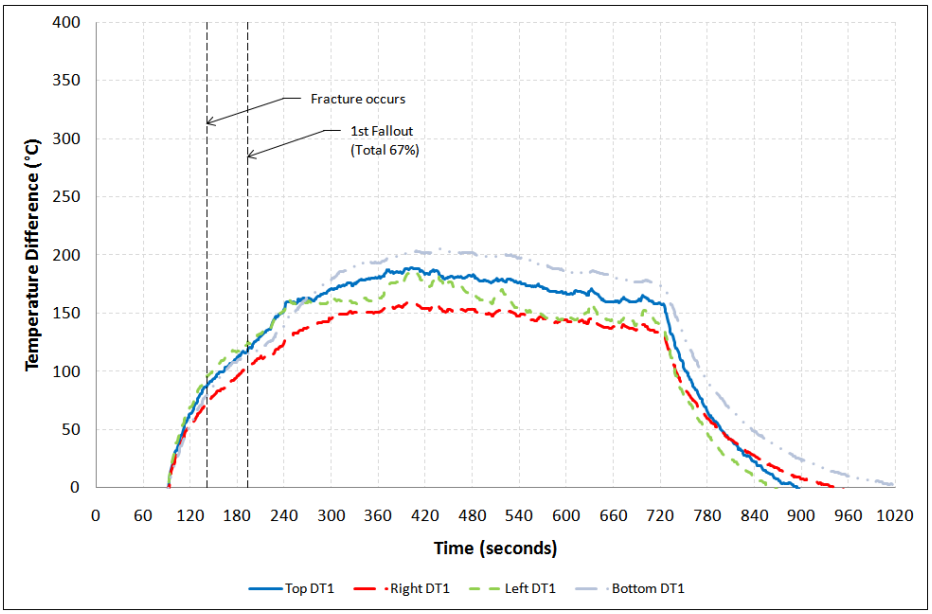

Figure 4-27: Temperature differences ΔT1 for experiment with sample 4 Test 37

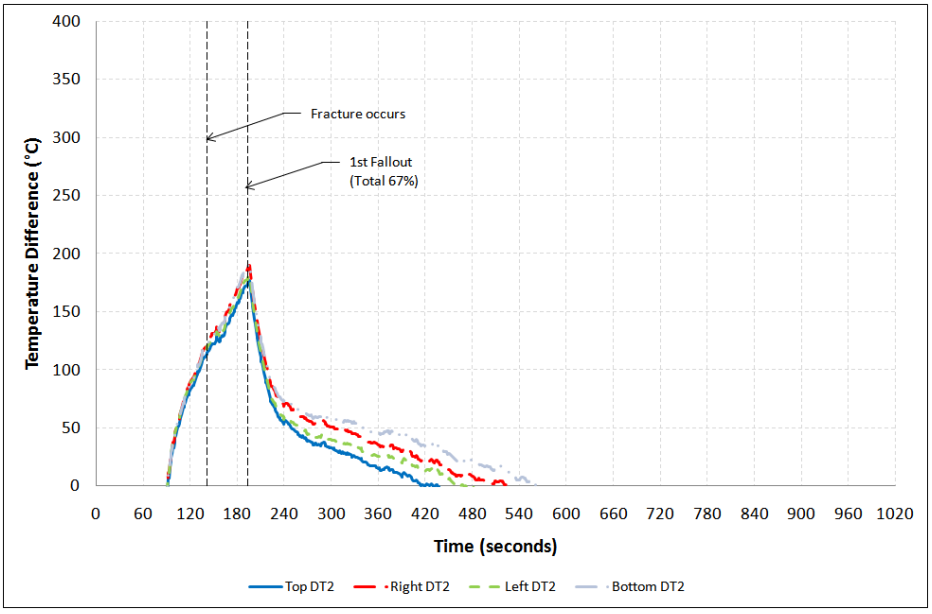

Figure 4-28: Temperature differences ΔT1 for experiment with sample 4 Test 37

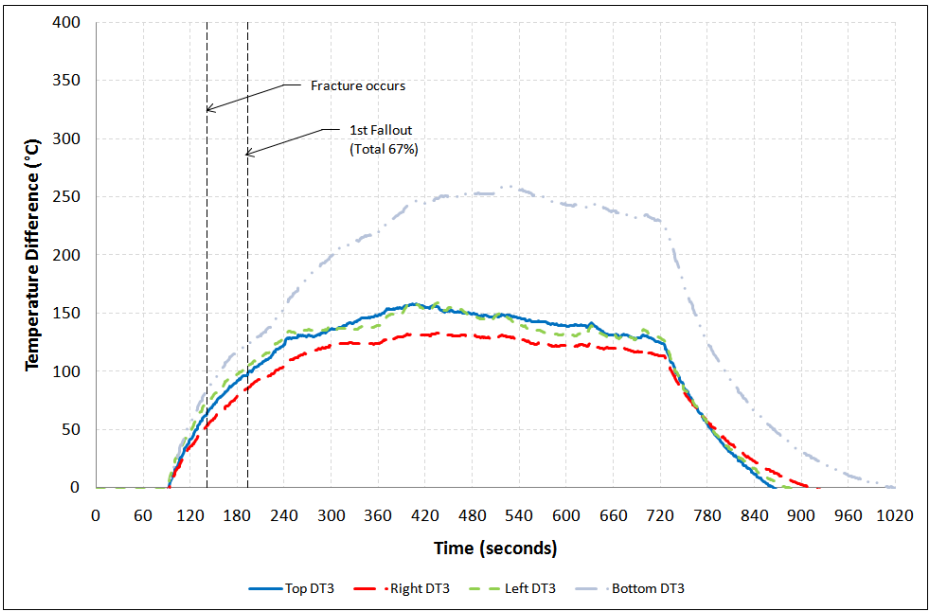

Figure 4-29: Temperature differences ΔT3 for experiment with sample 4 Test 37

The distributions of temperature differences ΔT1, ΔT2 and ΔT3 based on 4 mm and 6 mm thick glass samples are shown in Figure 4-30, Figure 4-31 and Figure 4-32. The mean temperature differences based on ΔT1, ΔT2 and ΔT3 were 98 °C ± 40 °C, 90 °C ± 43 °C, 92 °C ± 34 °C.

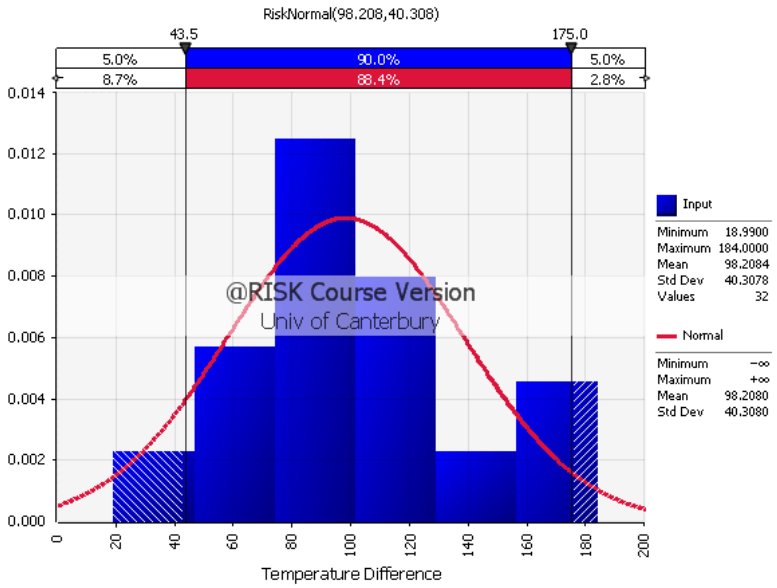

Figure 4-30: Distribution of temperature difference ΔT1 data based on experiments with 4 mm and 6 mm thick samples

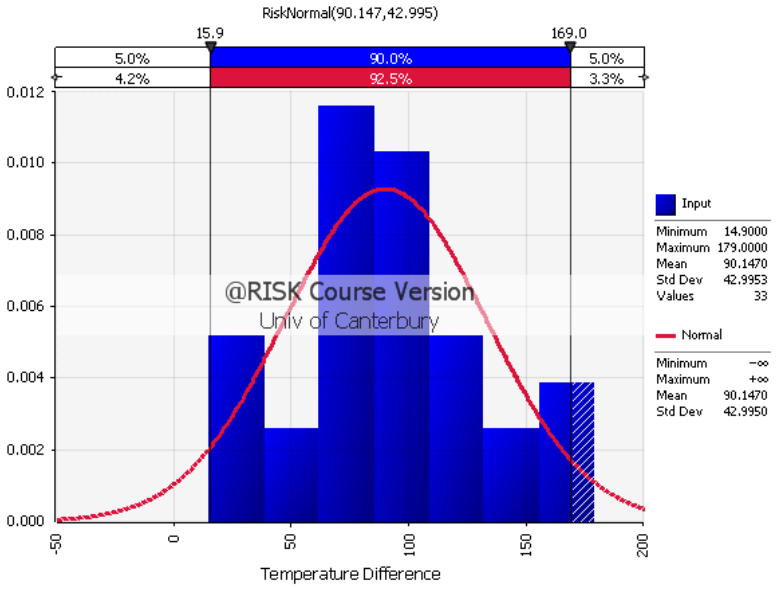

Figure 4-31: Distribution of temperature difference ΔT2 data based on experiments with 4 mm and 6 mm thick samples

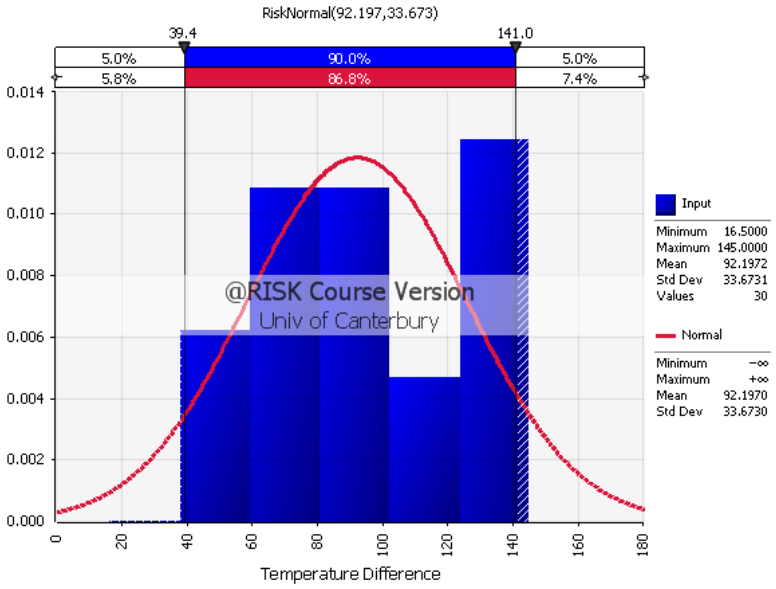

Figure 4-32: Distribution of temperature difference ΔT3 data based on experiments with 4 mm and 6 mm thick samples

The fracture temperature difference was obtained by re-arranging Equation (1) and replacing the terms T_∞ with T_{glass} and T_0 with T_{shade} to give,

$$T_{glass} - T_{shade} = \frac{\sigma_f}{E\beta} \tag{9}$$

A probabilistic simulation was carried out using Palisade @Risk to determine the distribution of temperature differences at fracture and sensitivity of the temperature difference to each input variable. The input variable distribution for each parameter is shown in Table 4-3. Figure 4-33 shows the generated distribution of temperature differences at fracture. Taking the range of temperature differences within the 5th and 95th percentile limits, the lower limit and upper limit of the predicted temperature difference at fracture is 55 °C and 129 °C. The predicted mean temperature difference at fracture is 89 °C.

Table 4-3: Input variable distributions for Palisade @Risk

Variable	Symbol	Distribution	Parameters	Reference
Fracture strength	σ_f	Weibull (3 parameter)	α = 2.56 β = 39.5 MPa Shift Factor = 28.9 MPa	Four-point bending test
Modulus of Elasticity	E	Normal	μ = 76.5 GPa σ = 4.0 GPa	Four-point bending test
Linear thermal expansion coefficient	β	Normal	μ = 9.5 x 10^{-6} /°C σ = 9.5 x 10^{-7} /°C	Parry (2002)

The output of the sensitivity analysis is shown in Figure 4-34. The figure shows that the most significant variable to determine the temperature difference at fracture is the fracture strength followed by the linear thermal expansion coefficient and modulus of elasticity.

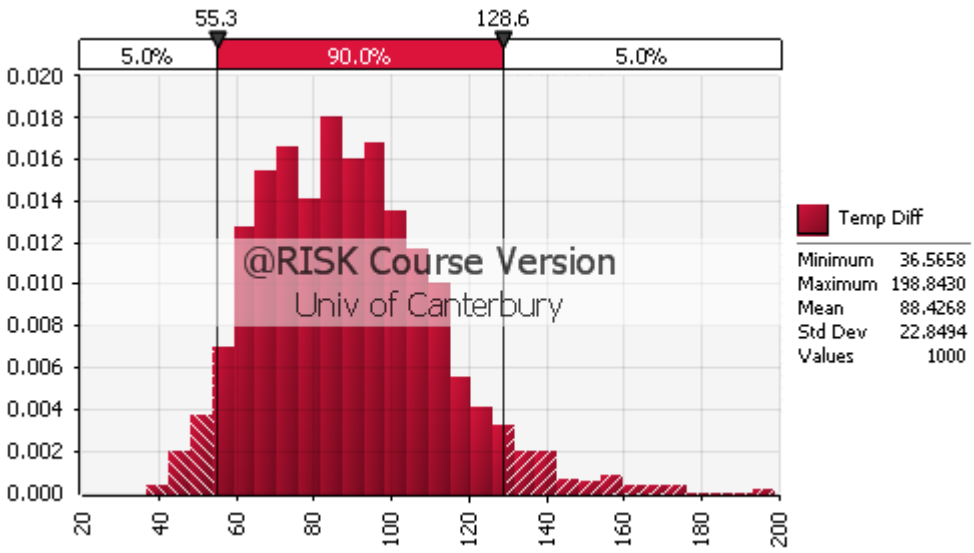

Figure 4-33: Probability distribution for temperature difference at fracture

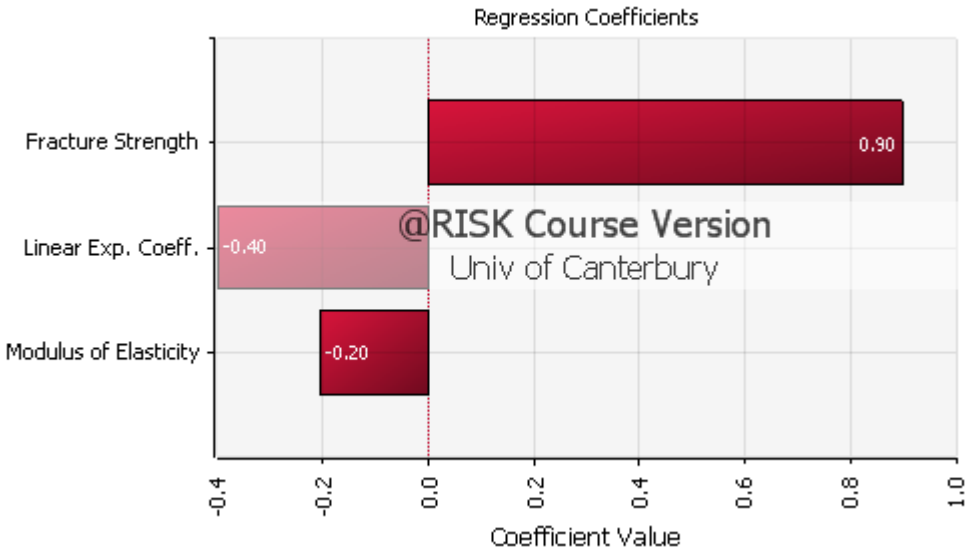

Figure 4-34: Sensitivity analysis for parameters used to determine temperature difference at fracture

Based on predicted temperature difference at fracture, the mean temperature difference, ΔT2 is the closest match followed by ΔT3 and ΔT1. However, the mean temperature difference, ΔT3 would be a more suitable criterion to use in order to model the glass fracture as the spread in the temperature difference data is less than that of ΔT2.

Theoretically, if the temperature at the centre of the glass pane is assumed to be the same as the temperature of the edge of the glass, ΔT1 would be equal to ΔT2. This assumption is valid if the applied heat flux on the glass pane is assumed to be uniform. Both temperature differences are a function of the temperatures of the exposed glass. However, the temperature difference ΔT3 is a function on the temperatures of the exposed and unexposed glass. In short, for simple computer application, ΔT1 and ΔT2 would suffice because the heat conduction through the thickness of the glass would not need to be determined.

4.8 Thermal Strains

A total of 10 experiments were fitted with strain gauges to measure the thermal strains induced in the glass during the experiments. Figure 4-35 show the thermal strain profiles for experiment with sample 4 Test 60. The thermal strain profiles for the remaining 9 experiments are available in Appendix D.

Prior to the fracture of the glass sample, the thermal strains increased linearly and once the glass fractured, the strains dropped suddenly as the glass relaxes due to the release of the thermal stresses within the glass. The strain profiles after the glass has fracture was disregarded as further heating of the glass sample will expose the strain gauges to temperatures higher than its maximum operating temperature of 80 °C and the readings were deemed unusable.

Table 4-4 show the summary of the thermal strains at fracture for the 10 experiments. From the table, the thermal strains at fracture range from 239 μstrain to 697 μstrain. The amount of thermal strain induced in a piece of glass pane appears to be independent of the type of beading. The thermal strains at fracture recorded in this research are similar in order of magnitude to the range of thermal strains at fracture reported by Pagni and Joshi (1991a) shown in Table 2-1.

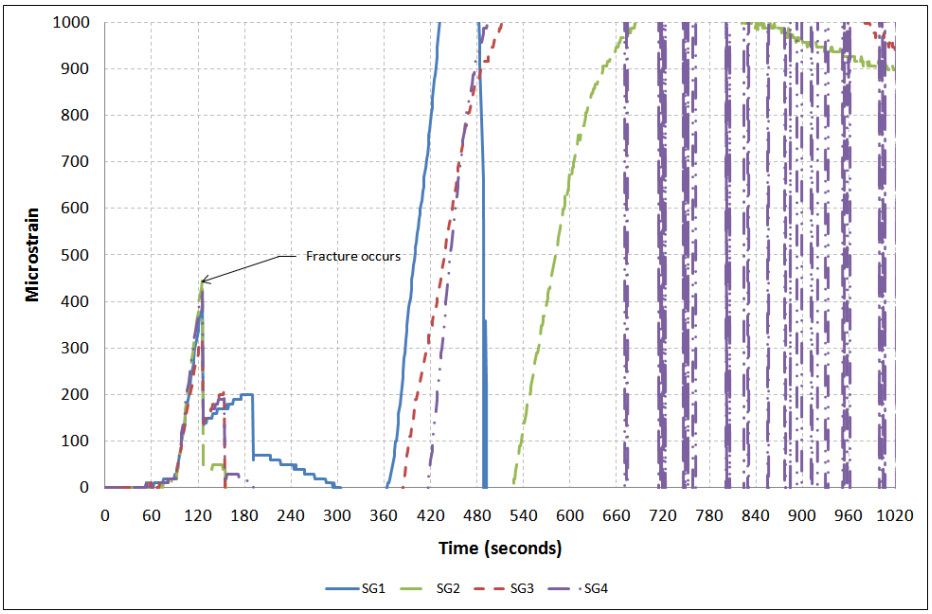

Figure 4-35: Thermal strain profiles for experiment with sample 4 Test 60

Table 4-4: Summary of thermal strains at glass fracture

Experiment sample	Type of Beading	Thermocouple Attachment	Strain at SG1 (µstrain)	Strain at SG2 (µstrain)	Strain at SG3 (µstrain)	Strain at SG4 (µstrain)
4 Test 60	Kaowool	No	399	448*	319	428
4 Test 61	Kaowool	Yes	349	697*	598	478
4 Test 62	Rubber	No	349	408*	369	339
4 Test 63	Kaowool	No	389*	339	169	249
4 Test 64	Rubber	Yes	379	428	488*	N/A
6 Test 47	Kaowool	Yes	209	239*	209	169
6 Test 48	Kaowool	No	319	379*	349	299
6 Test 49	Kaowool	No	209	N/A	289*	269
6 Test 50	Rubber	No	399	498*	130	399
6 Test 52	Rubber	Yes	528	618	658*	428
*Maximum value, N/A – Not Available						

4.9 Glass Fallout Time Histories

Figure 4-36 to Figure 4-39 show the crack pattern and fallout on some of the experiment samples that displayed fallout behaviour. All fallouts reported occurred during the heating stage of the experiments unless notified otherwise. The photos and some sketches of the crack patterns are available in Appendix G. The amount of glass fallout was estimated using 50 mm x 50 mm grids drawn on the glass sample prior to each experiment. There were 100 grids within the exposed area of the glass. Therefore, the amount of glass fallout corresponded to the number grids where fallout has occurred. It should be noted that glass fallout did not occur in all experiments. Generally, glass fallout occurred at some time after the glass has fractured.

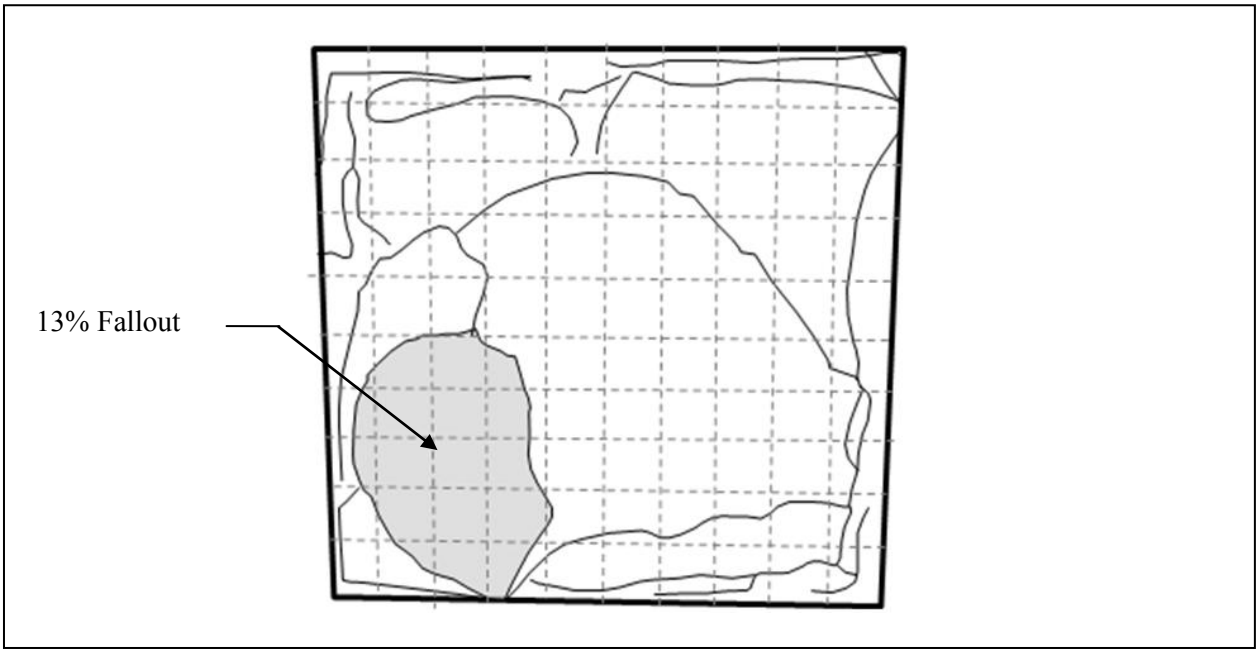

Figure 4-36: Crack pattern and amount of fallout for experiment with sample 4 Test 2 (4 mm thick glass sample glazed with rubber beading and has thermocouples attached)

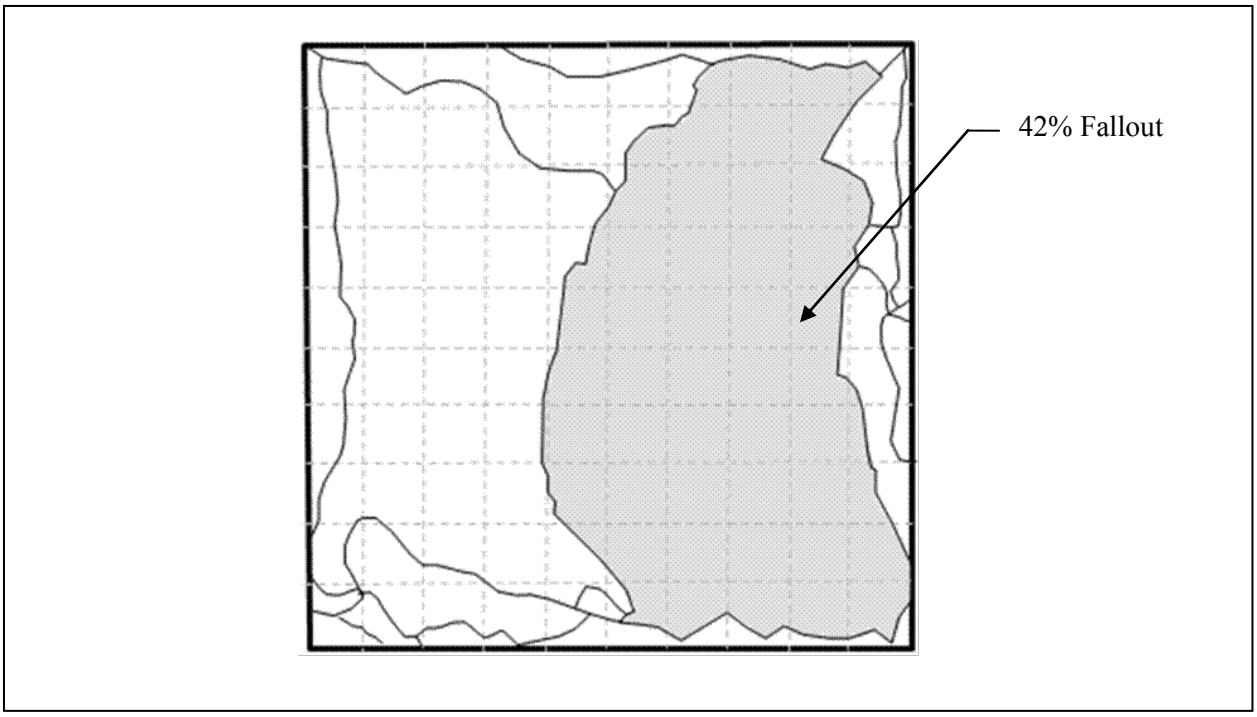

Figure 4-37: Crack pattern and amount of fallout for experiment with sample 4 Test 17 (4 mm thick glass sample glazed with kaowool beading and has no thermocouples attached)

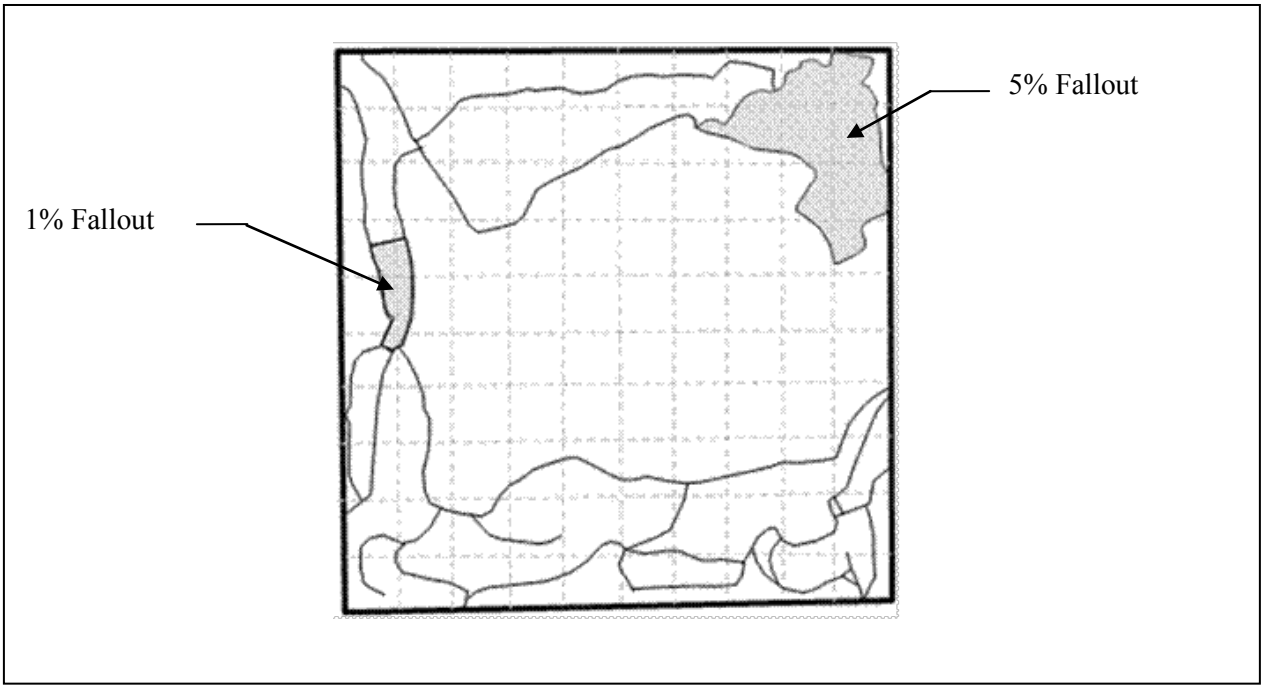

Figure 4-38: Crack pattern and amount of fallout for experiment with sample 6 Test 33 (6 mm thick glass sample glazed with kaowool beading and has thermocouples attached)

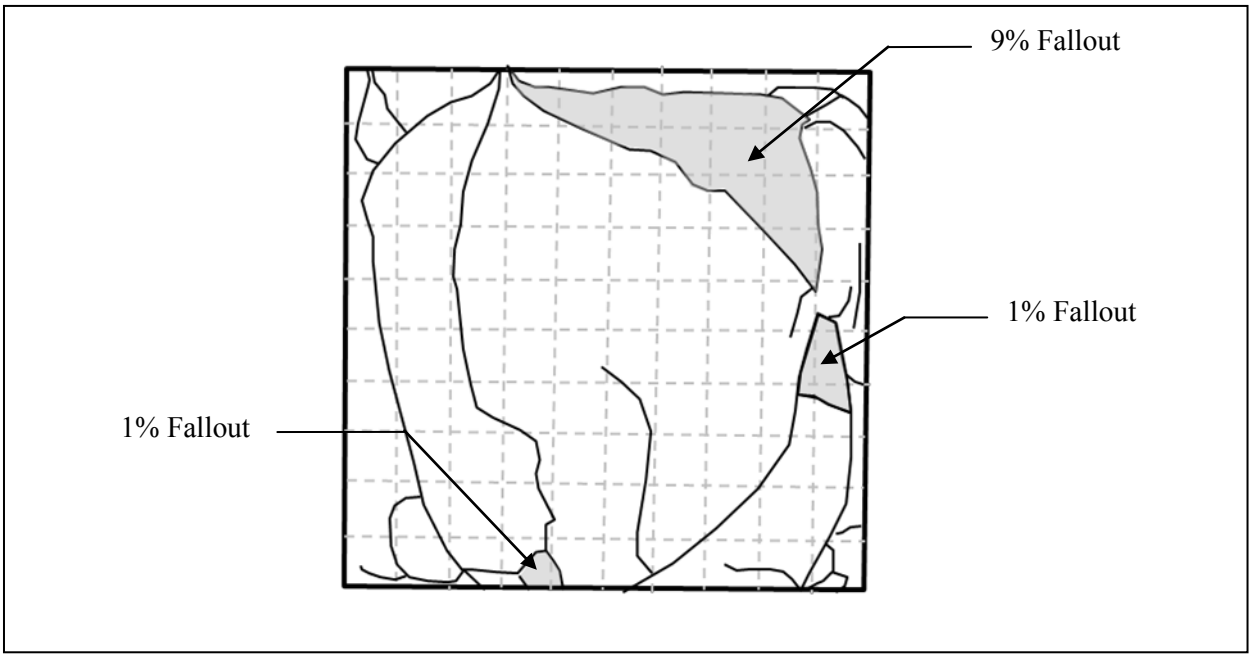

Figure 4-39: Crack pattern and amount of fallout for experiment with sample 6 Test 53 (6 mm thick glass sample glazed with rubber and has no thermocouples attached)

In order for glass to fall out, fracture has to occur. During the experiments, some glass fallout occurred immediately after fracture while most occurred at some time after fracture has taken place. Figure 4-40 to Figure 4-47 show the glass fallout time histories for all the experiments that displayed fallout behaviour. Based on the glass fallout time histories, the glass fallout occurrence was random with the 4 mm thick glass samples displaying more glass fallout occurrence compared with the 6 mm thick glass samples.

In the experiments with thermocouples attached onto the glass samples glazed with rubber beading, fallouts were recorded in 3 out of 9 experiments involving the 4 mm thick glass samples while fallouts were recorded in 4 out of 8 experiments involving the 6 mm thick glass samples.

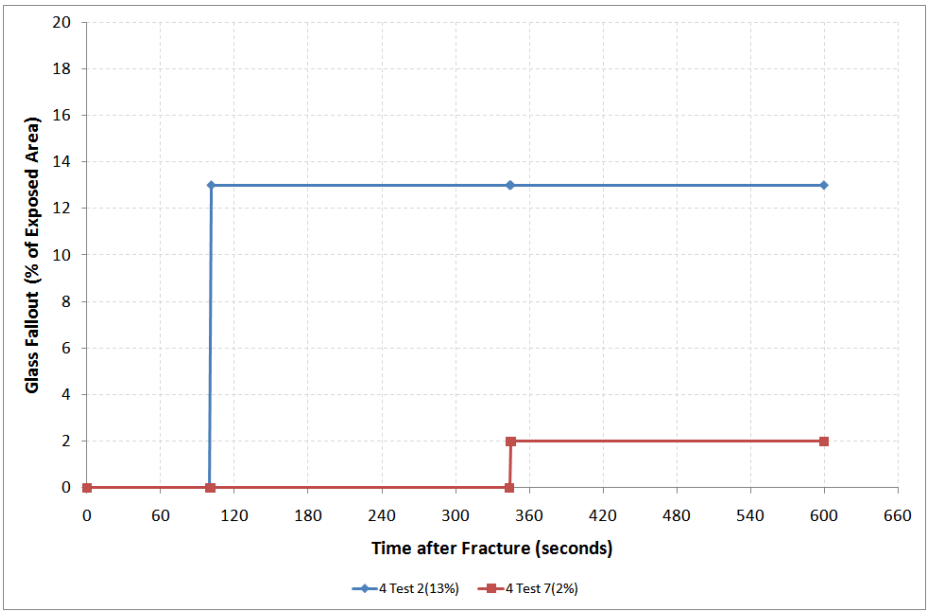

Figure 4-40: Glass fallout time histories for 4 mm thick samples glazed with rubber beading and have thermocouples attached (Fallout history of experiment sample 4 Test 57 not available)

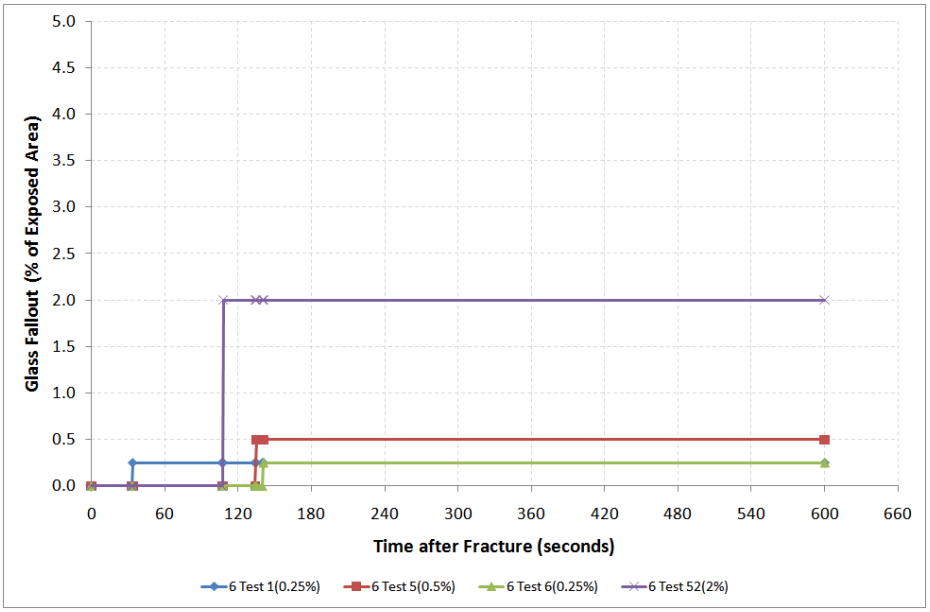

Figure 4-41: Glass fallout time histories for 6 mm thick samples glazed with rubber beading and have thermocouples attached

In the experiments with no thermocouples attached onto the glass samples glazed with rubber beading, fallouts were recorded in 12 out of 15 experiments involving the 4 mm thick glass samples while fallout was recorded in 1 experiment out of 10 experiments involving the 6 mm thick glass samples.

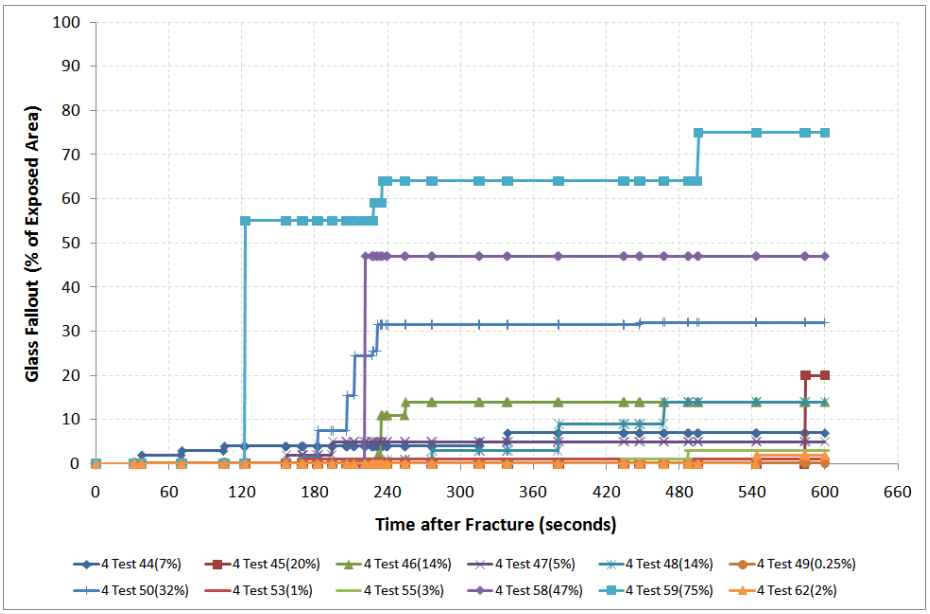

Figure 4-42: Glass fallout time histories for 4 mm thick samples glazed with rubber beading and have no thermocouples attached

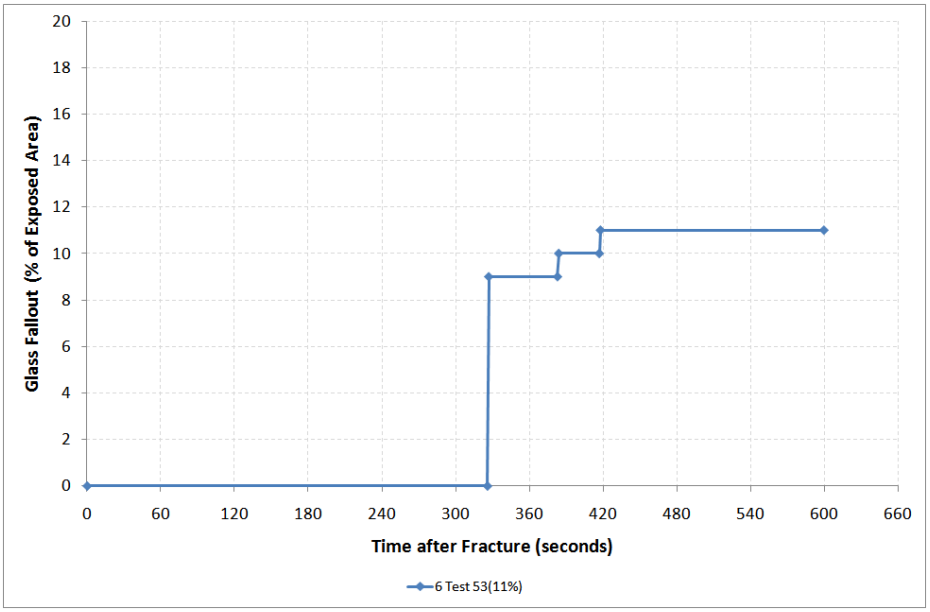

Figure 4-43: Glass fallout time history for 6 mm thick samples glazed with rubber beadings and have no thermocouples attached

In the experiments with thermocouples attached onto the glass samples glazed with kaowool beading, fallouts were recorded in 8 out of 12 experiments involving the 4mm thick glass samples while fallouts were recorded in 3 out of 7 experiments involving the 6 mm thick glass samples.

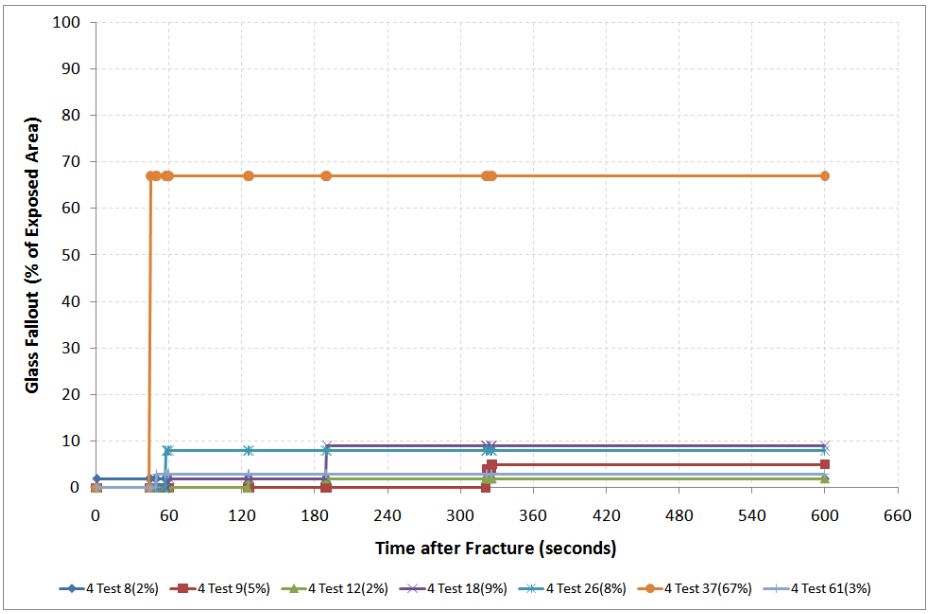

Figure 4-44: Glass fallout time histories for 4 mm thick samples glazed with kaowool beading and have thermocouples attached (Fallout history of experiment sample 4 Test 28 not recorded)

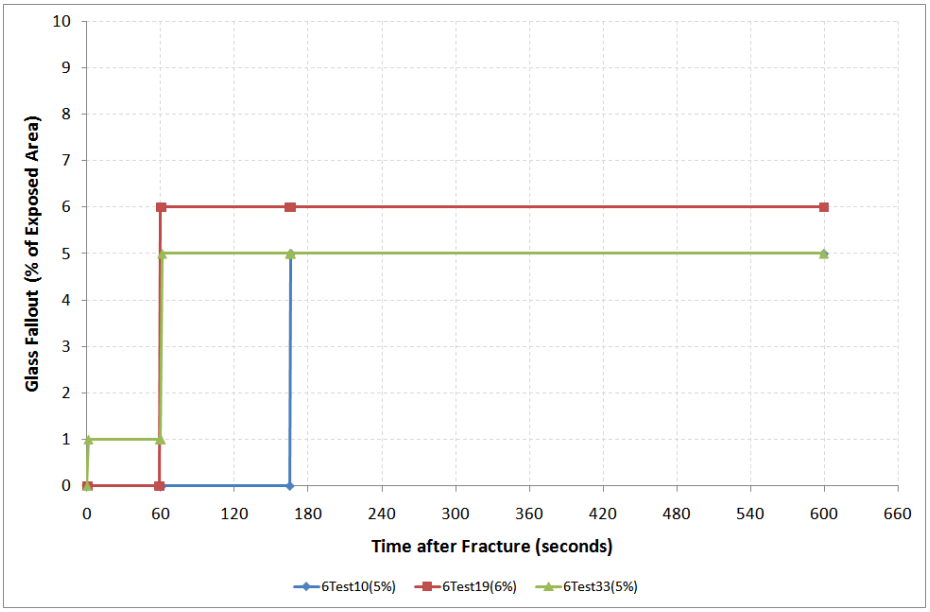

Figure 4-45: Glass fallout time histories for 6 mm thick samples glazed with kaowool beading and have thermocouples attached

In the experiments with no thermocouples attached onto the glass samples glazed with kaowool beading, fallouts were recorded in 25 out of 27 experiments involving the 4 mm thick glass samples while fallouts were recorded in 13 out of 29 experiments involving the 6 mm thick glass samples.

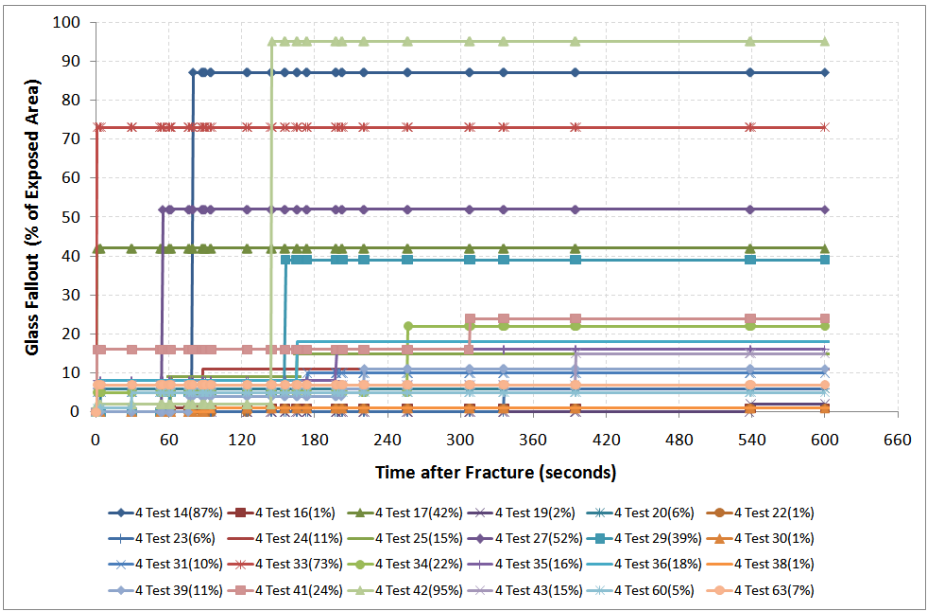

Figure 4-46: Glass fallout time histories for 4 mm thick samples glaze with kaowool beading and have no thermocouples attached (Fallout history of experiment sample 4 Test 32 not recorded)

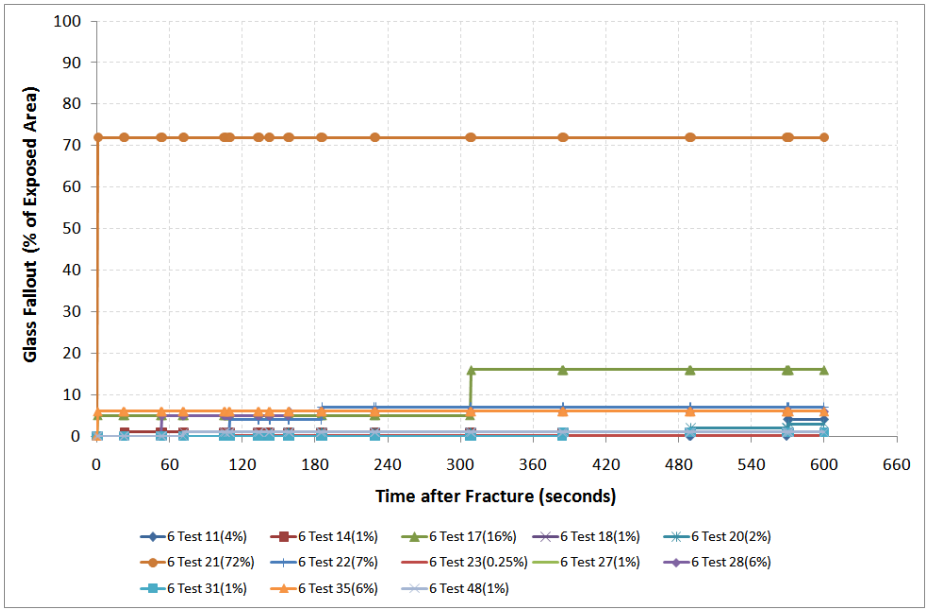

Figure 4-47: Glass fallout time histories for 6 mm thick samples glazed with kaowool beading and have no thermocouples attached

4.10 Time to Glass Fracture

Figure 4-48 and Figure 4-49 show the distribution of times to fracture for the 4 mm and 6 mm thick glass samples. The mean times to fracture are 38 seconds and 46 seconds for the 4 mm and 6 mm thick glass

samples respectively. The glass fallout histories are plotted from the time the glass samples fracture in the experiments. The heating stage in all of the experiments lasted for 630 seconds. Based on the mean times to fracture, the glass fallout histories are plotted to up to an arbitrarily chosen 600 seconds.

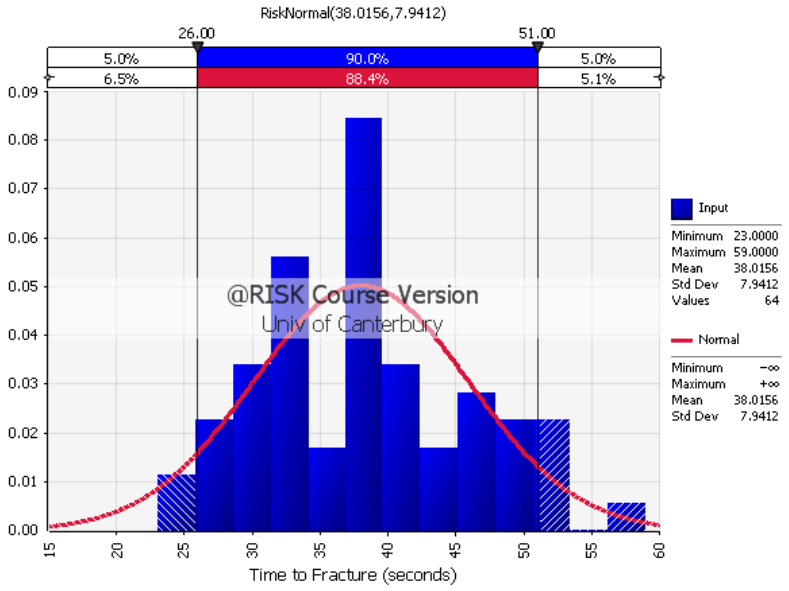

Figure 4-48: Distribution of times to fracture data for 4 mm thick glass samples

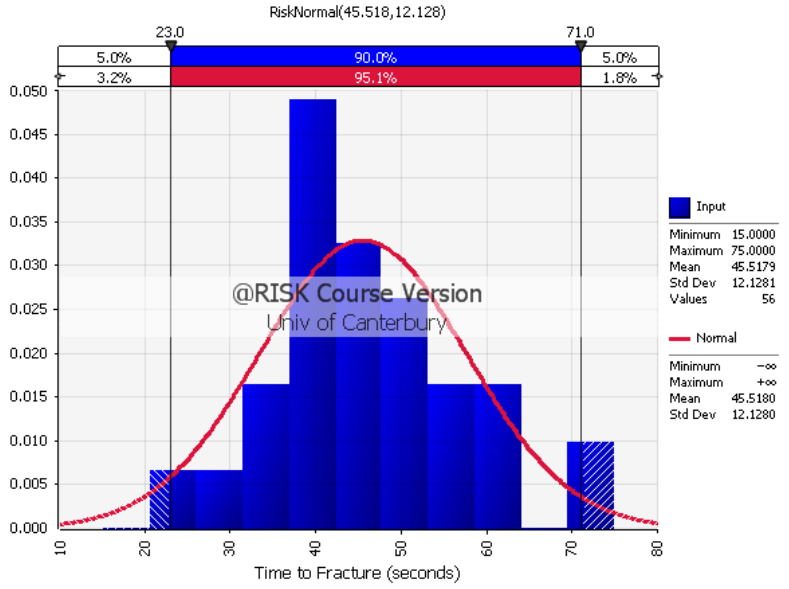

Figure 4-49: Distribution of times to fracture data for 6 mm thick glass samples

The time for a heated glass to fracture can be predicted either using lumped heat capacity model or heat transfer modelling using the fracture criteria.

4.10.1 Prediction of Time to Glass Fracture based on Lumped Heat Capacity Model

The time to fracture based on the lumped heat capacity model is given as,

$$t = \frac{\delta \rho c_p}{h} \ln\left[\frac{\dot{q}''}{\dot{q}'' - \dot{q}''_{crit}}\right] \tag{10}$$

The derivation of Equation (10) can be found in Appendix K. This simple lumped heat capacity model assumes that the applied heat flux is constant and the temperature gradient across the thickness of the glass is small. When comparing the temperature gradients between the 4 mm and 6 mm thick glass, the 6 mm will intuitively have a steeper temperature gradient. This assumption can be verified using the Biot number.

The Biot number is given as,

$$Bi = \frac{hL_c}{k} \tag{11}$$

When the Biot number is less than 0.1, it means that heat is conducted faster inside the body than the heat convection away from the surface of the body so the temperature gradient within the body can be neglected.

According to Equation (6) in Keski-Rahkoken (1988), the characteristic length, L_c is taken as the thickness of the glass pane.

Sincaglia and Barnett (1997) provided a simplified correlation to estimate the convective heat transfer coefficient which is a function of the temperature of the fire environment and velocity of the hot gases. The correlation is as follows,

$$h = h_{\min} + (h_{\min} - h_{\max})\frac{(T_u - 300)}{100} \tag{12}$$

where h_{min} = 5 W/m^2.K and h_{max} is 50 W/m^2.K

The summary of critical heat fluxes for glass fracture from various researches is shown in Table 4-5.

Table 4-5: Summary of critical heat flux for ordinary float glass from various researches

$\dot{q}''_{crit}$ (kW/m^2)	Reference	Glass Thickness used in Research
4 - 5	Mowrer (1997)	Not mentioned
3	Shields et al. (2002)	6 mm
5	Harada et al. (2000)	3 mm

The convective heat transfer coefficient was estimated using the relationship $\dot{q}''_{crit} = h(T_\infty - T_{glass})$ for convective heat transfer. The temperature difference, $T_\infty - T_{glass}$ was taken as the temperature difference at fracture for simplicity. The temperature difference at fracture was taken as 93 °C or 93 K as this was the average temperature difference determined from the experiments as shown in Table 4-6. The average temperature was based on the average thermocouple readings.

Table 4-6: Summary of temperature difference for convective heat transfer in experiments

Experiment sample	Average gas temperature at fracture (°C)	Average glass temperature at fracture on exposed face (°C)	Average Temperature difference at fracture (°C)
4 Test1	126	113	13
4 Test 2	163	155	8
4 Test 3	166	117	49
4 Test 5	236	169	67
4 Test 6	178	132	46
4 Test 7	240	95	145
4 Test 8	296	131	164

Table 4-6 **(con't)**

Experiment sample	Average gas temperature at fracture (°C)	Average glass temperature at fracture on exposed face (°C)	Average Temperature difference at fracture (°C)
4 Test 9	200	49	151
4 Test 10	258	132	126
4 Test 11	236	32	203
4 Test 12	268	78	190
4 Test 13	292	56	236
4 Test 18	279	70	208
4 Test 21	250	120	130
4 Test 26	192	141	52
4 Test 28	158	78	80
4 Test 37	183	121	61
4 Test 52	132	97	34
4 Test 57	109	89	20
4 Test 61	170	80	90
4 Test 64	138	75	63
6 Test 3	234	139	95
6 Test 4	151	137	14
6 Test 5	191	94	97
6 Test 6	247	129	118
6 Test 7	178	93	85
6Test 8	216	177	39
6 Test 9	249	95	154

Table 4-6 **(con't)**

Experiment sample	Average gas temperature at fracture (°C)	Average glass temperature at fracture on exposed face (°C)	Average Temperature difference at fracture (°C)
6 Test 10	235	106	130
6 Test 29	173	98	74
6 Test 33	178	108	70
6 Test 42	140	107	33
6 Test 47	147	103	43
6 Test 52	150	74	76
Average	199	106	93
Note: Temperature difference data from experiment samples 6 Test 1 and 6 Test 19 not available.			

At $\dot{q}''_{crit}$ = 3 kW/m^2, h = 0.032 kW/m^2.K or 32 /m^2.K

At $\dot{q}''_{crit}$ = 5 kW/m^2, h = 0.054 W/m^2.K or 54 /m^2.K

Based on the lower and upper limit of the convective heat transfer coefficient proposed by Singcalia et al. (1997), a range between 30 kW/m^2.K and 50 kW/m^2.K was chosen.

The thermal conductivity of glass is taken as 0.76 W/m.K based on the recommended value by Parry (2002).

Table 4-7 shows a summary of the Biot numbers calculated for the 4 mm and 6 mm thick glass samples using the convective heat coefficients determined earlier. The calculated Biot numbers confirms that the application of the lumped heat capacity model is less accurate for thicker glass since the Biot number for a 6 mm thick glass is greater compared with the Biot number for a 4 mm thick glass given the same heat transfer coefficient.

From the table, it can be seen that the Biot numbers exceeded 0.1 which means a temperature gradient exist across the thickness of the glass pane. This raises the question whether the lumped heat capacity model is suitable to be used to predict the time to glass fracture.

Table 4-7: Biot numbers calculated for 4 mm and 6 mm thick glass samples using convective heat coefficients of 30 W/m^2.K and 50 W/m^2.K

Glass Thickness mm	h W/m^2.K	L_c m	k W/m.K	Bi
4	30	0.004	0.76	0.16
4	50	0.004	0.76	0.26
6	30	0.006	0.76	0.24
6	50	0.006	0.76	0.39

Figure 4-50 and Figure 4-51 show the comparison between the actual time and predicted time using the lumped heat capacity model to fracture for the 4 mm and 6 mm thick glass samples.

The figures show that the actual times to fracture for the 6 mm thick glass samples are more scattered than the actual times to fracture for the 4 mm thick glass which was expected. Although the glass were not uniformly heated across its thickness as discussed and shown earlier using the Biot number, the lumped heat capacity model is still a simple tool that could be used to predict the time to glass fracture.

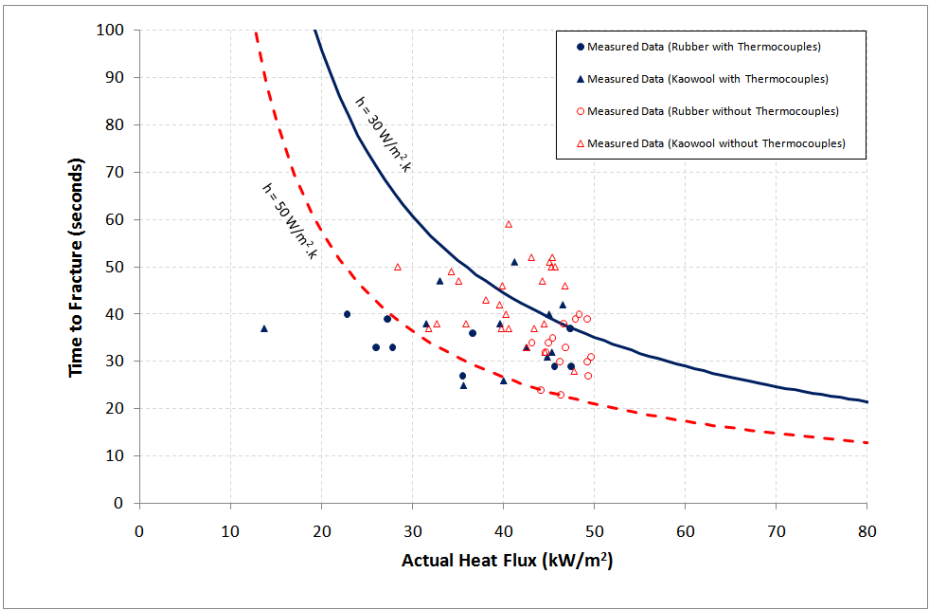

Figure 4-50: Comparison between actual and predicted time to fracture for 4 mm thick glass samples

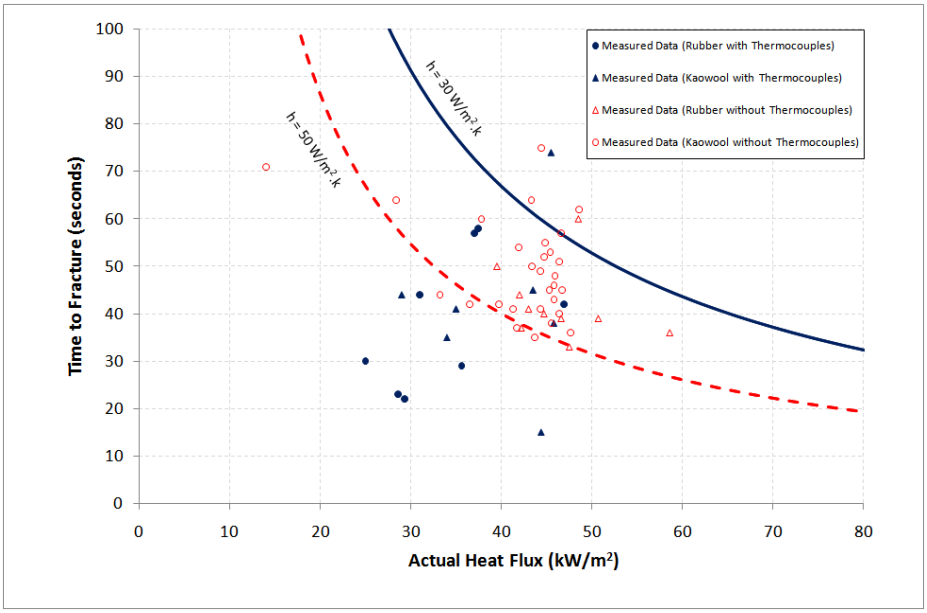

Figure 4-51: Comparison between actual and predicted time to fracture for 6 mm thick glass samples

The summary of the percentage of experiments where the time to fracture is within the predicted times to fracture is shown in Table 4-8. When the times to fracture of all the glass samples are viewed wholly, there is a 60% that the predicted time to fracture will be within the predicted range.

Table 4-8: Summary of percentage of experiments where the time to first crack that is within the predicted times to first crack

Experiment Sample Characteristics	Percentage experiments where the time to first crack is within the predicted times to first crack
4 mm thick glass sample glazed with rubber beading and has thermocouples attached (based on total 9 experiments)	44.4%
4 mm thick glass sample glazed with kaowool beading and has thermocouples attached (based on total 12 experiments)	50.0%
4 mm thick glass sample glazed with rubber beading and has no thermocouples attached (based on total 15 experiments)	73.3%
4 mm thick glass sample glazed with kaowool beading and has no thermocouples attached (based on total 25 experiments)	64.0%

Table 4-8 **(con't)**

Experiment Sample Characteristics	Percentage experiments where the time to first crack is within the predicted times to first crack
All 4 mm thick glass samples (based on total 61 experiments)	60.7%
6 mm thick glass sample glazed with rubber beading and has thermocouples attached (based on total 8 experiments)	37.5%
6 mm thick glass sample glazed with kaowool beading and has thermocouples attached (based on total 7 experiments)	28.6%
6 mm thick glass sample glazed with rubber beading and has no thermocouples attached (based on total 10 experiments)	70.0%
6 mm thick glass sample glazed with kaowool beading and has no thermocouples attached (based on total 29 experiments)	69.0%
All 6 mm thick glass samples (based on total 54 experiments)	59.3%
All glass samples (based on total 115 experiments)	60.0%
Note: Radiant heat flux readings were not available in 2 experiments.	

4.10.2 Prediction of Time to Glass Fracture based on the Fracture Criterion

This method requires a heat transfer model, which did not form part of this research, to calculate the temperature profile across the thickness of the glass pane at a given time. The time for the average temperature across the thickness to reach the temperature difference defined by the fraction criterion was taken as the time to glass fracture.

Figure 4-52 to Figure 4-55 show the temperature differences at glass fracture for the 4 mm and 6 mm glass samples glazed with either the rubber or kaowool beading where $\Delta T1$, $\Delta T2$ and $\Delta T3$ represents the local exposed edge, local exposed centre and local bulk temperature difference.

It was observed from Figure 4-52 that 7 out of 9 experiments had $\Delta T1$ between the earlier predicted ranges of temperature difference of 55°C to 129°C when fracture is expected to occur while 7 out of 9 experiments had $\Delta T2$ between the predicted ranges of temperature difference. For $\Delta T3$, there were 5 out of 9 experiments that were within the ranges of predicted temperature difference.

In Figure 4-53, 5 out of 10 experiments had ΔT1 between the predicted ranges of temperature difference, 5 out of 12 experiments had ΔT2 between the predicted ranges of temperature difference and 5 out of 10 experiments had ΔT3 within the ranges of temperature difference.

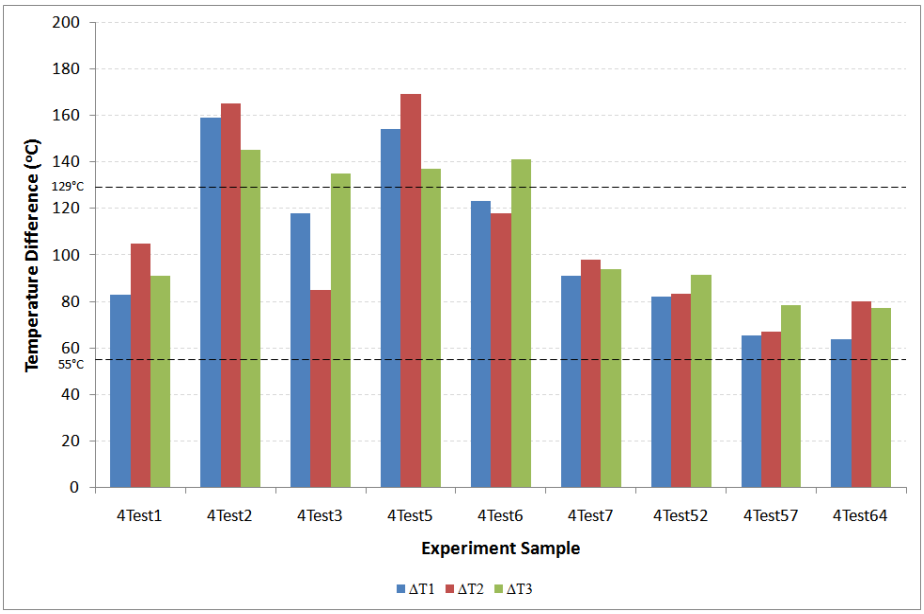

Figure 4-52: Comparison of temperature differences at glass fracture for 4 mm thick glass samples glazed with rubber beading with the predicted temperature differences at fracture

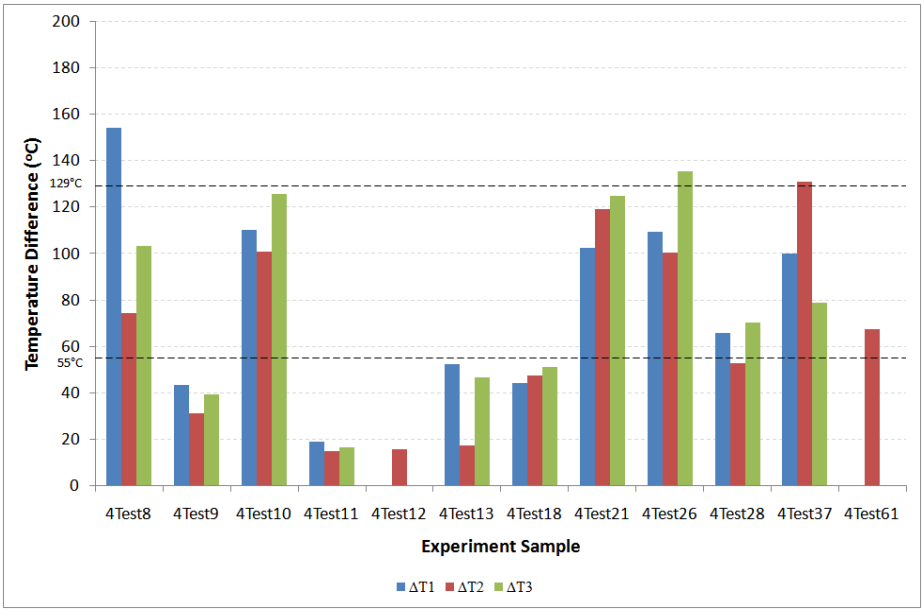

Figure 4-53: Comparison of temperature differences at glass fracture for 4 mm thick glass samples glazed with kaowool beading with the predicted temperature differences at fracture

In Figure 4-54, 5 out of 7 experiments had ΔT1 within the ranges of temperature difference, 5 out of 7 experiments had ΔT2 within the range of temperature difference and 6 out of 7 experiments had ΔT3 within the ranges of temperature difference.

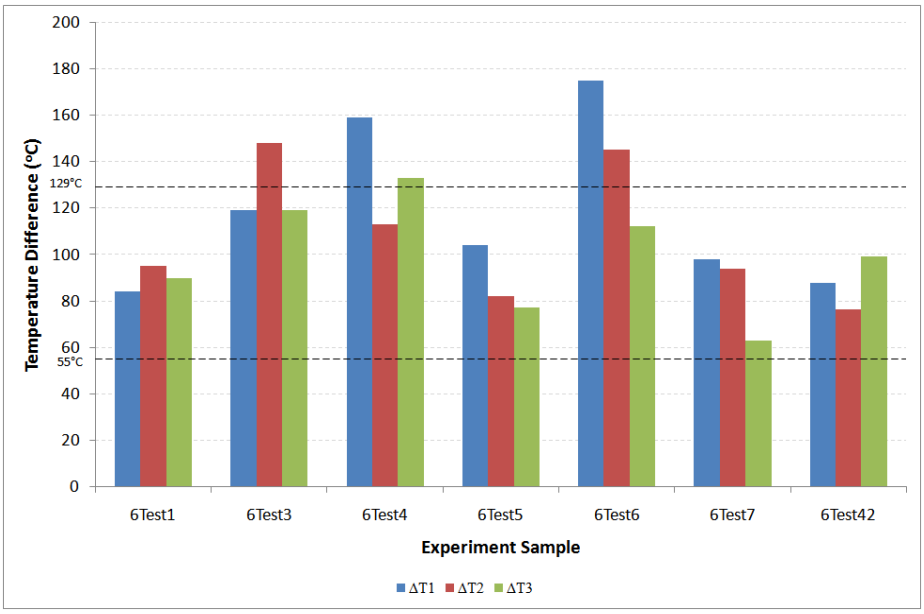

Figure 4-54: Comparison of temperature differences at glass fracture for 6 mm thick glass samples glazed with rubber beading with the predicted temperature differences at fracture

In Figure 4-55, 3 out of 5 experiments had ΔT1 within the ranges of temperature difference, 2 out of 4 experiments had ΔT2 within the range of temperature difference and 2 out of 3 experiments had ΔT3 within the ranges of temperature difference.

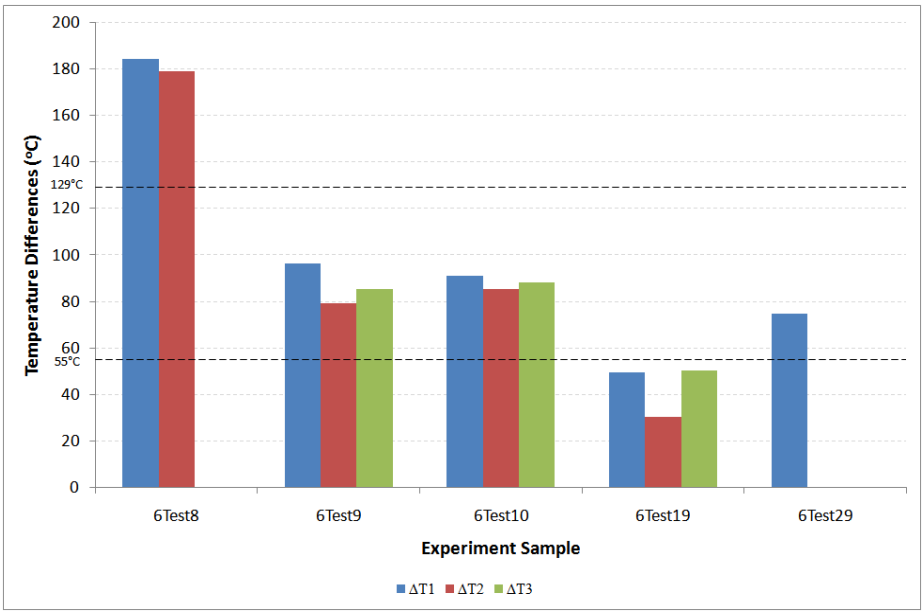

Figure 4-55: Comparison of temperature differences at glass fracture for 6 mm thick glass samples glazed with kaowool beading with the predicted temperature differences at fracture

Table 4-9: Summary of percentage of temperature differences at fracture that are within the predicted temperature differences

Experimental Sample Variation	Percentage experiments fractures within range of temperature differences (55°C to 129°C)		
	ΔT1	ΔT2	ΔT3
4 mm thick glass sample glazed with rubber beading	77.8%	77.8%	55.6%
4 mm thick glass sample glazed with kaowool beading	50.0%	41.7%	50.0%
6 mm thick glass sample glazed with rubber beading	71.4%	71.4%	85.7%
6 mm thick glass sample glazed with kaowool beading	60.0%	50.0%	66.7%
All glass samples	64.5%	59.4%	62.1%

It can be seen from Table 4-9, that the actual temperature differences were within the predicted temperature different range in 60% of the experiments. It should be noted that this method is generally applied to a zone-model where the glass is heated by a hot layer rather than direct radiation from the fire such as in this research. It was observed from Table 4-9, that there was better agreement between the actual and predicted temperature differences at fracture for glass samples glazed with rubber beading.

5 GLASS FALLOUT PREDICTION MODEL

5.1 Basis for Model

The glass fallout prediction model is based on the distribution characteristic of the glass fallout data collected during the experiments. Figure 5-1 and Figure 5-2 show examples of the glass fallout data that were fitted with the exponential probability distribution curve at the chosen times after fracture, in this case 1 second and 600 seconds respectively. The respective descending cumulative distribution curves are shown in Figure 5-3 and Figure 5-4. Figure 5-3 and Figure 5-4 describe the probability for a percentage of glass area to fallout at 1 second and 600 seconds after glass fracture.

The methodology used to derive the required parameters for the glass prediction fallout model, which were based on the distribution curves as shown in Figure 5-3 and Figure 5-4 is explained in Chapter 5.3.

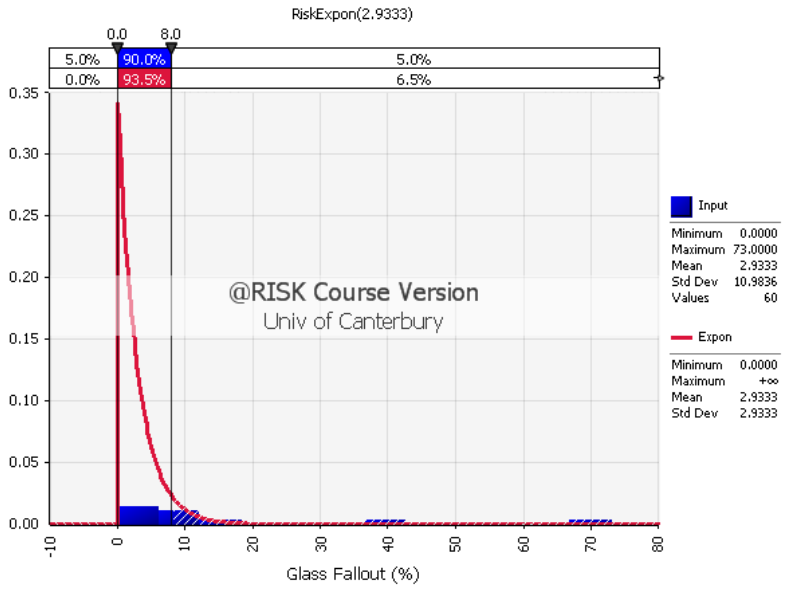

Figure 5-1: Probability exponential distribution curve fitted to glass fallout data from experiments with 4 mm thick samples at 1 seconds after glass facture

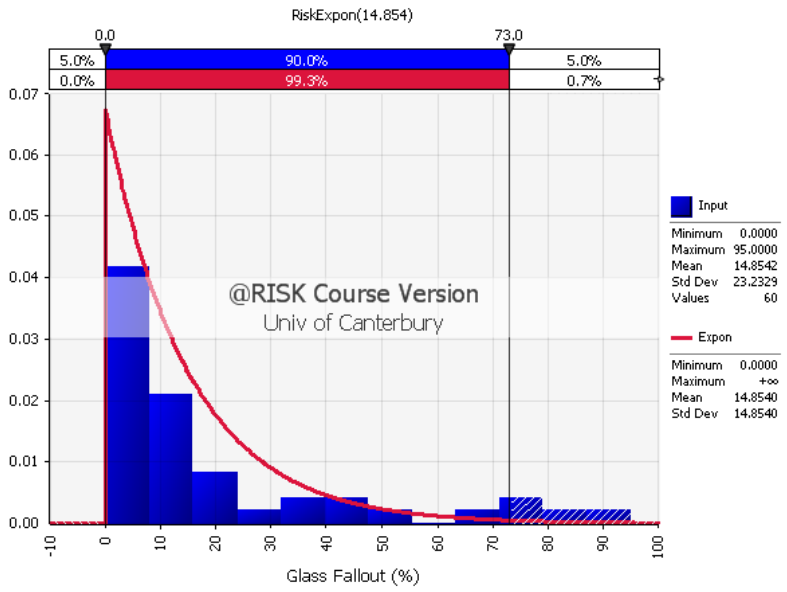

Figure 5-2: Probability exponential distribution curve fitted to glass fallout data from experiments with 4 mm thick samples at 600 seconds after glass facture

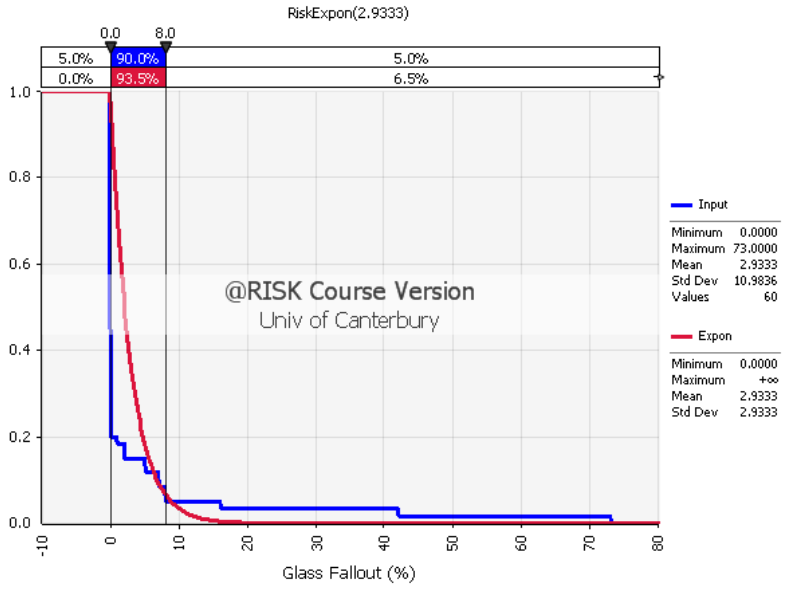

Figure 5-3: Descending cumulative exponential distribution curve fitted to glass fallout data from experiments with 4 mm thick samples at 1 second after glass fracture

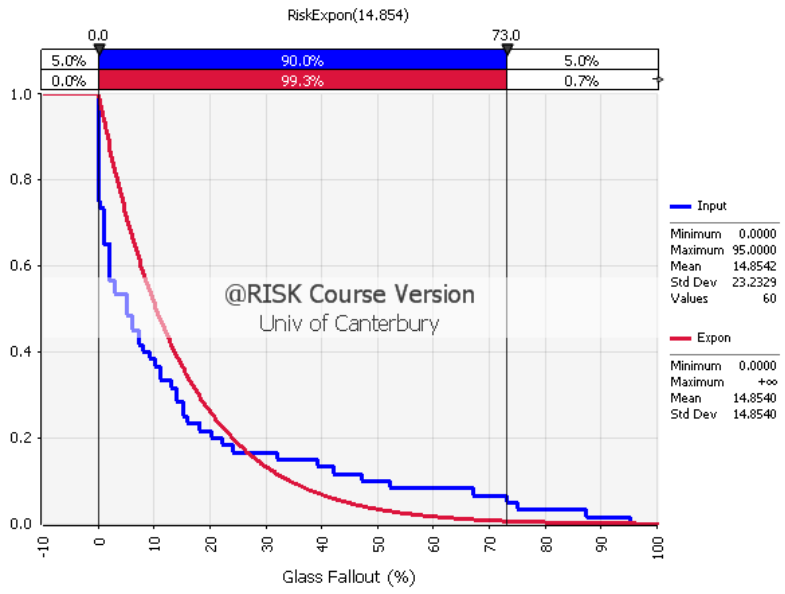

Figure 5-4: Descending cumulative exponential distribution curve fitted to glass fallout data from experiments with 4 mm thick samples at 600 seconds after glass fracture

As the glass fallout data were shown to have the characteristic of an exponential distribution function, the use of the distribution function to describe the fallout behaviour at a point in time after glass facture was deemed suitable. However, it should be noted that the exponential distribution curve will under-predict the amount glass fallout by visually inspection of Figure 5-3 and Figure 5-4.

5.2 Exponential Distribution

The exponential probability distribution function is given as,

$$f(x) = \lambda e^{-\lambda x} \tag{13}$$

for $x \geq 0,\ \lambda > 0$

and the cumulative distribution function is given as,

$$F(x) = 1 - e^{-\lambda x} \tag{14}$$

The exponential distribution has the following characteristics,

Mean = $\frac{1}{\lambda}$

Standard deviation = $\frac{1}{\lambda}$

The success rate (λ) is the only distributional parameter in the distribution function with parameter x being the random variable.

According to Mun (2006), this distribution is widely used to describe events that re-occur at random points in time. An example of the application of the exponential distribution is to describe the time between failures of electronic equipment.

The cumulative distribution function would have to be described in a descending manner rather than ascending since this research has shown that the small amount of glass fallouts (if any) are more likely to occur compared with large amount of fallouts.

For descending cumulative distribution,

$$F(x) = 1 - (1 - e^{-\lambda x}) \tag{15}$$

Rearranging Equation (15),

$$x = -\frac{\ln[F(x)]}{\lambda} \tag{16}$$

where now x is the potential amount of glass fallout defined as the percentage (%) with respect to the exposed glass area.

The final relationship between glass fallout potential and probability of fallout is now given as,

$$\text{Glass fallout potential (\%)} = -\frac{\ln[P_{fallout}]}{\lambda} \tag{17}$$

where the potential glass fallout is capped at 100%.

5.3 Exponential Distribution Parameter

The Palisade @Risk software was used to obtain the required parameter (λ) for the exponential distribution function. In Palisade @Risk, the distribution parameter λ is defined as the inverse of the continuous scale parameter β, so $\lambda = \frac{1}{\beta}$ where $\beta > 0$.

At every time step where fallout was reported for a group of experiments with similar characteristics such as those with attached thermocouples, glass thickness or type of beading, an exponential distribution curve was fitted to the glass fallout data. This is shown in Figure 5-1 and Figure 5-2 where β = 2.933 and 14.854 respectively. As $\lambda = \frac{1}{\beta}$, the respective λ value is 0.341 and is 0.0673.

A trendline was fitted to the plots of λ using the Microsoft Excel 2007 chart function and an equation function describing the trendline was obtained through the chart function.

5.4 Prediction Model based Experimental Data

The prediction models based on the different characteristics of the experiment samples are described in this section. It should be noted that for certain experiment sample characteristics, there were not sufficient fallout data to derive the exponential distribution parameter plot for the prediction model.

5.4.1 Prediction Model based on 4 mm Thick Samples Glazed with Rubber Beading and have no Thermocouples Attached (Fallouts only)

This prediction model is based on 12 available experimental samples displaying fallout behaviour. Figure 5-5 shows the exponential distribution function parameter, plotted as a function of time after fracture, based on the experimental fallout data. From the figure, an empirical function of $\lambda = 3103.4t_1^{-1.819}$ was obtained. Substituting the function into Equation (17) yields,

$$\text{Glass fallout potential (\%)} = \text{Min}\left(-\frac{\ln\left[P_{fallout}\right]t_1^{1.819}}{3103.4}, 100\right)$$

where $t_1 \leq 600$ seconds

A plot of the glass fallout potential with respect to the probability of glass fallout is shown in

Figure 5-6. The distribution of actual radiant heat fluxes imposed on the glass samples is shown in Figure 5-7.

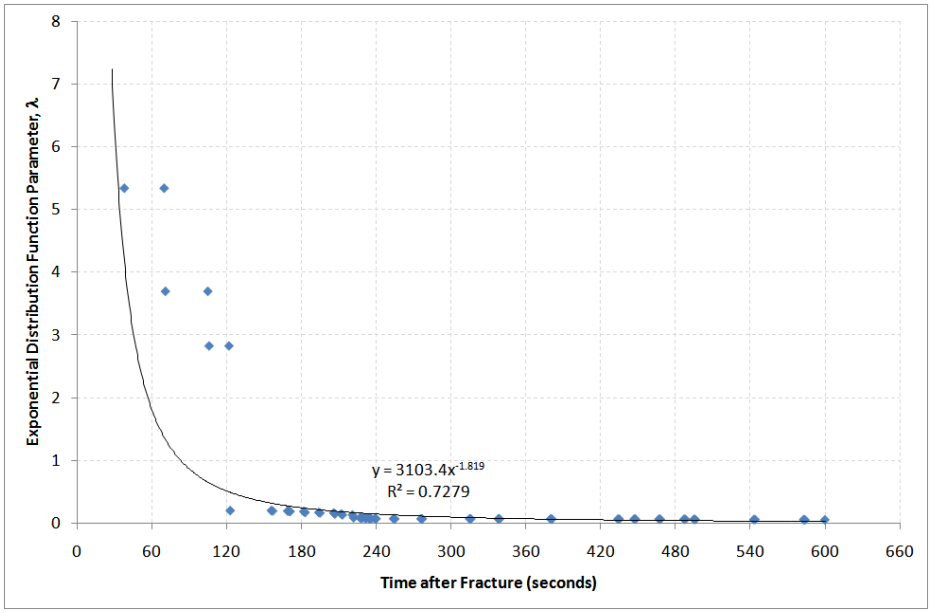

Figure 5-5: Exponential distribution function parameter for 4 mm thick samples glazed with rubber beading and has no thermocouples attached

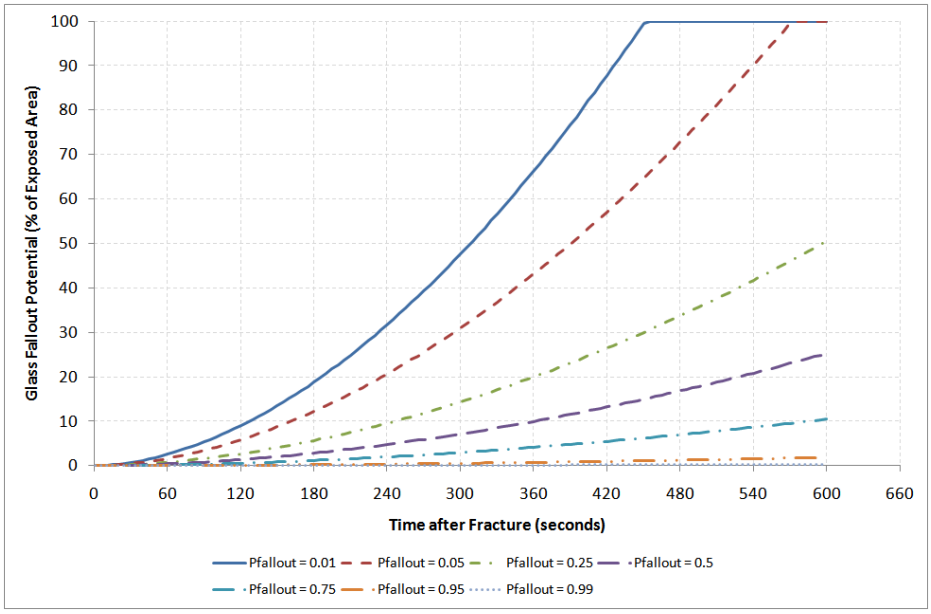

Figure 5-6: Glass fallout potential based on 4 mm thick samples glazed with rubber beading and has no thermocouples attached

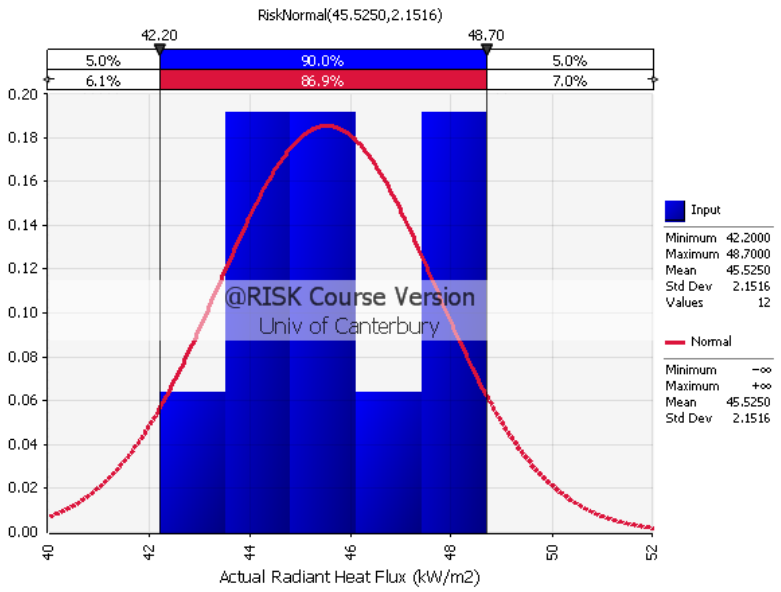

Figure 5-7: Distribution of actual radiant heat flux data for experiments with 4 mm thick samples glazed with rubber beading and has no thermocouples attached

5.4.2 Prediction Model based on 4 mm Thick Samples Glazed with Kaowool Beading and have Thermocouples Attached (Fallouts only)

This prediction model is based on 7 available experimental samples displaying fallout behaviour. Figure 5-8 shows the exponential distribution function parameter, plotted as a function of time after fracture, based on the experimental fallout data. From the figure, an empirical function of $\lambda = 0.1536 t_1^{-0.124}$ was obtained. Substituting the function into Equation (17) yields,

$$\text{Glass fallout potential (\%)} = \text{Min}\left(-\frac{\ln\left[P_{fallout}\right] t_1^{0.124}}{0.1536}, 100\right)$$

where $t_1 \leq 600$ seconds

A plot of the glass fallout potential with respect to the probability of glass fallout is shown in Figure 5-9. The distribution of actual radiant heat fluxes imposed on the glass samples is shown in Figure 5-10.

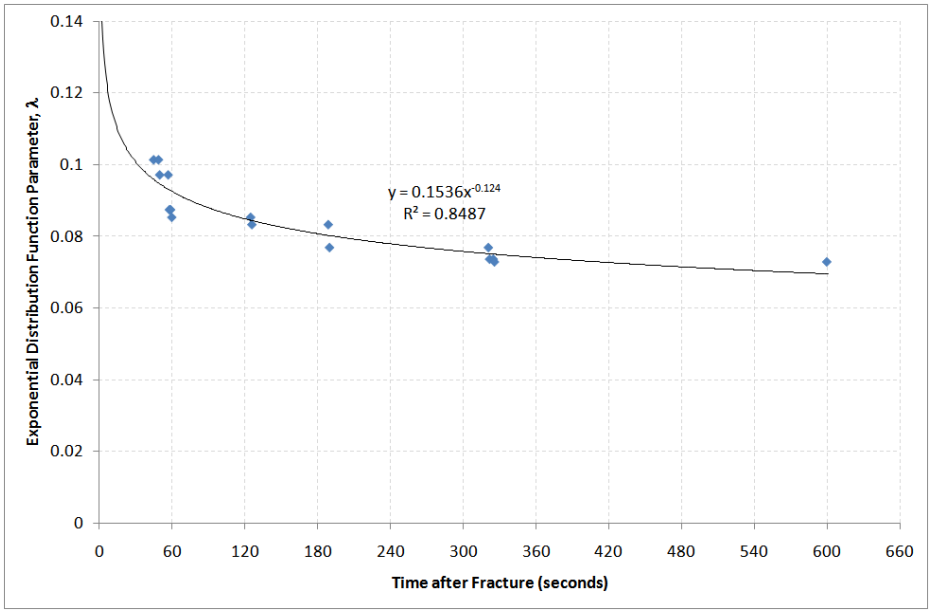

Figure 5-8: Exponential distribution function parameter for 4 mm thick samples glazed with kaowool beading and has thermocouples attached

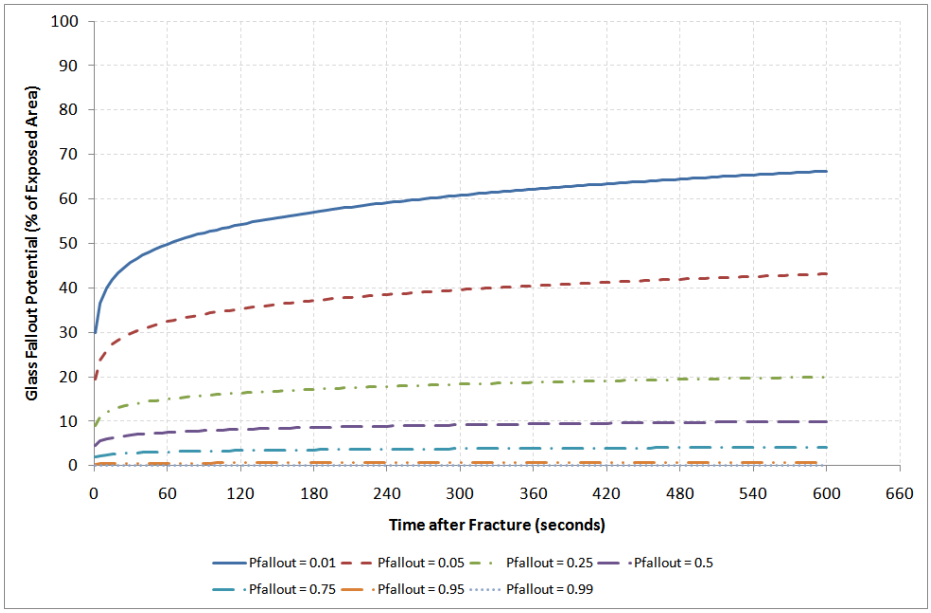

Figure 5-9: Glass fallout potential based on 4 mm thick samples glazed with kaowool beading and has thermocouples attached

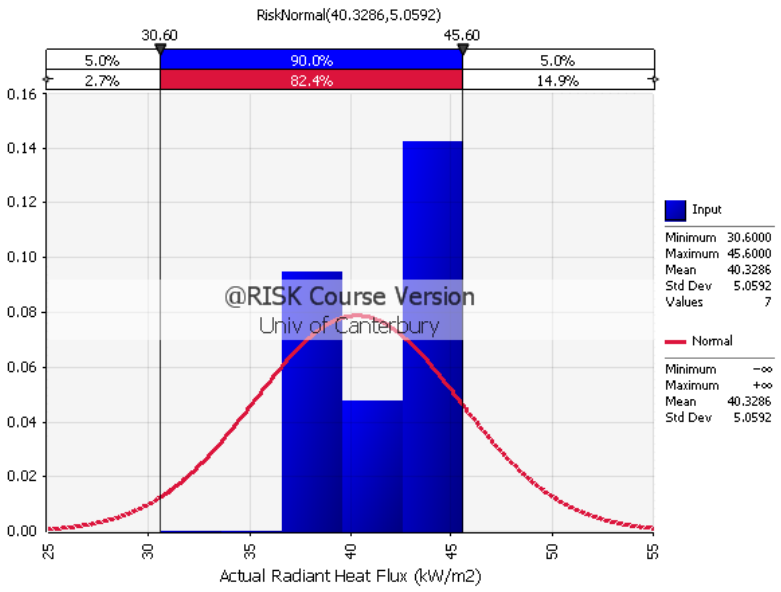

Figure 5-10: Distribution of actual radiant heat flux data for experiments with 4 mm thick samples glazed with kaowool beadings and has thermocouples attached

5.4.3 Prediction Model based on 4 mm Thick Samples Glazed with Kaowool Beading and have no Thermocouples Attached (Fallouts only)

This prediction model is based on 24 available experimental samples displaying fallout behaviour. Figure 5-11 shows the exponential distribution function parameter, plotted as a function of time after fracture, based on the experimental fallout data. From the figure, an empirical function of $\lambda = 0.2397 t_1^{-0.277}$ was obtained. Substituting the function into Equation (17) yields,

$$\text{Glass fallout potential (\%)} = \text{Min}\left(-\frac{\ln\left[P_{fallout}\right] t_1^{0.277}}{0.2397}, 100\right)$$

where $t_1 \leq 600$ seconds

A plot of the glass fallout potential with respect to the probability of glass fallout is shown in Figure 5-12. The distribution of actual radiant heat fluxes imposed on the glass samples is shown in Figure 5-13.

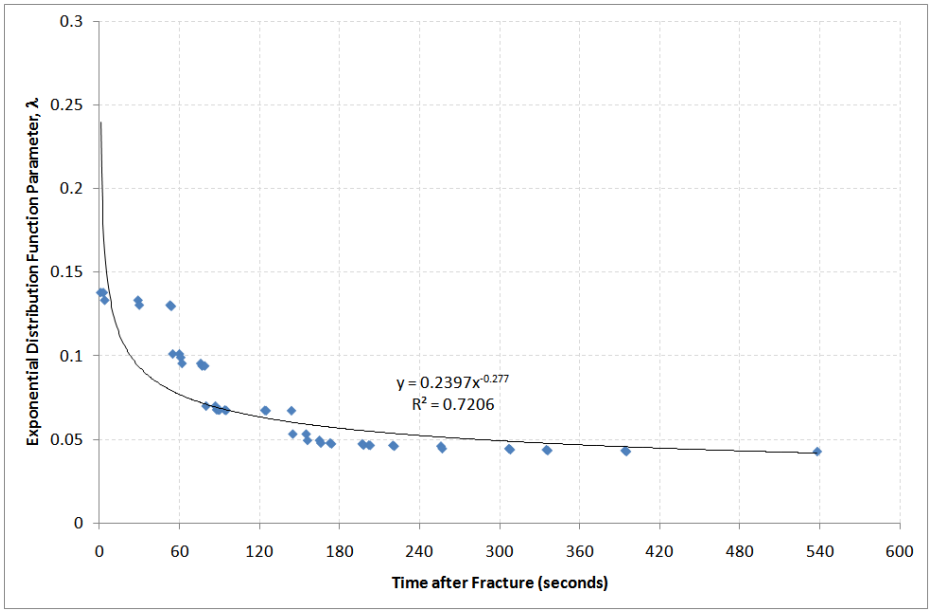

Figure 5-11: Exponential distribution function parameter for 4 mm thick samples glazed with kaowool beading and has no thermocouples attached

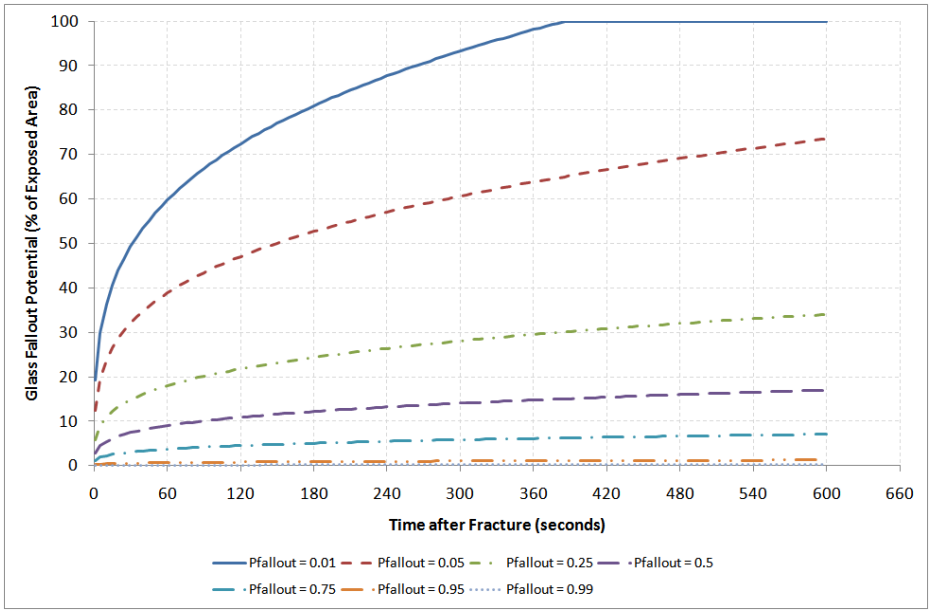

Figure 5-12: Glass fallout potential based on 4 mm thick samples glazed with kaowool beading and has no thermocouples attached

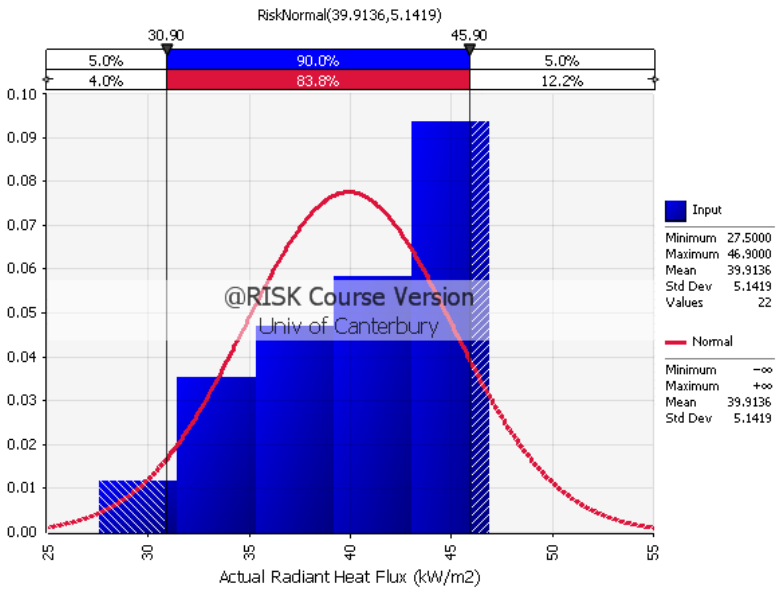

Figure 5-13: Distribution of actual radiant heat flux data for experiments with 4 mm thick samples glazed with kaowool beading and has no thermocouples attached

5.4.4 Prediction Model based on 4 mm Thick Samples with Fallout Only

This prediction model is based on 45 available experimental samples displaying fallout behaviour. Figure 5-14 shows the exponential distribution function parameter, plotted as a function of time after fracture, based on the experimental fallout data. From the figure, an empirical function of $\lambda = 0.7104 t_1^{-0.432}$ was obtained. Substituting the function into Equation (17) yields,

$$\text{Glass fallout potential (\%)} = \text{Min}\left(-\frac{\ln\left[P_{fallout}\right] t_1^{0.432}}{0.7104}, 100\right)$$

where $t_1 \leq 600$ seconds

A plot of the glass fallout potential with respect to the probability of glass fallout is shown in Figure 5-15. The distribution of actual radiant heat fluxes imposed on the glass samples is shown in Figure 5-16.

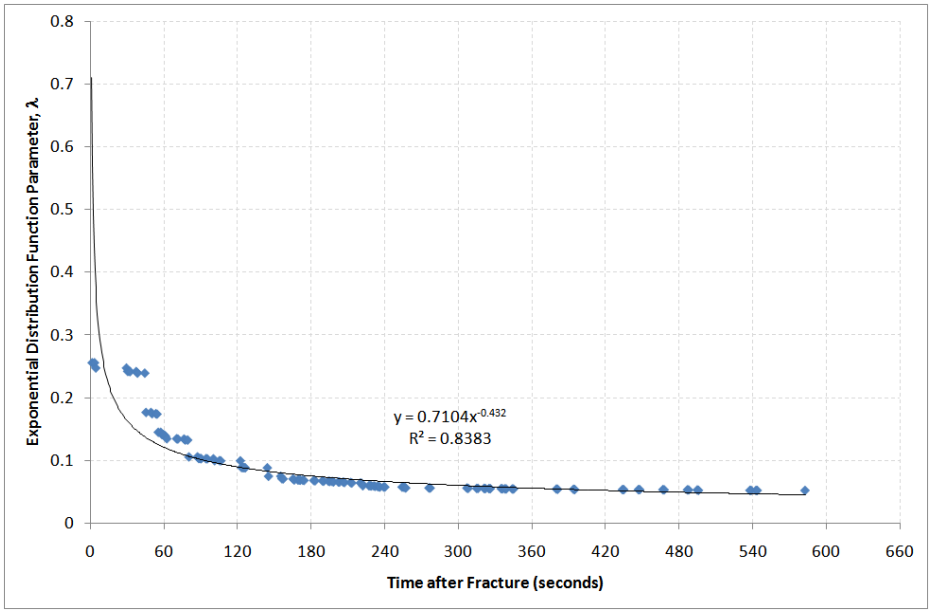

Figure 5-14: Exponential distribution function parameter for 4 mm thick samples with fallouts only

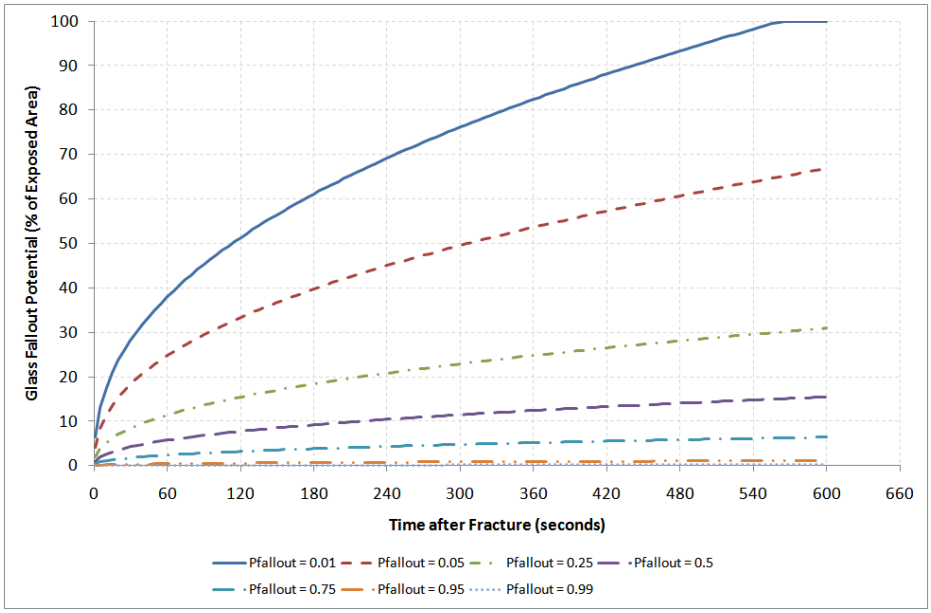

Figure 5-15: Glass fallout potential based on 4 mm thick samples with fallouts only

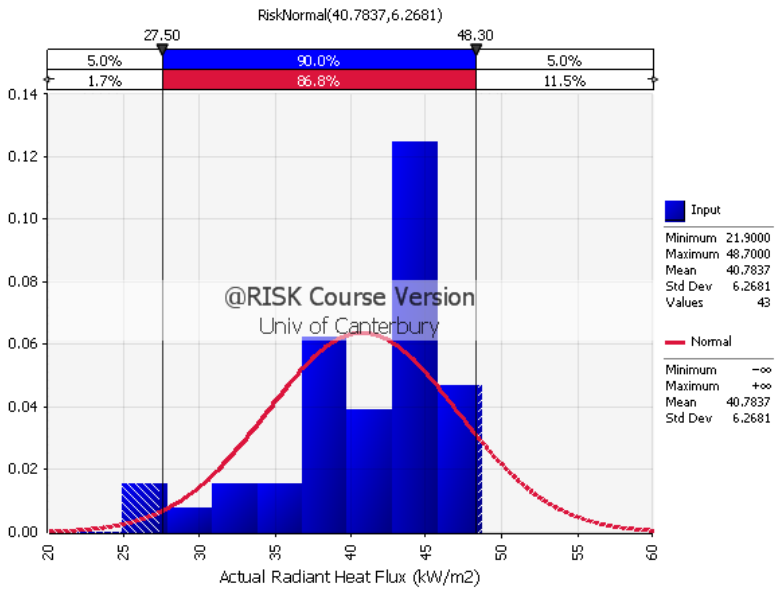

Figure 5-16: Distribution of actual radiant heat flux data for experiments with 4 mm thick samples with fallouts only

5.4.5 Prediction Model based on all 4 mm Thick Samples

This prediction model is based on 60 available experimental samples irrespective of the fallout behaviour. Figure 5-17 shows the exponential distribution function parameter, plotted as a function of time after fracture, based on the experimental fallout data. From the figure, an empirical function of $\lambda = 0.9438 t_1^{-0.432}$ was obtained. Substituting the function into Equation (17) yields,

$$\text{Glass fallout potential (\%)} = \text{Min}\left(-\frac{\ln\left[P_{fallout}\right] t_1^{0.432}}{0.9438}, 100\right)$$

where $t_1 \leq 600$ seconds

A plot of the glass fallout potential with respect to the probability of glass fallout is shown in Figure 5-18. The distribution of actual radiant heat fluxes imposed on the glass samples is shown in Figure 5-19.

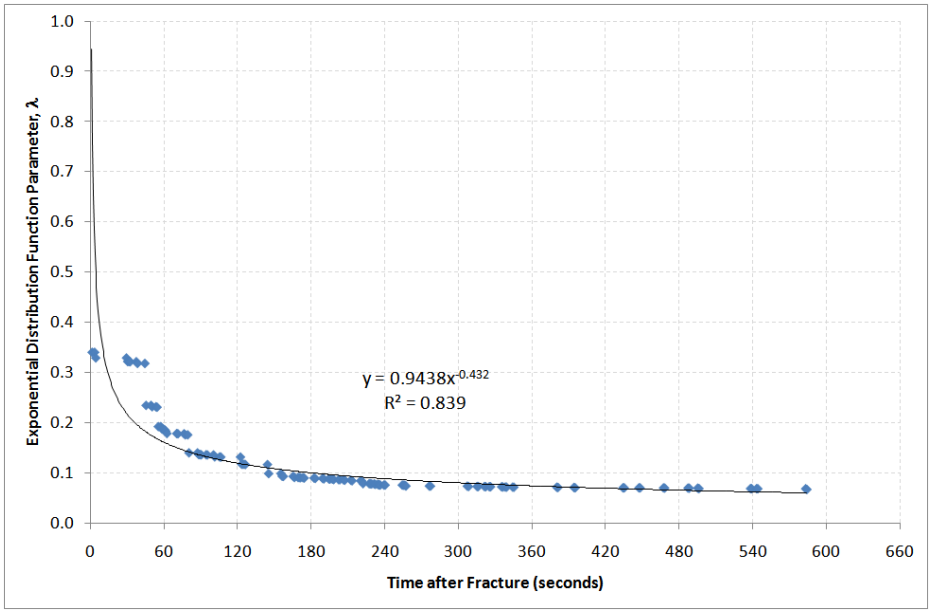

Figure 5-17: Exponential distribution function parameter for all 4 mm thick samples

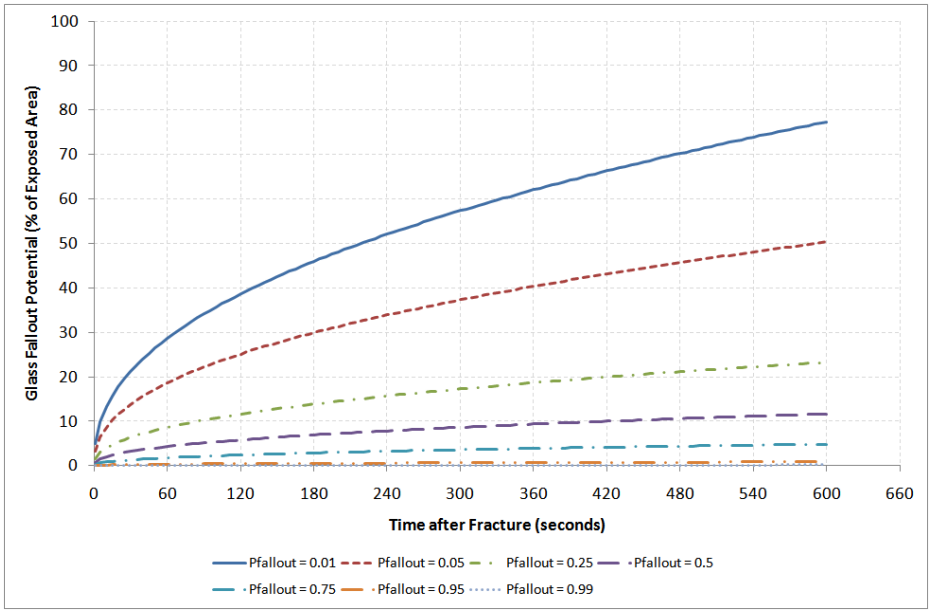

Figure 5-18: Glass fallout potential based on all 4 mm thick samples

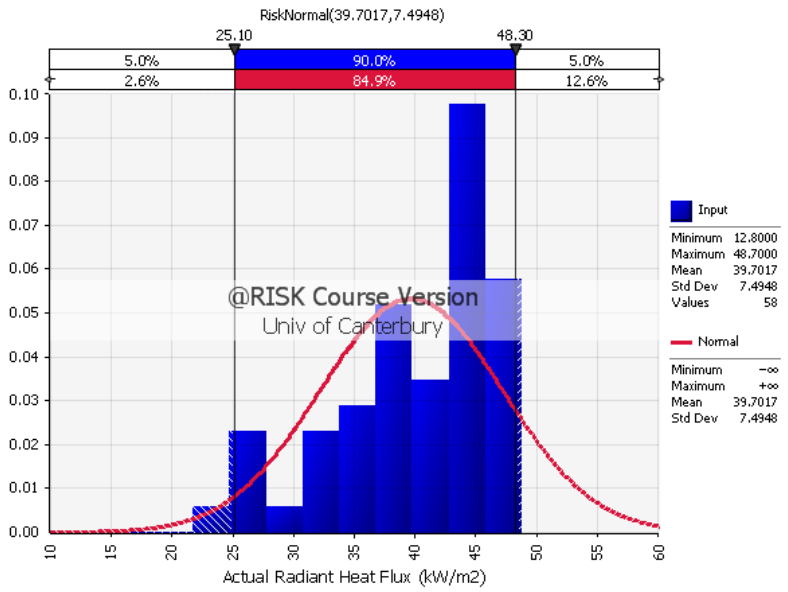

Figure 5-19: Distribution of actual radiant heat flux data for experiments with all 4 mm thick samples

5.4.6 Prediction Model based on all 4 mm Thick Samples with Thermocouples Attached

This prediction model is based on 19 available experimental samples irrespective of the fallout behaviour. Figure 5-20 shows the exponential distribution function parameter, plotted as a function of time after fracture, based on the experimental fallout data. From the figure, an empirical function of $\lambda = 0.5419 t_1^{-0.195}$ was obtained. Substituting the function into Equation (17) yields,

$$\text{Glass fallout potential (\%)} = \text{Min}\left(-\frac{\ln\left[P_{fallout}\right] t_1^{0.195}}{0.5419}, 100\right)$$

where $t_1 \leq 600$ seconds

A plot of the glass fallout potential with respect to the probability of glass fallout is shown in Figure 5-21. The distribution of actual radiant heat fluxes imposed on the glass samples is shown in Figure 5-22.

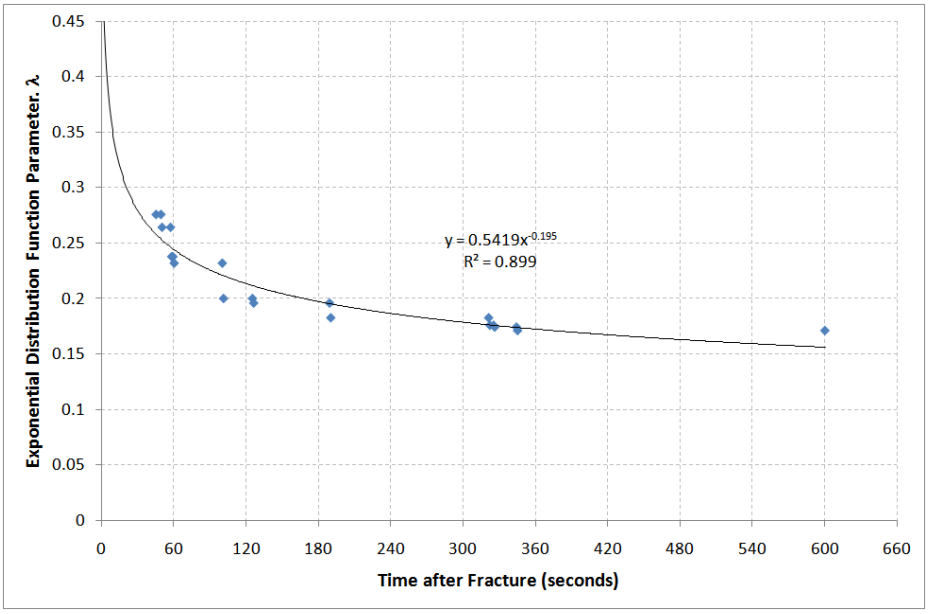

Figure 5-20: Exponential distribution function parameter for all 4 mm thick samples with thermocouples attached

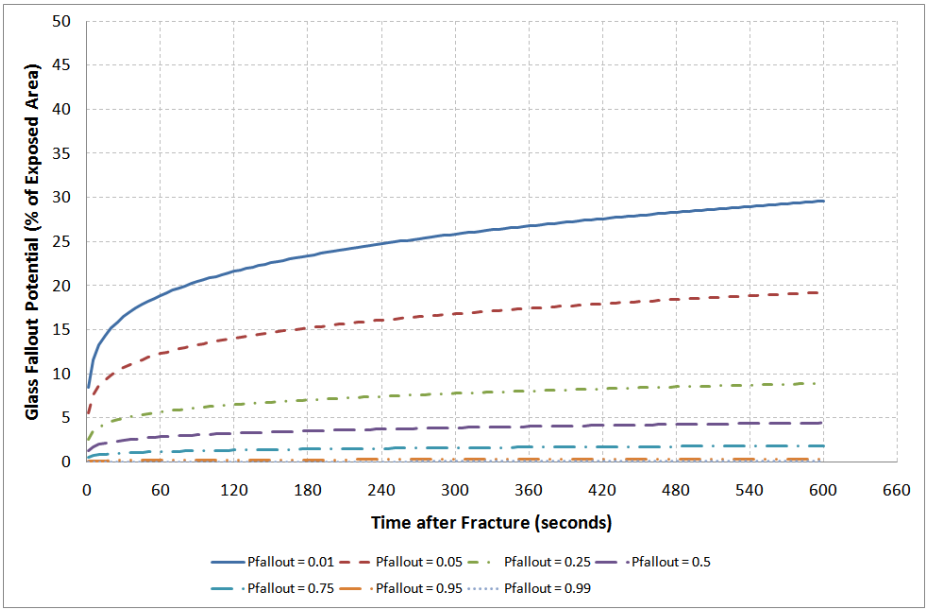

Figure 5-21: Glass fallout potential based on all 4 mm thick samples with thermocouples attached

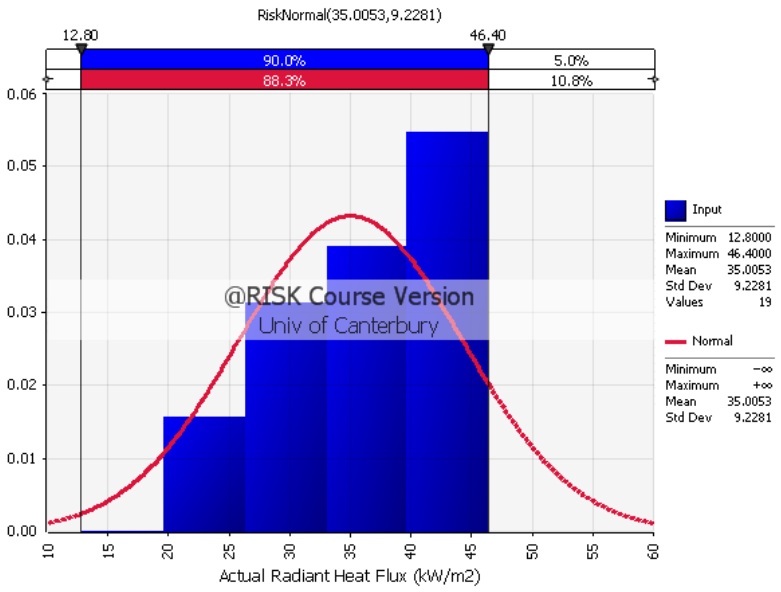

Figure 5-22: Distribution of actual radiant heat flux data for experiments with all 4 mm thick samples with thermocouples attached

5.4.7 Prediction Model based on all 4 mm Thick Samples with No Thermocouples Attached

This prediction model is based on 41 available experimental samples irrespective of the fallout behaviour. Figure 5-23 shows the exponential distribution function parameter based on the experimental fallout data. From the figure, an empirical function of $\lambda = 0.6376t_1^{-0.400}$ was obtained. Substituting the function into Equation (17) yields,

$$\text{Glass fallout potential (\%)} = \text{Min}\left(-\frac{\ln\left[P_{fallout}\right]t_1^{0.400}}{0.6376}, 100\right)$$

where $t_1 \leq 600$ seconds

A plot of the glass fallout potential with respect to the probability of glass fallout is shown in Figure 5-24. The distribution of actual radiant heat fluxes imposed on the glass samples is shown in Figure 5-25.

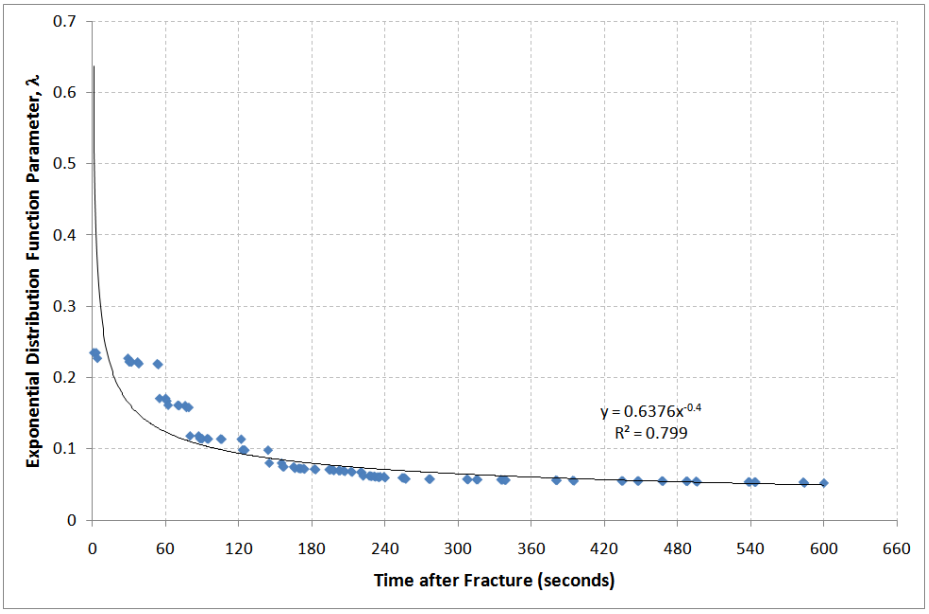

Figure 5-23: Exponential distribution function parameter for all 4 mm thick samples with no thermocouples attached

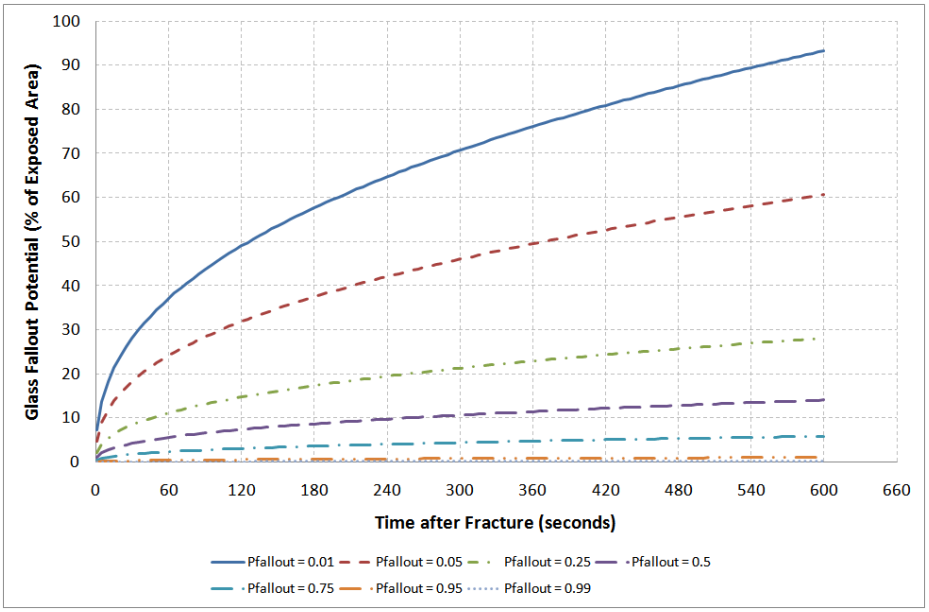

Figure 5-24: Glass fallout potential based on all 4 mm thick samples with no thermocouples attached

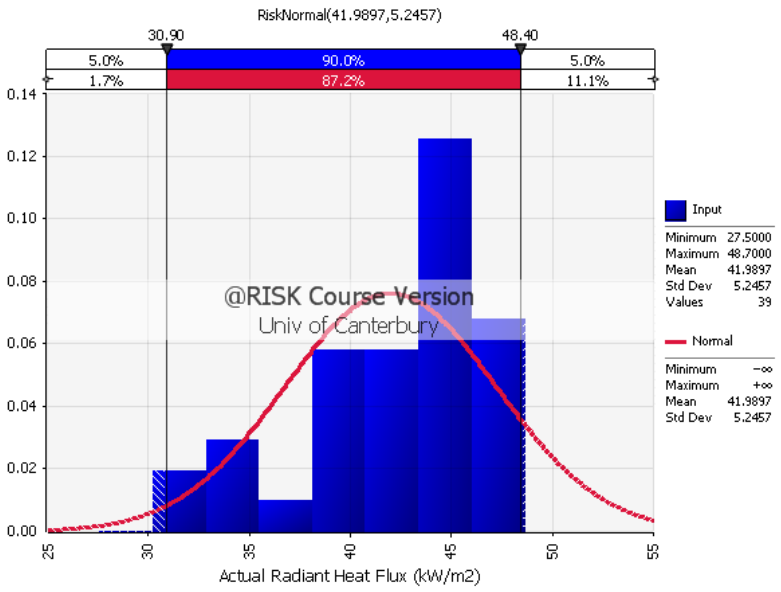

Figure 5-25: Distribution of actual radiant heat flux data for experiments with all 4 mm thick samples with no thermocouples attached

5.4.8 Prediction Model based on 4 mm Thick Samples with Thermocouples Attached (Fallouts only)

This prediction model is based on 9 available experimental samples displaying fallout behaviour. Figure 5-26 shows the exponential distribution function parameter, plotted as a function of time after fracture, based on the experimental fallout data. From the figure, an empirical function of $\lambda = 0.2567 t_1^{-0.195}$ was obtained. Substituting the function into Equation (17) yields,

$$\text{Glass fallout potential (\%)} = \text{Min}\left(-\frac{\ln\left[P_{fallout}\right] t_1^{0.195}}{0.2567}, 100\right)$$

where $t_1 \leq 600$ seconds

A plot of the glass fallout potential with respect to the probability of glass fallout is shown in Figure 5-27. The distribution of actual radiant heat fluxes imposed on the glass samples is shown in Figure 5-34.

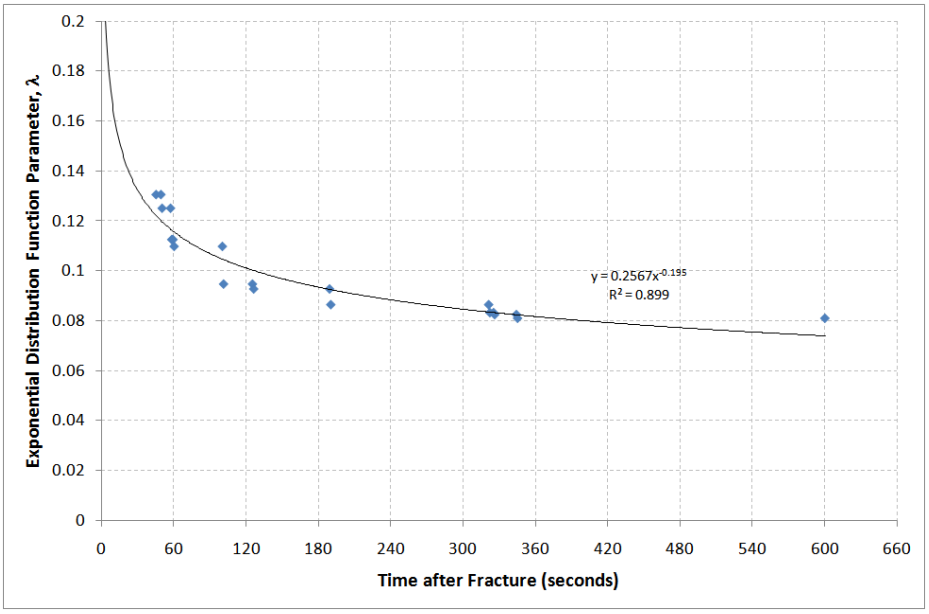

Figure 5-26: Exponential distribution function parameter for 4 mm thick samples with thermocouples attached (Fallouts only)

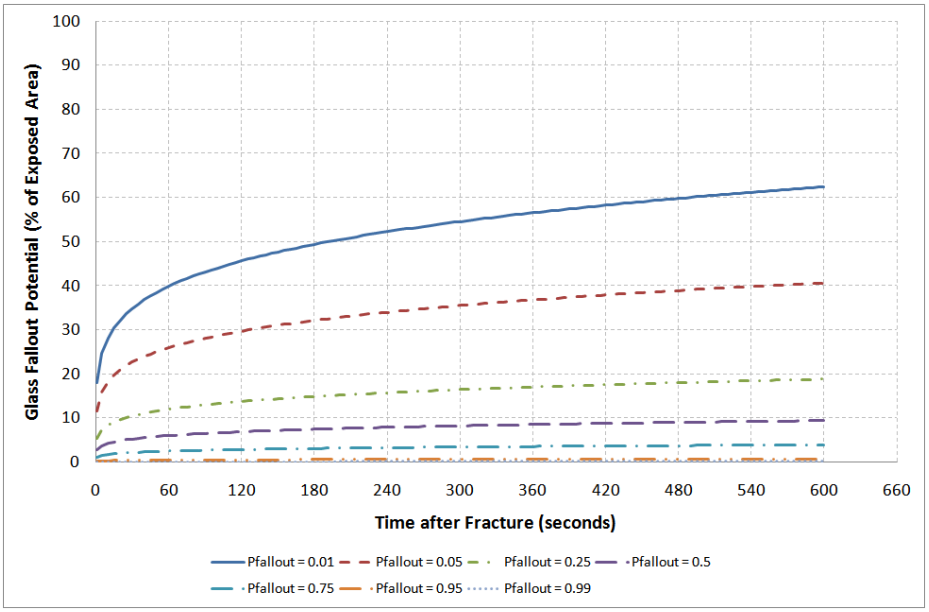

Figure 5-27: Glass fallout potential based on 4 mm thick samples with thermocouples attached (Fallouts only)

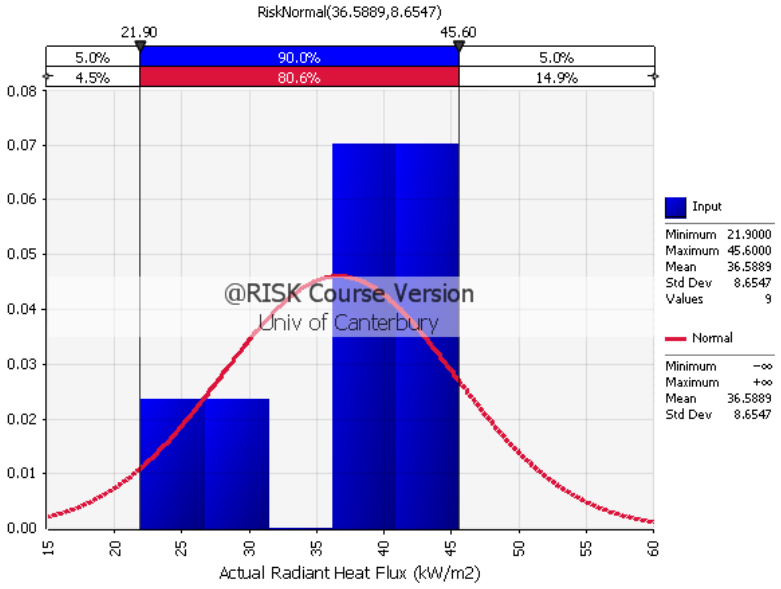

Figure 5-28: Distribution of actual radiant heat flux data for experiments with 4 mm thick samples with thermocouples attached (Fallouts only)

5.4.9 Prediction Model based on 4 mm Thick Samples with No Thermocouples Attached (Fallouts only)

This prediction model is based on 36 available experimental samples displaying fallout behaviour. Figure 5-29 shows the exponential distribution function parameter, plotted as function of time after fracture, based on the experimental fallout data. From the figure, an empirical function of $\lambda = 0.5601 t_1^{-0.400}$ was obtained. Substituting the function into Equation (17) yields,

$$\text{Glass fallout potential (\%)} = \text{Min}\left(-\frac{\ln\left[P_{fallout}\right] t_1^{0.4}}{0.5601}, 100\right)$$

where $t_1 \leq 600$ seconds

A plot of the glass fallout potential with respect to the probability of glass fallout is shown in Figure 5-36. The distribution of actual radiant heat fluxes imposed on the glass samples is shown in Figure 5-31.

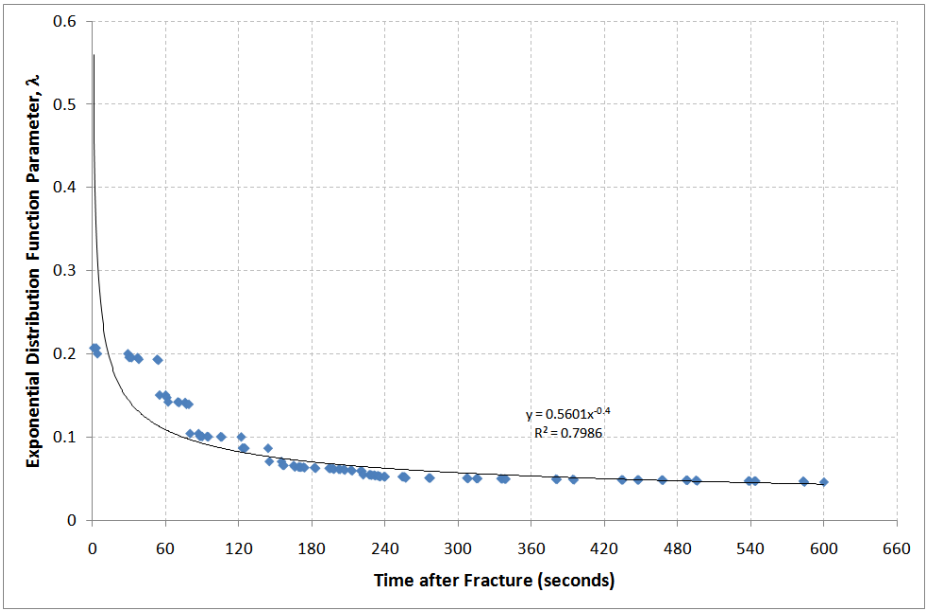

Figure 5-29: Exponential distribution function parameter for 4 mm thick samples with no thermocouples attached (Fallouts only)

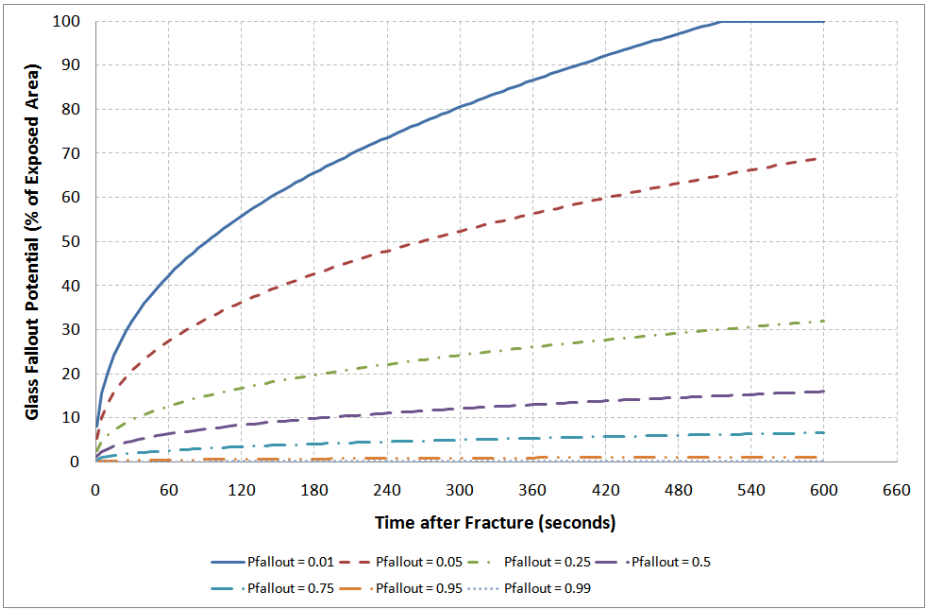

Figure 5-30: Glass fallout potential based on 4 mm thick samples with no thermocouples attached (Fallouts only)

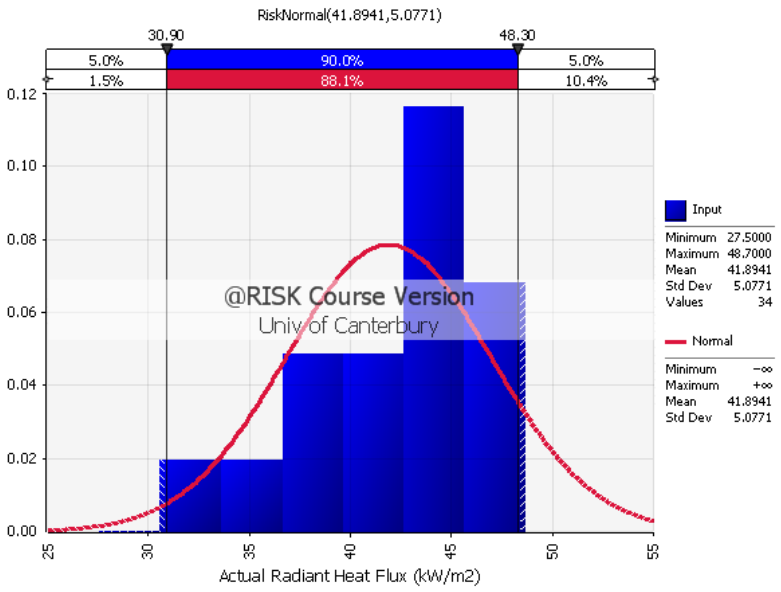

Figure 5-31: Distribution of actual radiant heat flux data for experiments with 4 mm thick samples with no thermocouples attached (Fallouts only)

5.4.10 Prediction Model based on 6 mm Thick Samples Glazed with Kaowool Beading and have no Thermocouples Attached (Fallouts only)

This prediction model is based on 13 available experimental samples displaying fallout behaviour. Figure 5-32 shows the exponential distribution function parameter, plotted as a function of time after fracture, based on the experimental fallout data. From the figure, an empirical function of $\lambda = 0.1912 t_1^{-0.075}$ was obtained. Substituting the function into Equation (17) yields,

$$\text{Glass fallout potential (\%)} = \text{Min}\left(-\frac{\ln\left[P_{fallout}\right] t_1^{0.075}}{0.1912}, 100\right)$$

where $t_1 \leq 600$ seconds

A plot of the glass fallout potential with respect to the probability of glass fallout is shown in Figure 5-33. The distribution of actual radiant heat fluxes imposed on the glass samples is shown in Figure 5-34.

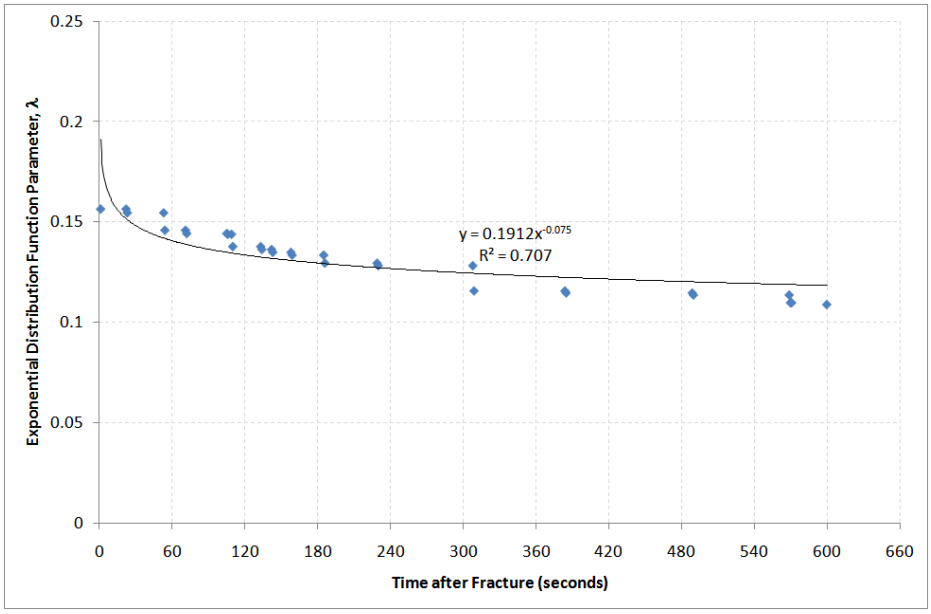

Figure 5-32: Exponential distribution function parameter for 6 mm thick samples glazed with kaowool beading and has no thermocouples attached

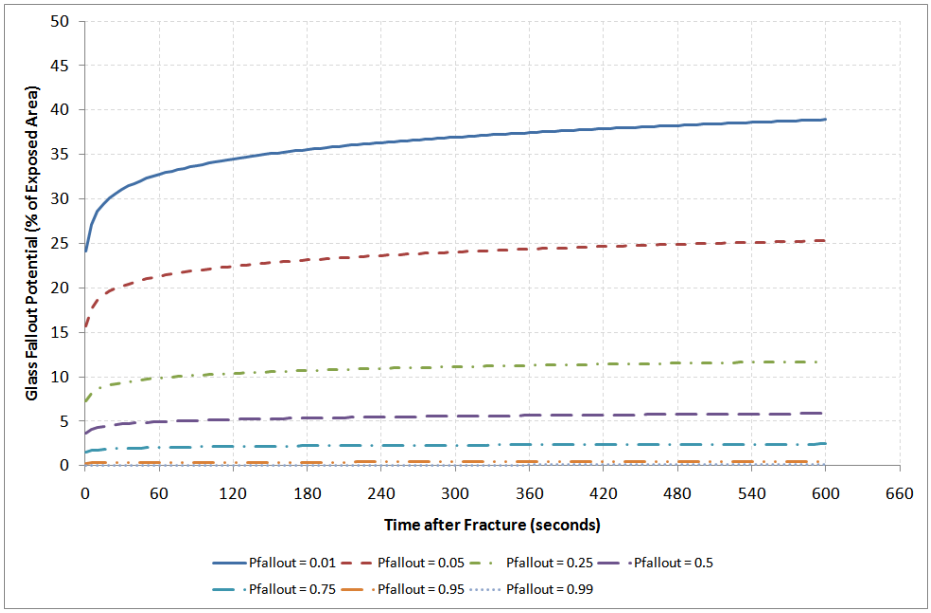

Figure 5-33: Glass fallout potential based on 6 mm thick samples glazed with kaowool beading and has no thermocouples attached

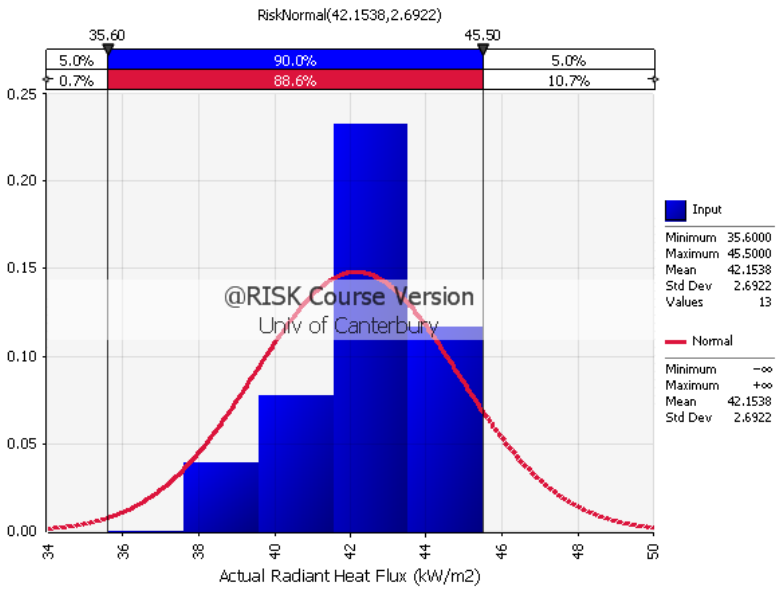

Figure 5-34: Distribution of actual radiant heat flux data for experiments with 6 mm thick samples glazed with kaowool beading and has no thermocouples attached

5.4.11 Prediction Model based on 6 mm Thick Samples with Fallout Only

This prediction model is based on 21 available experimental samples displaying fallout behaviour. Figure 5-35 shows the exponential distribution function parameter, plotted as a function of time after fracture, based on the experimental fallout data. From the figure, an empirical function of $\lambda = 0.3698 t_1^{-0.139}$ was obtained. Substituting the function into Equation (17) yields,

$$\text{Glass fallout potential (\%)} = \text{Min}\left(-\frac{\ln\left[P_{fallout}\right] t_1^{0.139}}{0.3698}, 100\right)$$

where $t_1 \leq 600$ seconds

A plot of the glass fallout potential with respect to the probability of glass fallout is shown in Figure 5-36. The distribution of actual radiant heat fluxes imposed on the glass samples is shown in Figure 5-37.

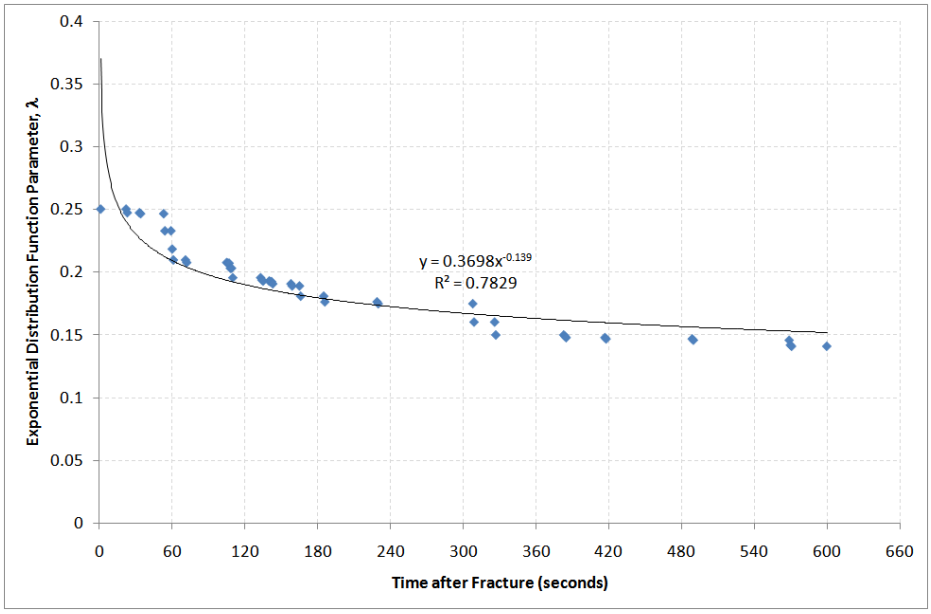

Figure 5-35: Exponential distribution function parameter for 6 mm thick samples with fallouts only

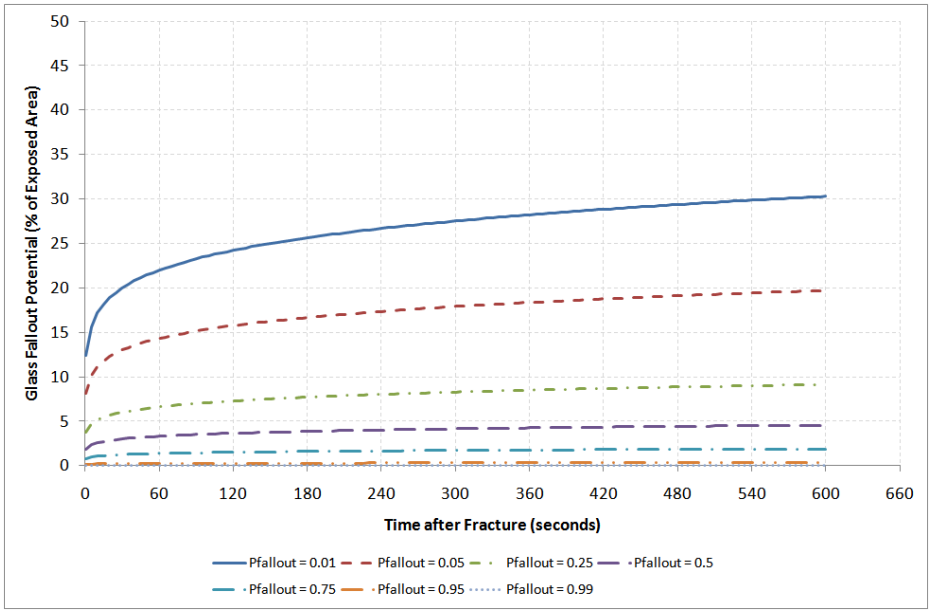

Figure 5-36: Glass fallout potential based on 6 mm thick samples with fallouts only

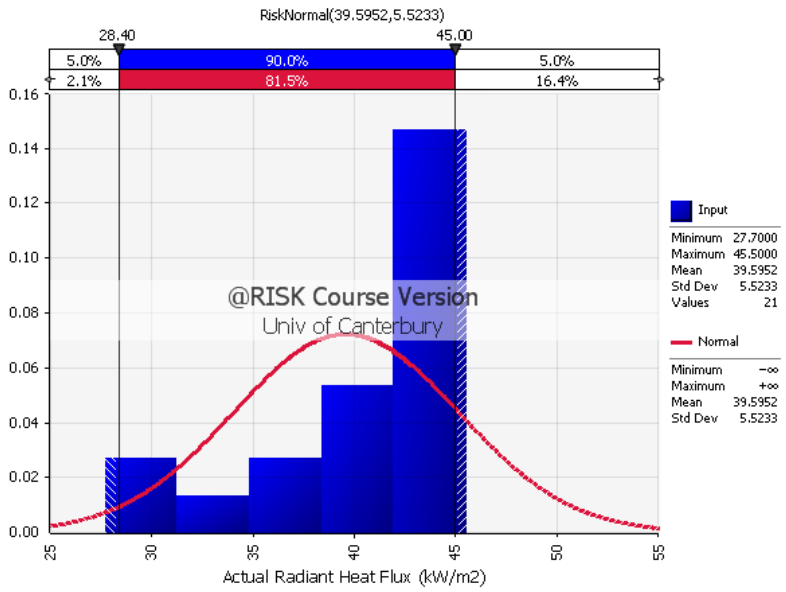

Figure 5-37: Distribution of actual radiant heat flux data for experiments with 6 mm thick samples with fallouts only

5.4.12 Prediction Model based on all 6 mm Thick Samples

This prediction model is based on 54 available experimental samples irrespective of fallout behaviour. Figure 5-38 shows the exponential distribution function parameter, plotted as a function of time after fracture, based on the experimental fallout data. From the figure, an empirical function of $\lambda = 0.951 t_1^{-0.139}$ was obtained. Substituting the function into Equation (17) yields,

$$\text{Glass fallout potential (\%)} = \text{Min}\left(-\frac{\ln\left[P_{fallout}\right] t_1^{0.139}}{0.951}, 100\right)$$

where $t_1 \leq 600$ seconds

A plot of the glass fallout potential with respect to the probability of glass fallout is shown in Figure 5-39. The distribution of actual radiant heat fluxes imposed on the glass samples is shown in Figure 5-40.

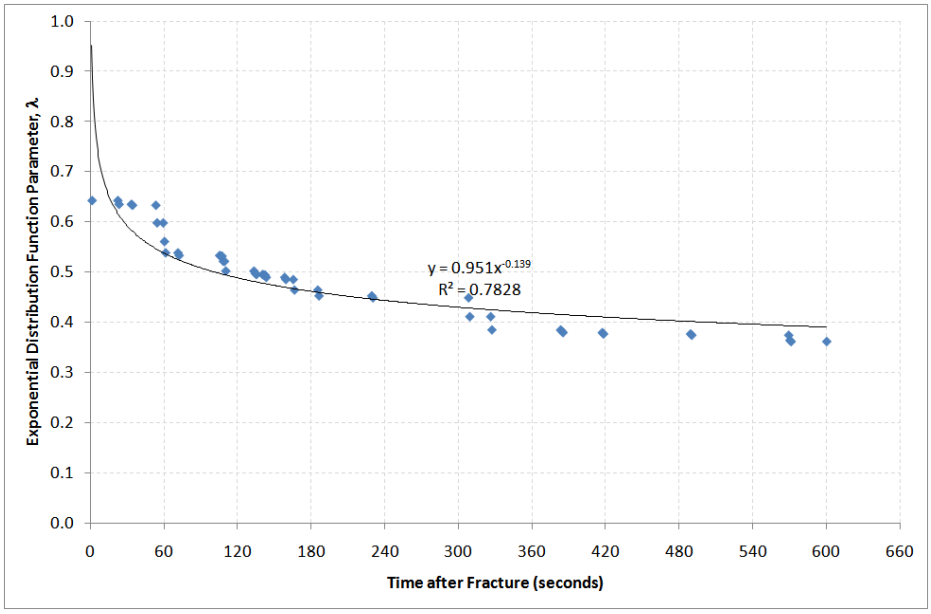

Figure 5-38: Exponential distribution function parameter for all 6 mm thick samples

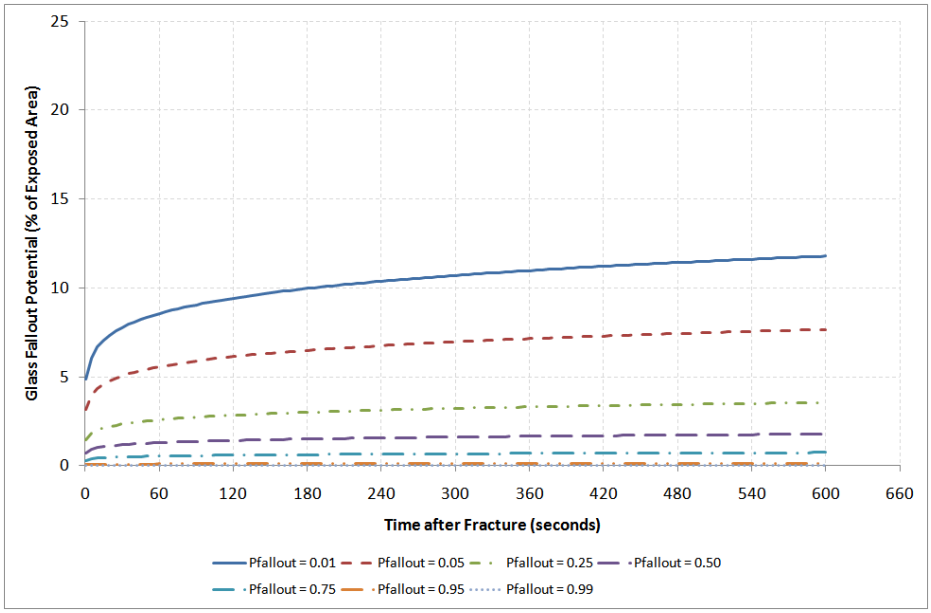

Figure 5-39: Glass fallout potential based on all 6 mm thick samples

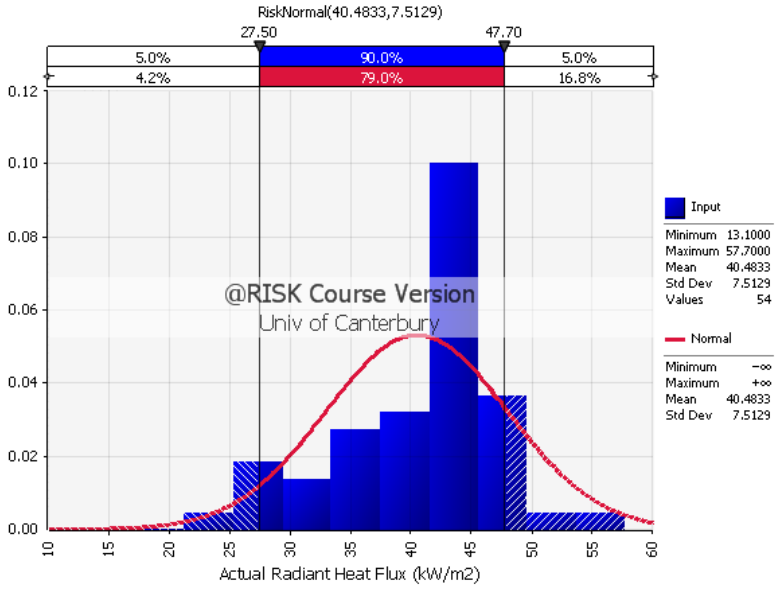

Figure 5-40: Distribution of actual radiant heat flux data for experiments with all 6 mm thick glass samples

5.4.13 Prediction Model based on all 6 mm Thick Samples with Thermocouples Attached

This prediction model is based on 15 available experimental samples irrespective of fallout behaviour. Figure 5-38 shows the exponential distribution function parameter, plotted as a function of time after fracture, based on the experimental fallout data. From the figure, an empirical function of $\lambda = 3.0713 t_1^{-0.217}$ was obtained. Substituting the function into Equation (17) yields,

$$\text{Glass fallout potential (\%)} = \text{Min}\left(-\frac{\ln\left[P_{fallout}\right] t_1^{0.217}}{3.0713}, 100\right)$$

where $t_1 \leq 600$ seconds

A plot of the glass fallout potential with respect to the probability of glass fallout is shown in Figure 5-39. The distribution of actual radiant heat fluxes imposed on the glass samples is shown in Figure 5-40.

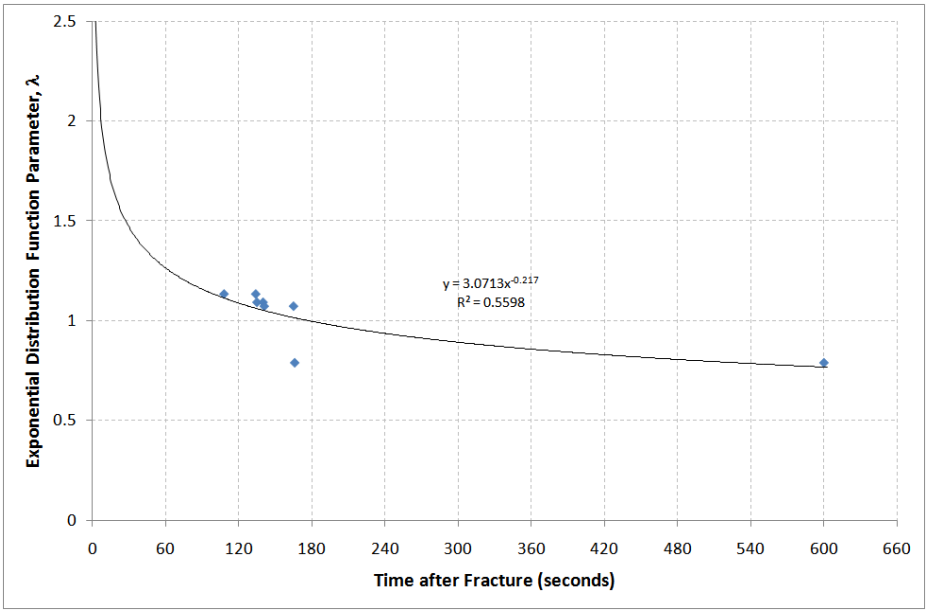

Figure 5-41: Exponential distribution function parameter for all 6 mm thick samples with thermocouples attached

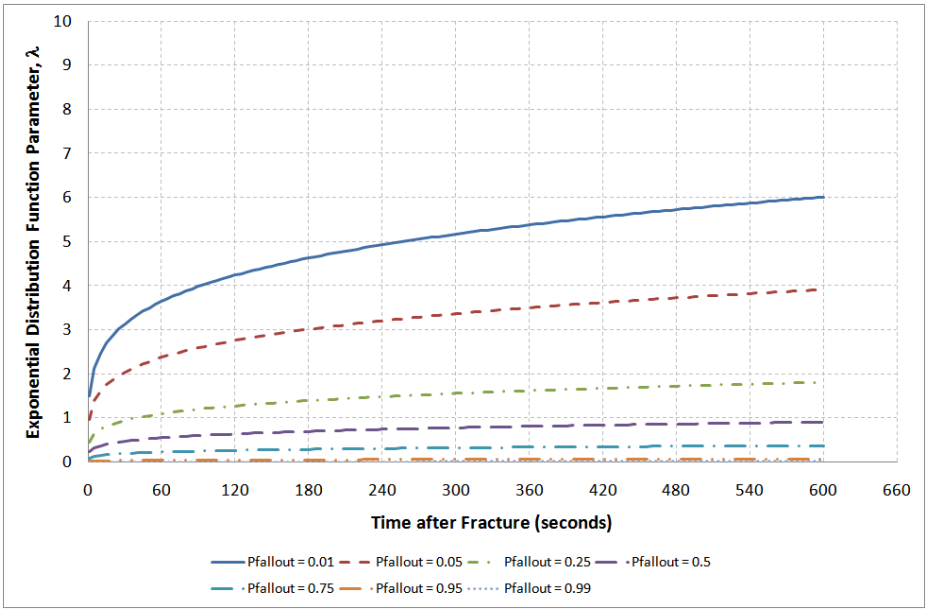

Figure 5-42: Glass fallout potential based on all 6 mm thick samples with thermocouples attached

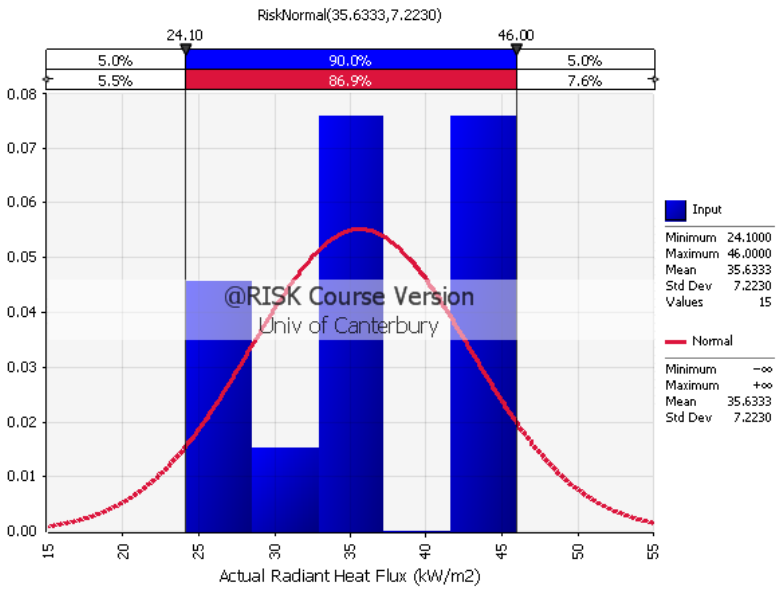

Figure 5-43: Distribution of actual radiant heat flux data for experiments with all 6 mm thick glass samples with thermocouples attached

5.4.14 Prediction Model based on all 6 mm Thick Samples with No Thermocouples Attached

This prediction model is based on 39 available experimental samples irrespective of fallout behaviour. Figure 5-44 shows the exponential distribution function parameter, plotted as function of time after fracture, based on the experimental fallout data. From the figure, an empirical function of $\lambda = 0.6147 t_1^{-0.095}$ was obtained. Substituting the function into Equation (17) yields,

$$\text{Glass fallout potential (\%)} = \text{Min}\left(-\frac{\ln\left[P_{fallout}\right] t_1^{0.095}}{0.6147}, 100\right)$$

where $t_1 \leq 600$ seconds

A plot of the glass fallout potential with respect to the probability of glass fallout is shown in Figure 5-45. The distribution of actual radiant heat fluxes imposed on the glass samples is shown in Figure 5-46.

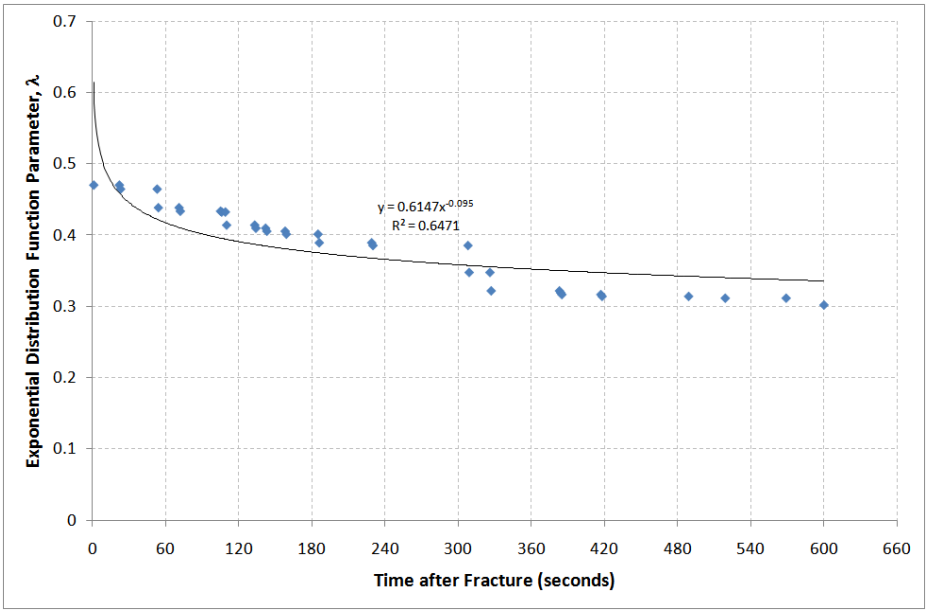

Figure 5-44: Exponential distribution function parameter for all 6 mm thick samples with no thermocouples attached

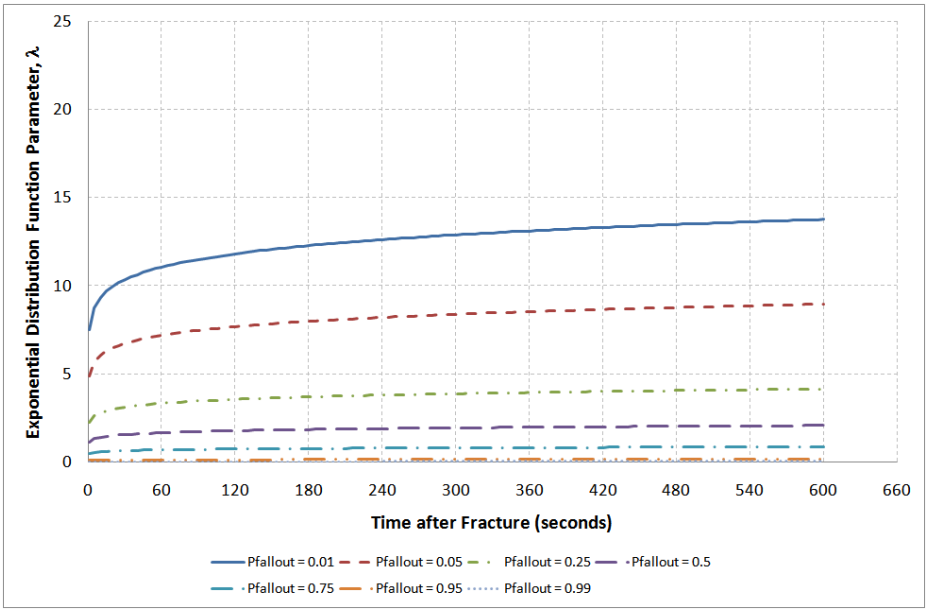

Figure 5-45: Glass fallout potential based on all 6 mm thick samples with no thermocouples attached

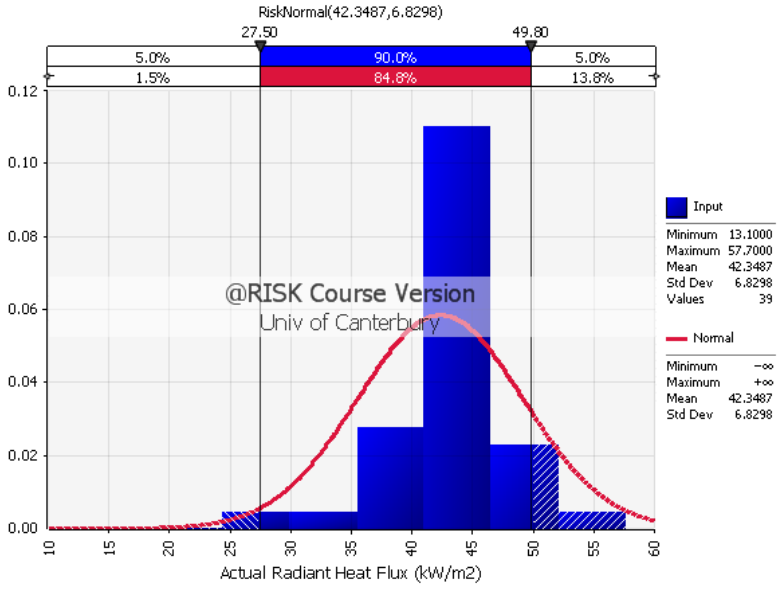

Figure 5-46: Distribution of actual radiant heat flux data for experiments with all 6 mm thick glass samples with no thermocouples attached

5.4.15 Prediction Model based on all 6 mm Thick Samples with Thermocouples Attached (Fallouts only)

This prediction model is based on 7 available experimental samples irrespective of fallout behaviour.. Figure 5-47 shows the exponential distribution function parameter, plotted as a function of time after fracture, based on the experimental fallout data. From the figure, an empirical function of $\lambda = 71.607 t_1^{-0.961}$ is obtained. Substituting the function into Equation (17) yields,

$$\text{Glass fallout potential (\%)} = \text{Min}\left(-\frac{\ln\left[P_{fallout}\right] t_1^{0.961}}{71.607}, 100\right)$$

where $t_1 \leq 600$ seconds

A plot of the glass fallout potential with respect to the probability of glass fallout is shown in Figure 5-48. The distribution of actual radiant heat fluxes imposed on the glass samples is shown in Figure 5-49.

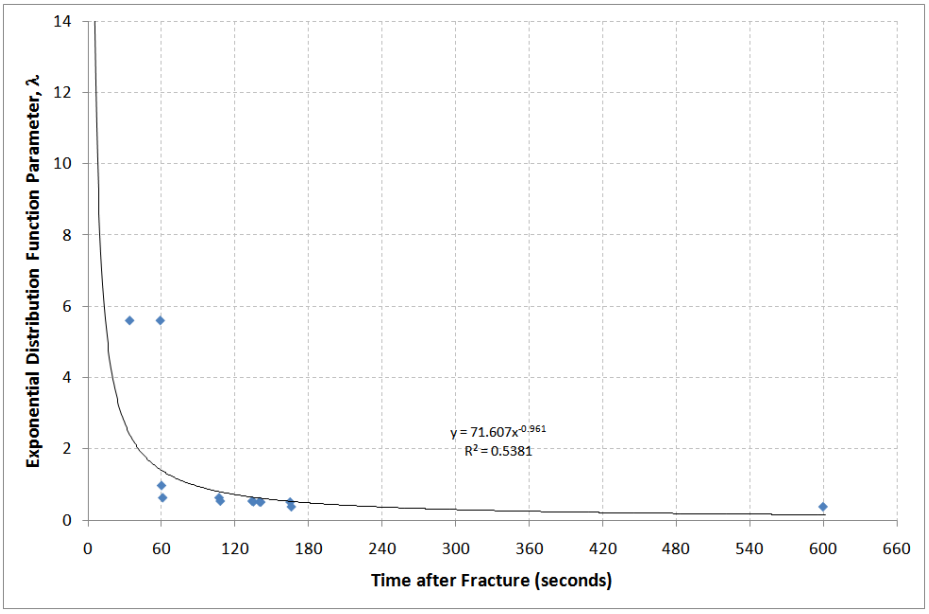

Figure 5-47: Exponential distribution function parameter for all 6 mm thick samples with thermocouples attached (Fallouts only)

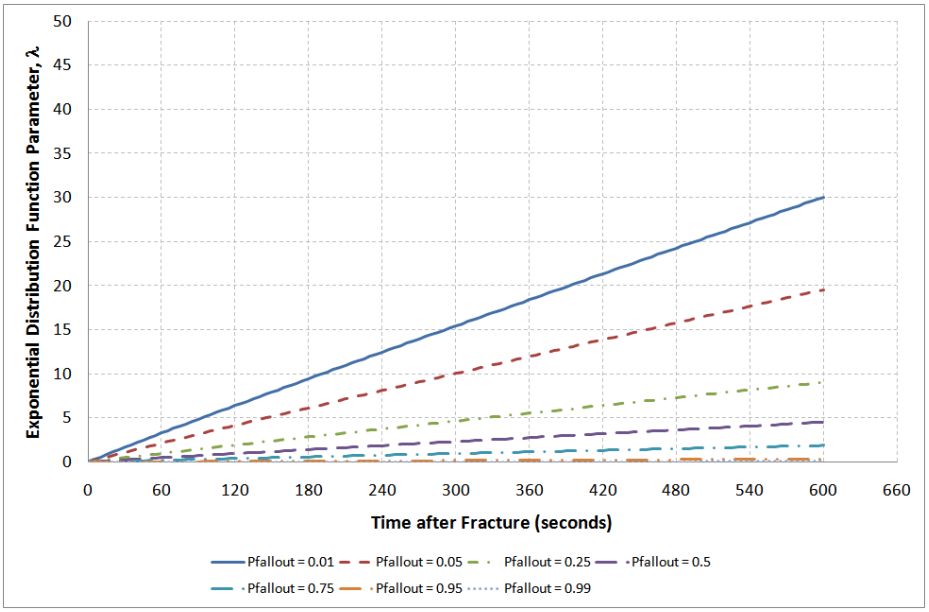

Figure 5-48: Glass fallout potential based on all 6 mm thick samples with thermocouples attached (Fallouts only)

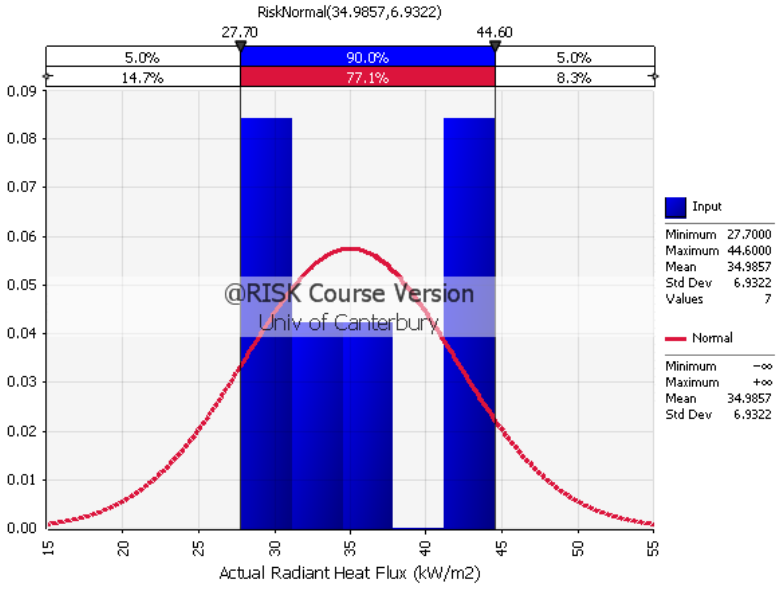

Figure 5-49: Distribution of actual radiant heat flux data for experiments with all 6 mm thick glass samples with thermocouples attached (Fallouts only)

5.4.16 Prediction Model based on all 6 mm Thick Samples with No Thermocouples Attached (Fallouts only)

This prediction model is based on 14 available experimental samples irrespective of fallout behaviour. Figure 5-50 shows the exponential distribution function parameter, plotted as a function of time after fracture, based on the experimental fallout data. From the figure, an empirical function of $\lambda = 0.239t_1^{-0.097}$ was obtained. Substituting the function into Equation (17) yields,

$$\text{Glass fallout potential (\%)} = \text{Min}\left(-\frac{\ln\left[P_{fallout}\right]t_1^{0.097}}{0.239}, 100\right)$$

where $t_1 \leq 600$ seconds

A plot of the glass fallout potential with respect to the probability of glass fallout is shown in Figure 5-51. The distribution of actual radiant heat fluxes imposed on the glass samples is shown in Figure 5-52.

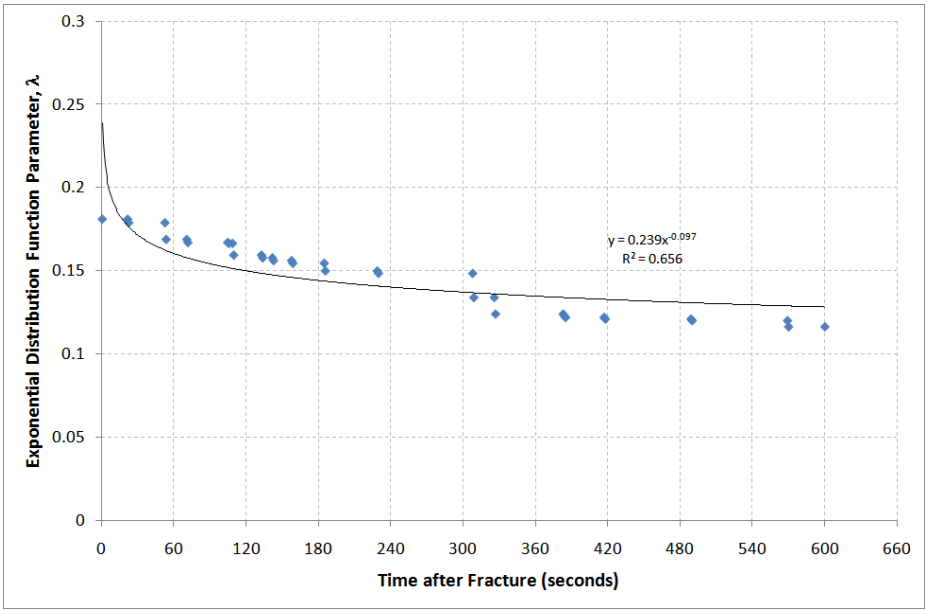

Figure 5-50: Exponential distribution function parameter for all 6 mm thick samples with no thermocouples attached (Fallouts only)

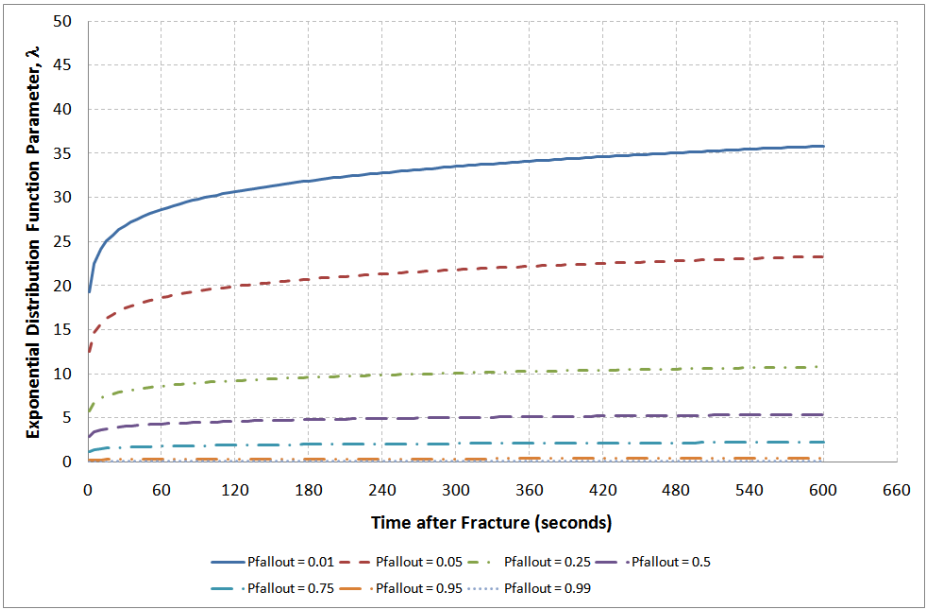

Figure 5-51: Glass fallout potential based on all 6 mm thick samples with no thermocouples attached (Fallouts only)

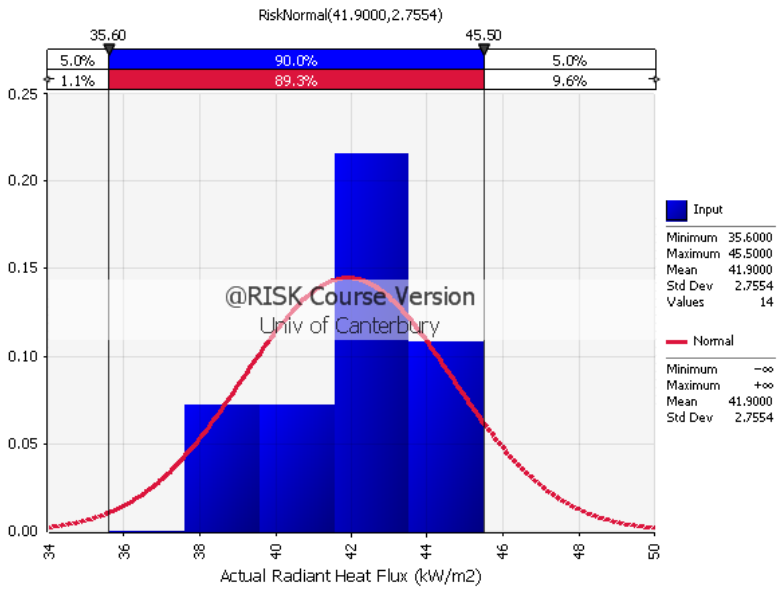

Figure 5-52: Distribution of actual radiant heat flux data for experiments with all 6 mm thick glass samples with no thermocouples attached (Fallout only)

5.4.17 Comparison between Glass Fallout Prediction Models for Glass Samples with Different Characteristics

The glass prediction model based on the 4 mm thick samples show that the experiment samples that have thermocouples attached will predict less glass fallout compared with the samples that have no thermocouples attached.

The fallout results from the experiments with 4 mm thick samples glazed with kaowool and rubber beadings and have no thermocouples attached are used to determine whether the type of beading used has an effect on the fallout behaviour. Figure 5-6 and Figure 5-12 show that the type of beading used will affect the amount and time to glass fallout. However, the sample size with the kaowool beading used was twice the sample size with the rubber beading. So, the observation based on the two figures is not considered conclusive due to the difference in sample sizes. In terms of probability, 12 out of 15 samples glazed with rubber beading had fallen out during the experiments compared with 25 out of 27 samples glazed with kaowool beading. This comparison shows that the probability of glass fallout in a sample glazed with rubber beading is similar to a sample glazed with kaowool beading. Furthermore, it was observed during the experiments, that there was still residual edge glass attached in the window frame when fallout occurred. Based on these observations, it was concluded that the type of glazing beading did not influence the fallout behaviour of the glass.

Based on the prediction models for the 4 mm thick glass and 6 mm thick glass, the general trend is that the 4 mm thick glass will have a higher amount of fallout compared with the 6 mm thick glass when the glass panes are exposed to similar radiant heat flux intensity. The probability of glass fallout is also higher for the 4 mm thick glass compared with the 6 mm thick glass under a given radiant heat flux.

5.4.18 General Equation for Glass Fallout Prediction Model

The general equation for the glass fallout prediction model is expressed as,

$$\text{Glass fallout potential (\%)} = \text{Min}\left(-\frac{\ln\left[P_{fallout}\right] t_1^{\,a_1}}{b_1}\ , 100\right) \qquad (18)$$

where $t_1 \leq 600$ seconds

Table 5-1: Summary of parameters and sample sizes for glass fallout prediction model with various experiment sample characteristics and actual radiant heat flux

Experiment Sample Characteristics	a_1	b_1	Actual Radiant heat flux (kW/m^2)	Sample Size
4 mm thick samples glazed with rubber beading and have no thermocouples attached (Fallouts only)	1.819	3103.4	42 – 49 (46)	12
4 mm thick samples glazed with kaowool beading and have thermocouples attached (Fallouts only)	0.124	0.1536	31 – 46 (40)	7
4 mm thick samples glazed with kaowool beading and have no thermocouples attached (Fallouts only)	0.277	0.2397	28 – 47 (40)	24
4 mm thick samples with fallouts only	0.432	0.7014	22 – 49 (41)	45

Table 5-1 **(con't)**

Experiment Sample Characteristics	a_1	b_1	Actual Radiant heat flux (kW/m^2)	Sample Size
All 4 mm thick samples	0.432	0.9438	13 – 49 (39)	60
All 4 mm thick samples with thermocouples attached	0.195	0.5419	13 – 46 (35)	19
All 4 mm thick samples with no thermocouples attached	0.400	0.6376	28 – 49 (42)	41
All 4 mm thick samples with thermocouples attached (Fallouts only)	0.195	0.2567	22 – 46 (37)	9
4 mm thick samples with no thermocouples attached (Fallouts only)	0.400	0.5601	28 – 49 (42)	36
6 mm thick samples glazed with kaowool beading and have no thermocouples attached (Fallouts only)	0.075	0.1912	36 – 46 (42)	13
6 mm thick samples with fallouts only	0.139	0.3698	28 – 46 (40)	21
All 6 mm thick samples	0.139	0.9510	13 – 58 (41)	54
All 6 mm thick samples with thermocouples attached	0.217	3.0713	24 – 46 (36)	15
All 6 mm thick samples with no thermocouples attached	0.095	0.6147	13 – 58 (42)	39
6 mm thick samples with thermocouples attached (Fallouts only)	0.961	71.6070	28 – 45 (35)	7
6 mm thick samples with no thermocouples attached (Fallouts only)	0.097	0.2390	36 – 46 (42)	14
Note: Mean actual radiant heat flux shown in bracket				

Two types of probabilities are used in the glass fallout prediction methodology. The Bayesian probability is used to describe the probability of glass fallout in the glass fallout prediction model while the Frequency probability is used to describe the probability of glass fallout determined from the results of the experiments. The Bayesian probability deals with the concept of uncertainties and probabilities are assigned based on an individual's belief in the occurrence of an event. The Frequency probability is based on the occurrence of an event determined from trials carried out.

The term "probability of glass fallout occurrence" will be used to describe the probability associated with the Frequency probability while the term "probability of glass fallout" will apply to the Bayesian probability. The probability of glass fallout occurrence for various experimental sample characteristics is summarised in Table 5-2.

It is recognized that actual windows do not have thermocouples attached onto the glass panes. In order to apply the results from the experiments to actual windows, the parameters from the experiments with samples with no thermocouples attached irrespective of beading type were used in the glass fallout prediction model. These parameters are summarised in Table 5-3 to Table 5-5.

Table 5-2: Probability of glass fallout occurrence for various experimental sample characteristics

Experimental Sample Characteristics	Probability of glass fallout
All 4 mm thick samples (Based on 63 experiments)	0.7619
All 4 mm thick samples with thermocouples attached (Based on 21 experiments)	0.5238
All 4 mm thick samples with no thermocouples attached (Based on 42 experiments)	0.8810
All 6 mm thick samples (Based on 54 experiments)	0.3889
All 6 mm thick samples with thermocouples attached (Based on 15 experiments)	0.4667
All 6 mm thick samples with no thermocouples attached (Based on 39 experiments)	0.3590

Table 5-3: Probability of glass fallout occurrence for different glass thicknesses

Glass Thickness	Probability of glass fallout occurrence
4 mm	0.881
6 mm	0.359

Table 5-4: Parameters for glass prediction model for different glass thickness based on all experiments irrespective of fallout behaviour

Glass Thickness	a_1	b_1
4 mm	0.400	0.6376
6 mm	0.095	0.6147

Table 5-5: Parameters for glass prediction model for different glass thickness based on experiments displaying fallout behaviour only

Glass Thickness	a_1	b_1
4 mm	0.400	0.5601
6 mm	0.097	0.2390

5.4.19 Procedure to use Glass Fallout Prediction Model

The recommended steps to use the glass fallout prediction model to predict the amount of glass fallout of single glazing in a fire is summarised in the flowcharts shown in Figure 5-53 and Figure 5-54. Numerical simulation in the form of a computer program (e.g. BRANZFire) could be used to carry out the heat transfer analysis and determine the time to glass fracture. In the absence of a computer program, the heat transfer analysis can be carried out manually and the time to glass facture can be determined using the lumped heat capacity method.

It should be noted that the probability of glass fallout ($P_{fallout}$) in the glass prediction model should not be taken directly from Table 5-3 as the probability of glass fallout occurrence in the table is based on

the fallout data from the experiments irrespective of the amount of fallout which was discussed earlier. Further studies are still required into the selection of the glass fallout probability for analysis purposes and this subject is not covered in this research report.

Two flowcharts are provided to guide the user to use the glass fallout prediction model. The main difference between the flowcharts is that Flowchart B includes an additional step that requires the user to select the probability of glass fallout occurrence from Table 5-3.

The parameters in Table 5-3 are based on the fallout results with experiment samples displaying fallout behaviour only while the parameters in Table 5-4 used in the glass prediction model in Flowchart A are based on the results of experiments irrespective of fallout behaviour.

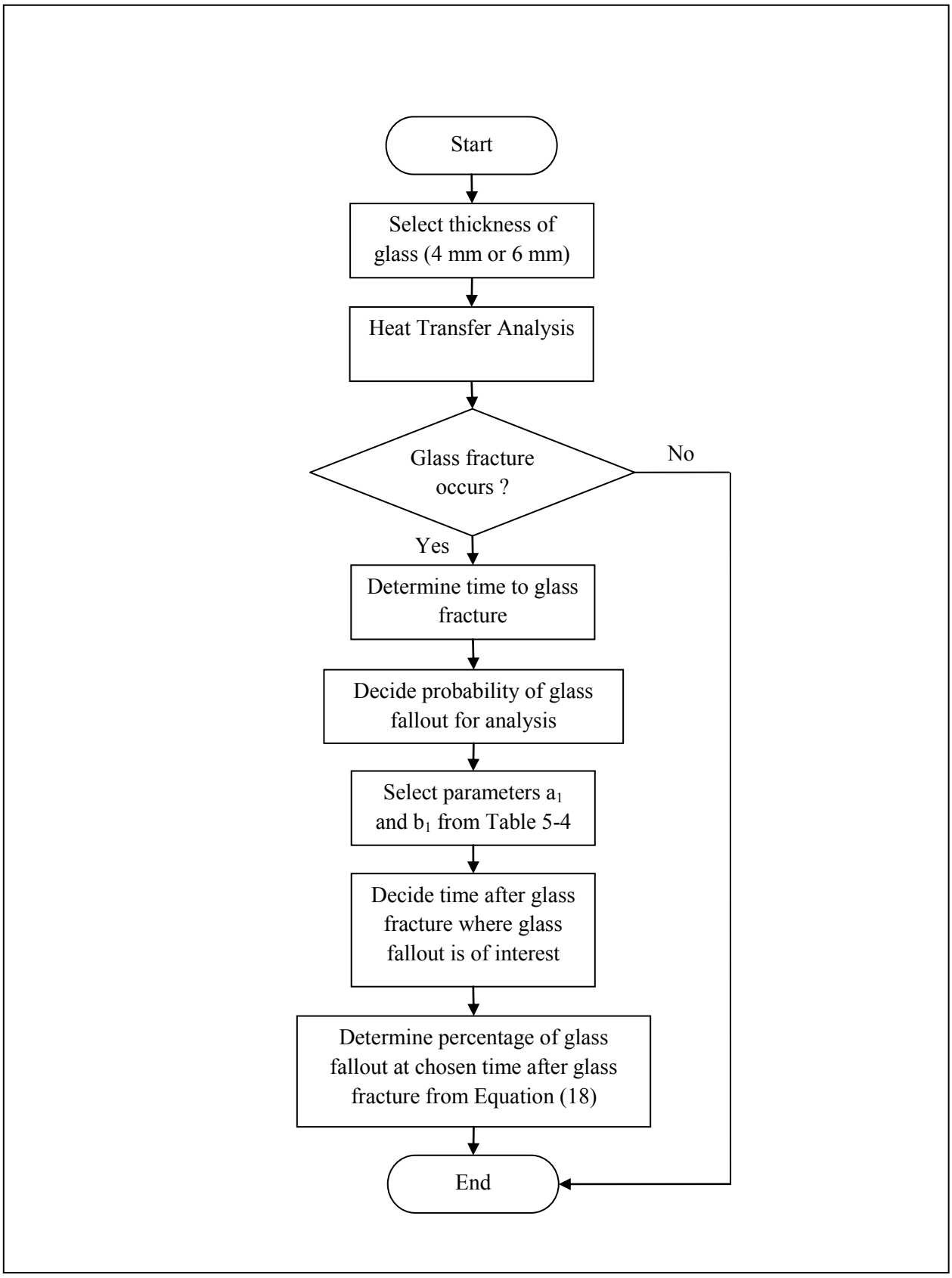

Figure 5-53: Flowchart A outlining the glass fallout prediction methodology

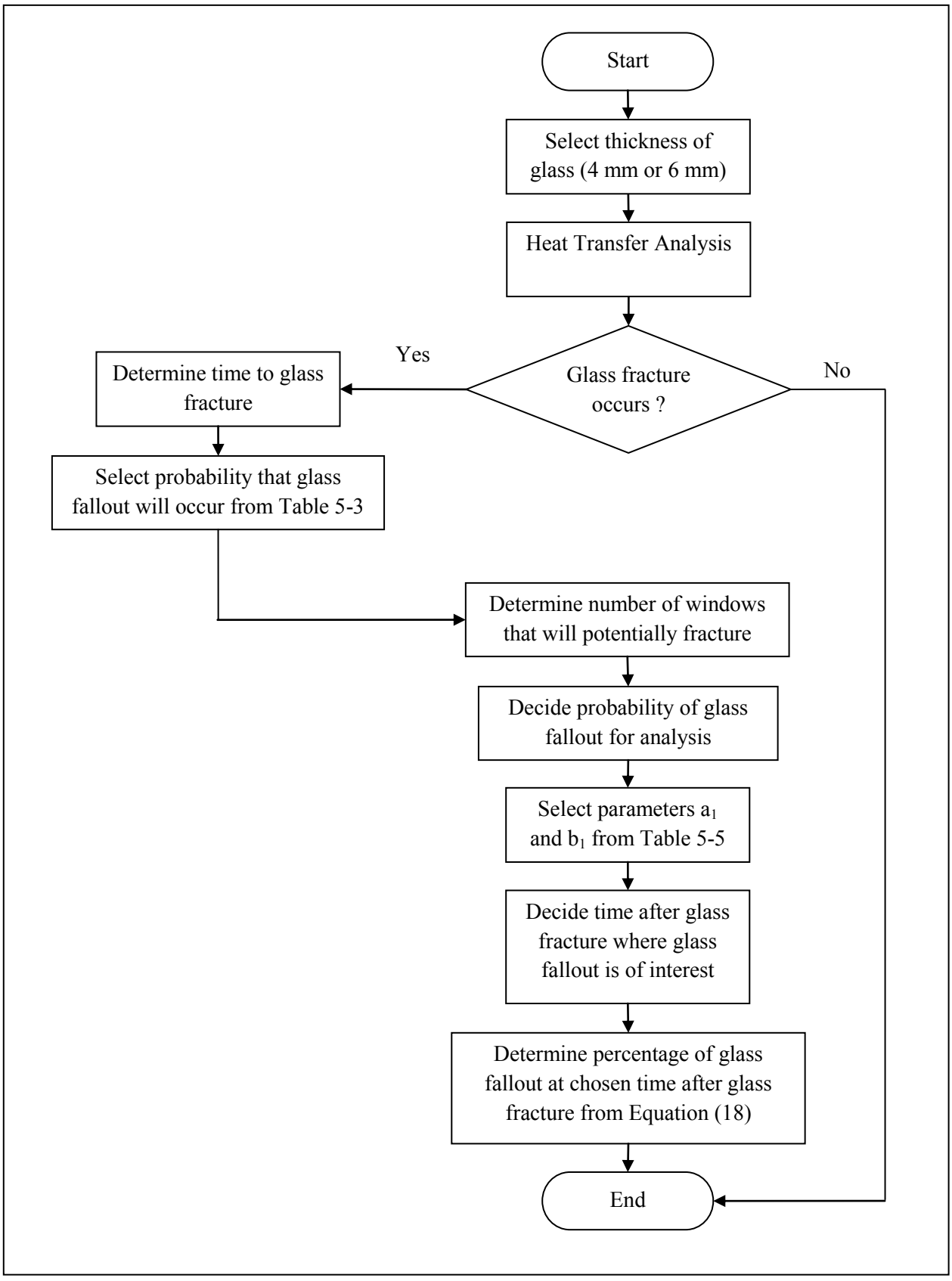

Figure 5-54: Flowchart B outlining the glass fallout prediction methodology

6 CONCLUSIONS

A total 117 experiments were carried involving 4 mm and 6 mm thick glass samples glazed with either rubber or kaowool beading. The samples were exposed to radiant heat fluxes ranging from 14 kW/m^2 to 59 kW/m^2. The average radiant heat flux from the experiment is although most of the heat fluxes ranged from 43 kW/m^2 to 47 kW/m^2.

Material properties for the glass samples were derived from the four-point bending test with twenty-four specimens. The mean fracture strength and modulus of elasticity of glass derived from the test data were 64 MPa ± 15 MPa and 76.5 ± 4.0 MPa respectively. The fracture strength and the modulus of elasticity can be described with a 3-parameter Weibull distribution and normal distribution respectively.

The time to glass fracture could be predicted using the lumped heat capacity method although the method is less accurate for 6 mm thick glass panes compared with 4 mm thick glass panes. The fracture criterion which is incorporated into fire modelling program with glass heat transfer routine can also be used to predict the time to glass fracture. However this method is highly dependent on the fracture strength of the glass. Based on the comparison between the predicted and actual times to glass fracture, there was good agreement with 60% of the experiments.

The mean temperature differences at glass fracture that were determined from the experimental data were between 90 °C to 98 °C. The temperature differences at glass fracture were predicted using the fracture criterion suggested by Keski-Rahkonen (1988). The predicted temperature differences at glass fracture ranged from 55 °C to 129 °C. Based on the comparison between the predicted and actual temperature differences at glass fracture, there was good agreement with 60% of the experiments

The measured thermal strains at fracture ranged between 239 μstrain to 697 μstrain.

The type of glazing beading did not influence the fallout behaviour of the glass as when fallout occurs, there were still residual edge glass attached in the window frame. The occurrence of fallout was also less likely and amount of fallout was lesser for a thicker piece of glass than that of a thinner piece of glass for a given heat flux.

Generally, when fallout behaviour was observed for a glass sample, the fallout took place at a time long after glass fracture and not immediately after the initial fracture. When a glass sample did exhibit fallout behaviour, the amount of fallout did not correspond to 100% of the window opening. The

occurrence, time and amount of glass fallout are random events.

The fallout behaviour of glass can be described with an exponential distribution and a glass fallout prediction model was derived for the 4 mm and 6 mm thick glass using the exponential distribution function. However, the application of the model is subjected to the limitations imposed by the conditions that exist in the experiments.

7 RECOMMENDATIONS FOR FURTHER WORK

Based on the experimental work and findings of this research, a number of issues arose and further work is required to look into these issues in more detail. In this research, 117 glass samples were exposed to radiant heat from a burner fire. However, these 117 glass samples consisted of samples with different characteristics as some samples were glazed with either kaowool or rubber beading, and had thermocouples attached onto the glass. In additional, two thicknesses were used in this research. In order to improve the reliability of the glass prediction model, more data would be required. Therefore, it is recommended that more similar experiments be carried out to improve the model.

During the course of this research, each glass sample was gently tapped by hand after each experiment to examine whether any additional force will induce the fractured glass samples to fallout. Generally, a gentle tap on the glass was sufficient to either cause the fractured glass sample to fallout or increase the amount of fallout where fallout had occurred. However, since cooling has taken place and the glass sample would have shrunk and increase the gap between the cracked glass pieces, fallout in most samples would have been inevitable. There is certainly a need to investigate the condition where there is pressure acting on the glass. A source of the pressure could be the expanding air in the compartment due to the fire. This condition is not simulated in this research as the "compartment effect" does not exist since air is constantly being extracted from the fire lab via the calorimeter hood. The "compartment effect" could be replicated by using a small-scale compartment and attaching the glass sample to one of the walls as discussed in the work by Shields (2001 and 2002). A compartment would also induce a "layering effect" where non-uniform heating that will induce a vertical thermal gradient on the glass panes.

Another recommendation would be introducing glass panes of various sizes into future researches. These sizes of these glass samples should represent the typical sizes of glass windows being used in the window industry so the results could be applied to actual conditions.

The types of window frames which are effectively the restraint condition for the glass could be varied to investigate the effects of different frames have on the fallout behaviour of the glass similar to the work carried out by Mowrer (1997) but with an larger sample size for each type of frame.

In this research, the glass samples were exposed to the radiant heat fluxes ranging from 13 kW/m^2 to 58 kW/m^2. The varying radiant heat flux levels are due to the turbulent nature of the flame and air flow in the fire lab. It is recommended that a radiant panel be used to achieve a steadier and uniform heat flux. The experiment should be carried out using radiant heat flux levels ranging of heat fluxes from a critical fracture flux but unlikely to cause the glass to fracture to a fully developed fire.

8 REFERENCES

Babraukas, V., *Glass Breakage in Fires*, World Wide Web, www.doctorfire.com/glass.html, Accessed 2nd March 2010.

Emmons, H. W., (1986), *The Needed Fire Science*, Proceedings of the First International Symposium on Fire Safety Science, Washing D.C., USA, pp. 33-53.

Harada, K., Enomoto, A., Uede, K., and Wakamatsu, T. (2000), *An Experimental Study on Glass Cracking and Fallout by Radiant Heat Exposure*. Proceedings of the Sixth International Symposium on Fire Safety Science, France, pp. 1063 – 1074.

Hietaniemi, J. (2005), *Probabilistic Simulation of Glass Fracture and Fallout in Fire,* VTT Working Papers 41, VTT Building and Transport, Finland.

Joshi, A. A., and Pagni, P. J. (1991b), *Users' Guide to BREAK1*, *The Berkeley Algorithm for Breaking Window Glass in Compartment Fire*, NIST-GCR-91-595.

Joshi, A. A., and Pagni, P. J. (1994a), *Fire-Induced Thermal Fields in Window Glass I – Theory*, Fire Safety Journal, Vol. 22, pp. 25 – 43.

Joshi, A. A., and Pagni, P. J. (1994b), *Fire-Induced Thermal Fields in Window Glass II – Experiments*, Fire Safety Journal, Vol. 22, pp. 45 – 65.

Kang, K. (2009), Assessment of a Model Development for Window Glass Breakage due to Fire Exposure in a Fire Model, Fire Safety Journal, Vol. 44, pp. 415 – 424, DOI: 10.1016/j.firesaf.2008.09.002.

Keshi-Rahkonen, O. (1988), *Breaking of Window Glass Close to Fire*, Fire and Materials, Vol. 12, pp. 61 – 69.

McGrattan, K. (2005), *Fire Dynamics Simulator (Version 4) – Technical Reference Guide*, NIST Special Publication 1018, July 2005.

McGrattan, K. (2006), *Fire Dynamics Simulator (Version 4) – Technical Reference Guide*, NIST Special Publication 1018, March 2006.

Mikhelson, I., (2004), *Structural Engineering Formulas*, McGraw-Hill, United States of America.

Mowrer, F. W. (1997), *Window breakage induced by exterior fires*, 2nd International Conference on Fire Research and Engineering (ICFRE2), Gaithersburg, MD, August 3 – 8, pp. 404-415.

Mun, J. (2006), *Modelling Risk: Applying Monte Carlo Simulation, Real Options Analysis, Forecasting, and Optimization Techniques*, John Wiley & Sons Inc, United States of America.

Pagni, P. J. And Joshi, A. A. (1991a), *Glass Breaking in Fires*, Fire Safety Science – Proceedings of the Third International Symposium, Hemisphere, Washington, D. C., pp. 791 - 802.

Pagni, P. J. (2003), *Thermal Glass Breakage*, Fire Safety Science – Proceedings of the Seventh International Symposium, Worcester, MA, pp. 3 - 22.

Parry, R. (2002), *Implementation of a Glass Fracture Module for the BRANZfire Compartment Fire Zone Modelling Software: A Research Project Report Presented as Partial Fulfilment of the Requirements for the Degree of Master of Engineering in Fire Engineering*, Department of Civil Engineering, University of Canterbury, Christchurch, New Zealand.

Pope, N. D., and Bailey, C. G. (2007), *Development of a Gaussian Glass Breakage Model within a Fire Field Model*, Fire Safety Journal, Vol. 42, Issue 5, July 2007, pp. 366 – 376, DOI: 10.1016/j.firesaf.2006.12.005.

Sincaglia, P. E., and Barnett J. R. (1997), *Development of a Glass Window Fracture Model for Zone-Type Computer Fire Codes*, Journal of Fire Protection Engineering, Vol. 8, pp. 101 – 118, DOI: 10.1177/104239159600800301.

Shields, T. J., Silcock, G. W. H., and Flood, M. F. (2001), *Performance of a Single Glazing Assembly Exposed to Enclosure Corner Fires of Increasing Severity*, Fire and Materials, Vol. 25, pp. 123 – 152, DOI: 10.1002/fam.764.

Shields, T. J., Silcock, G. W. H., and Flood, M. F. (2002), *Performance of a Single Glazing Assembly Exposed a Fire in the Centre of an Enclosure*, Fire and Materials, Vol. 26, pp. 51 – 75, DOI: 10.1002/fam.783.

Shields, T. J., Silcock, G. W. H., and Flood, M. F. (2005), *Behaviour of Double Glazing in Corner Fires*, Fire Technology, Vol. 41, pp. 37 – 65.

Skelly, M. J., Roby, R. J., and Beyler, C. L. (1991), *An Experimental Investigation of Glass Breakage in Compartment Fires*, Journal of Fire Protection Engineering, Vol. 3, No. 1, pp. 25 – 34, DOI: 10.1177/104239159100300103.

SNZ, *Glazing in Buildings*, NZS 4224.1:2008, New Zealand Standards, Wellington, New Zealand, 2008.

Wade, C. A. (2000), BRANZFIRE Tecnical Reference Guide, BRANZ Study Report 92, Building Research Association of New Zealand, Judgeford, New Zealand.

APPENDIX A - EXPERIMENTAL APPARATUS

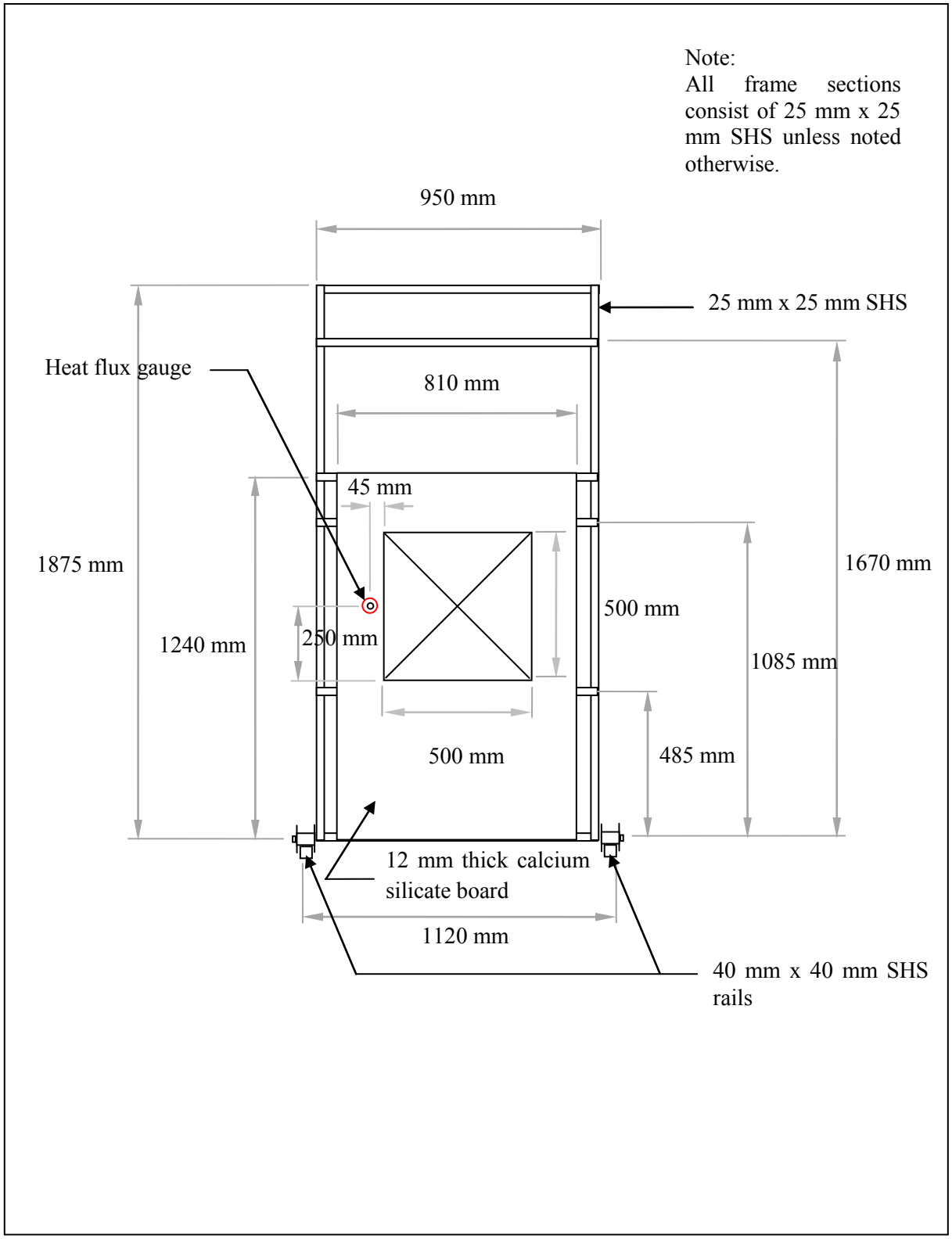

Figure A-1: Front (face exposed to fire) of main frame with glass sample not in place

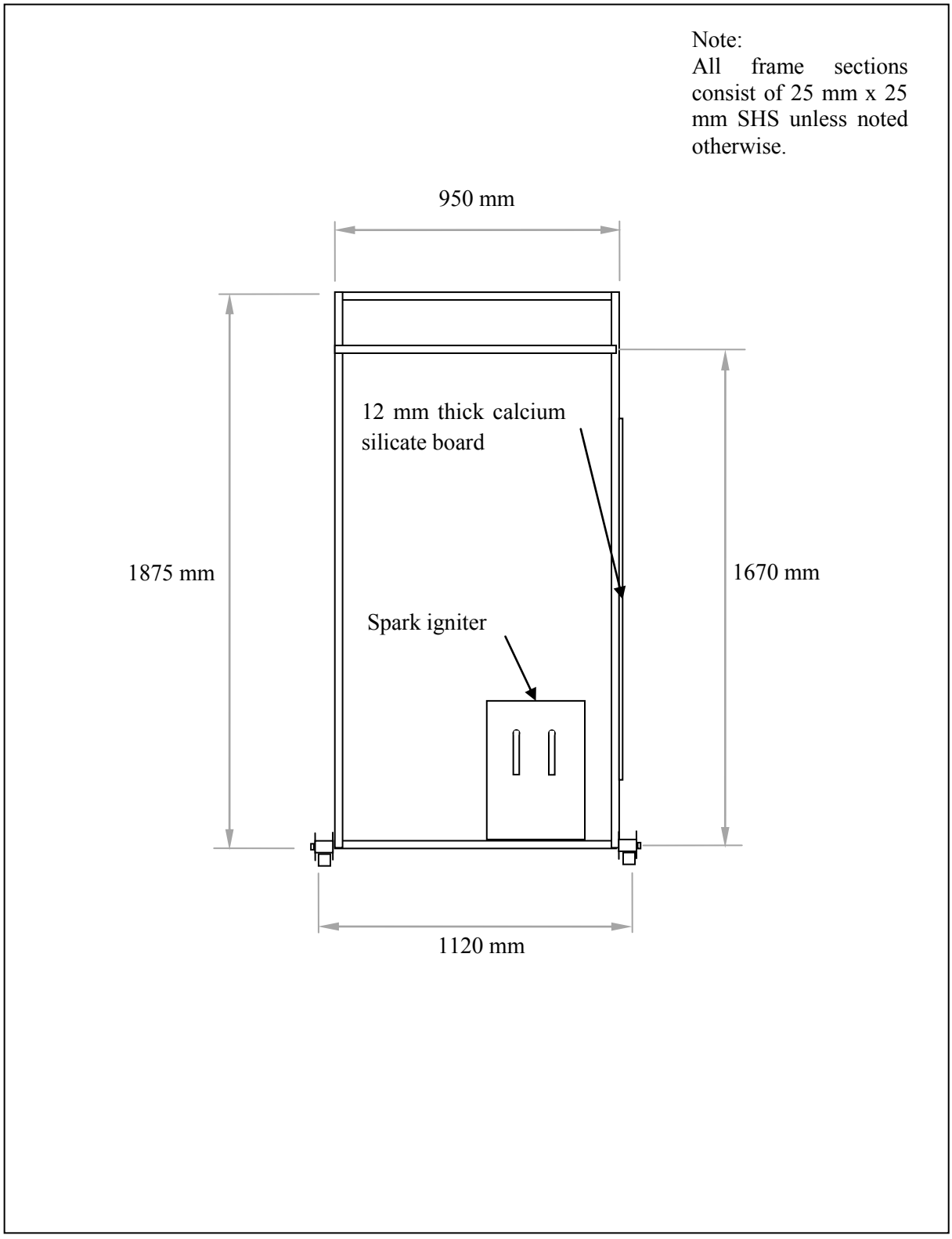

Figure A-2: Front view of radiation shield frame

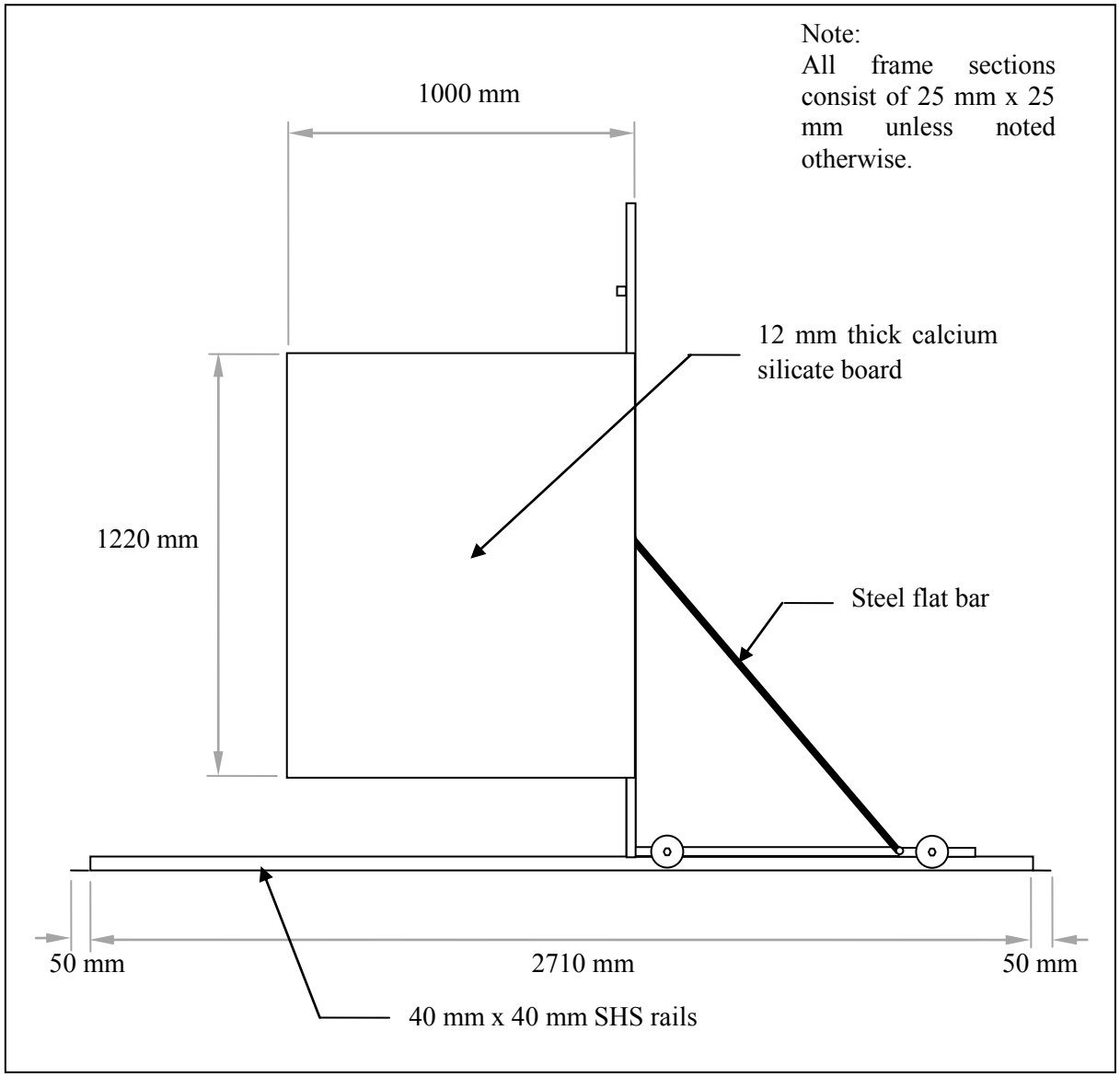

Figure A-3: Elevation view of radiation shield frame

APPENDIX B - EXPERIMENT SAMPLE CHARACTERISTICS

Table B-1: Summary of characteristics for 4 mm thick glass samples

Experiment Sample	Type of Beading	Glass Thermocouples Attached
4 Test 1	Rubber	Yes
4 Test 2	Rubber	Yes
4 Test 3	Rubber	Yes
4 Test 4	Not included in research	
4 Test 5	Rubber	Yes
4 Test 6	Rubber	Yes
4 Test 7	Rubber	Yes
4 Test 8	Kaowool	Yes
4 Test 9	Kaowool	Yes
4 Test 10	Kaowool	Yes
4 Test 11	Kaowool	Yes
4 Test 12	Kaowool	Yes
4 Test 13	Kaowool	Yes
4 Test 14	Kaowool	No
4 Test 15	Kaowool	No
4 Test 16	Kaowool	No

Table B-1 **(con't)**

Experiment Sample	Type of Beading	Glass Thermocouples Attached
4 Test 17	Kaowool	No
4 Test 18	Kaowool	Yes
4 Test 19	Kaowool	No
4 Test 20	Kaowool	No
4 Test 21	Kaowool	Yes
4 Test 22	Kaowool	No
4 Test 23	Kaowool	No
4 Test 24	Kaowool	No
4 Test 25	Kaowool	No
4 Test 26	Kaowool	Yes
4 Test 27	Kaowool	No
4 Test 28	Kaowool	Yes
4 Test 29	Kaowool	No
4 Test 30	Kaowool	No
4 Test 31	Kaowool	No
4 Test 32	Kaowool	No
4 Test 33	Kaowool	No
4 Test 34	Kaowool	No

Table B-1 **(con't)**

Experiment Sample	Type of Beading	Glass Thermocouples Attached
4 Test 35	Kaowool	No
4 Test 36	Kaowool	No
4 Test 37	Kaowool	Yes
4 Test 38	Kaowool	No
4 Test 39	Kaowool	No
4 Test 40	Kaowool	No
4 Test 41	Kaowool	No
4 Test 42	Kaowool	No
4 Test 43	Kaowool	No
4 Test 44	Rubber	No
4 Test 45	Rubber	No
4 Test 46	Rubber	No
4 Test 47	Rubber	No
4 Test 48	Rubber	No
4 Test 49	Rubber	No
4 Test 50	Rubber	No
4 Test 51	Rubber	No
4 Test 52	Rubber	Yes

Table B-1 **(con't)**

Experiment Sample	Type of Beading	Glass Thermocouples Attached
4 Test 53	Rubber	No
4 Test 54	Rubber	No
4 Test 55	Rubber	No
4 Test 56	Rubber	No
4 Test 57	Rubber	Yes
4 Test 58	Rubber	No
4 Test 59	Rubber	No
4 Test 60	Kaowool	No
4 Test 61	Kaowool	Yes
4 Test 62	Rubber	No
4 Test 63	Kaowool	No
4 Test 64	Rubber	Yes

Table B-2: Summary of characteristics for 6 mm thick glass samples

Experiment Sample	Type of Beading	Glass Thermocouples Attached
6 Test 1	Rubber	Yes
6 Test 2	Not included in research	
6 Test 3	Rubber	Yes
6 Test 4	Rubber	Yes

Table B-2 **(con't)**

Experiment Sample	Type of Beading	Glass Thermocouples Attached
6 Test 5	Rubber	Yes
6 Test 6	Rubber	Yes
6 Test 7	Rubber	Yes
6 Test 8	Kaowool	Yes
6 Test 9	Kaowool	Yes
6 Test 10	Kaowool	Yes
6 Test 11	Kaowool	No
6 Test 12	Kaowool	No
6 Test 13	Kaowool	No
6 Test 14	Kaowool	No
6 Test 15	Kaowool	No
6 Test 16	Kaowool	No
6 Test 17	Kaowool	No
6 Test 18	Kaowool	No
6 Test 19	Kaowool	Yes
6 Test 20	Kaowool	No
6 Test 21	Kaowool	No
6 Test 22	Kaowool	No
6 Test 23	Kaowool	No
6 Test 24	Kaowool	No
6 Test 25	Kaowool	No
6 Test 26	Kaowool	No
6 Test 27	Kaowool	No
6 Test 28	Kaowool	No

Table B-2 **(con't)**

Experiment Sample	Type of Beading	Glass Thermocouples Attached
6 Test 29	Kaowool	Yes
6 Test 30	Kaowool	No
6 Test 31	Kaowool	No
6 Test 32	Kaowool	No
6 Test 33	Kaowool	Yes
6 Test 34	Kaowool	No
6 Test 35	Kaowool	No
6 Test 36	Kaowool	No
6 Test 37	Kaowool	No
6 Test 38	Kaowool	No
6 Test 39	Kaowool	No
6 Test 40	Kaowool	No
6 Test 41	Rubber	No
6 Test 42	Rubber	Yes
6 Test 43	Rubber	No
6 Test 44	Rubber	No
6 Test 45	Rubber	No
6 Test 46	Rubber	No
6 Test 47	Kaowool	Yes
6 Test 48	Kaowool	No
6 Test 49	Kaowool	No
6 Test 50	Rubber	No
6 Test 51	Not included in research	
6 Test 52	Rubber	Yes

Table B-2 **(con't)**

Experiment Sample	Type of Beading	Glass Thermocouples Attached
6 Test 53	Rubber	No
6 Test 54	Rubber	No
6 Test 55	Rubber	No
6 Test 56	Rubber	No

APPENDIX C - TEMPERATURE PROFILES

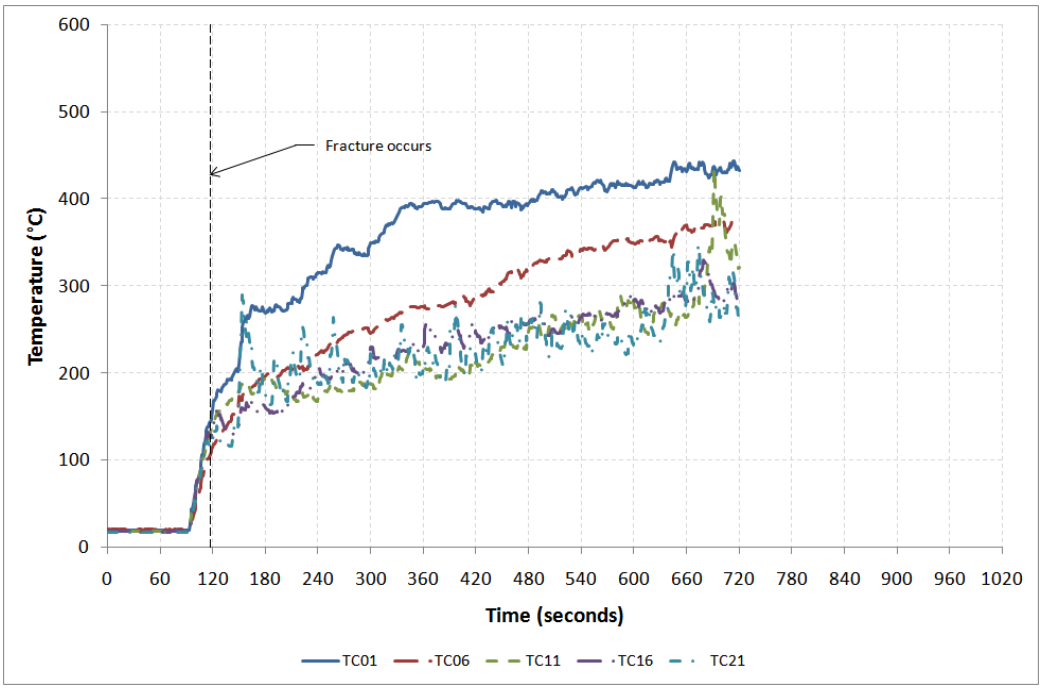

Figure C-1: Gas temperature profiles for experiment 4 Test 1

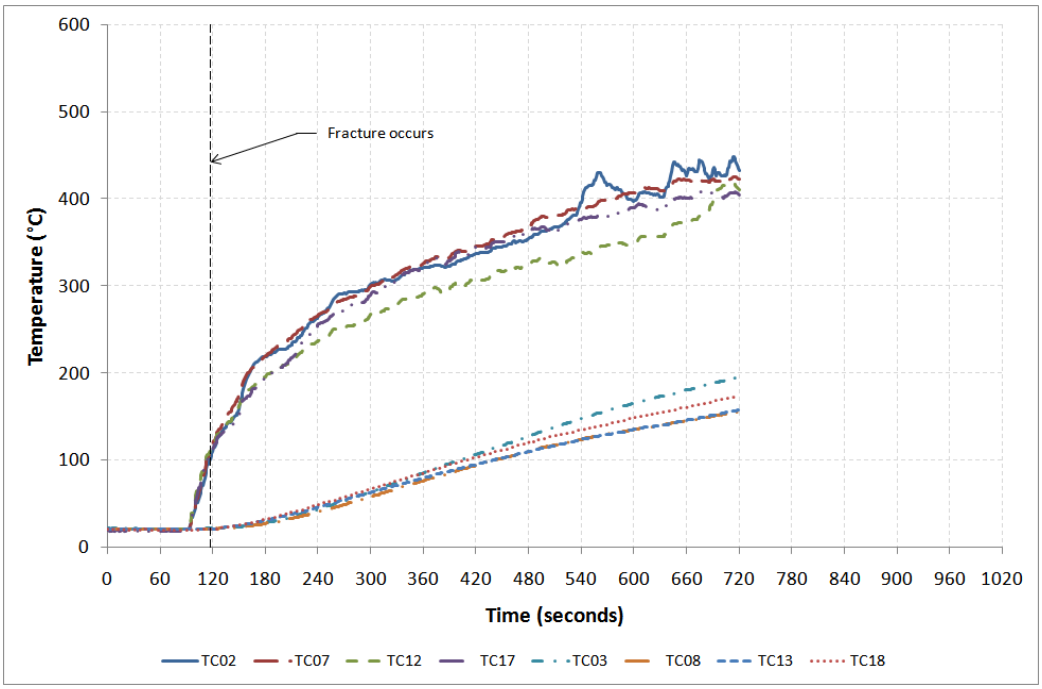

Figure C-2: Glass temperature profiles on exposed side for experiment 4 Test 1

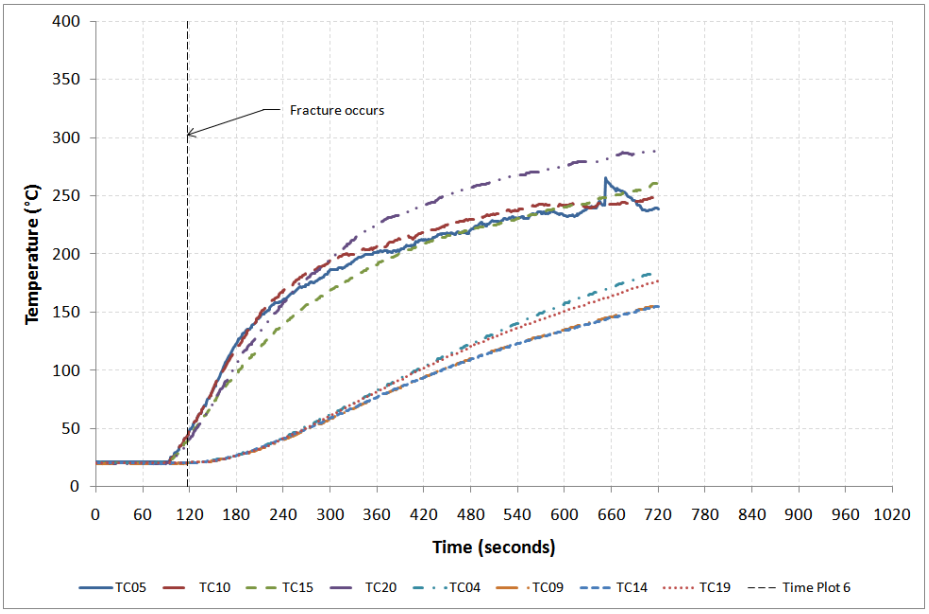

Figure C-3: Glass temperature profiles on unexposed side for experiment 4 Test 1

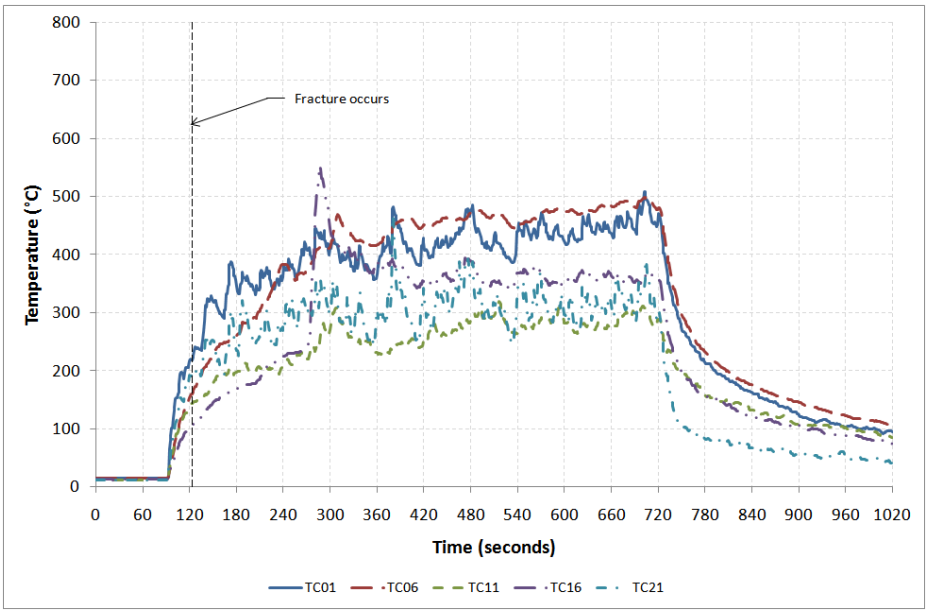

Figure C-4: Gas temperature profiles for experiment 4 Test 3

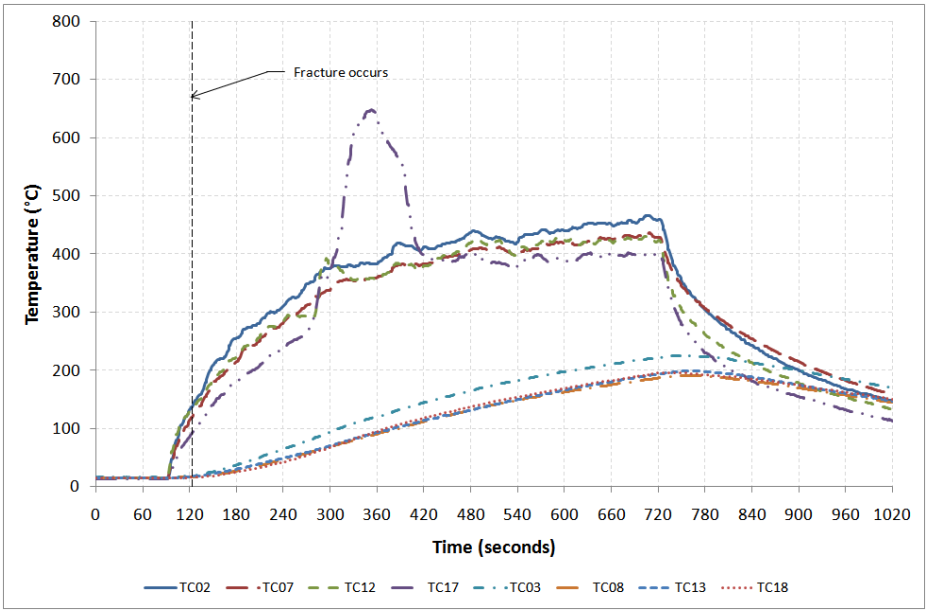

Figure C-5: Glass temperature profiles on exposed side for experiment 4 Test 3

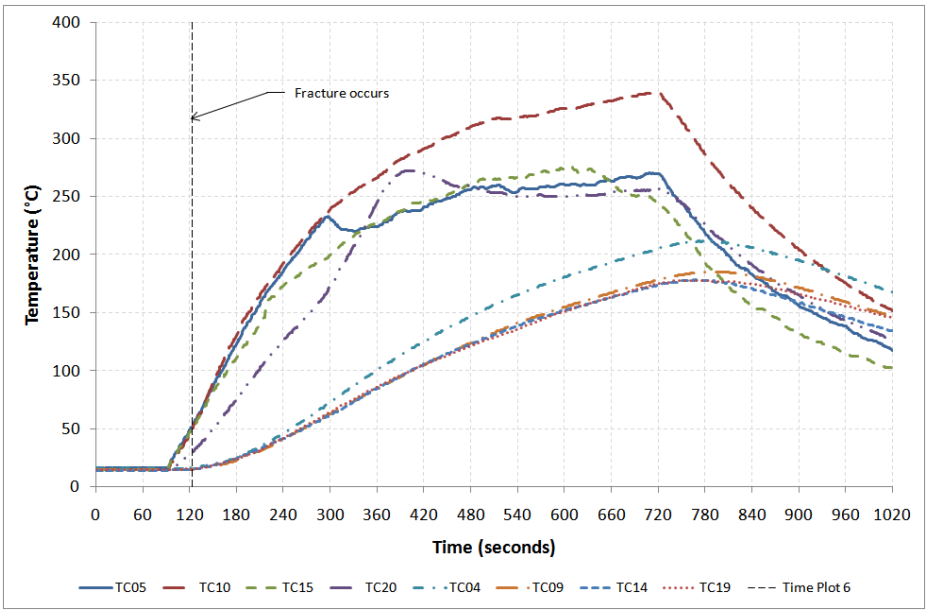

Figure C-6: Glass temperature profiles on unexposed side for experiment 4 Test 3

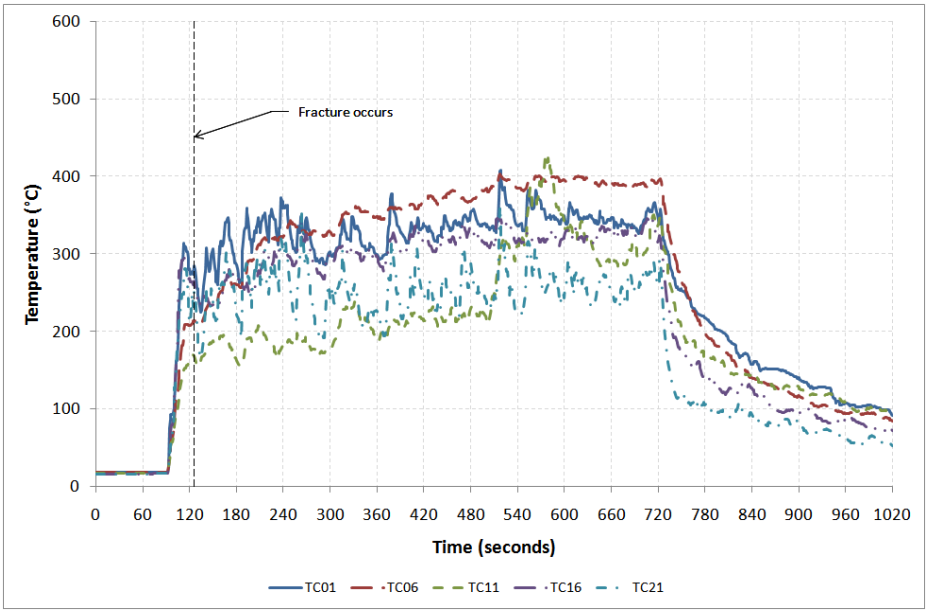

Figure C-7: Gas temperature profiles for experiment 4 Test 5

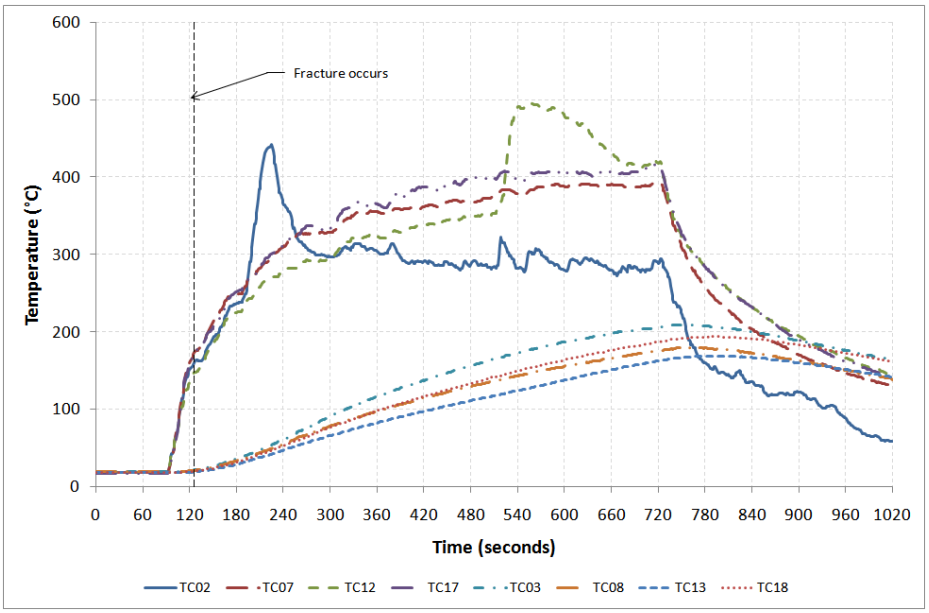

Figure C-8: Glass temperature profiles on exposed side for experiment 4 Test 5

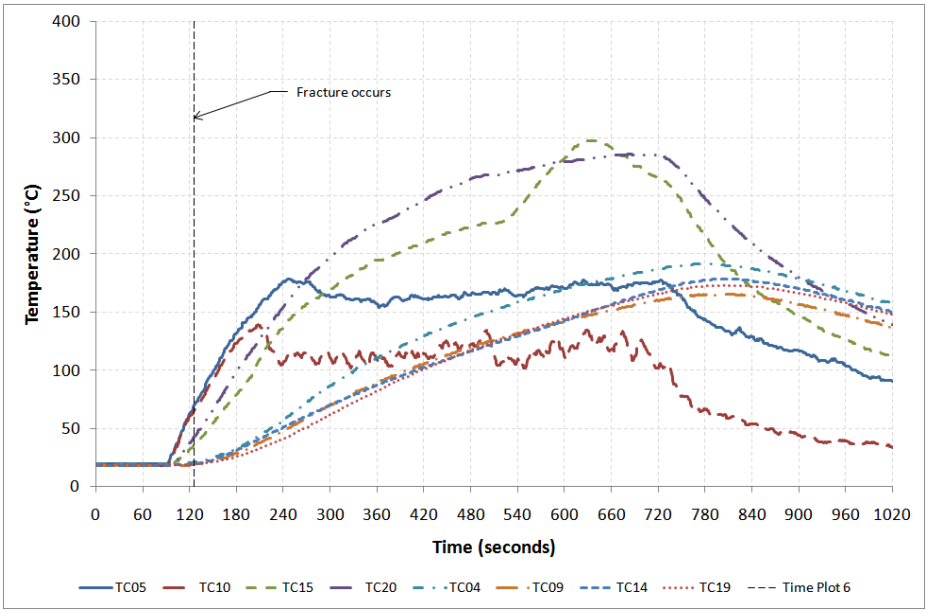

Figure C-9: Glass temperature profiles on unexposed side for experiment 4 Test 5

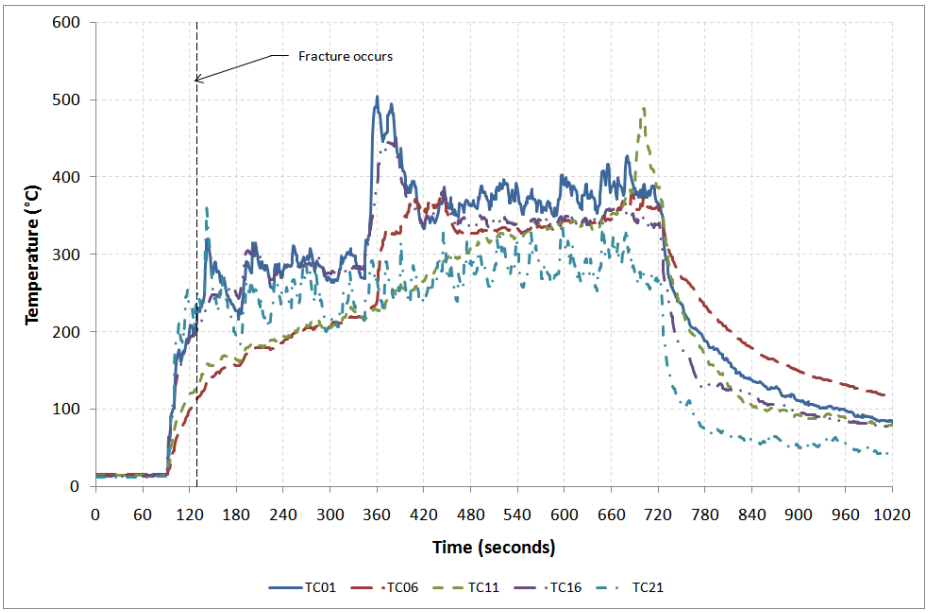

Figure C-10: Gas temperature profiles for experiment 4 Test 6

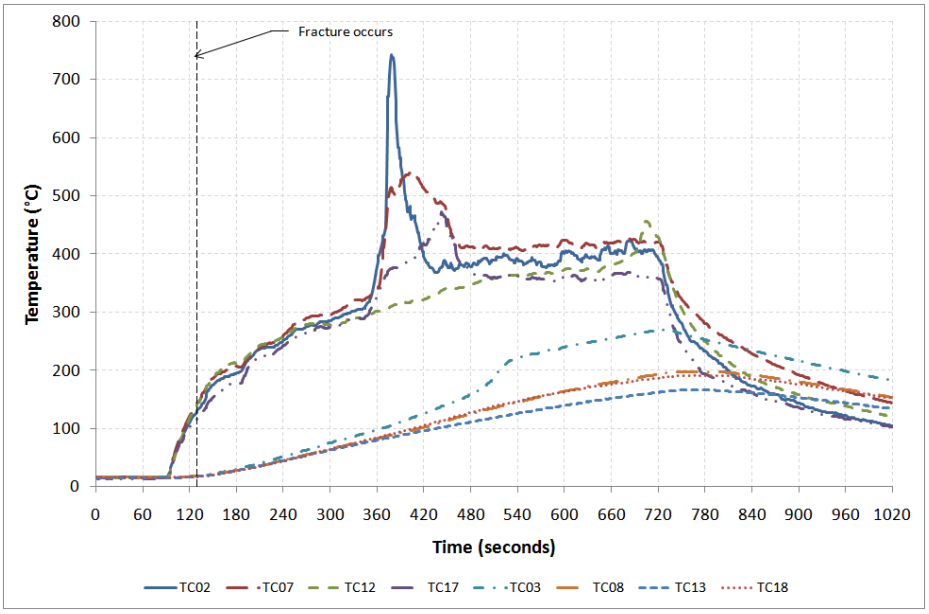

Figure C-11: Glass temperature profiles on exposed side for experiment 4 Test 6

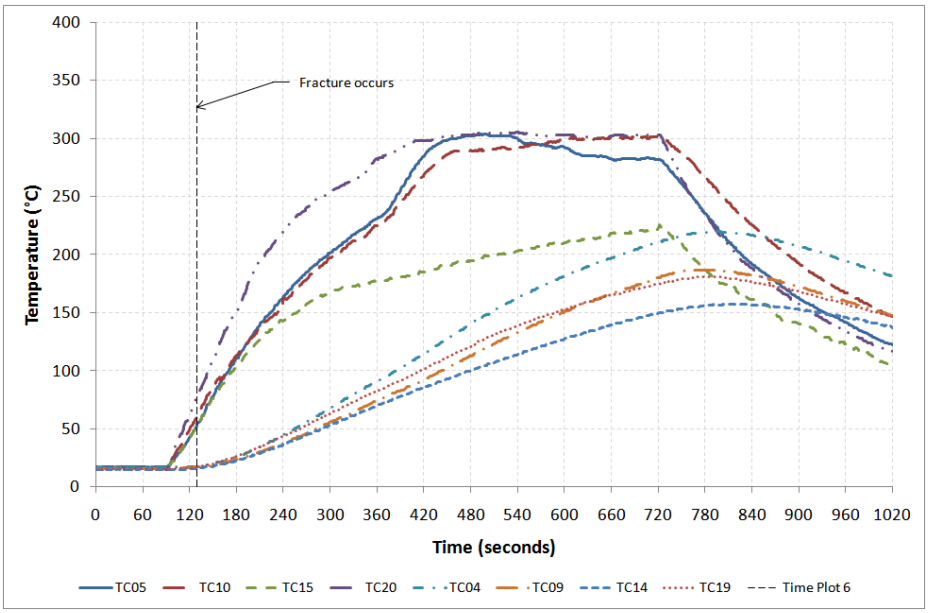

Figure C-12: Glass temperature profiles on unexposed side for experiment 4 Test 6

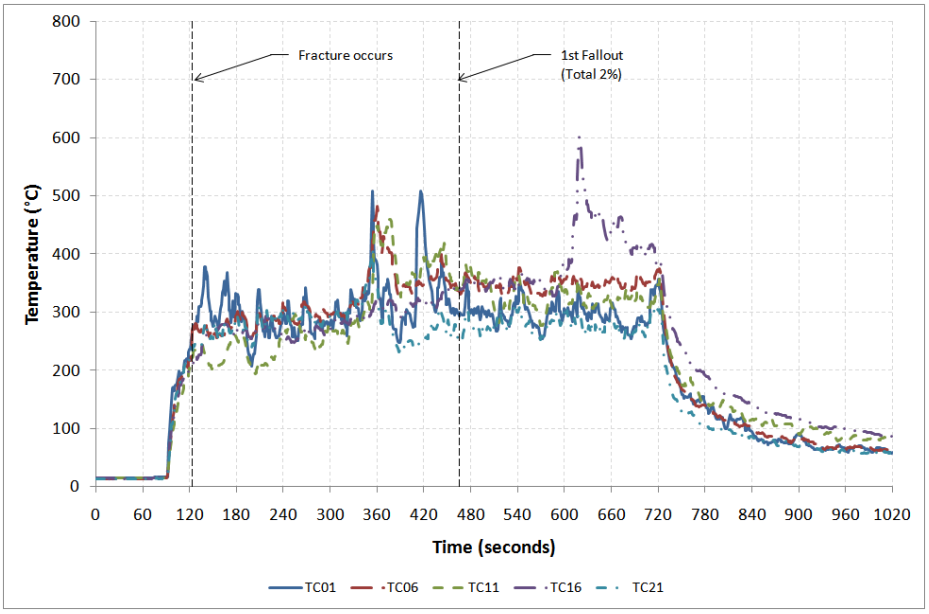

Figure C-13: Gas temperature profiles for experiment 4 Test 7

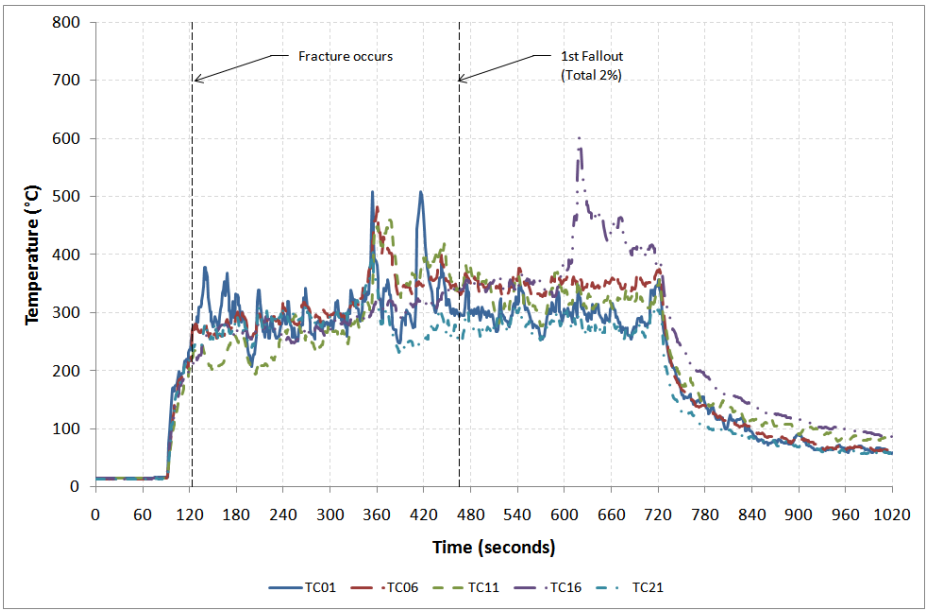

Figure C-14: Glass temperature profiles on exposed side for experiment 4 Test 7

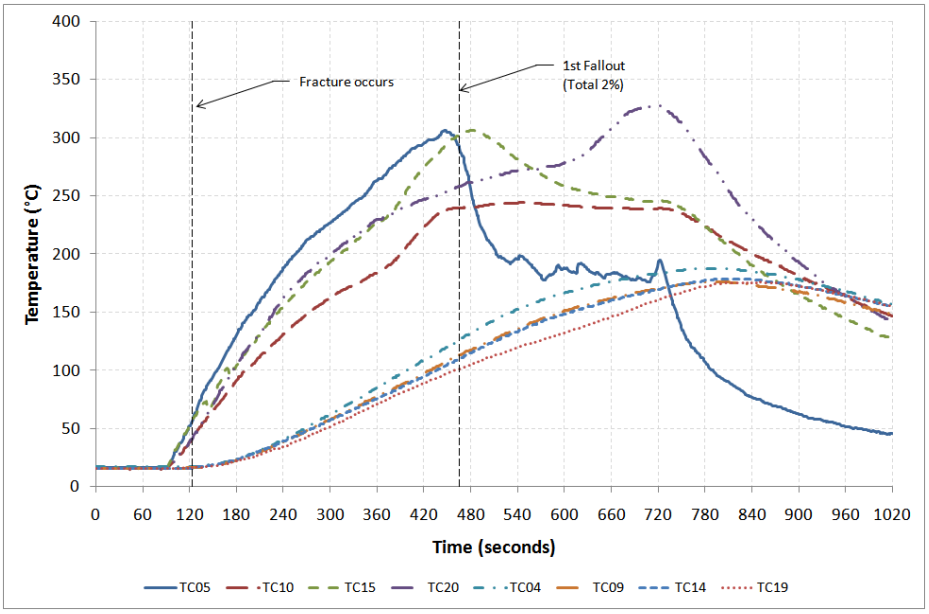

Figure C-15: Glass temperature profiles on unexposed side for experiment 4 Test 7

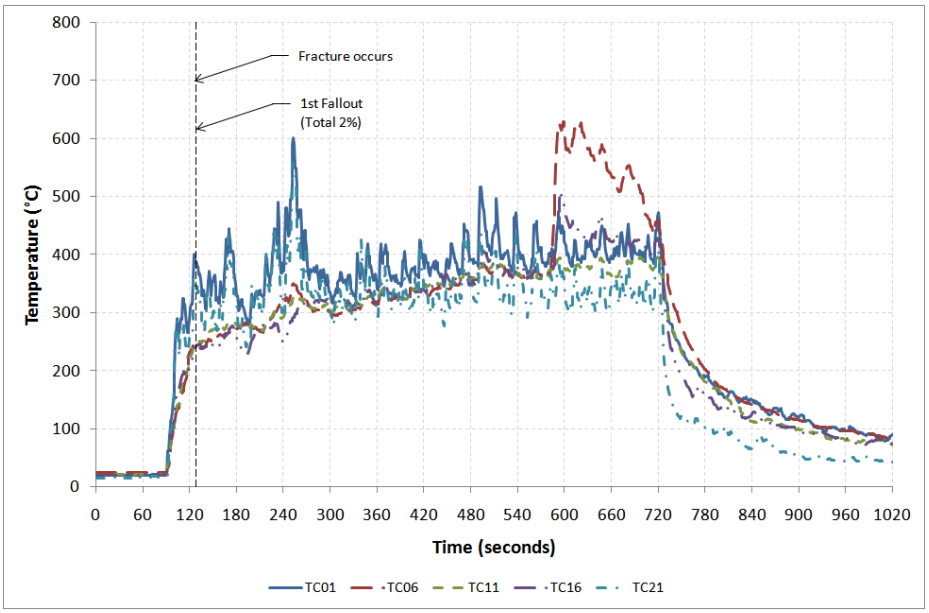

Figure C-16: Gas temperature profiles for experiment 4 Test 8

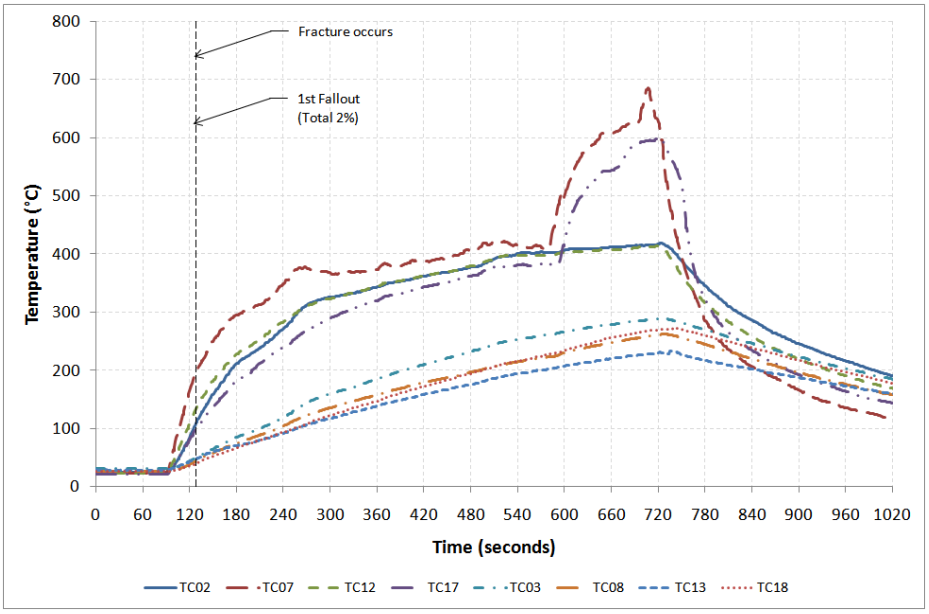

Figure C-17: Glass temperature profiles on exposed side for experiment 4 Test 8

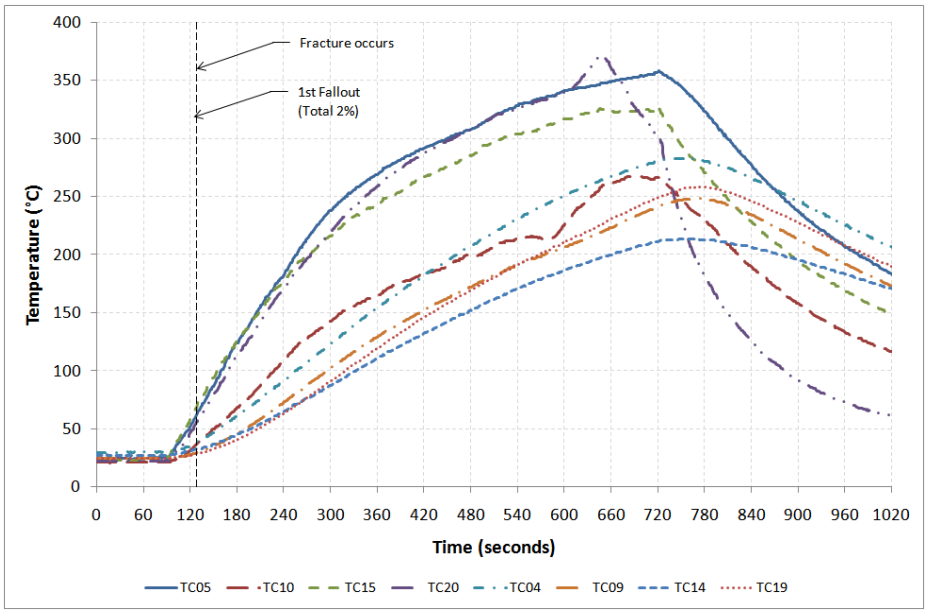

Figure C-18: Glass temperature profiles on unexposed side for experiment 4 Test 8

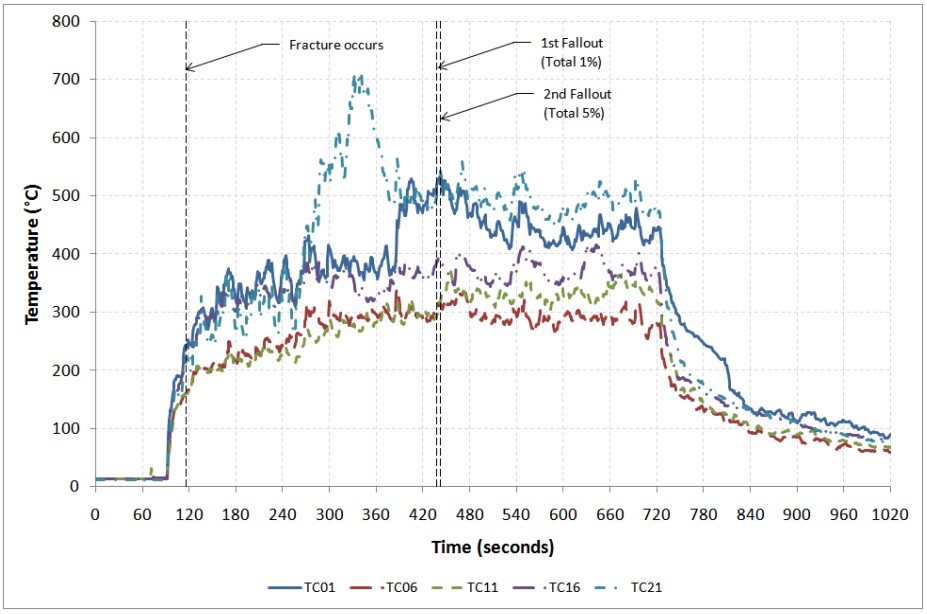

Figure C-19: Gas temperature profiles for experiment 4 Test 9

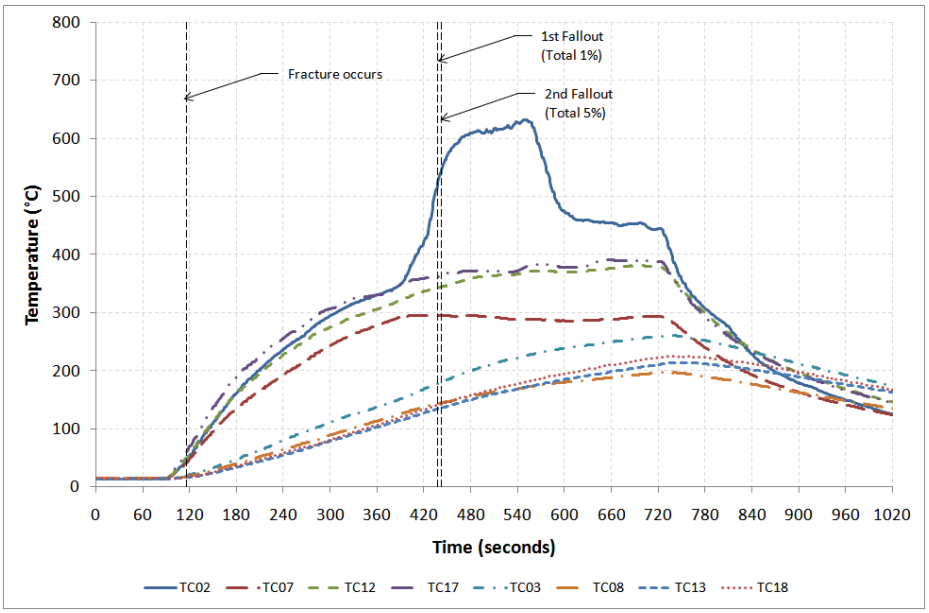

Figure C-20: Glass temperature profiles on exposed side for experiment 4 Test 9

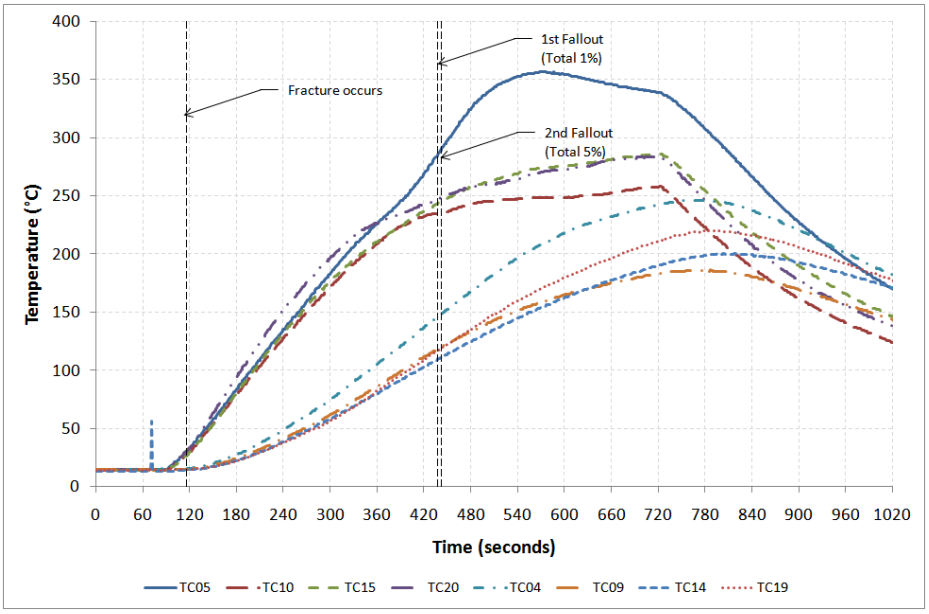

Figure C-21: Glass temperature profiles on unexposed side for experiment 4 Test 9

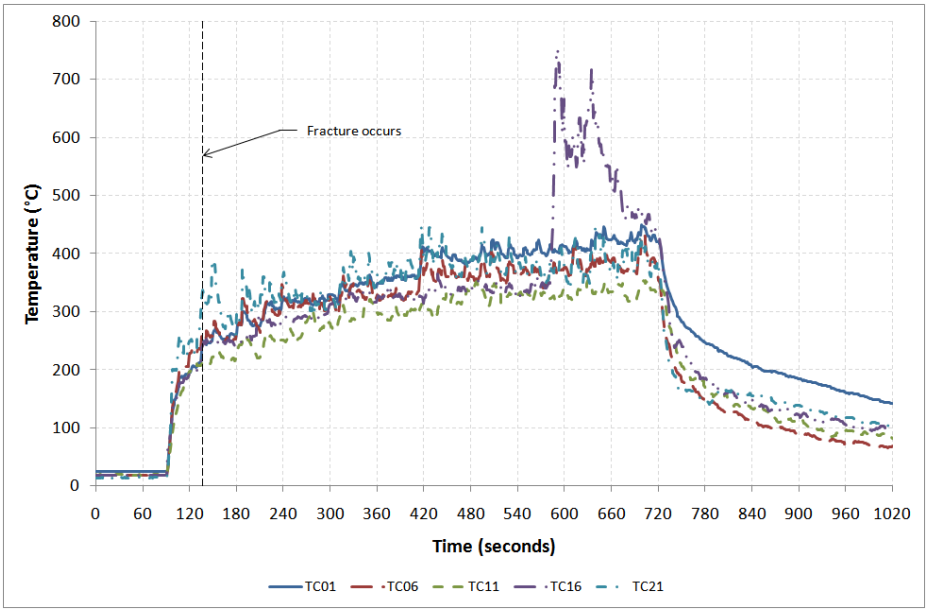

Figure C-22: Gas temperature profiles for experiment 4 Test 10

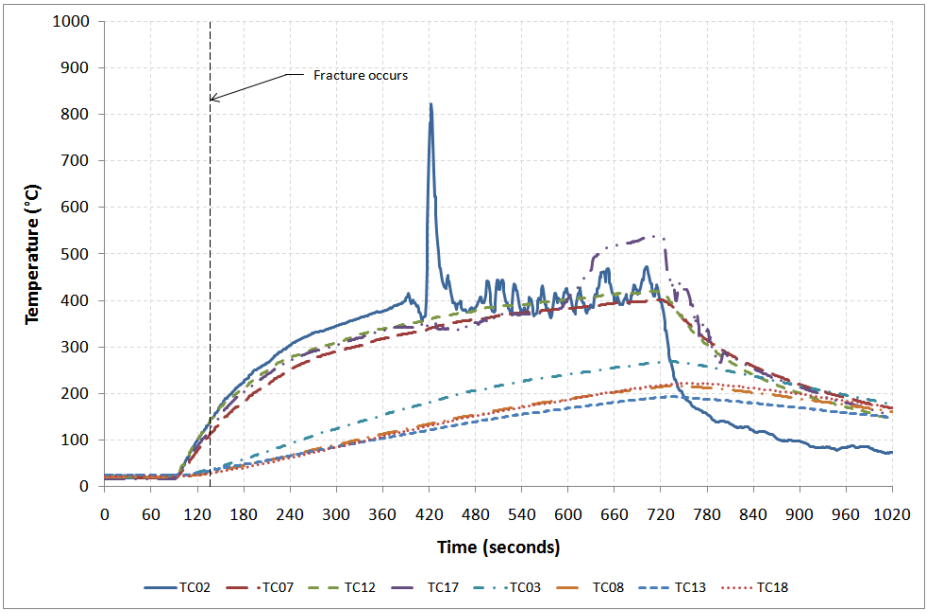

Figure C-23: Glass temperature profiles on exposed side for experiment 4 Test 10

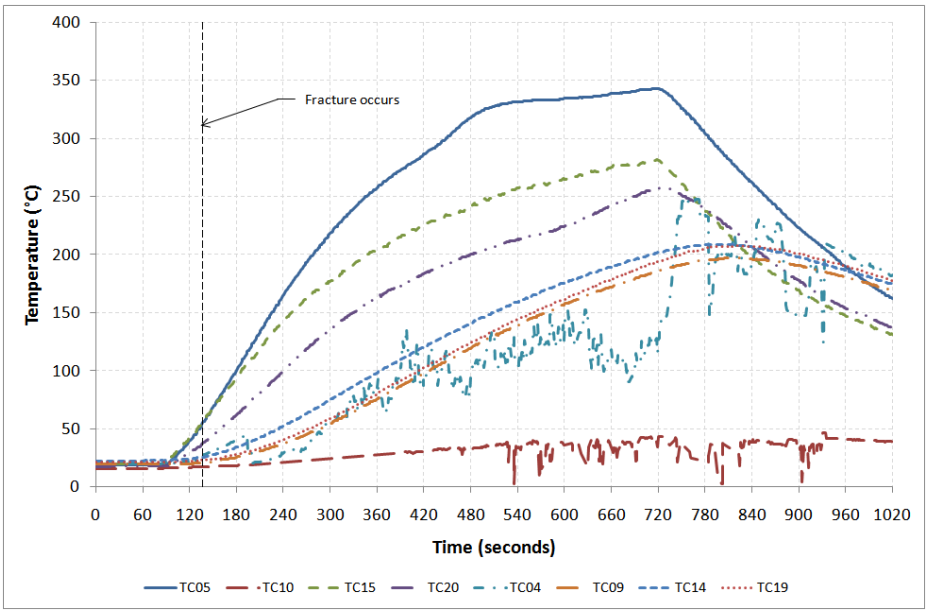

Figure C-24: Glass temperature profiles on unexposed side for experiment 4 Test 10

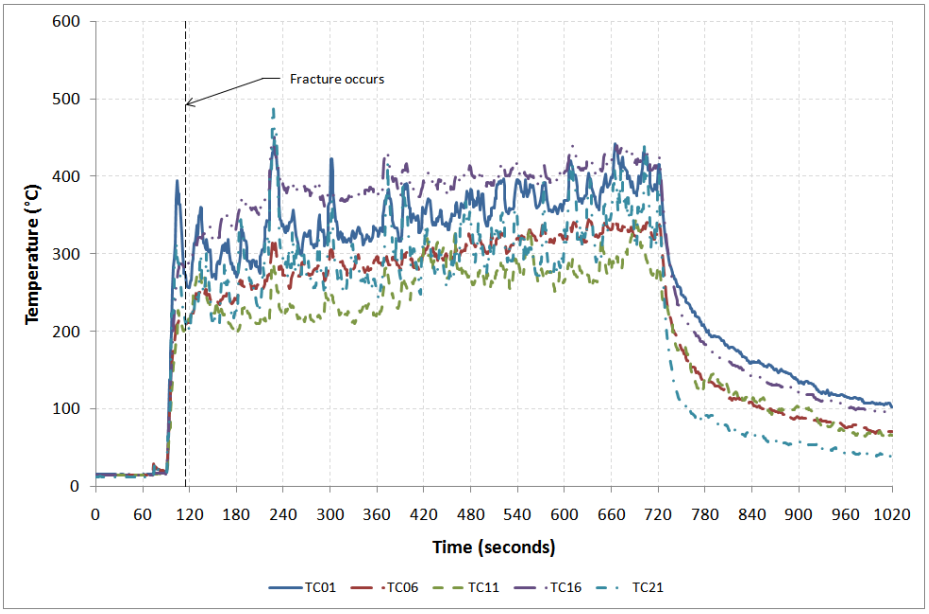

Figure C-25: Gas temperature profiles for experiment 4 Test 11

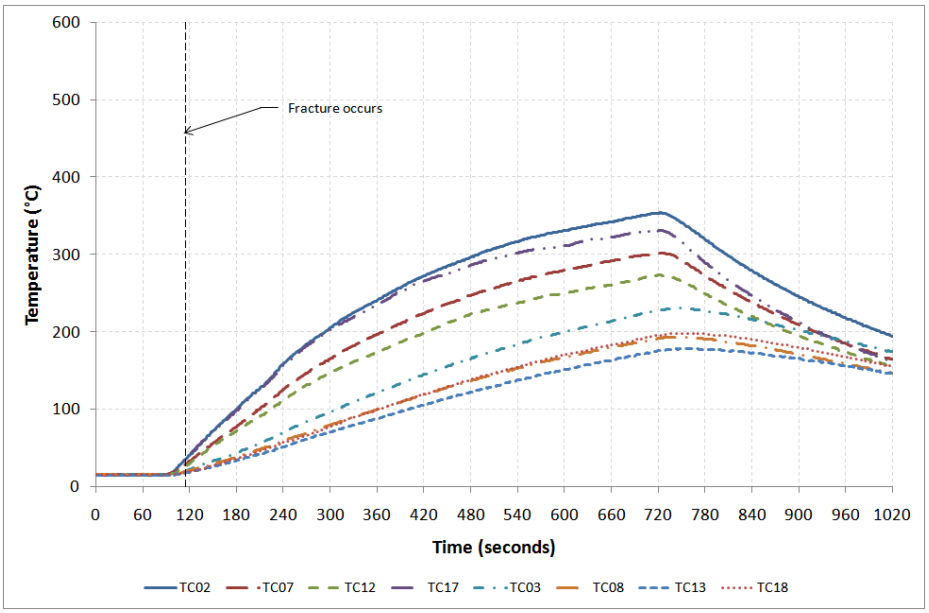

Figure C-26: Glass temperature profiles on exposed side for experiment 4 Test 11

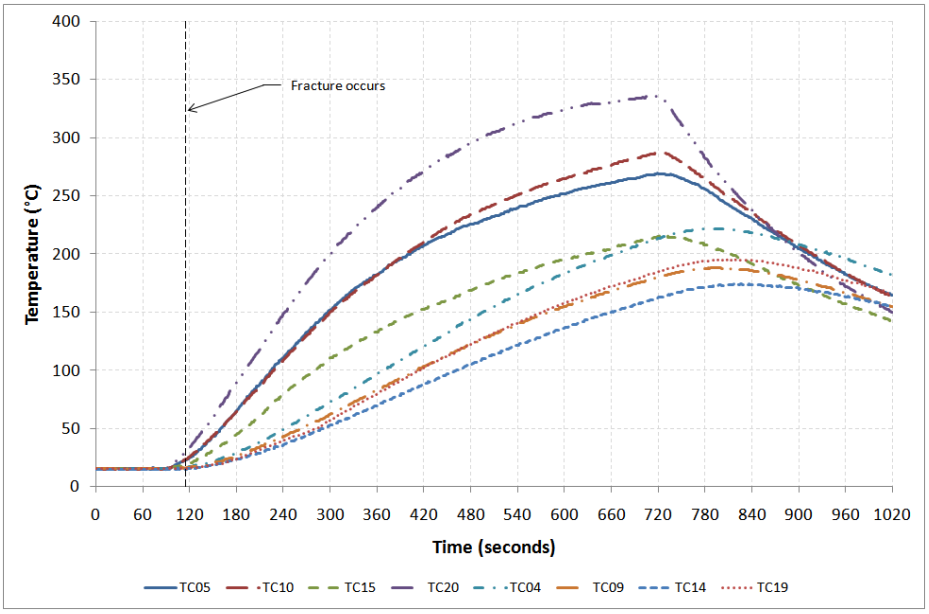

Figure C-27: Glass temperature profiles on unexposed side for experiment 4 Test 11

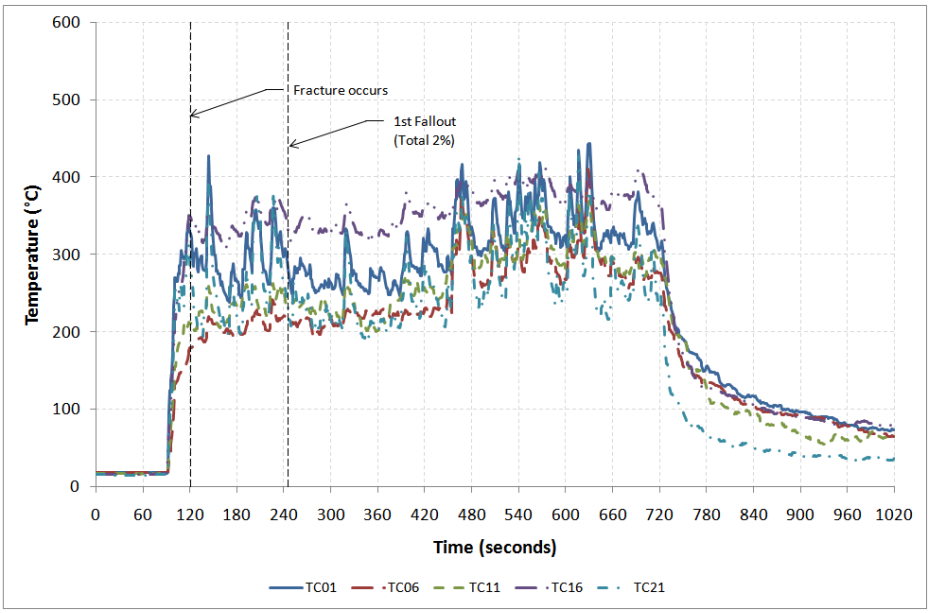

Figure C-28: Gas temperature profiles for experiment 4 Test 12

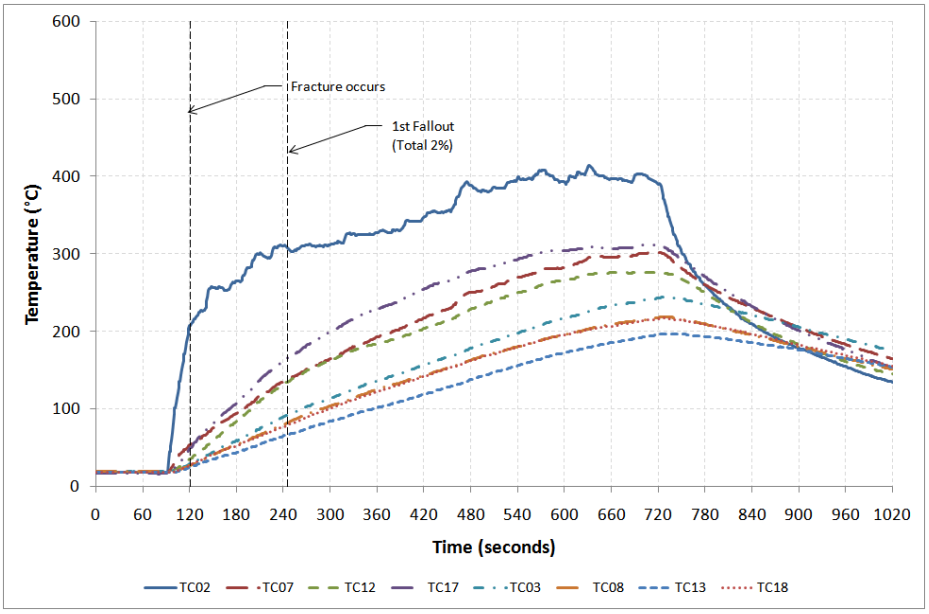

Figure C-29: Glass temperature profiles on exposed side for experiment 4 Test 12

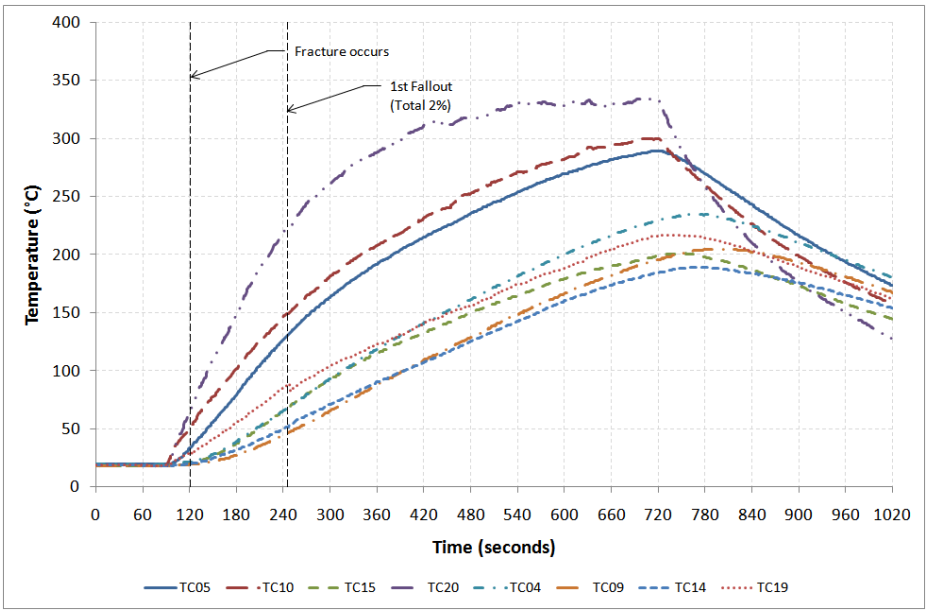

Figure C-30: Glass temperature profiles on unexposed side for experiment 4 Test 12

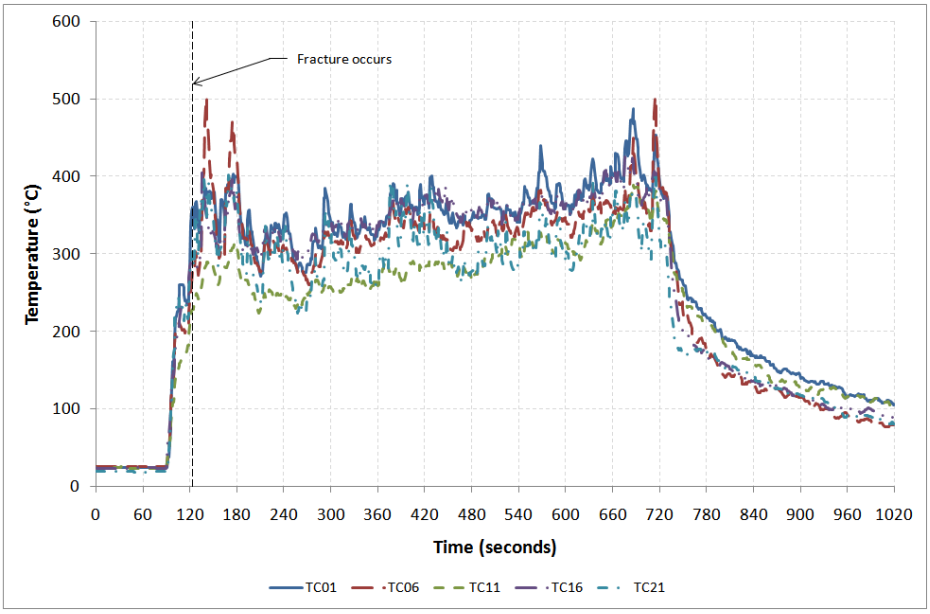

Figure C-31: Gas temperature profiles for experiment 4 Test 13

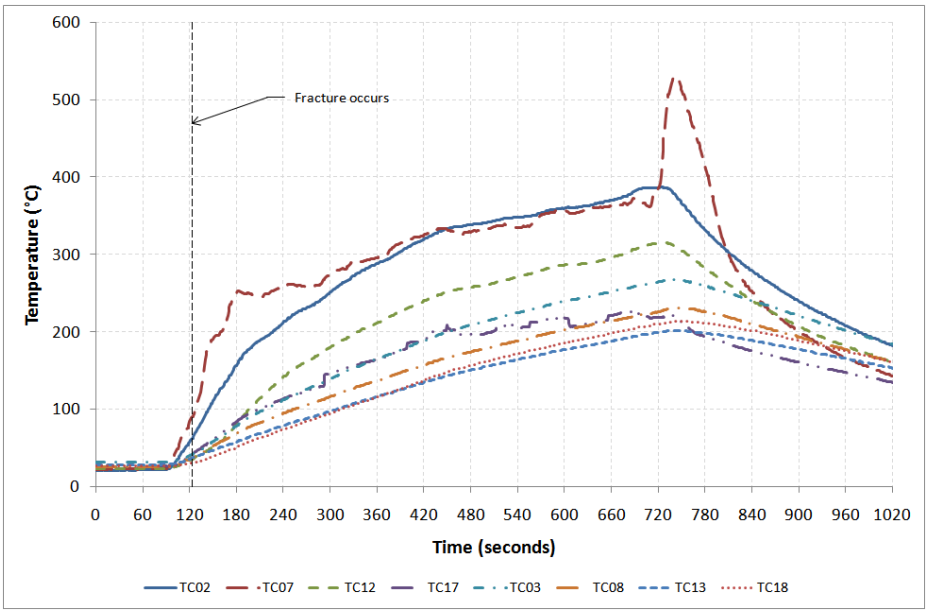

Figure C-32: Glass temperature profiles on exposed side for experiment 4 Test 13

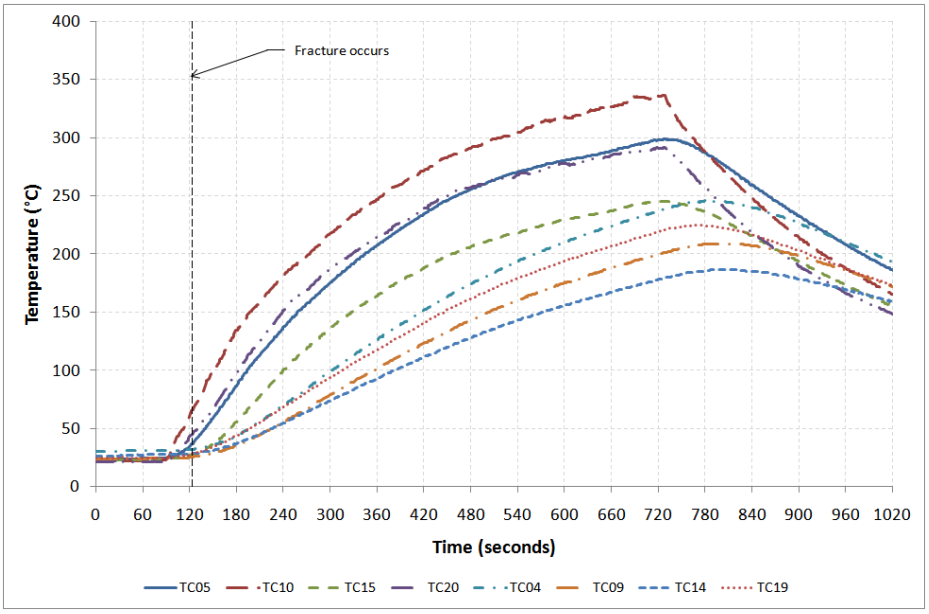

Figure C-33: Glass temperature profiles on unexposed side for experiment 4 Test 13

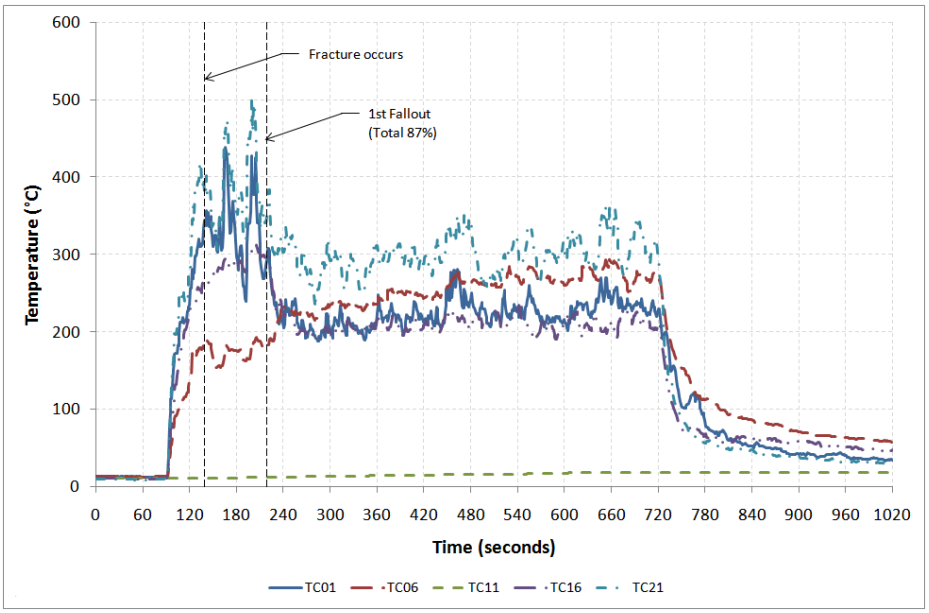

Figure C-34: Gas temperature profiles for experiment 4 Test 14

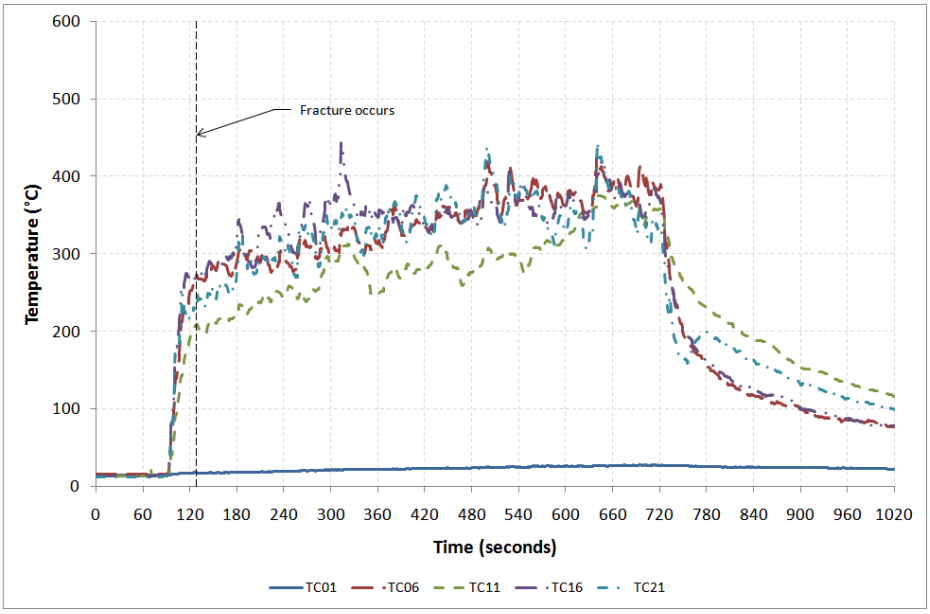

Figure C-35: Gas temperature profiles for experiment 4 Test 15

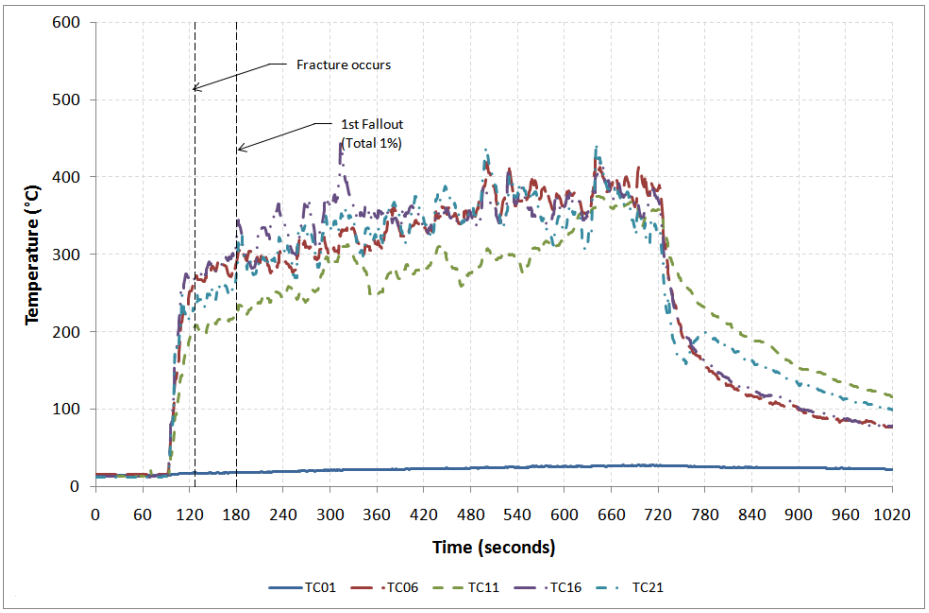

Figure C-36: Gas temperature profiles for experiment 4 Test 16

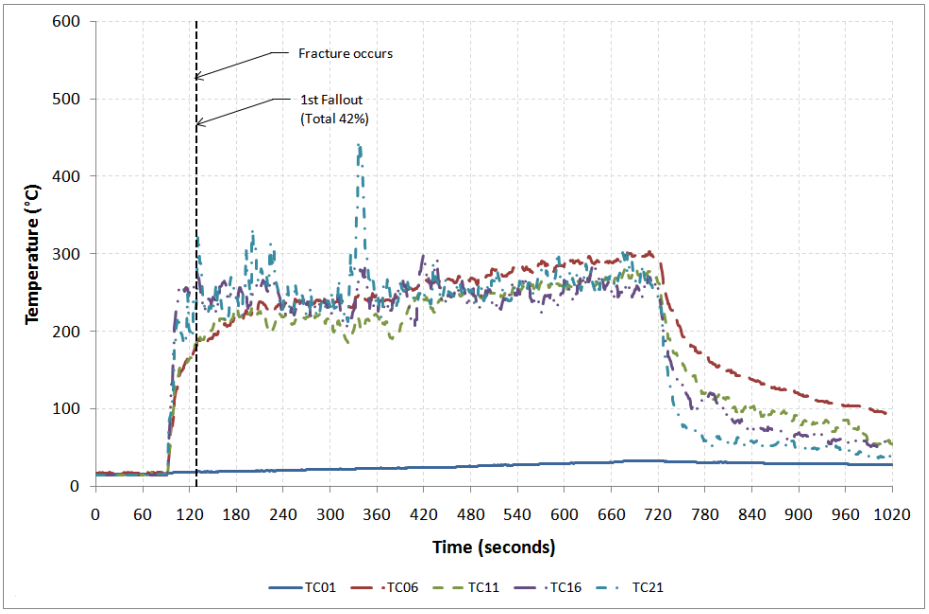

Figure C-37: Gas temperature profiles for experiment 4 Test 17

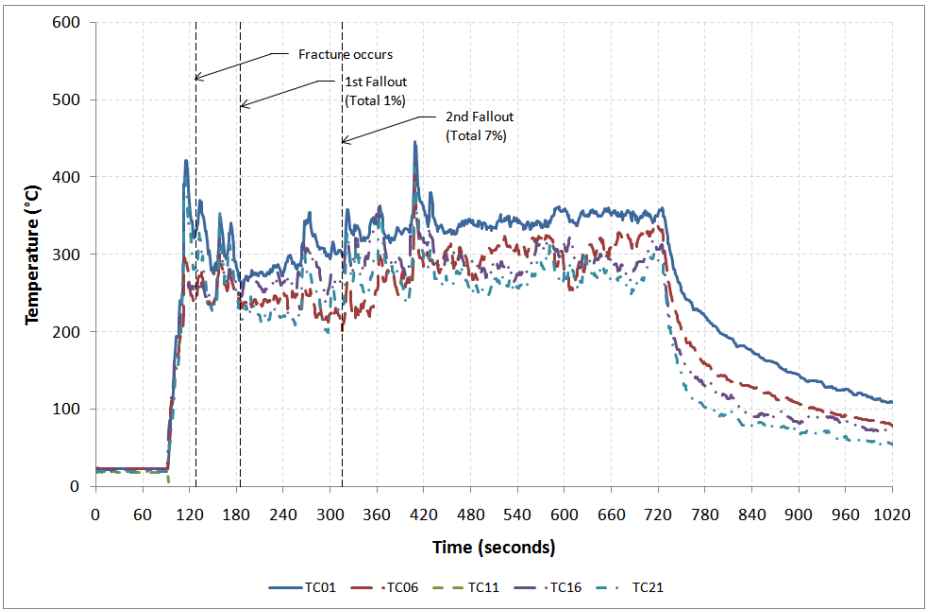

Figure C-38: Gas temperature profiles for experiment 4 Test 18

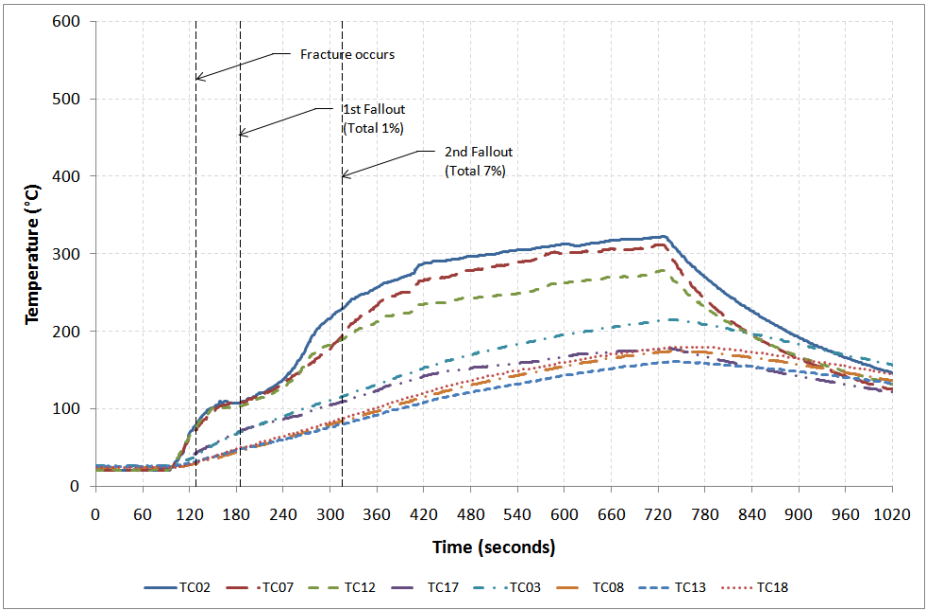

Figure C-39: Glass temperature profiles on exposed side for experiment 4 Test 18

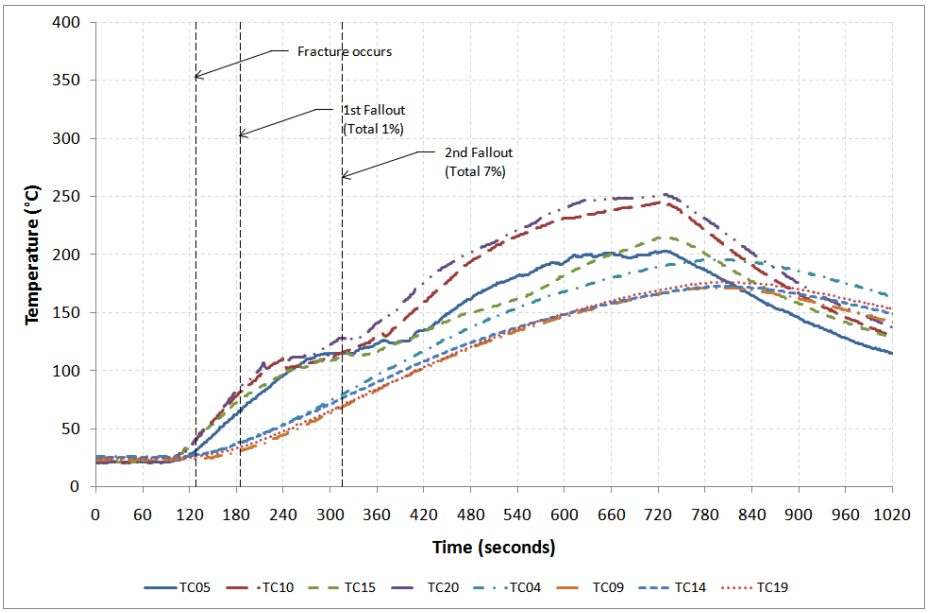

Figure C-40: Glass temperature profiles on unexposed side for experiment 4 Test 18

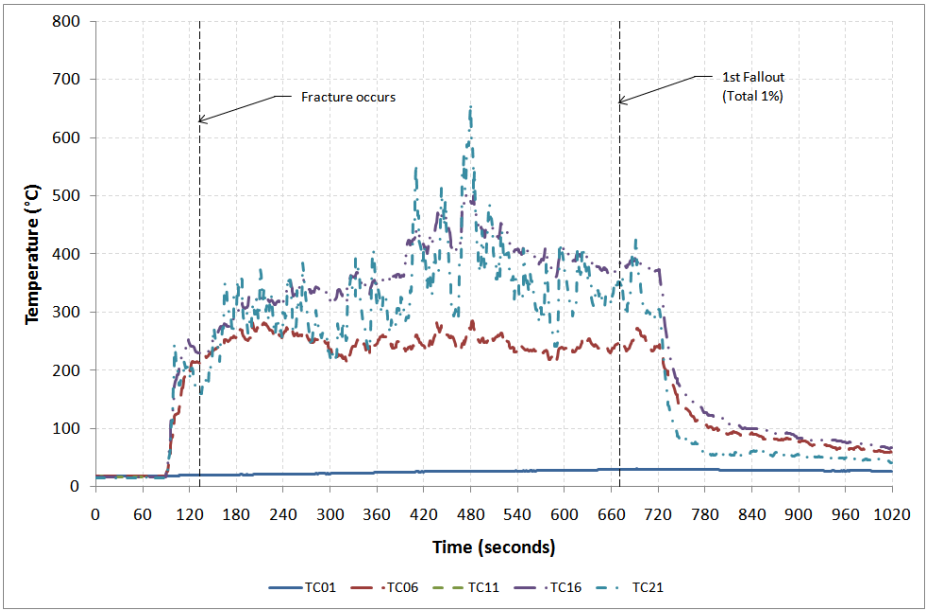

Figure C-41: Gas temperature profiles for experiment 4 Test 19

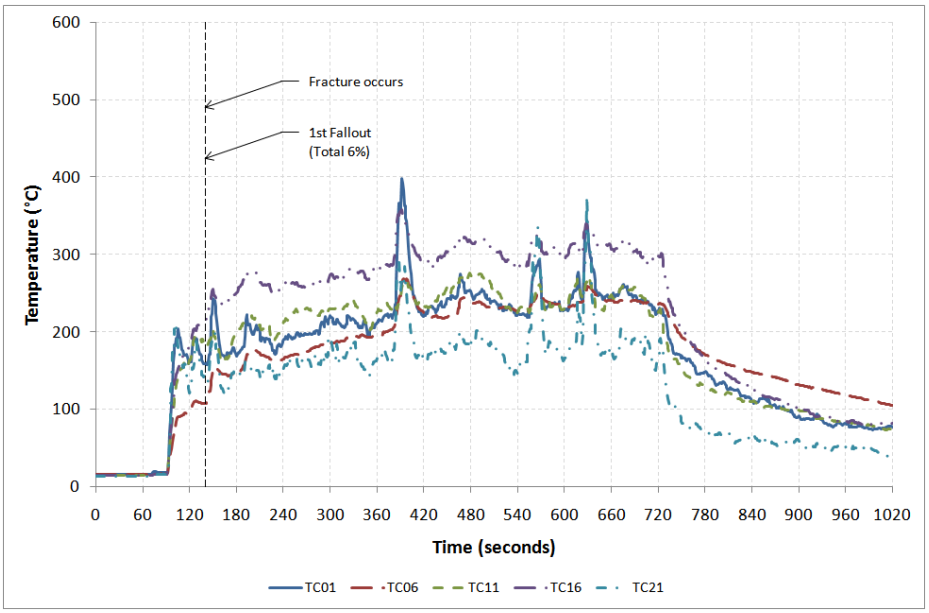

Figure C-42: Gas temperature profiles for experiment 4 Test 20

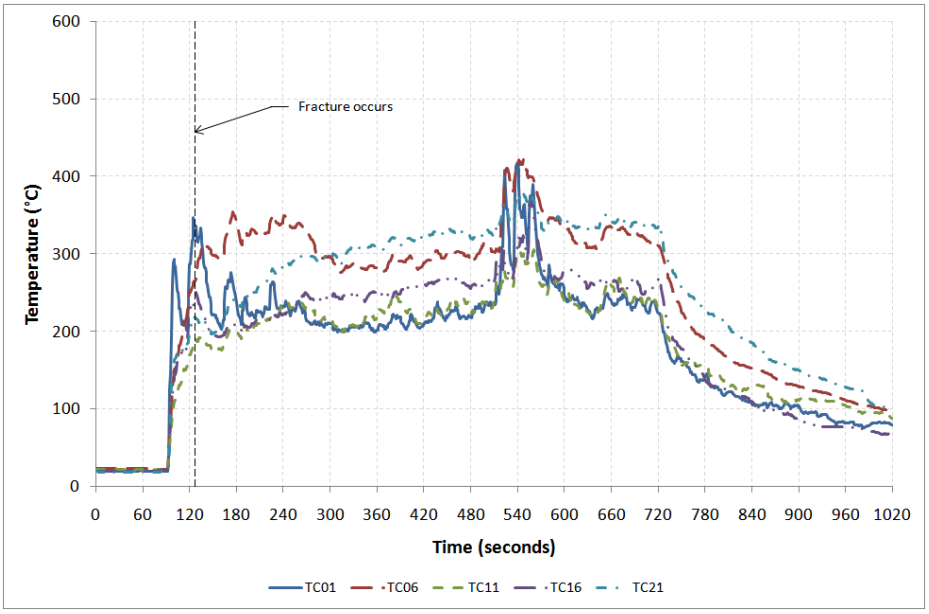

Figure C-43: Gas temperature profiles for experiment 4 Test 21

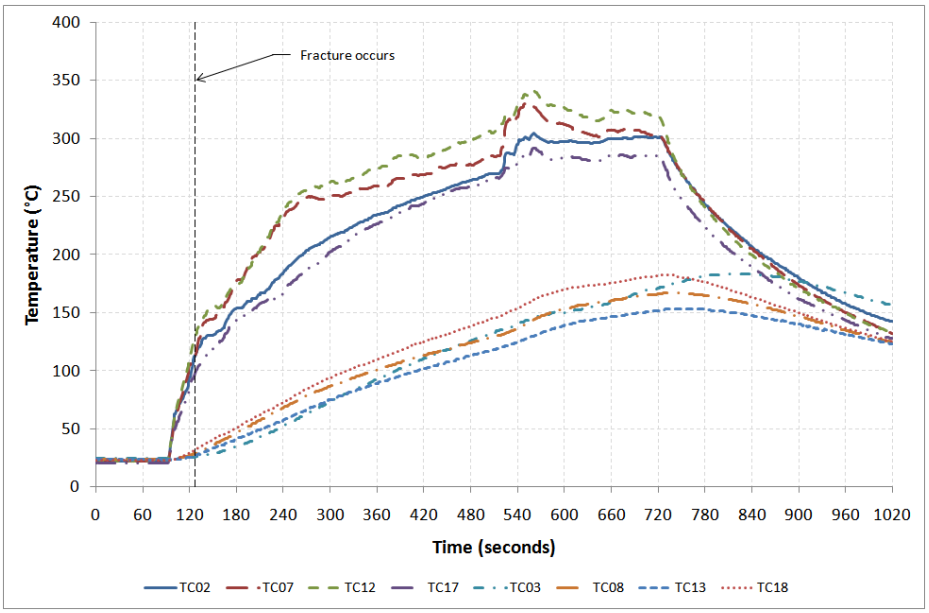

Figure C-44: Glass temperature profiles on exposed side for experiment 4 Test 21

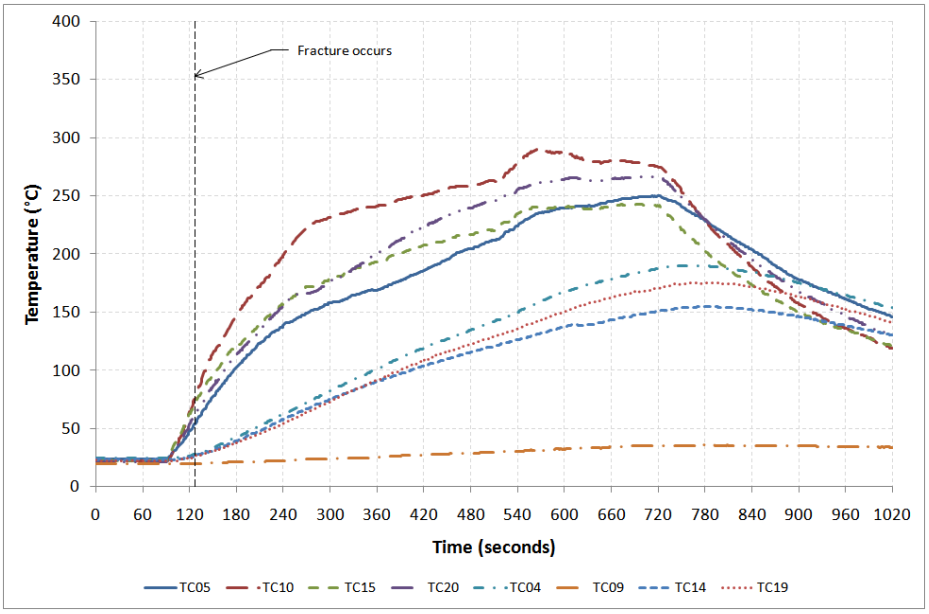

Figure C-45: Glass temperature profiles on unexposed side for experiment 4 Test 21

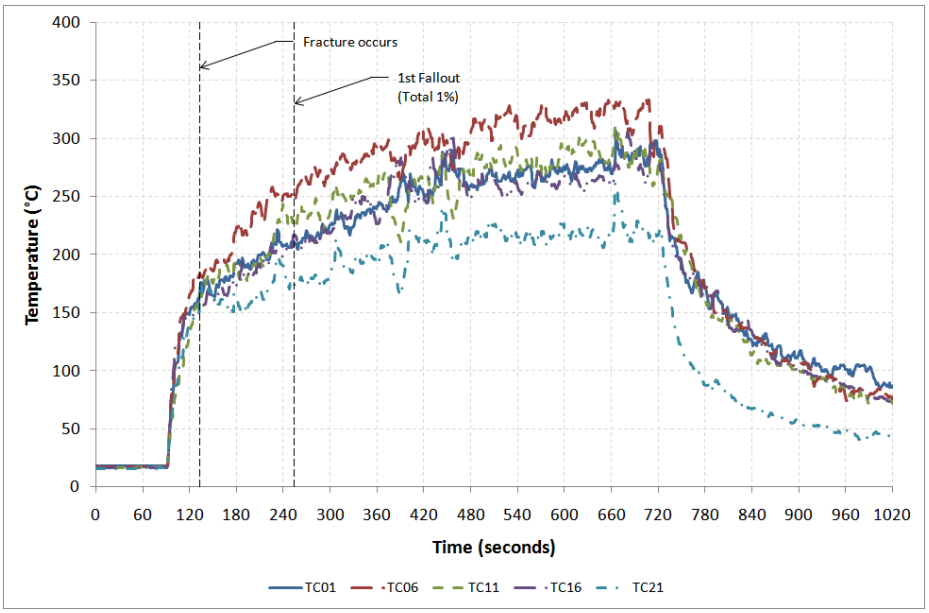

Figure C-46: Gas temperature profiles for experiment 4 Test 22

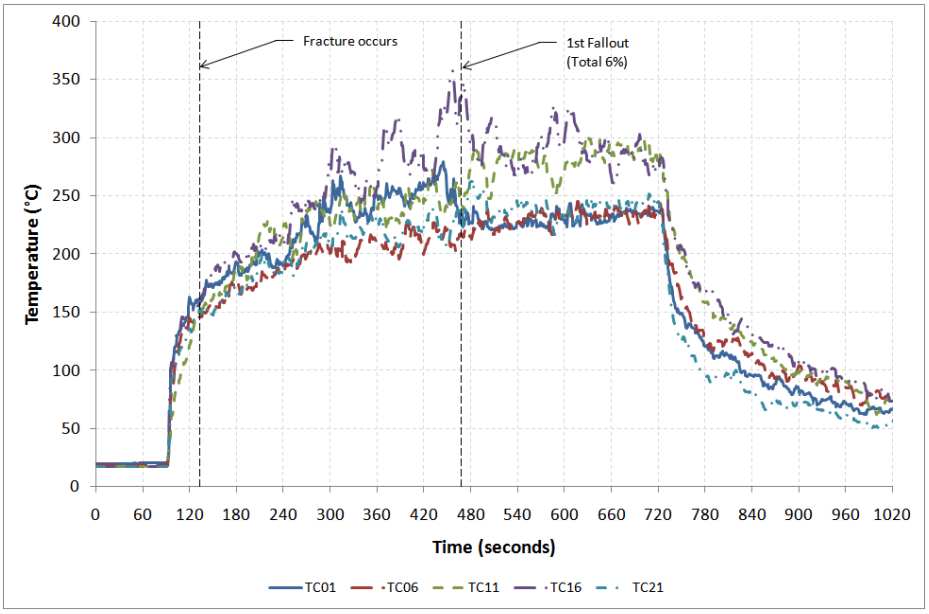

Figure C-47: Gas temperature profiles for experiment 4 Test 23

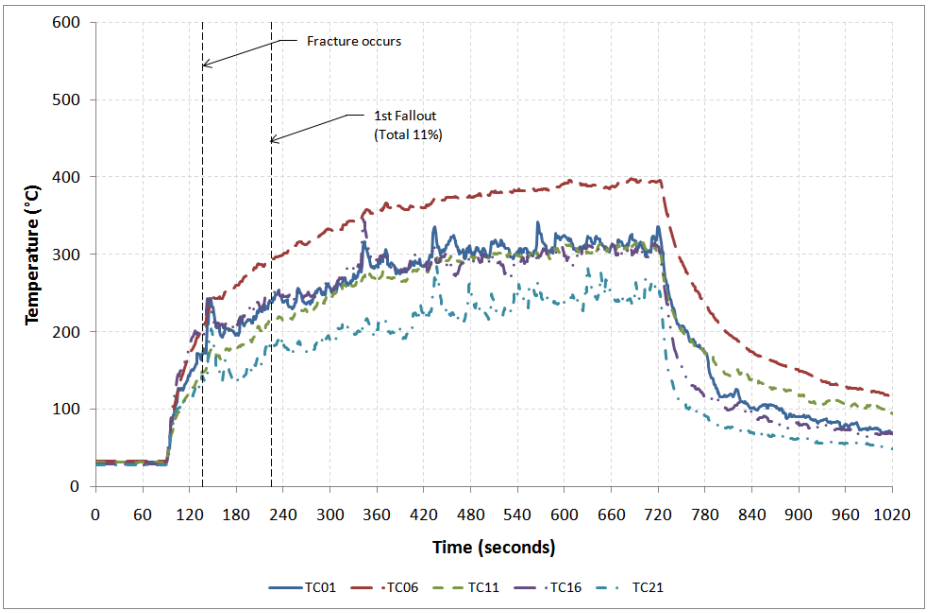

Figure C-48: Gas temperature profiles for experiment 4 Test 24

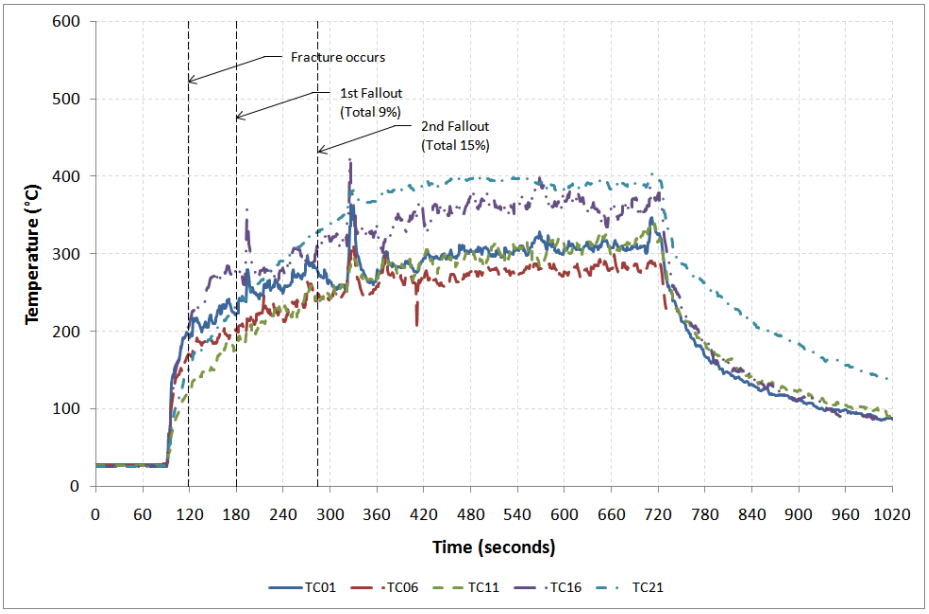

Figure C-49: Gas temperature profiles for experiment 4 Test 25

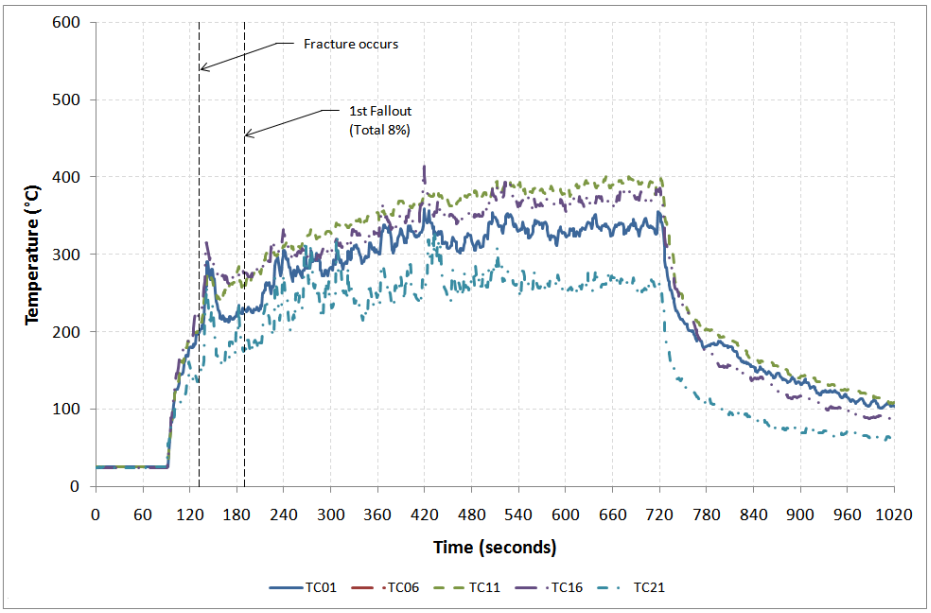

Figure C-50: Gas temperature profiles for experiment 4 Test 26

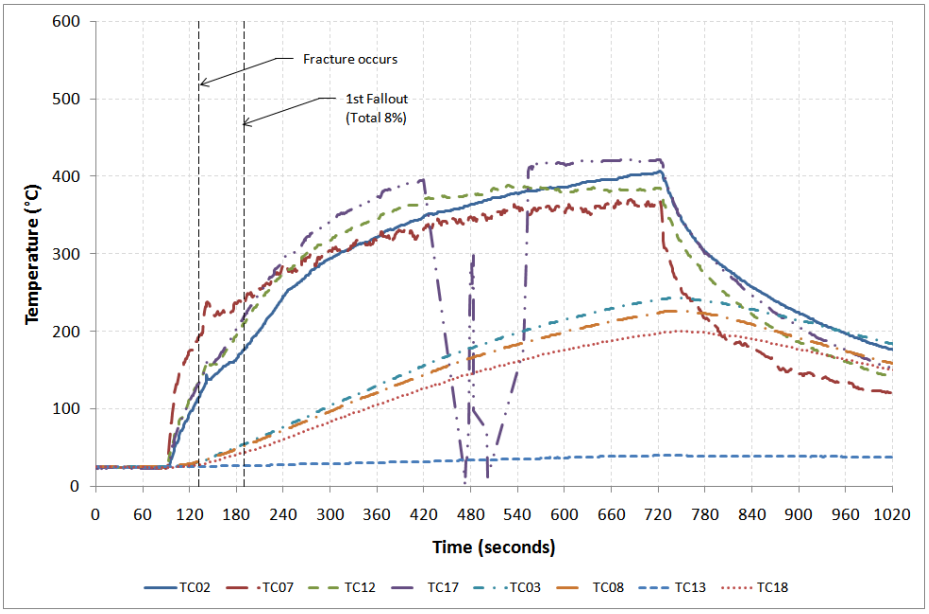

Figure C-51: Glass temperature profiles on exposed side for experiment 4 Test 26

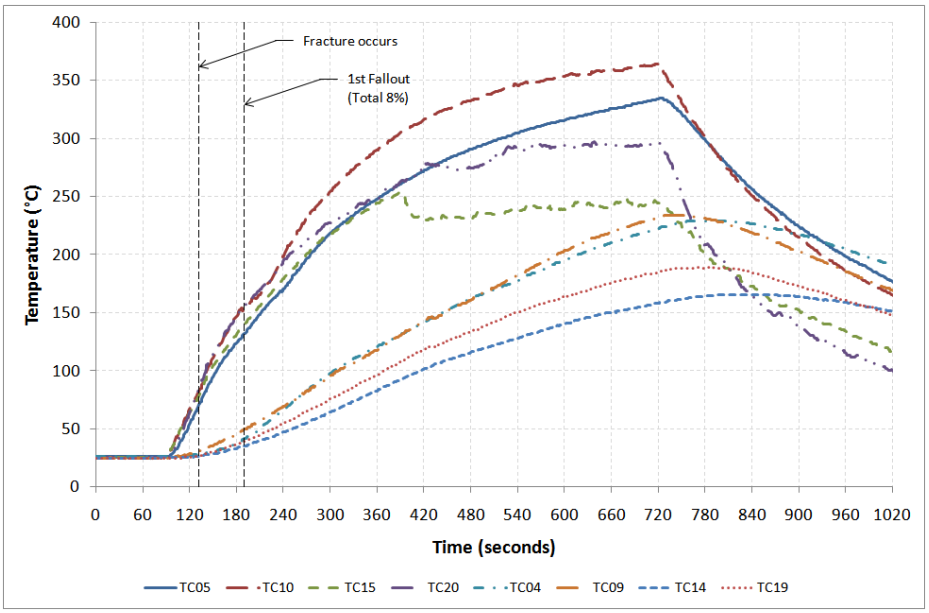

Figure C-52: Glass temperature profiles on unexposed side for experiment 4 Test 26

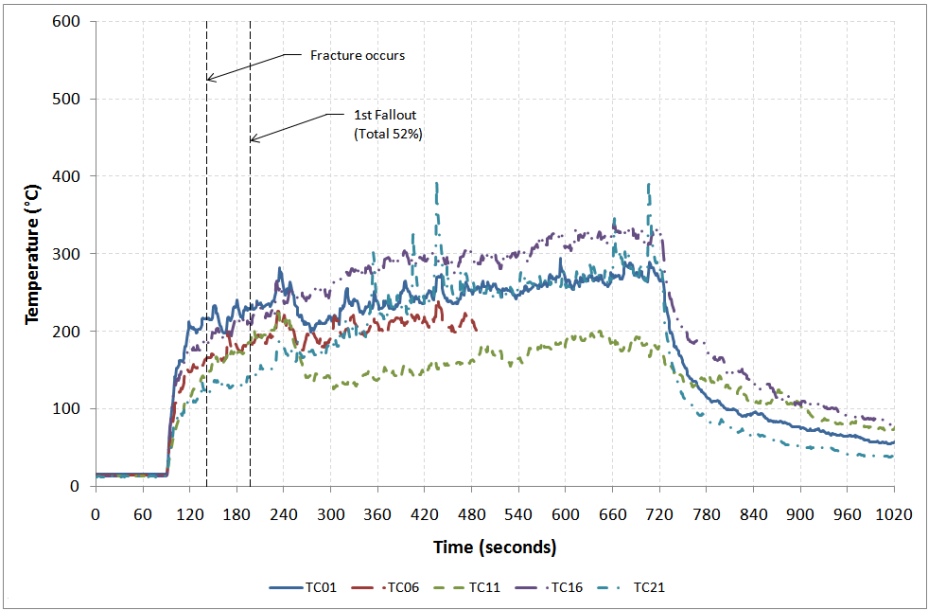

Figure C-53: Gas temperature profiles for experiment 4 Test 27

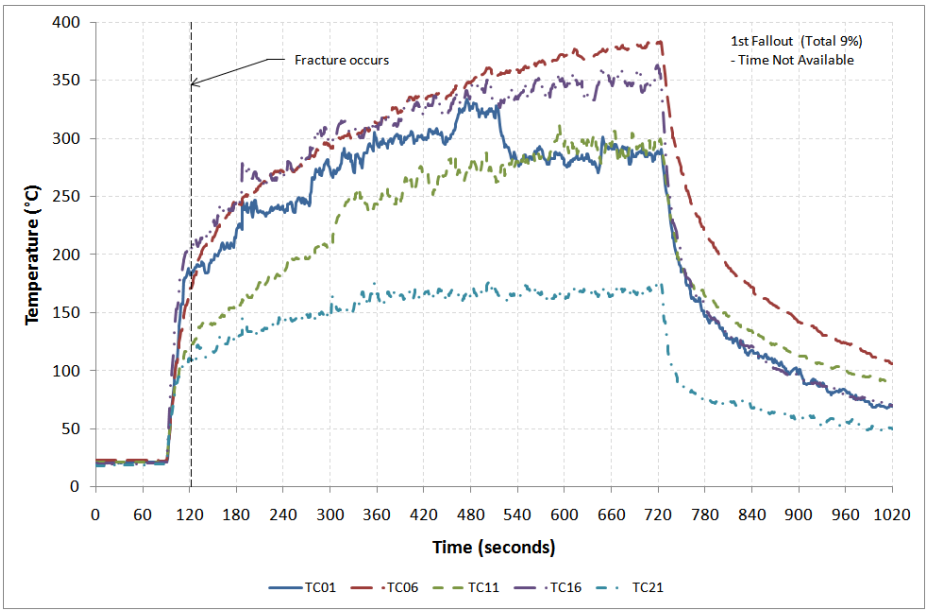

Figure C-54: Gas temperature profiles for experiment 4 Test 28

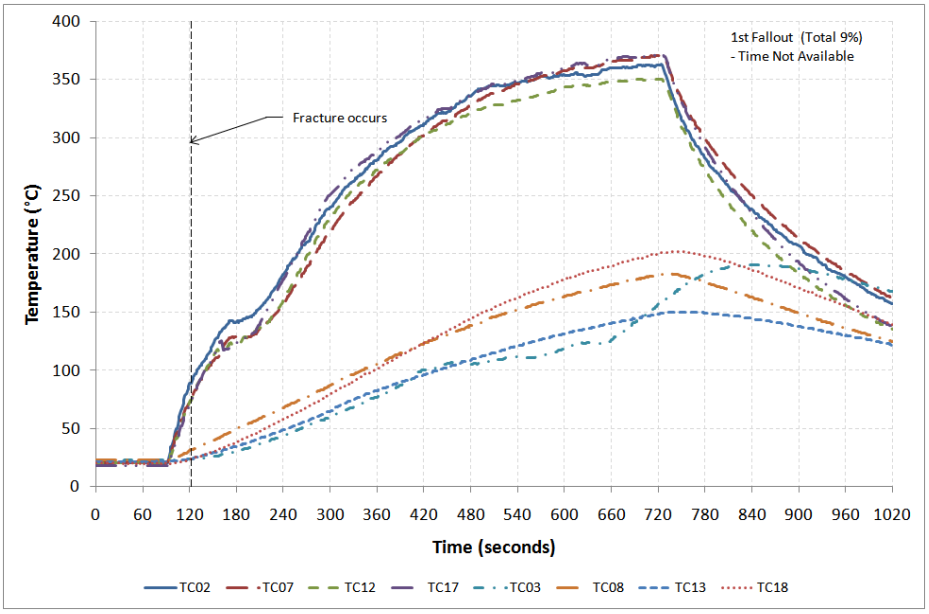

Figure C-55: Glass temperature profiles on exposed side for experiment 4 Test 28

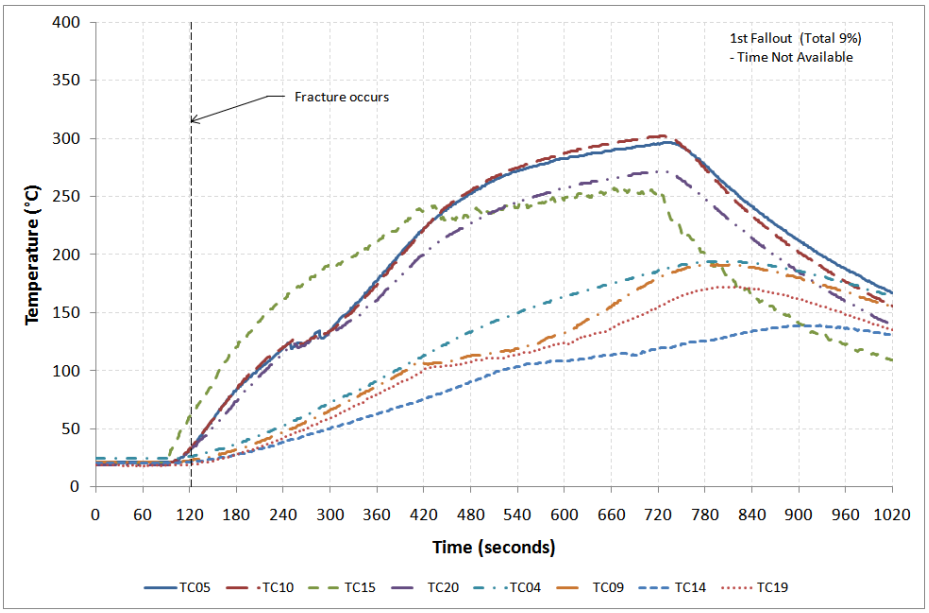

Figure C-56: Glass temperature profiles on unexposed side for experiment 4 Test 28

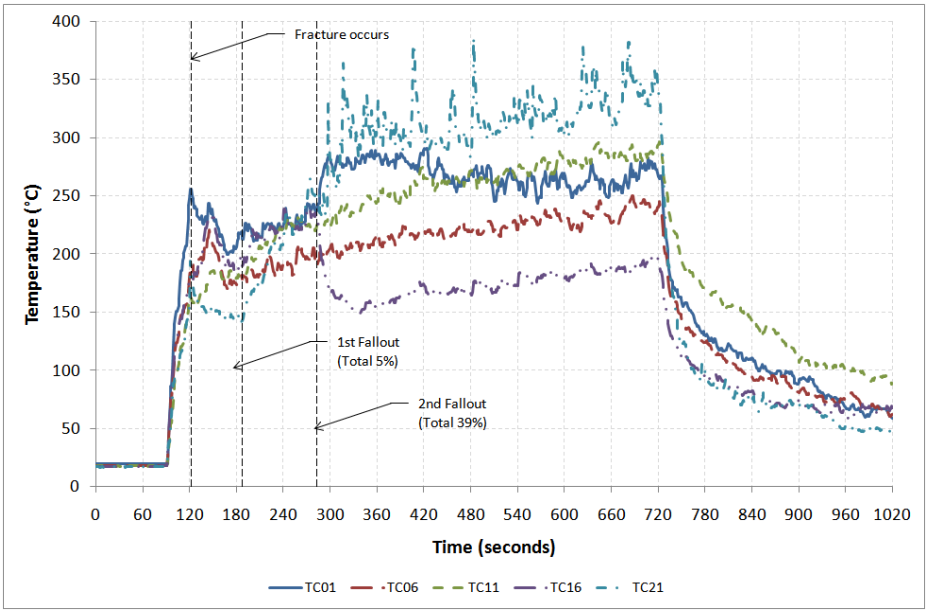

Figure C-57: Gas temperature profiles for experiment 4 Test 29

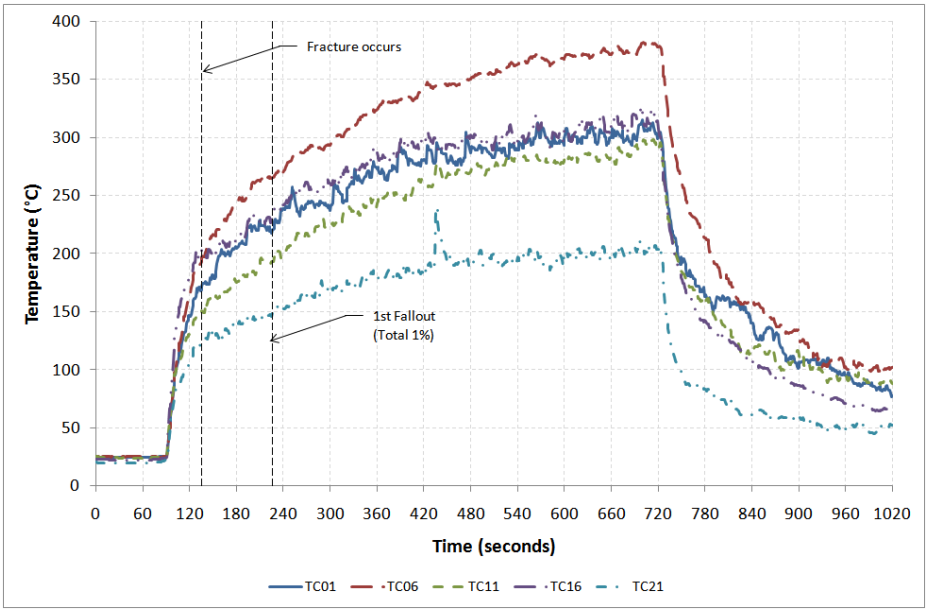

Figure C-58: Gas temperature profiles for experiment 4 Test 30

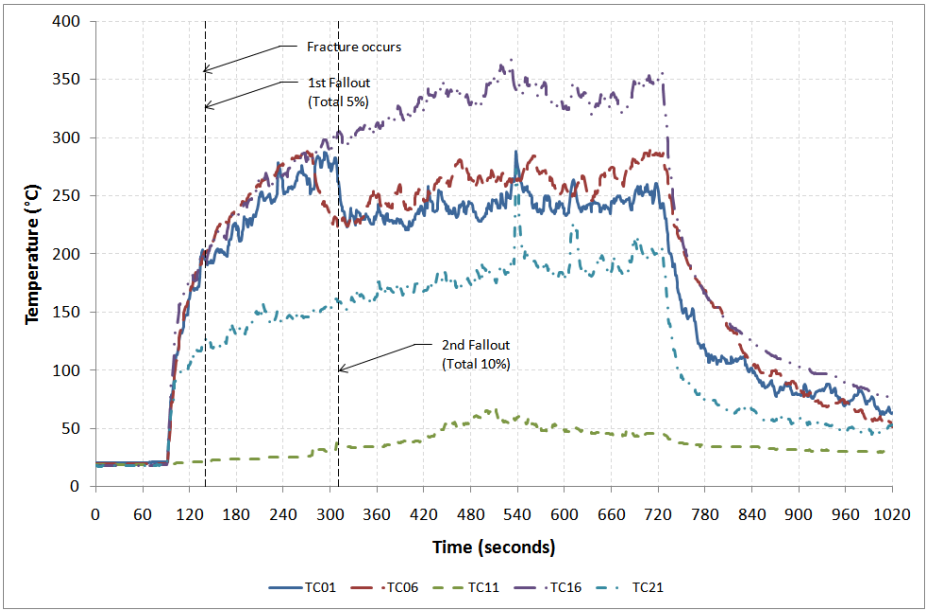

Figure C-59: Gas temperature profiles for experiment 4 Test 31

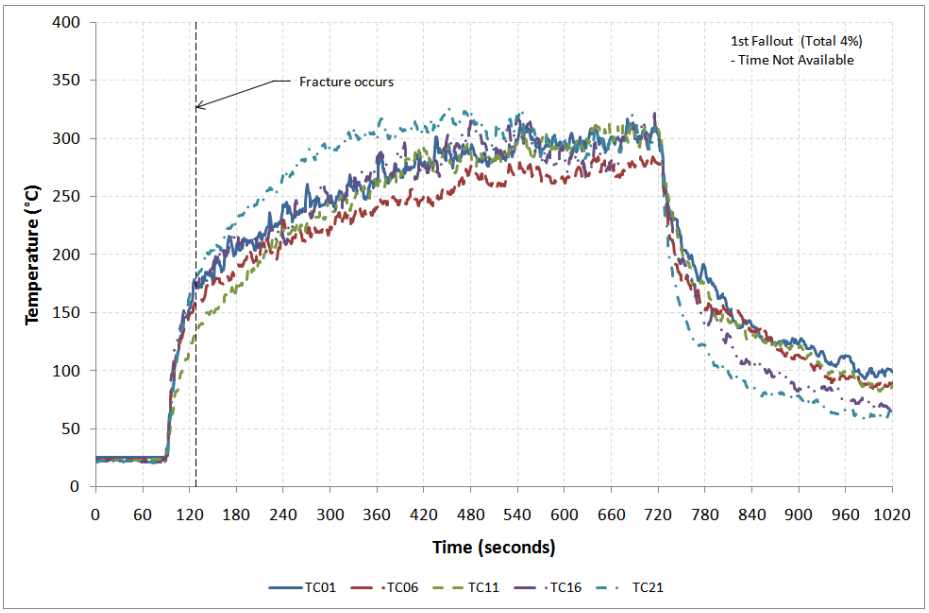

Figure C-60: Gas temperature profiles for experiment 4 Test 32

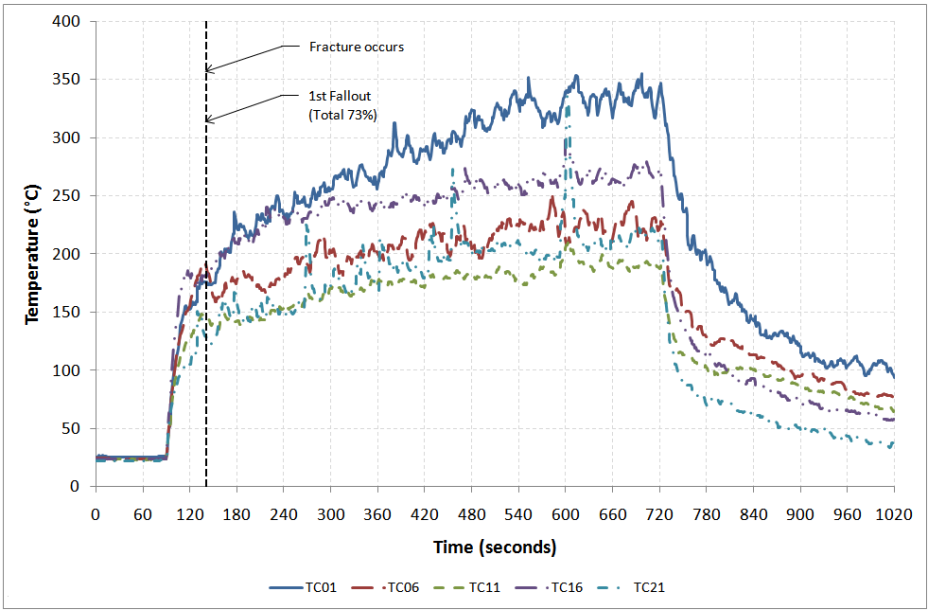

Figure C-61: Gas temperature profiles for experiment 4 Test 33

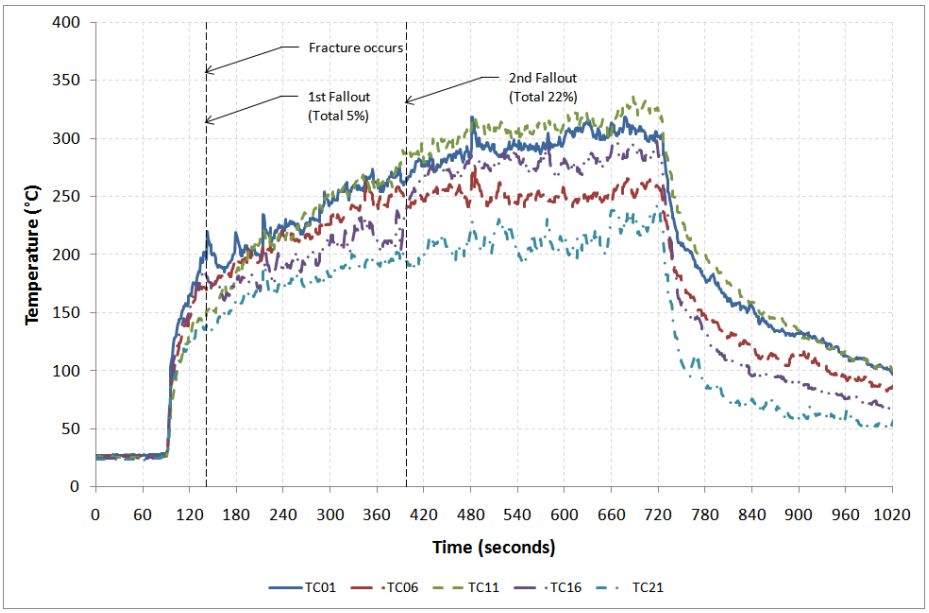

Figure C-62: Gas temperature profiles for experiment 4 Test 34

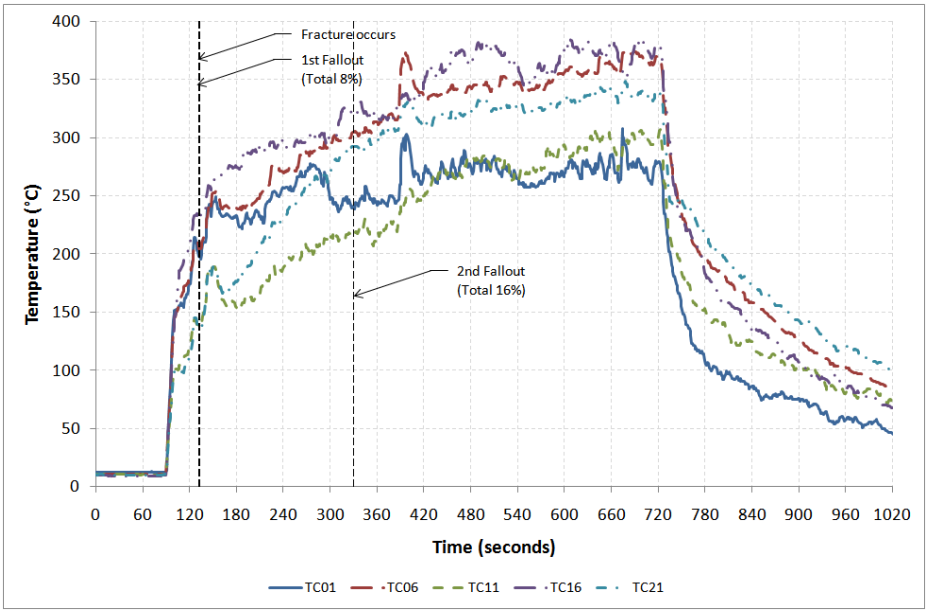

Figure C-63: Gas temperature profiles for experiment 4 Test 35

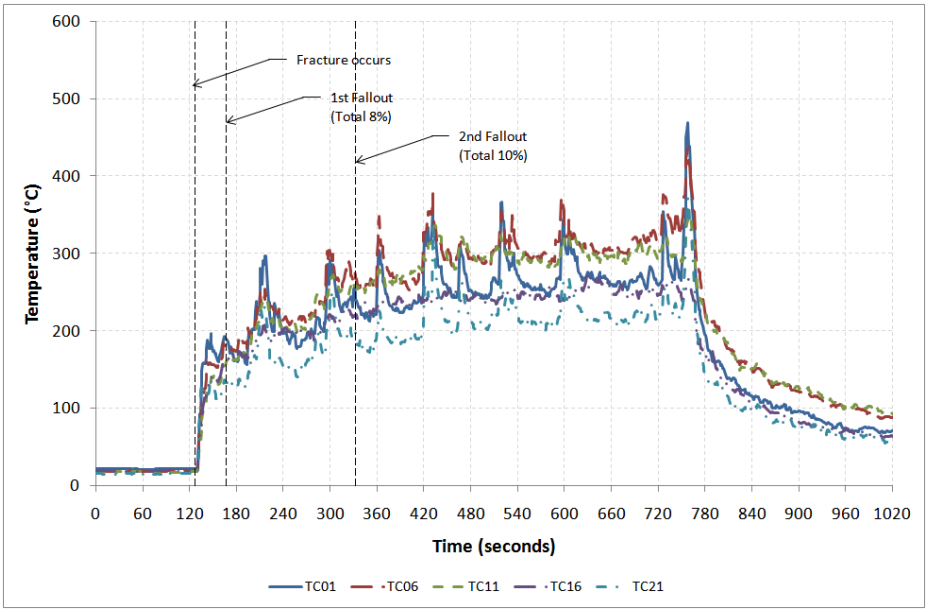

Figure C-64: Gas temperature profiles for experiment 4 Test 36

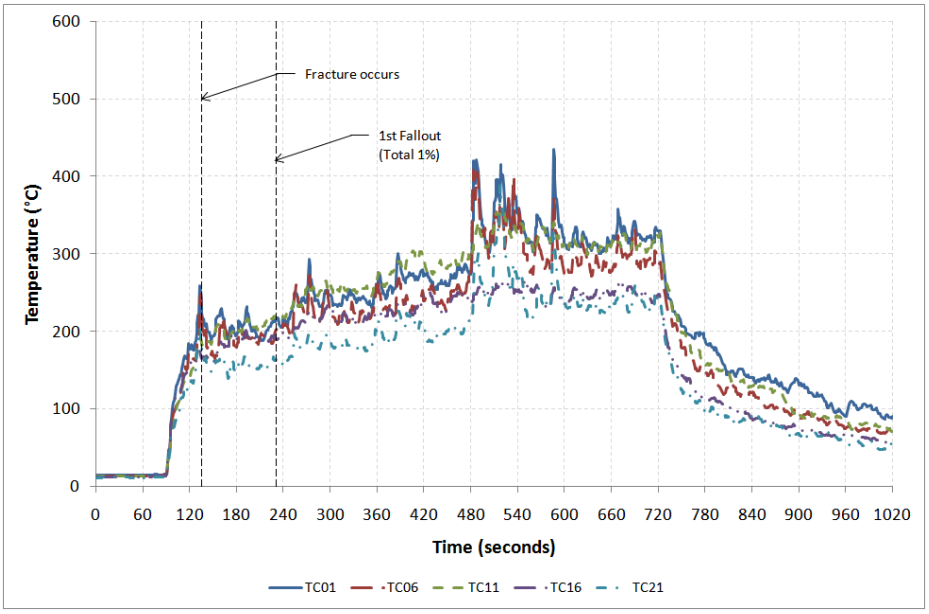

Figure C-65: Gas temperature profiles for experiment 4 Test 38

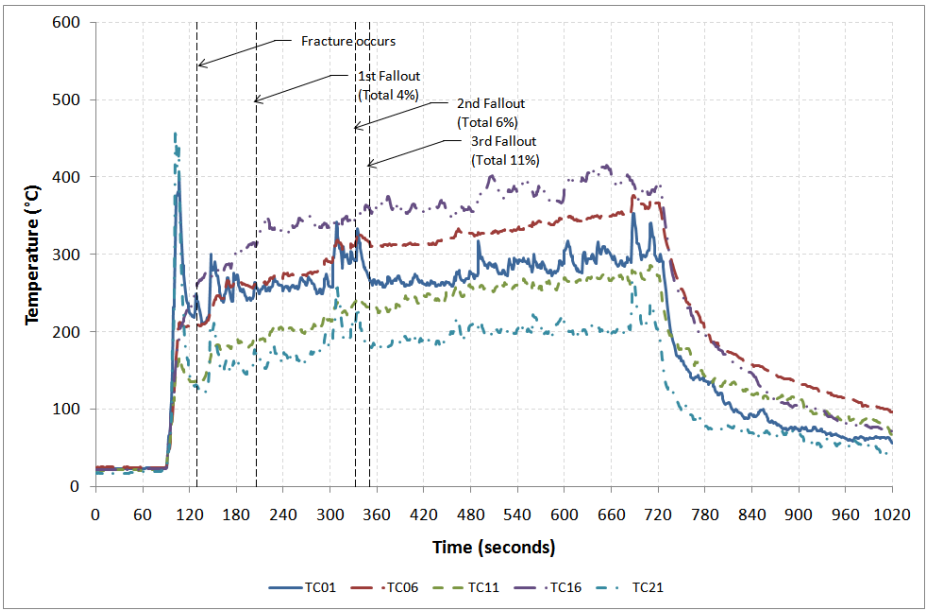

Figure C-66: Gas temperature profiles for experiment 4 Test 39

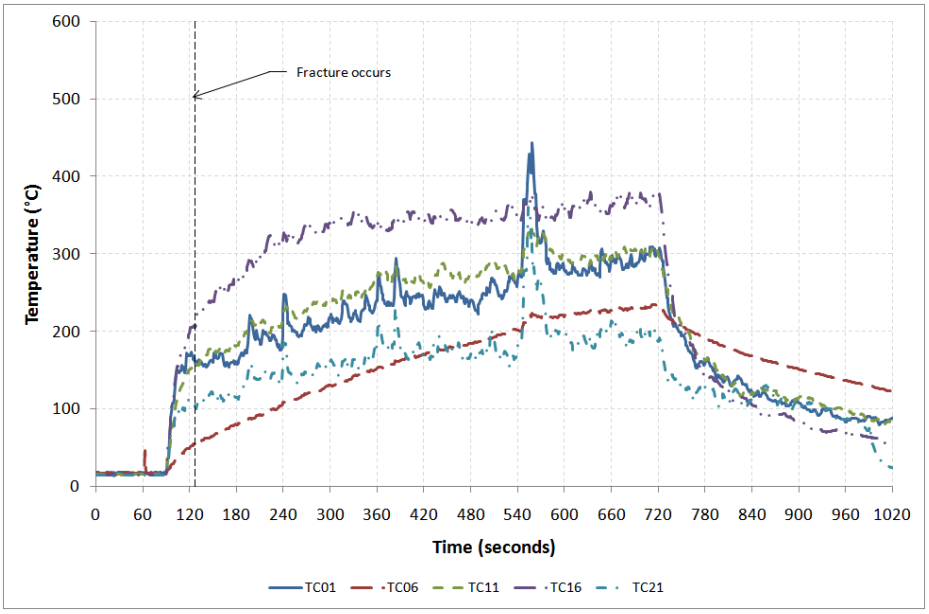

Figure C-67: Gas temperature profiles for experiment 4 Test 40

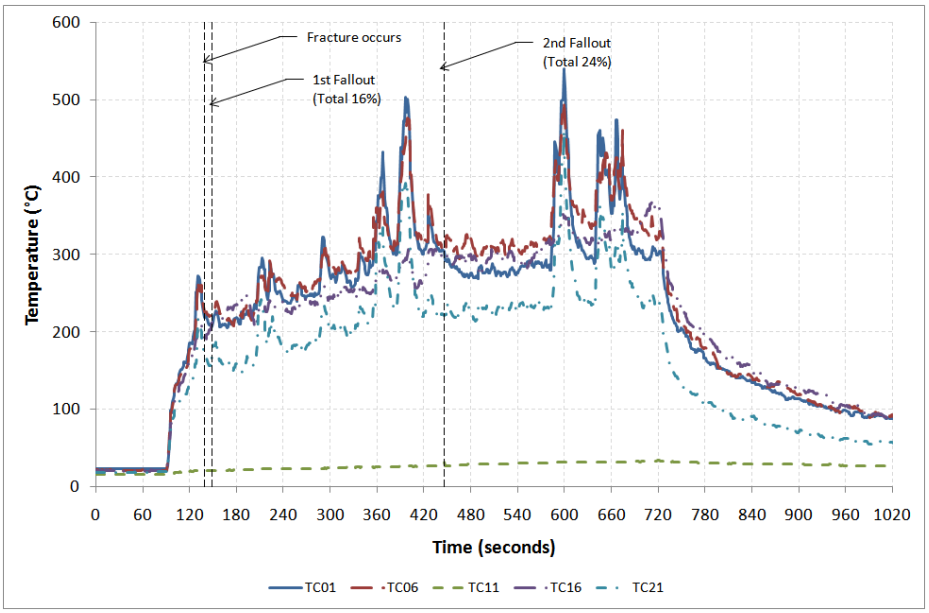

Figure C-68: Gas temperature profiles for experiment 4 Test 41

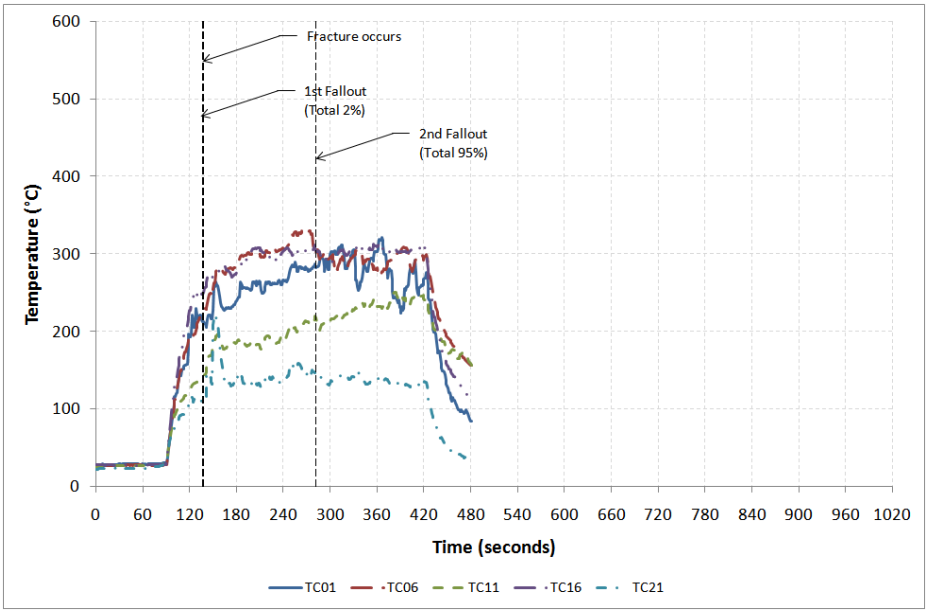

Figure C-69: Gas temperature profiles for experiment 4 Test 42

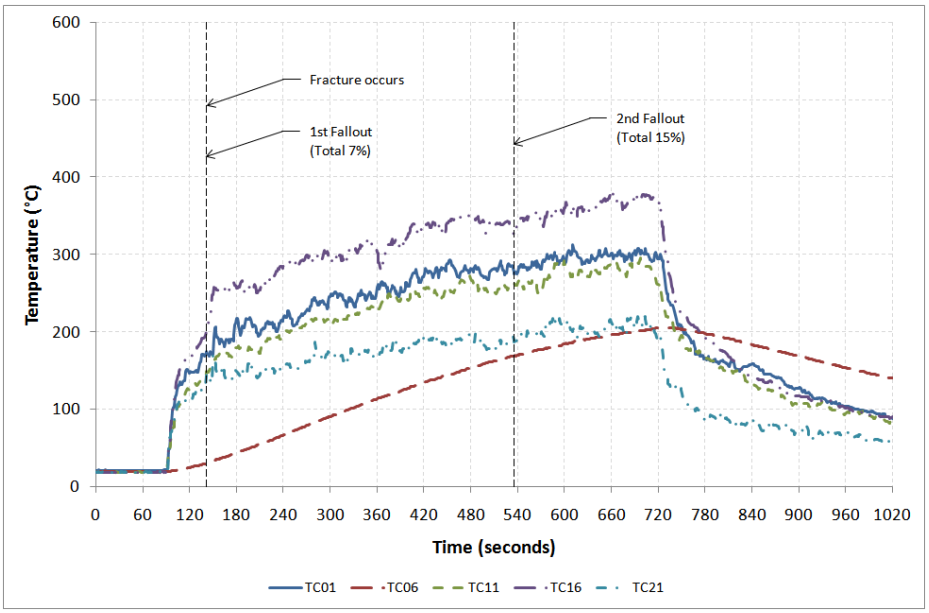

Figure C-70: Gas temperature profiles for experiment 4 Test 43

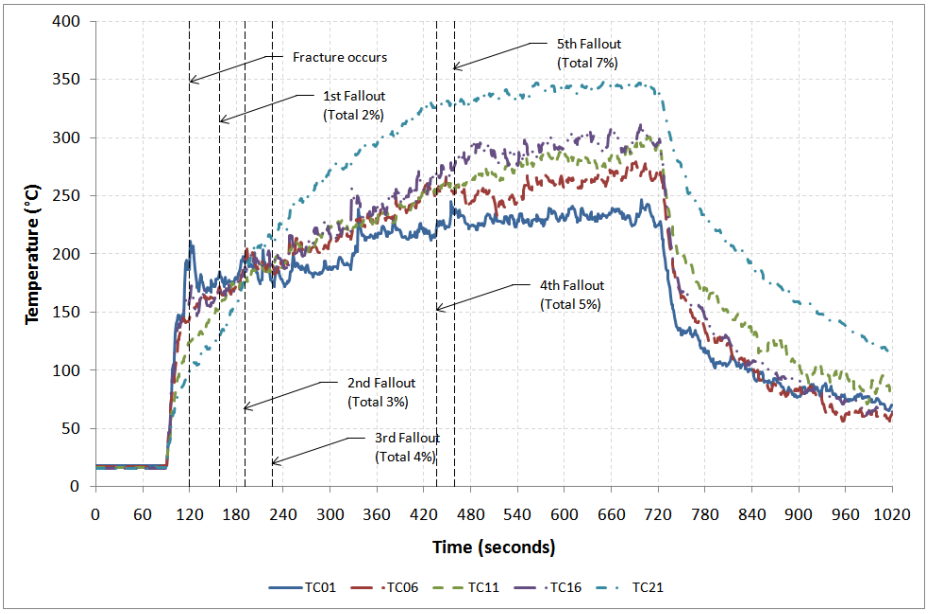

Figure C-71: Gas temperature profiles for experiment 4 Test 44

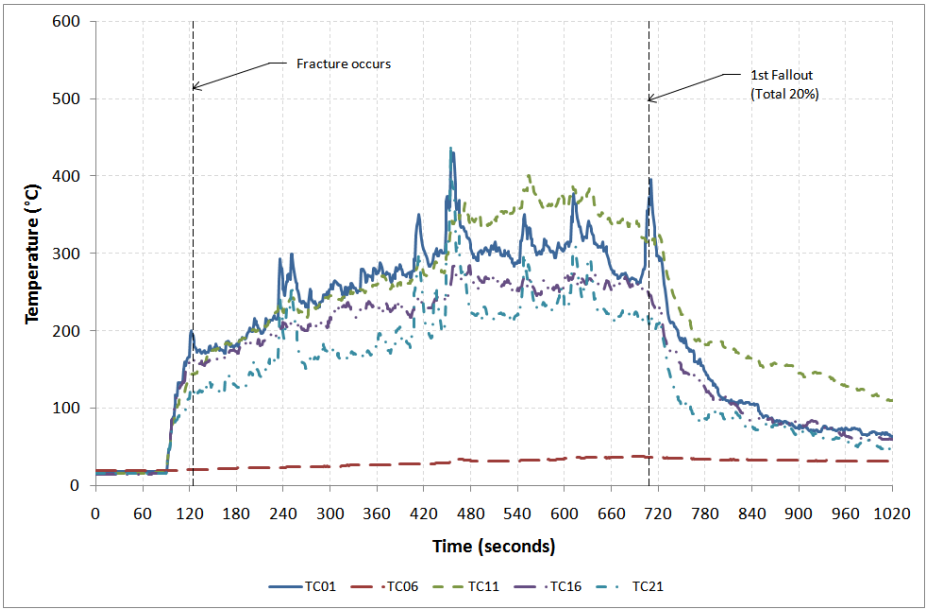

Figure C-72: Gas temperature profiles for experiment 4 Test 45

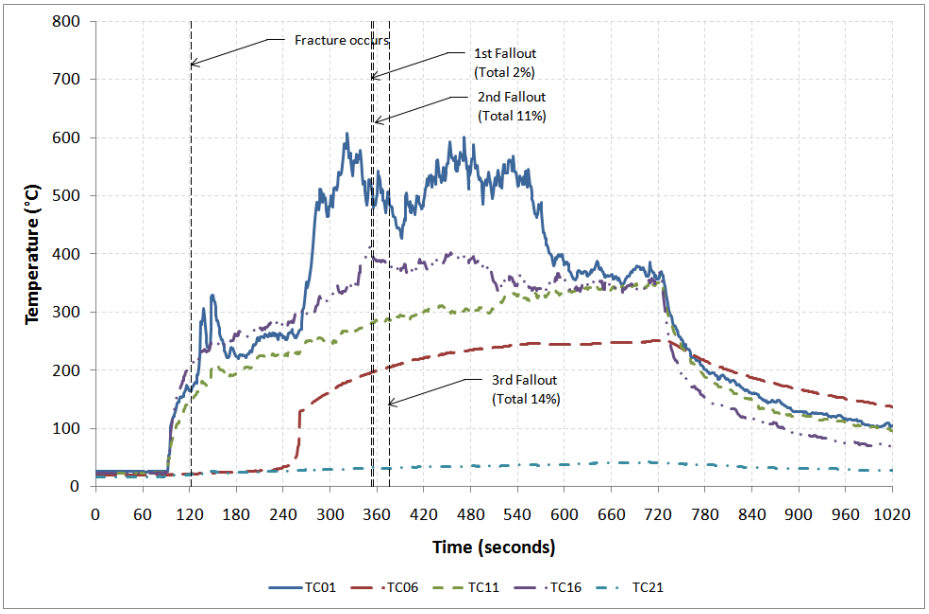

Figure C-73: Gas temperature profiles for experiment 4 Test 46

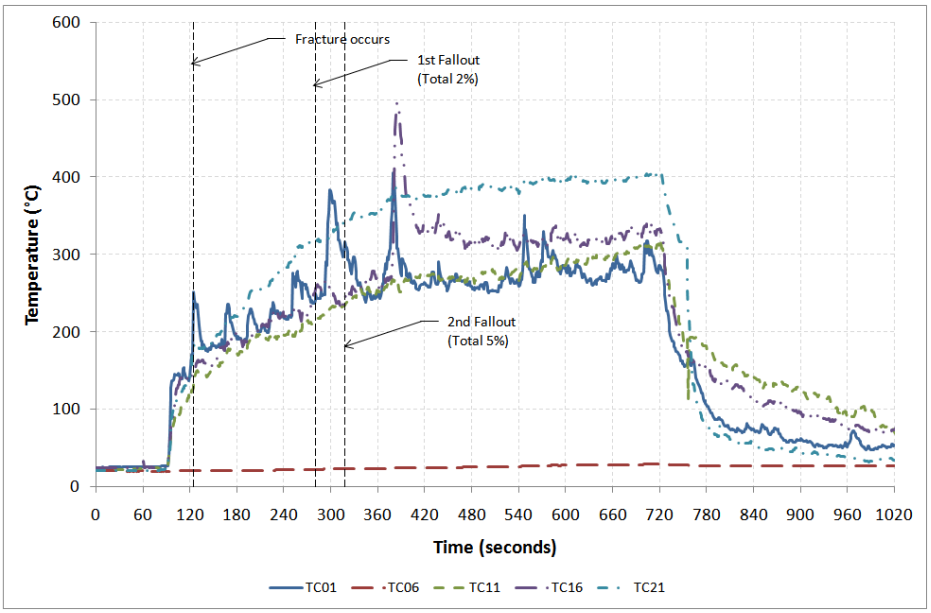

Figure C-74: Gas temperature profiles for experiment 4 Test 47

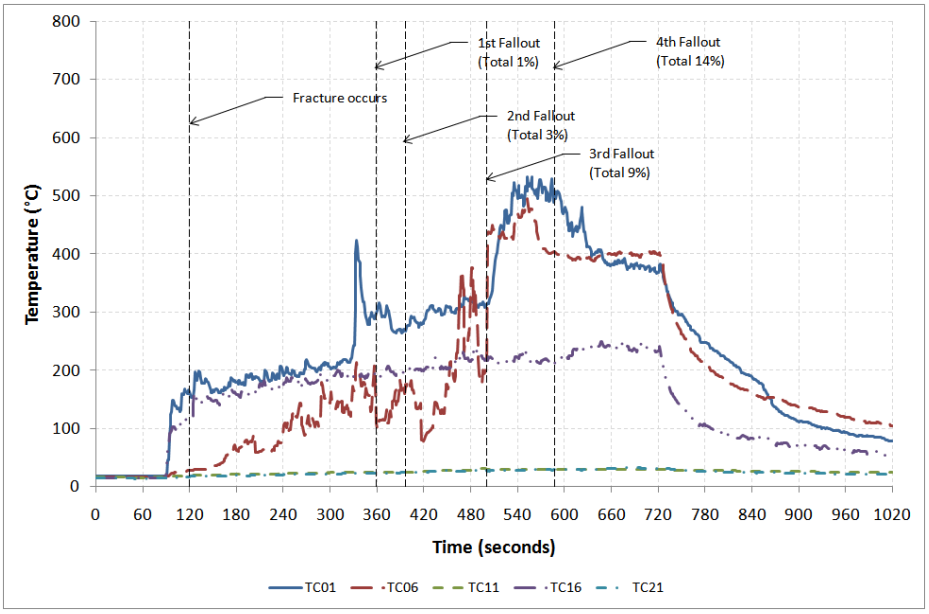

Figure C-75: Gas temperature profiles for experiment 4 Test 48

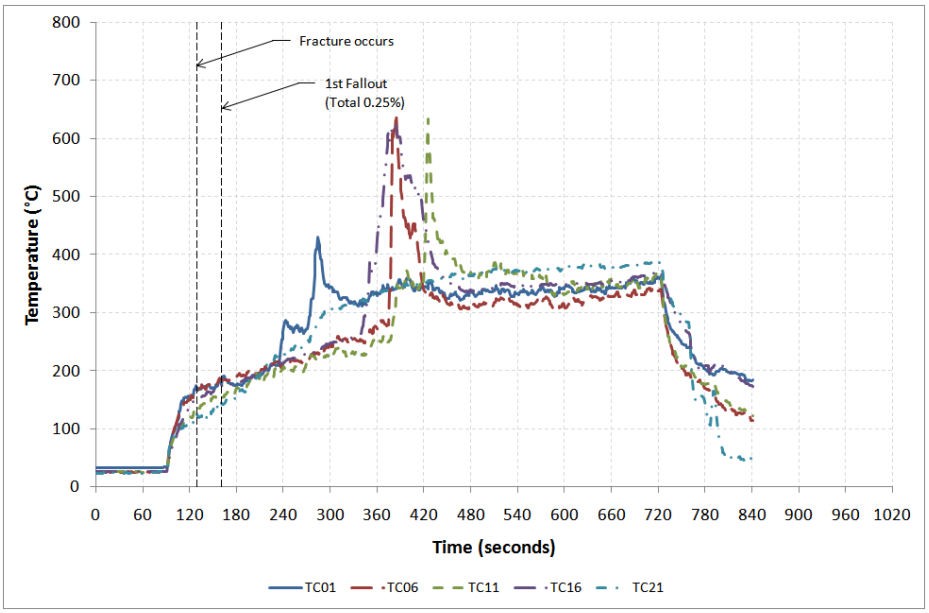

Figure C-76: Gas temperature profiles for experiment 4 Test 49

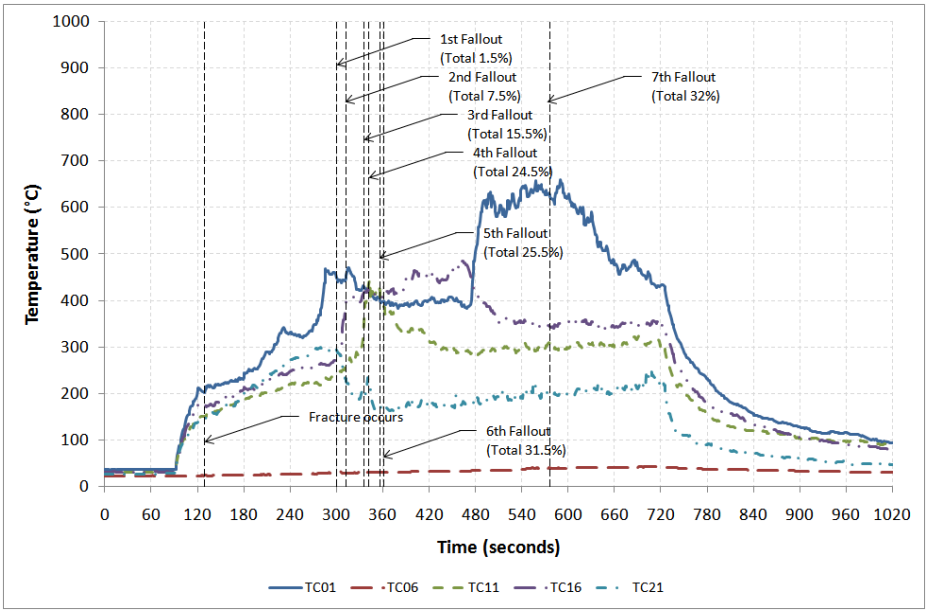

Figure C-77: Gas temperature profiles for experiment 4 Test 50

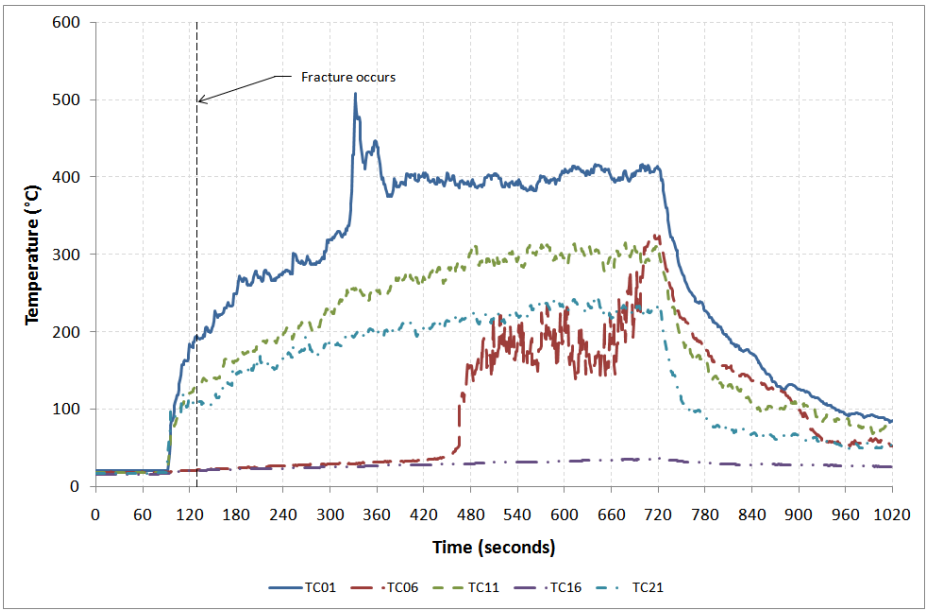

Figure C-78: Gas temperature profiles for experiment 4 Test 51

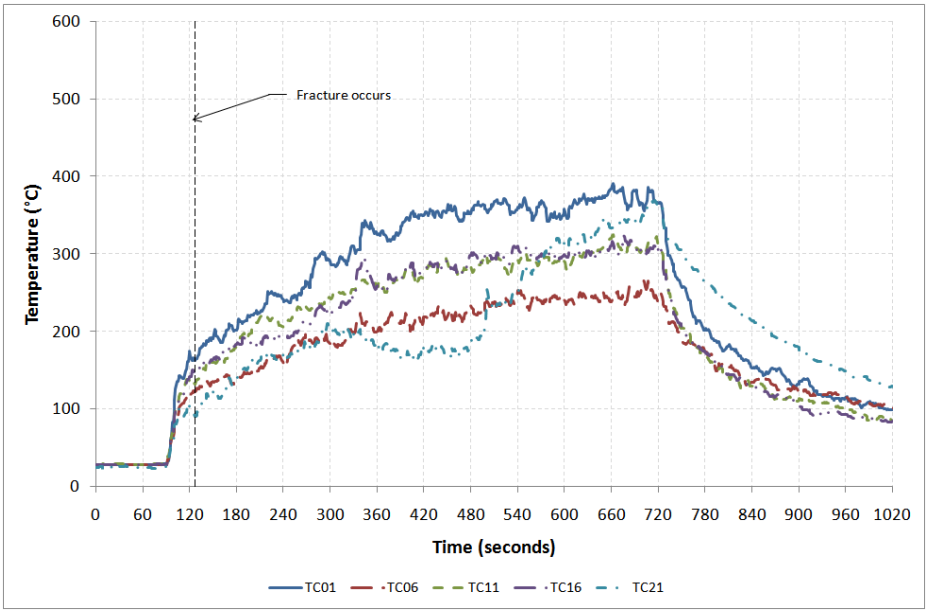

Figure C-79: Gas temperature profiles for experiment 4 Test 52

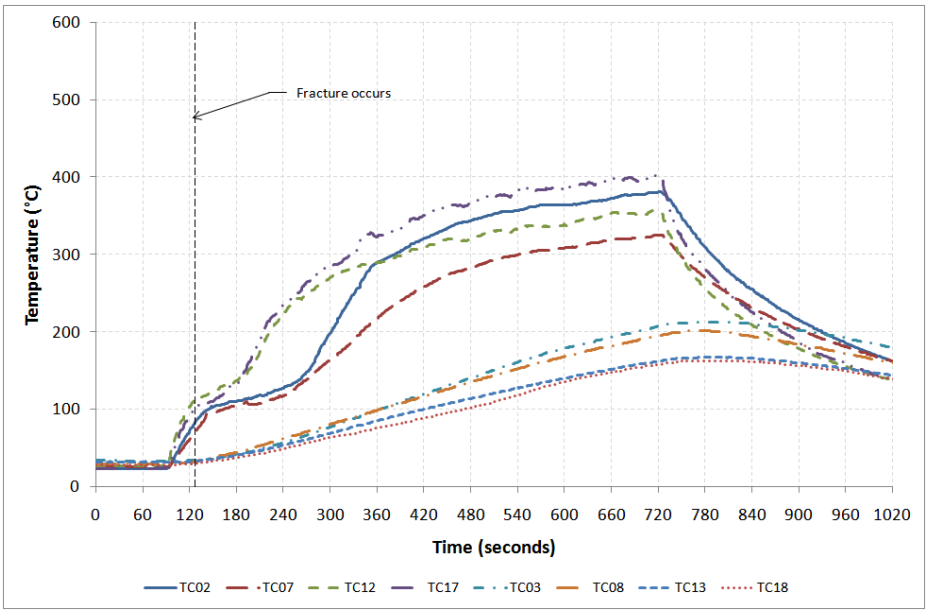

Figure C-80: Glass temperature profiles on exposed side for experiment 4 Test 52

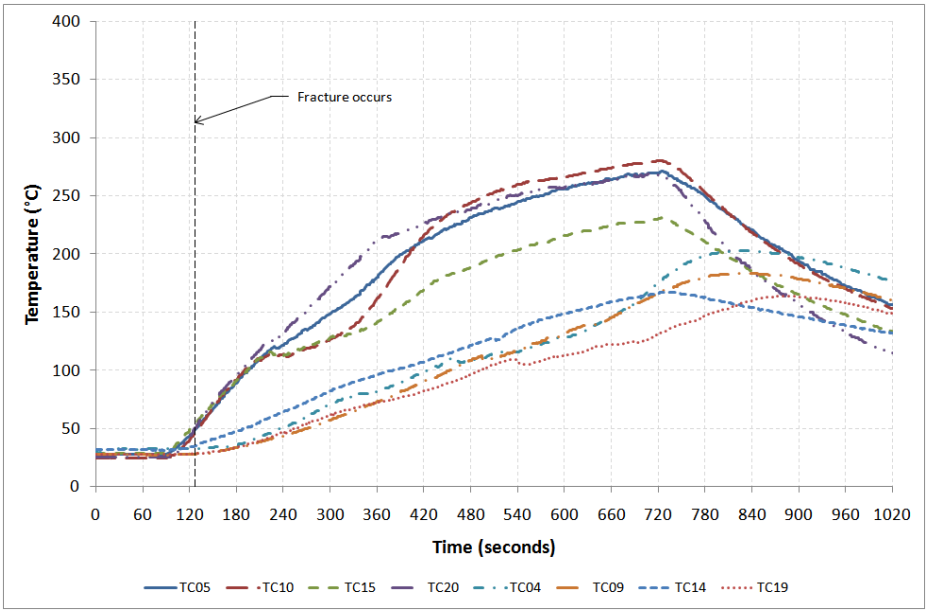

Figure C-81: Glass temperature profiles on unexposed side for experiment 4 Test 52

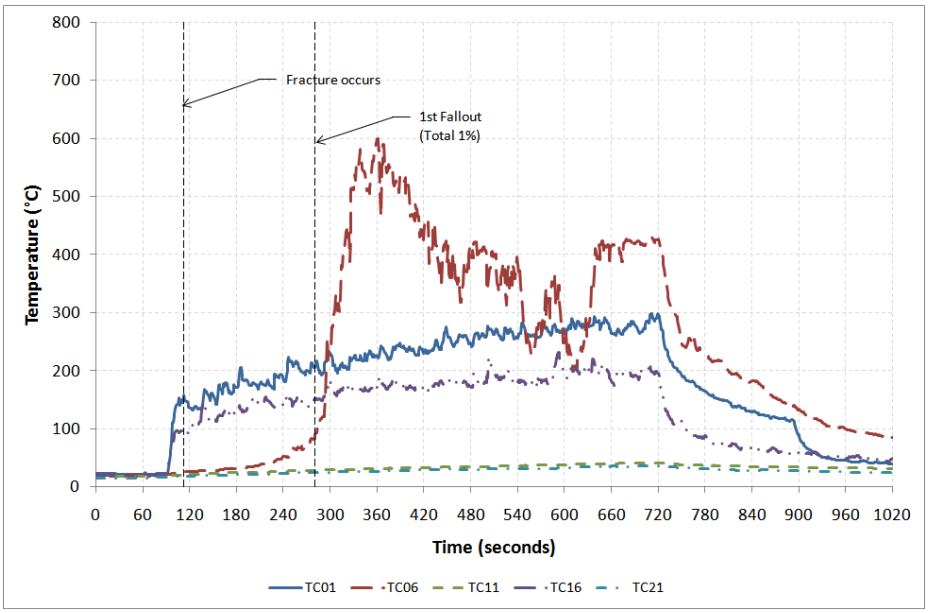

Figure C-82: Gas temperature profiles for experiment 4 Test 53

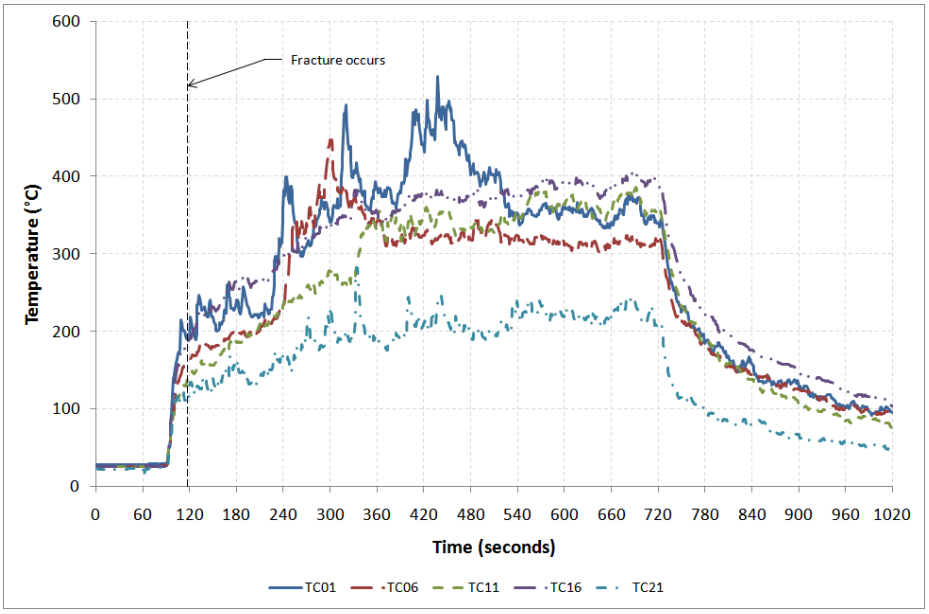

Figure C-83: Gas temperature profiles for experiment 4 Test 54

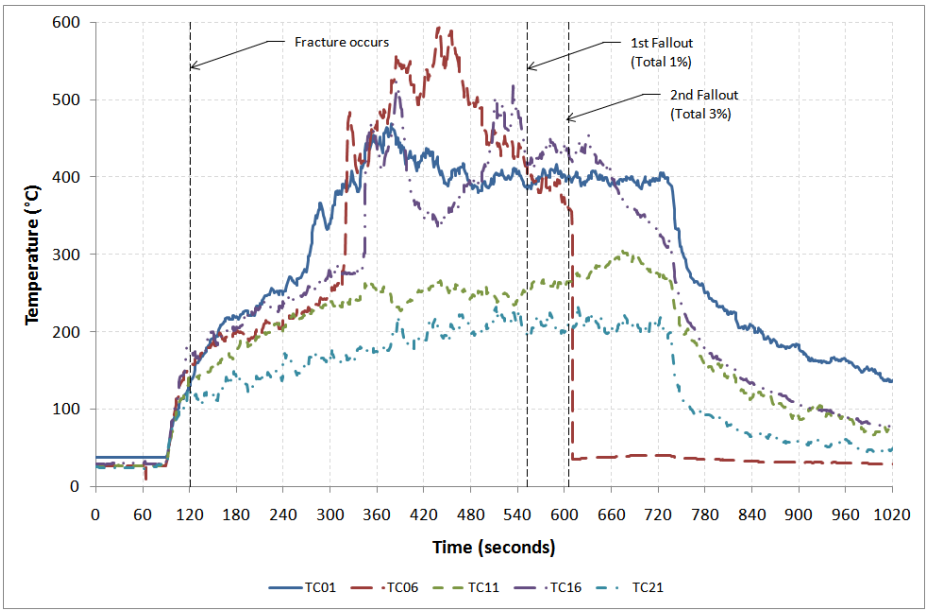

Figure C-84: Gas temperature profiles for experiment 4 Test 55

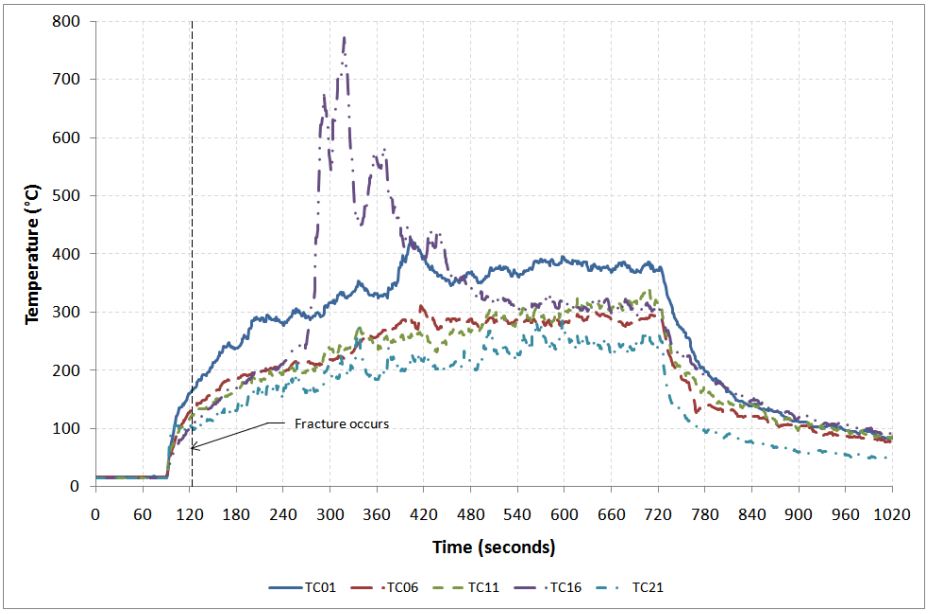

Figure C-85: Gas temperature profiles for experiment 4 Test 56

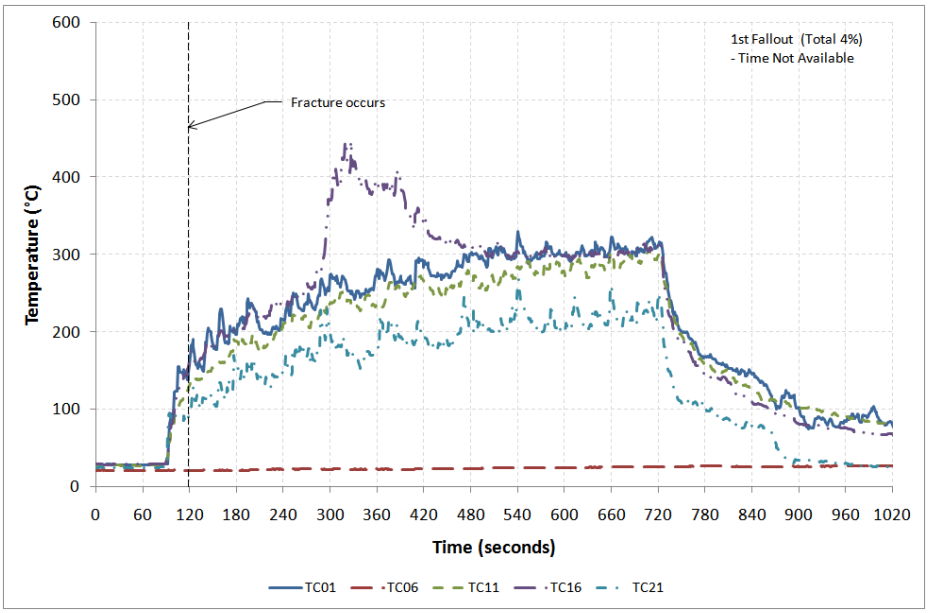

Figure C-86: Gas temperature profiles for experiment 4 Test 57

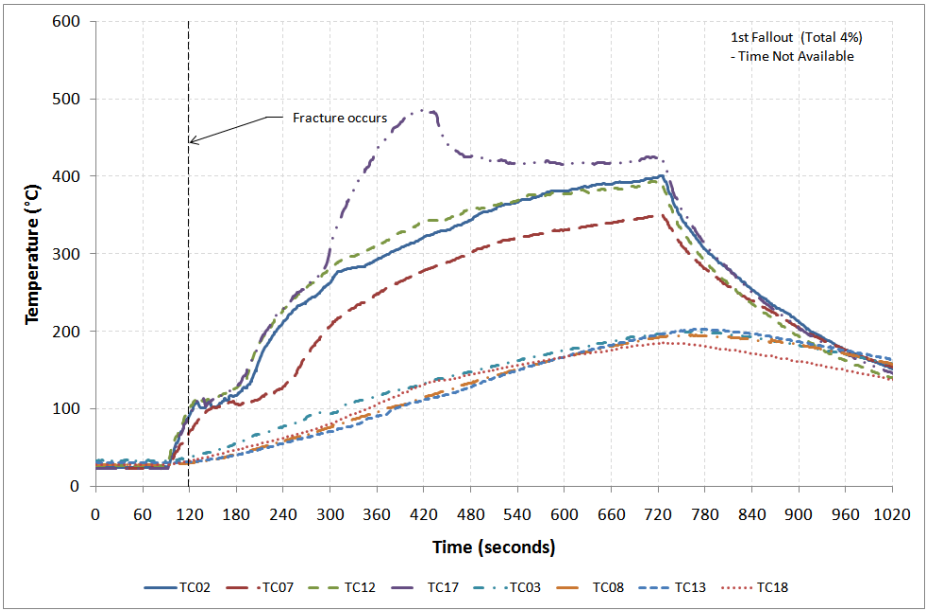

Figure C-87: Glass temperature profiles on exposed side for experiment 4 Test 57

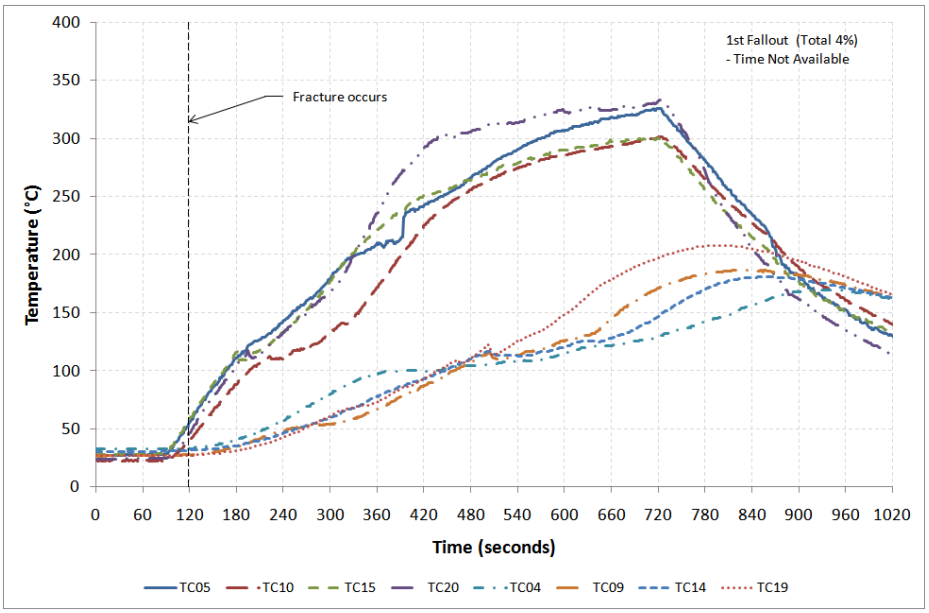

Figure C-88: Glass temperature profiles on unexposed side for experiment 4 Test 57

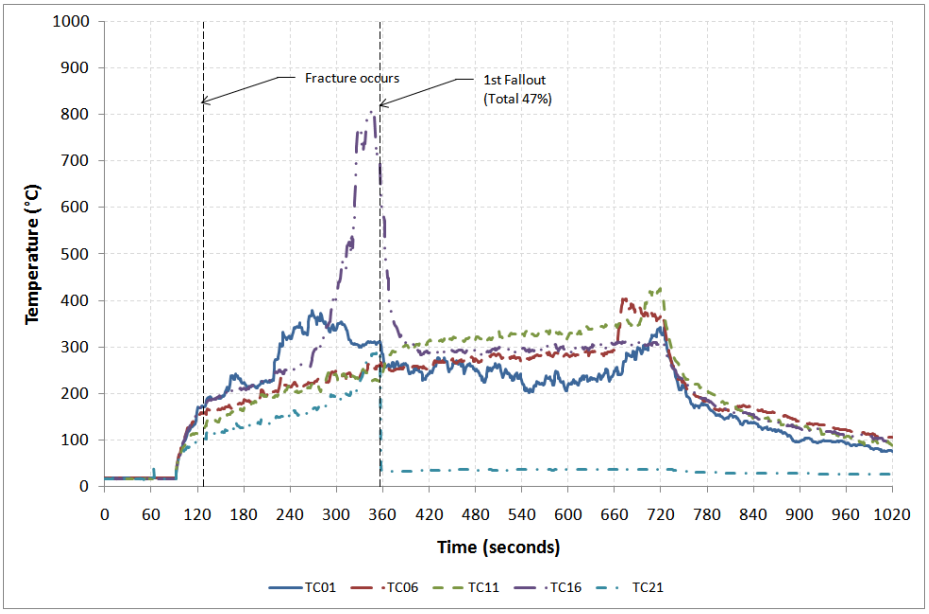

Figure C-89: Gas temperature profiles for experiment 4 Test 58

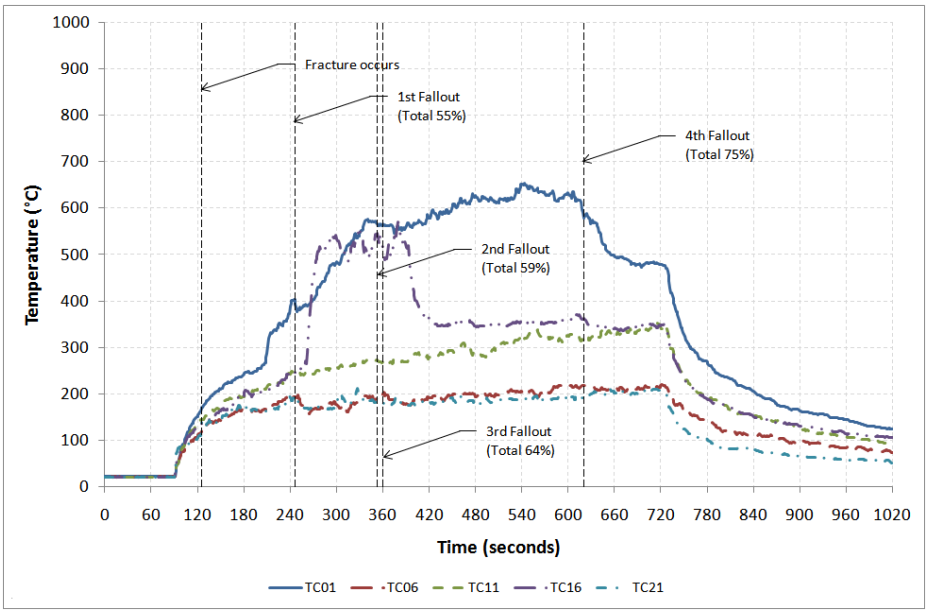

Figure C-90: Gas temperature profiles for experiment 4 Test 59

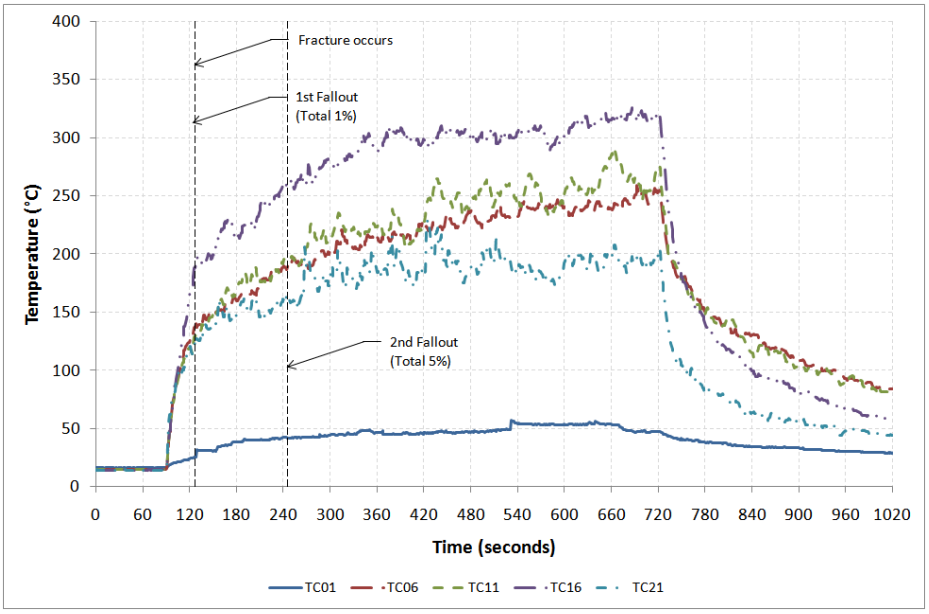

Figure C-91: Gas temperature profiles for experiment 4 Test 60

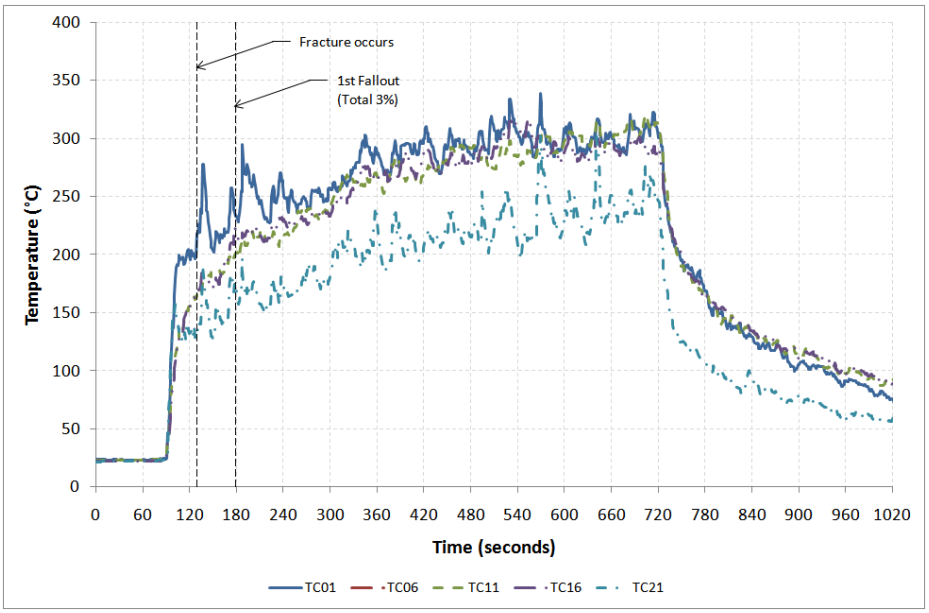

Figure C-92: Gas temperature profiles for experiment 4 Test 61 (TC06 reading not available)

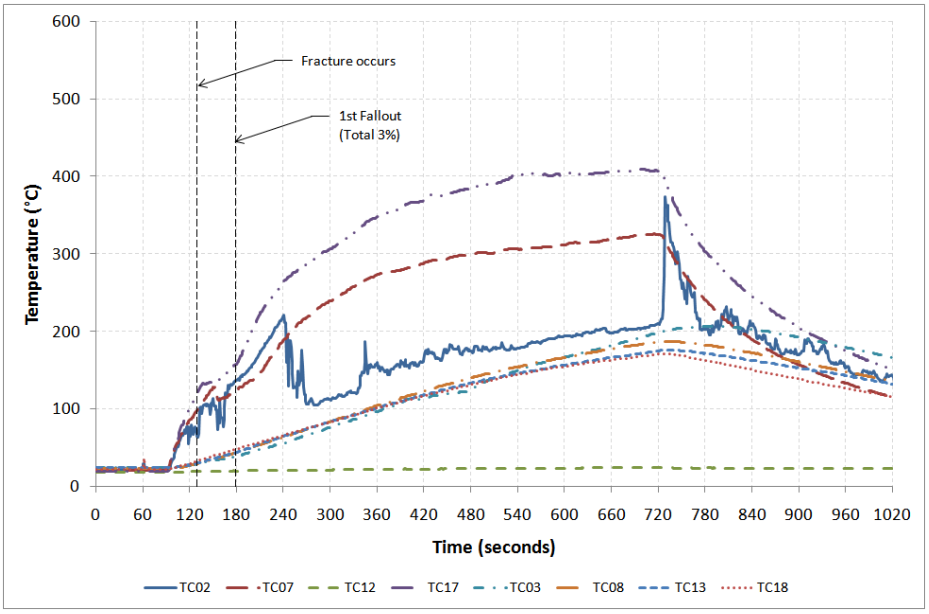

Figure C-93: Glass temperature profiles on exposed side for experiment 4 Test 61

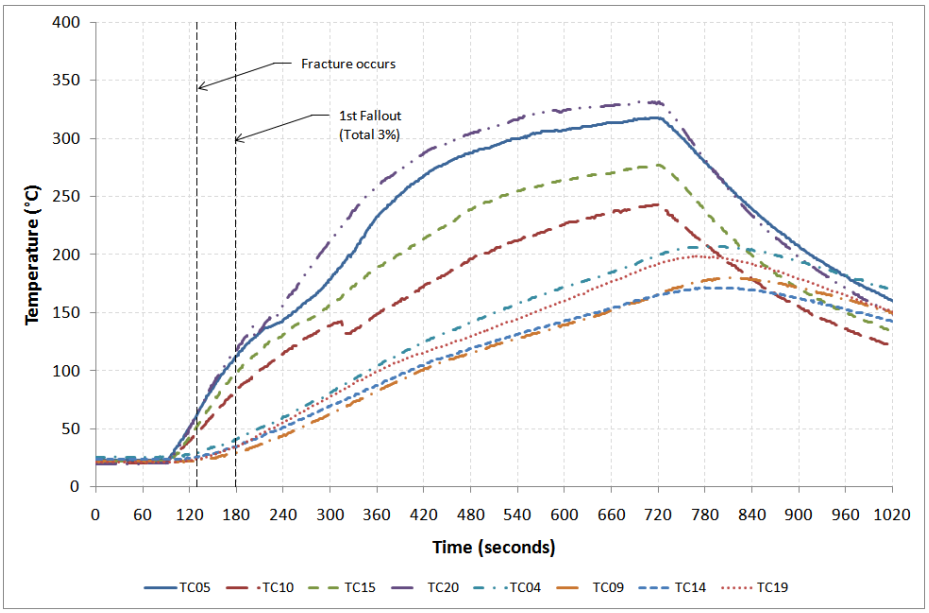

Figure C-94: Glass temperature profiles on unexposed side for experiment 4 Test 61

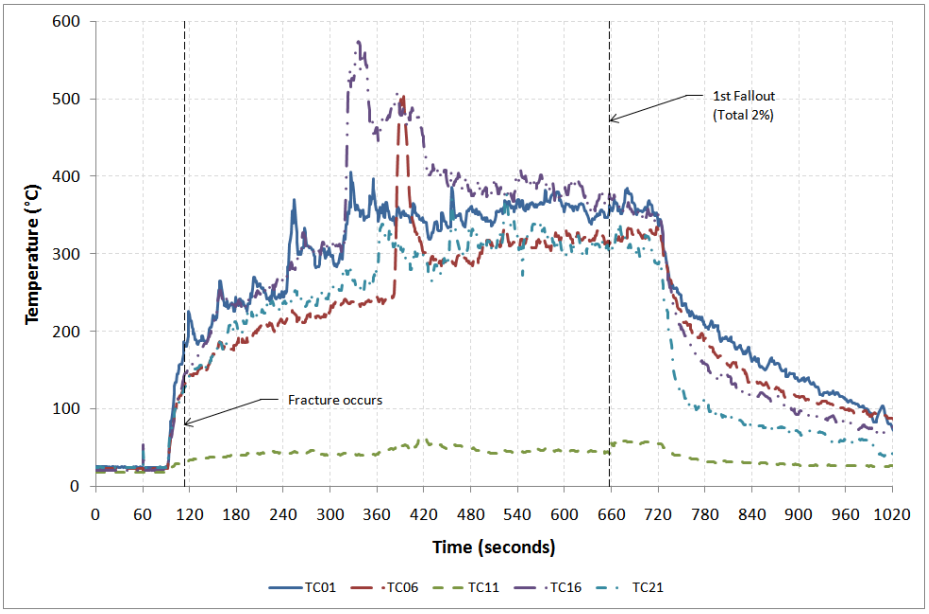

Figure C-95: Gas temperature profiles for experiment 4 Test 62

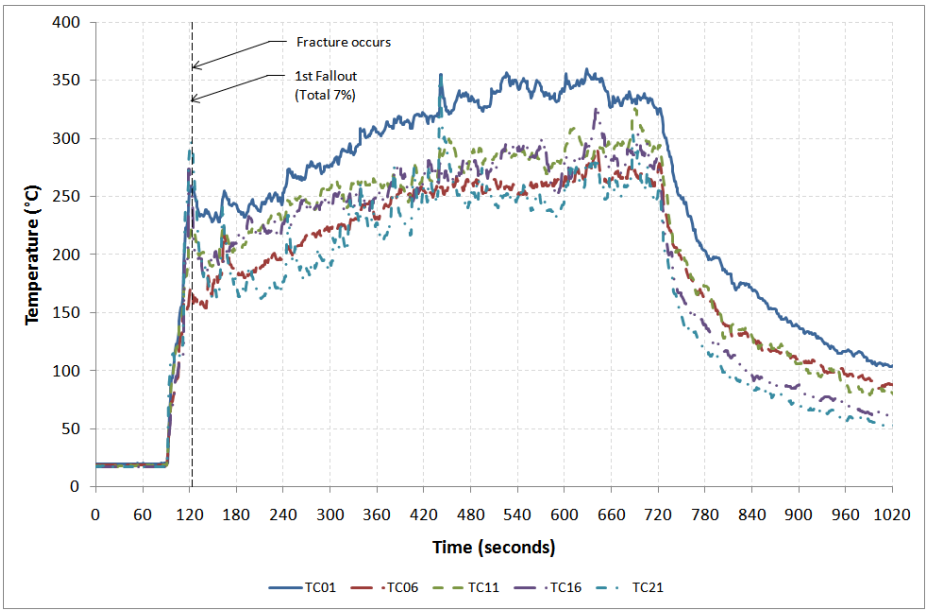

Figure C-96: Gas temperature profiles for experiment 4 Test 63

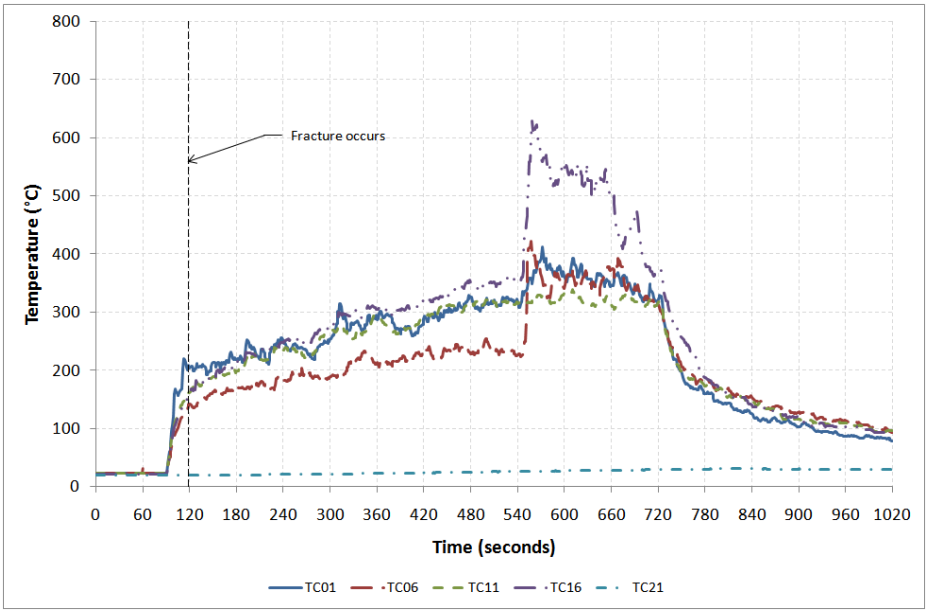

Figure C-97: Gas temperature profiles for experiment 4 Test 64

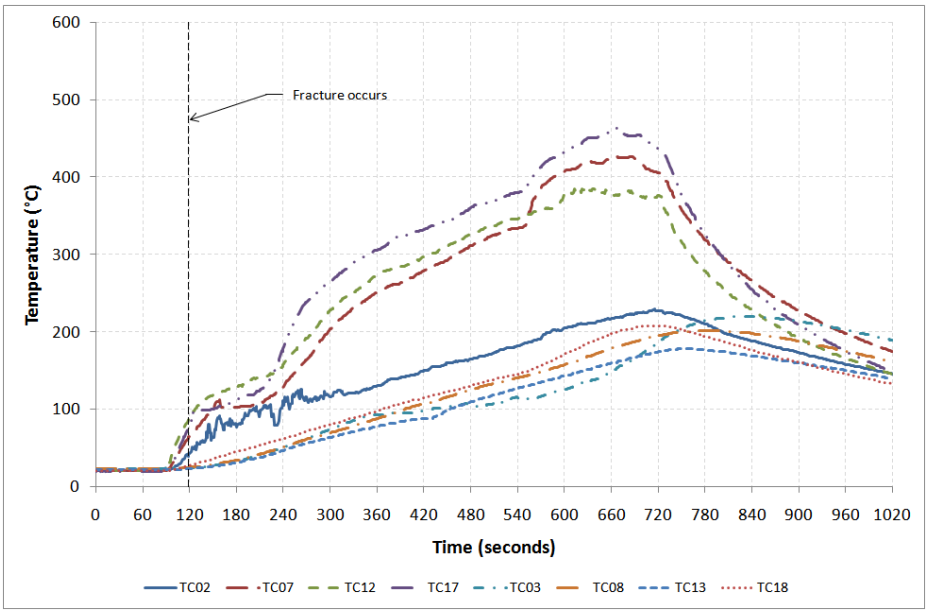

Figure C-98: Glass temperature profiles on exposed side for experiment 4 Test 64

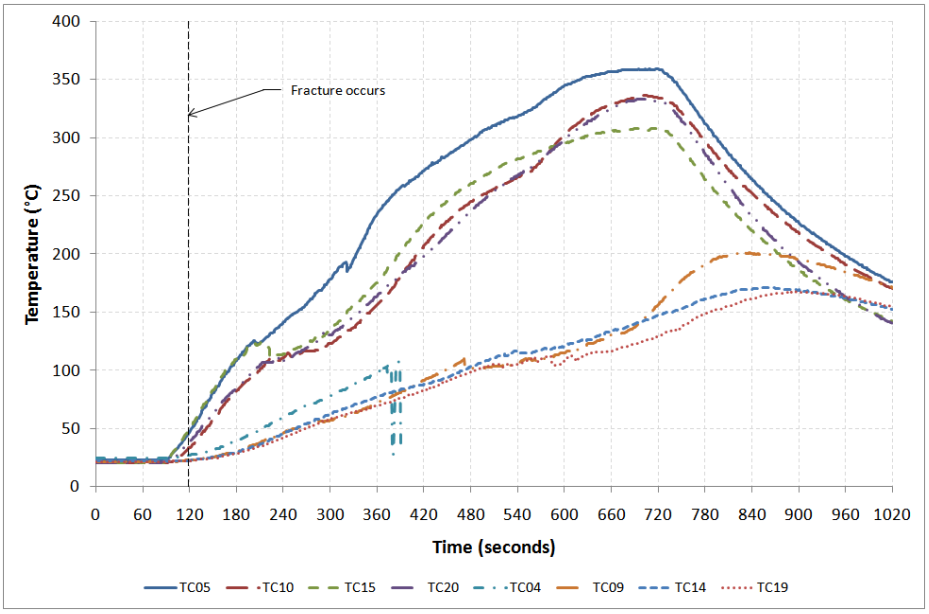

Figure C-99: Glass temperature profiles on unexposed side for experiment 4 Test 64

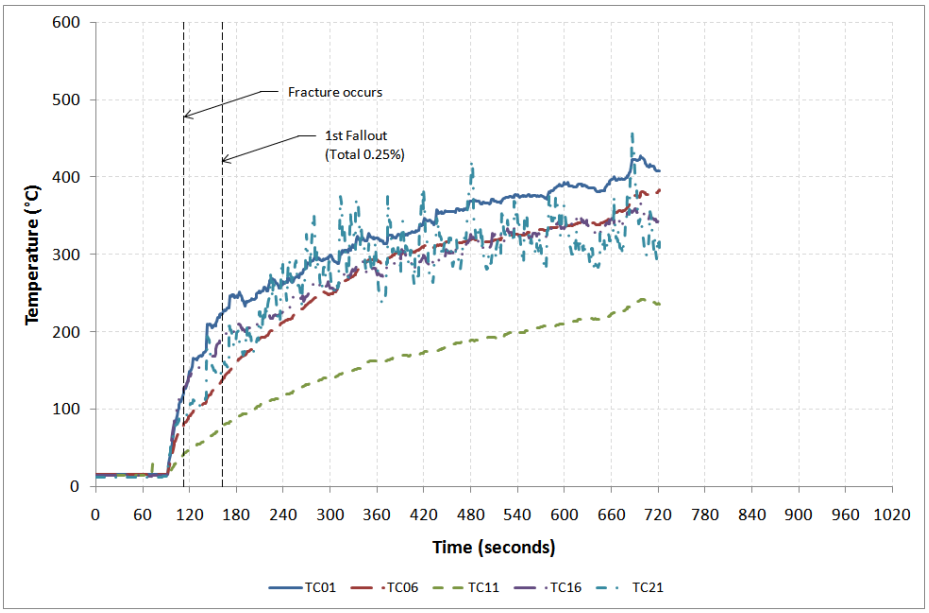

Figure C-100: Gas temperature profiles for experiment 6 Test 1

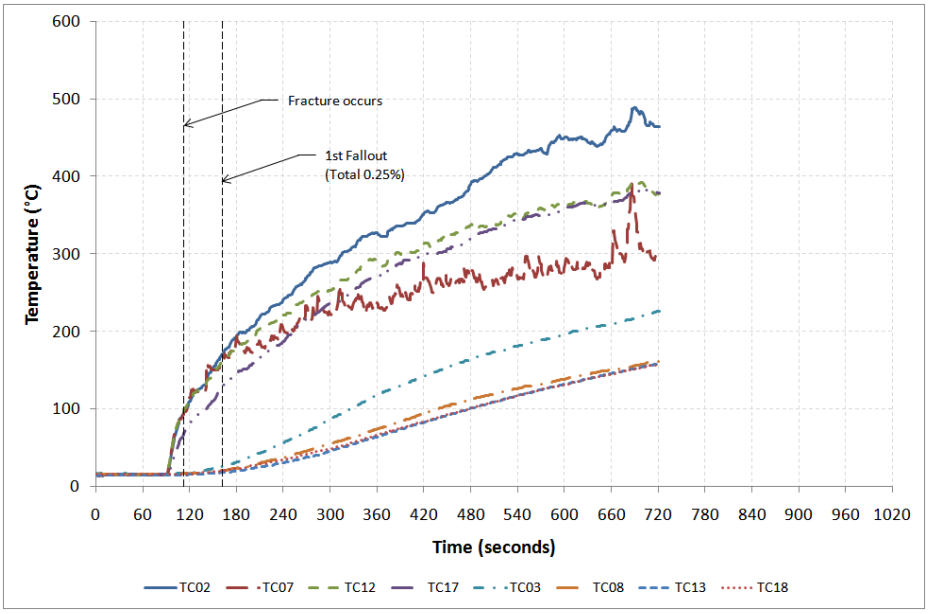

Figure C-101: Glass temperature profiles on exposed side for experiment 6 Test 1

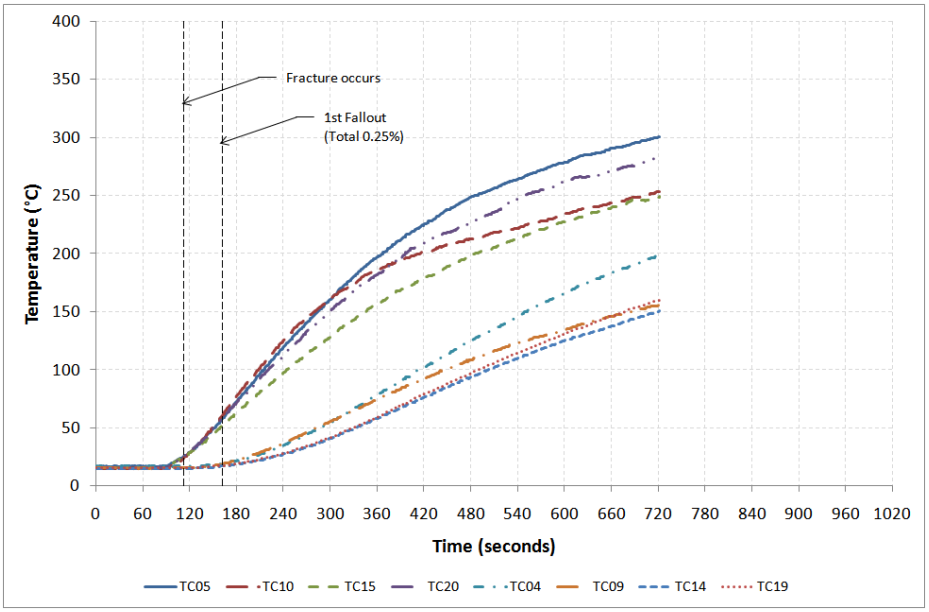

Figure C-102: Glass temperature profiles on exposed side for experiment 6 Test 1

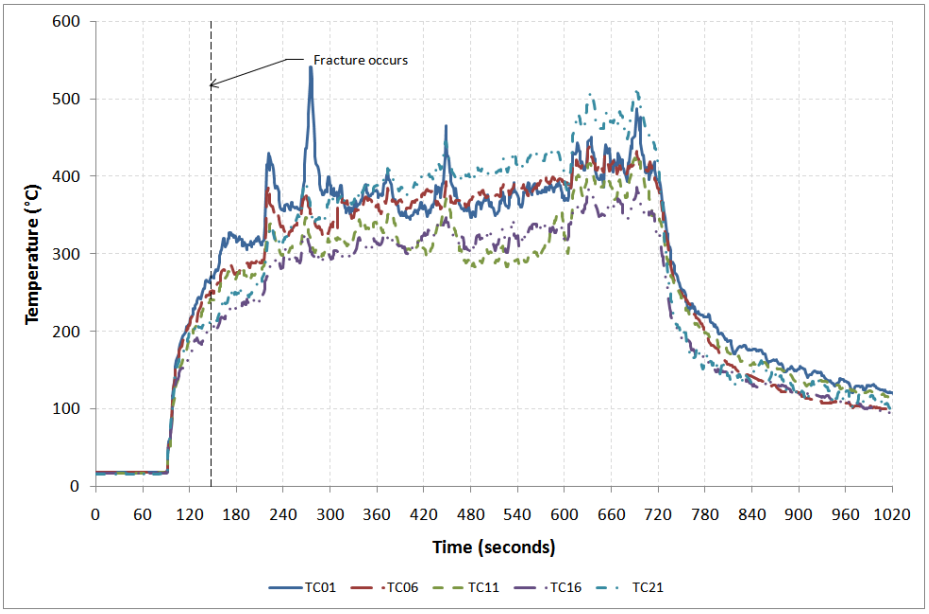

Figure C-103: Gas temperature profiles for experiment 6 Test 3

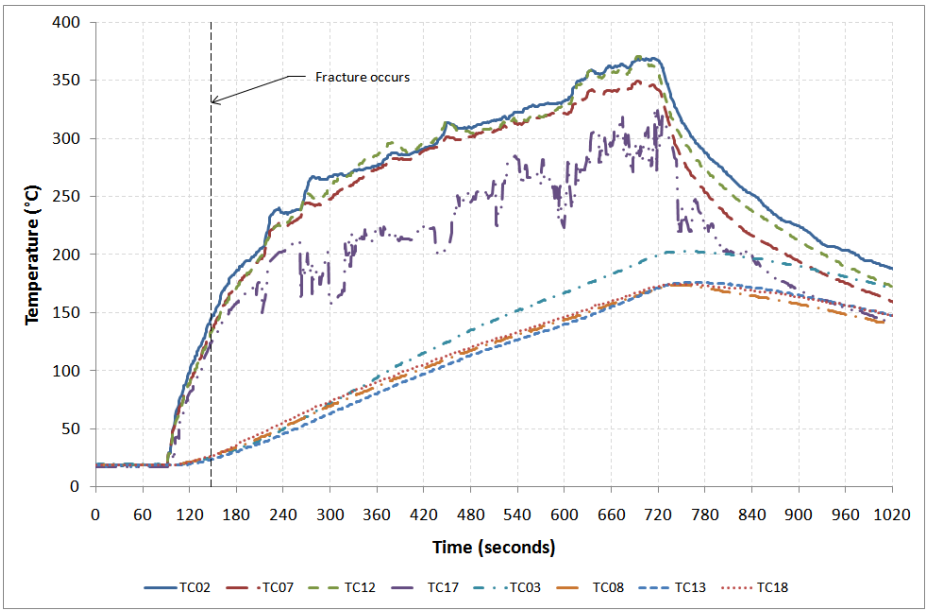

Figure C-104: Glass temperature profiles on exposed side for experiment 6 Test 3

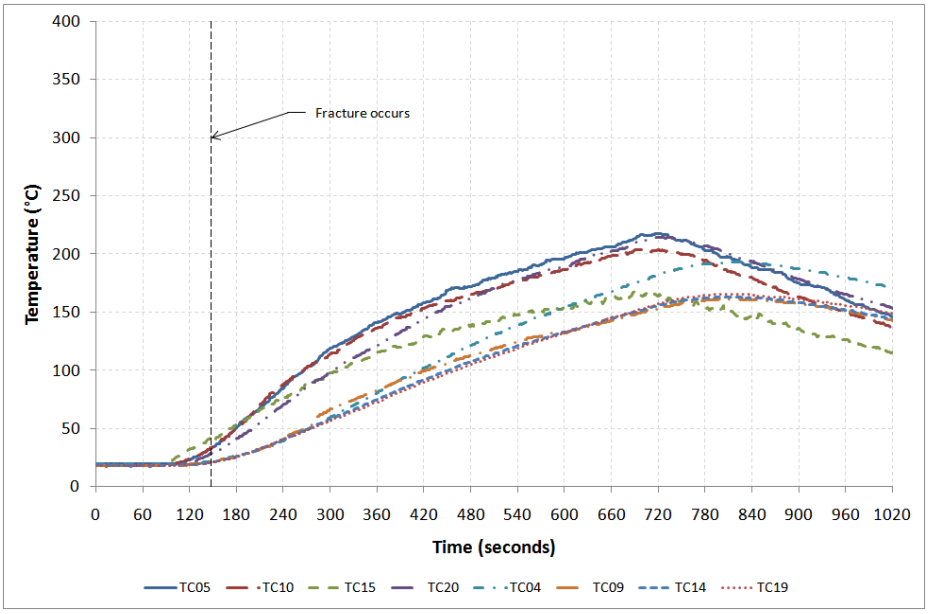

Figure C-105: Glass temperature profiles on unexposed side for experiment 6 Test 3

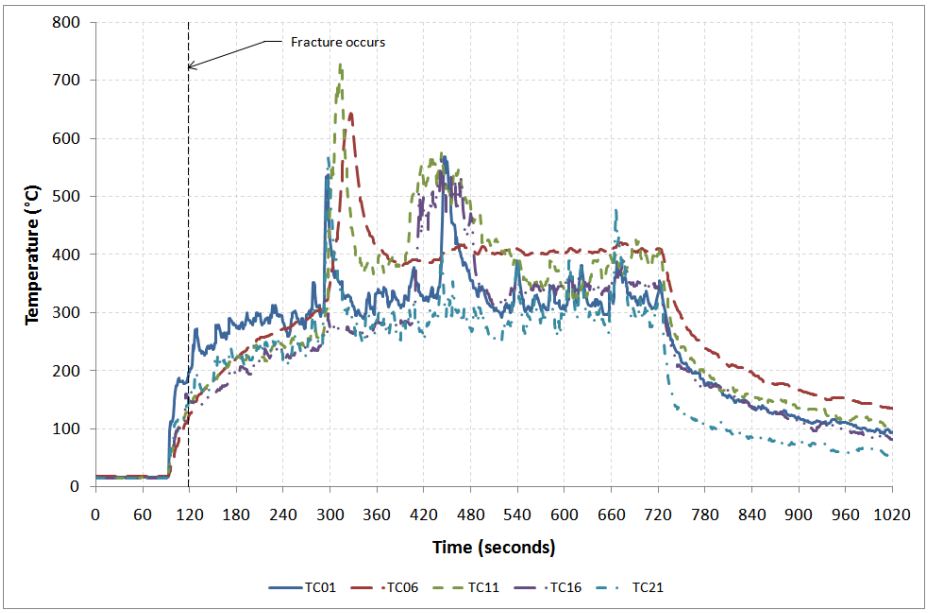

Figure C-106: Gas temperature profiles for experiment 6 Test 4

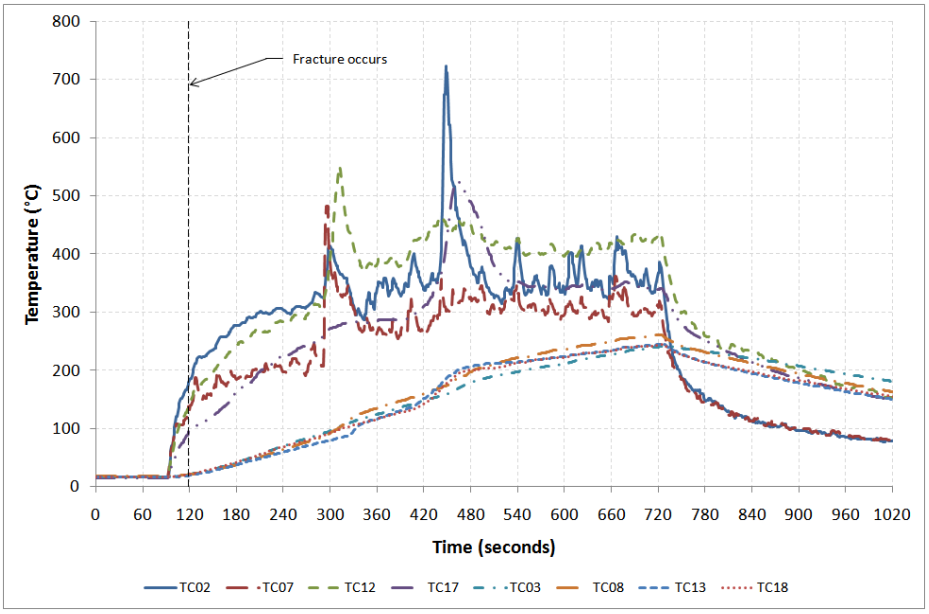

Figure C-107: Glass temperature profiles on exposed side for experiment 6 Test 4

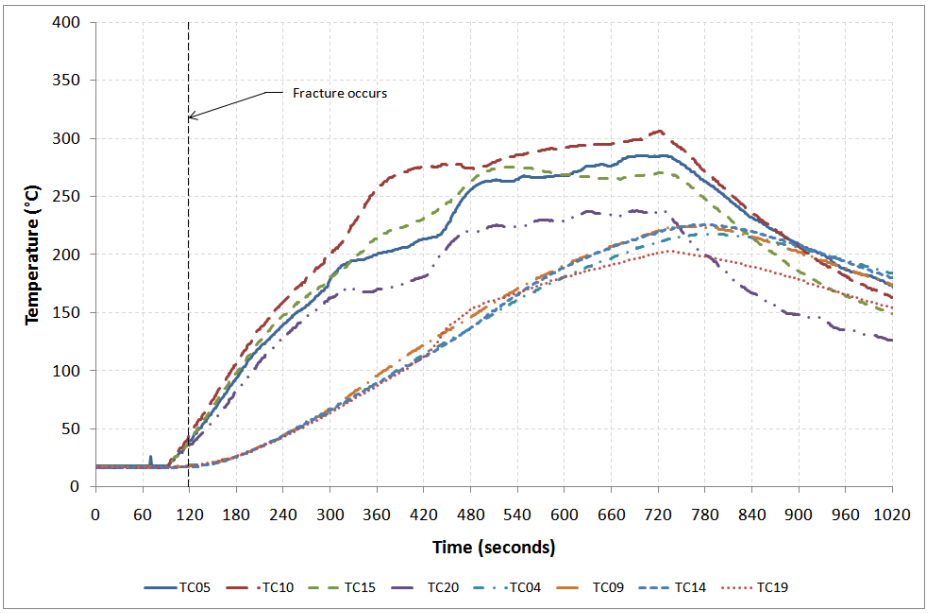

Figure C-108: Glass temperature profiles on unexposed side for experiment 6 Test 4

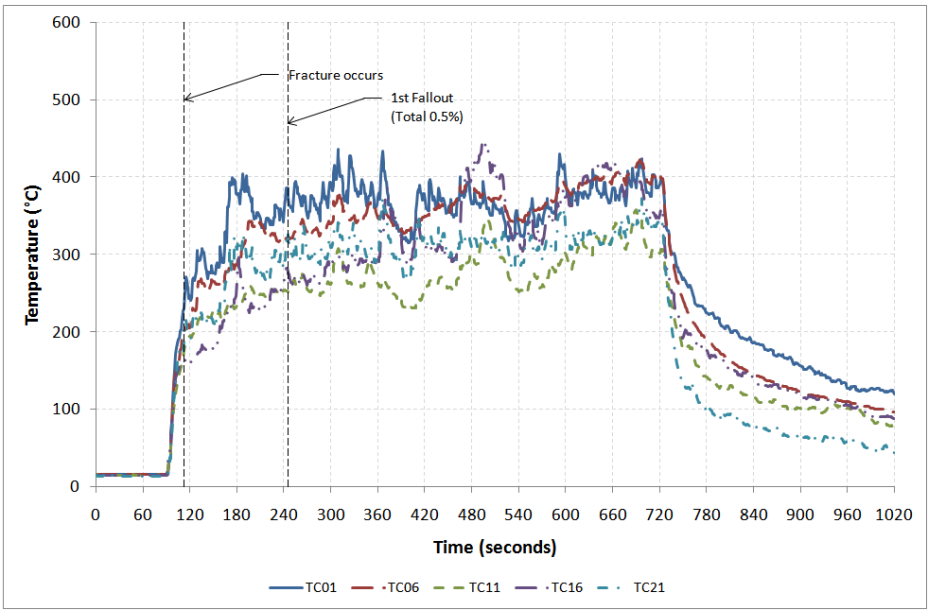

Figure C-109: Gas temperature profiles for experiment 6 Test 5

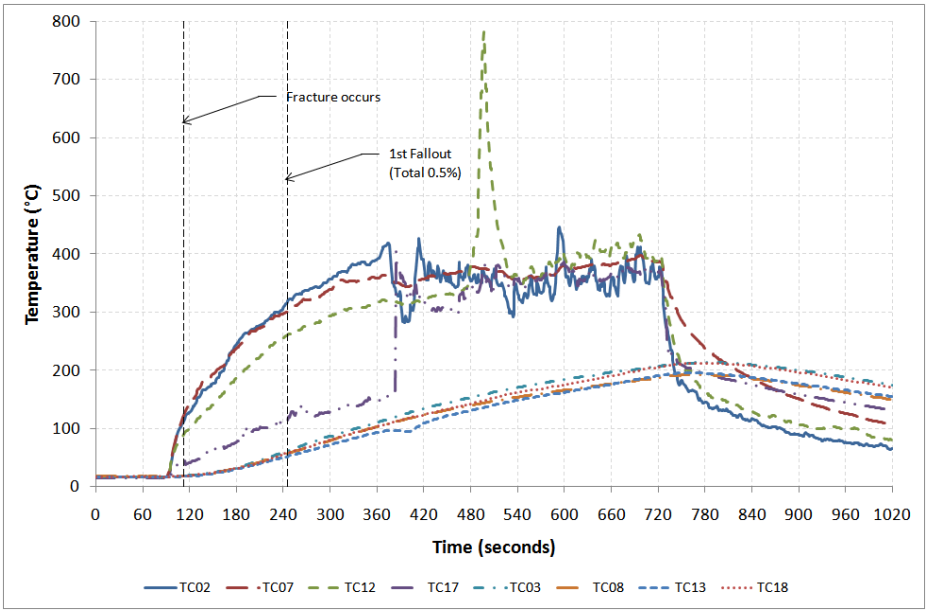

Figure C-110: Glass temperature profiles on exposed side for experiment 6 Test 5

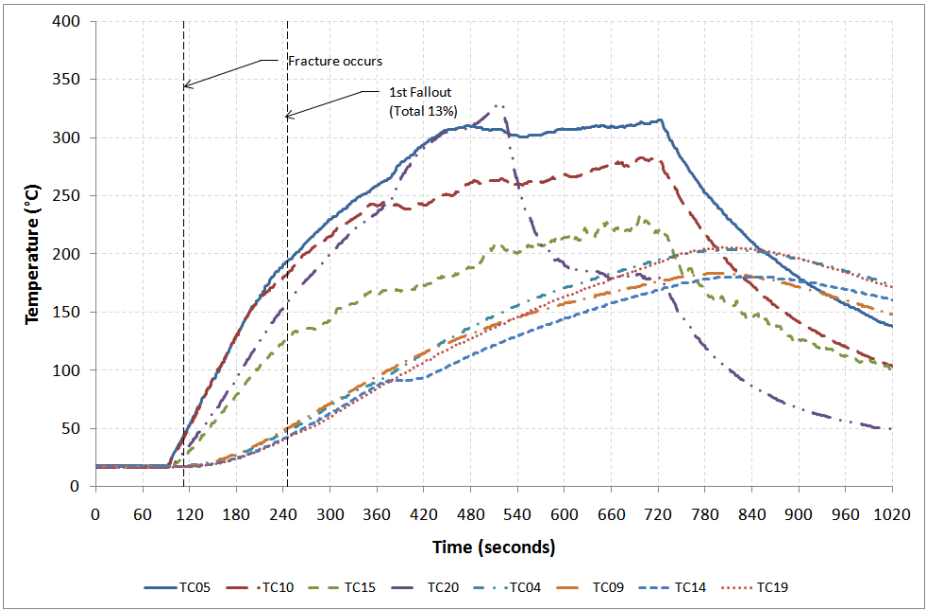

Figure C-111: Glass temperature profiles on unexposed side for experiment 6 Test 5

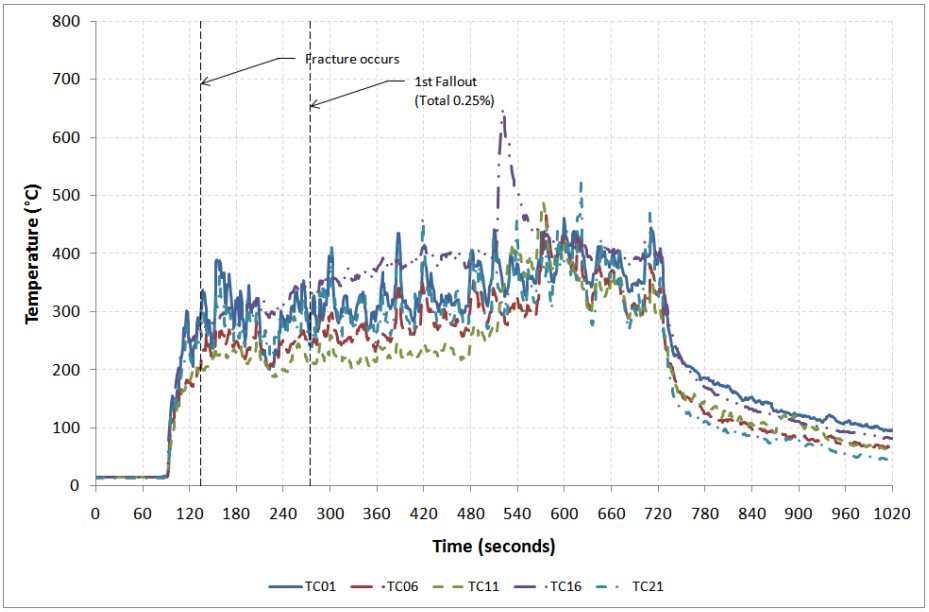

Figure C-112: Gas temperature profiles for experiment 6 Test 6

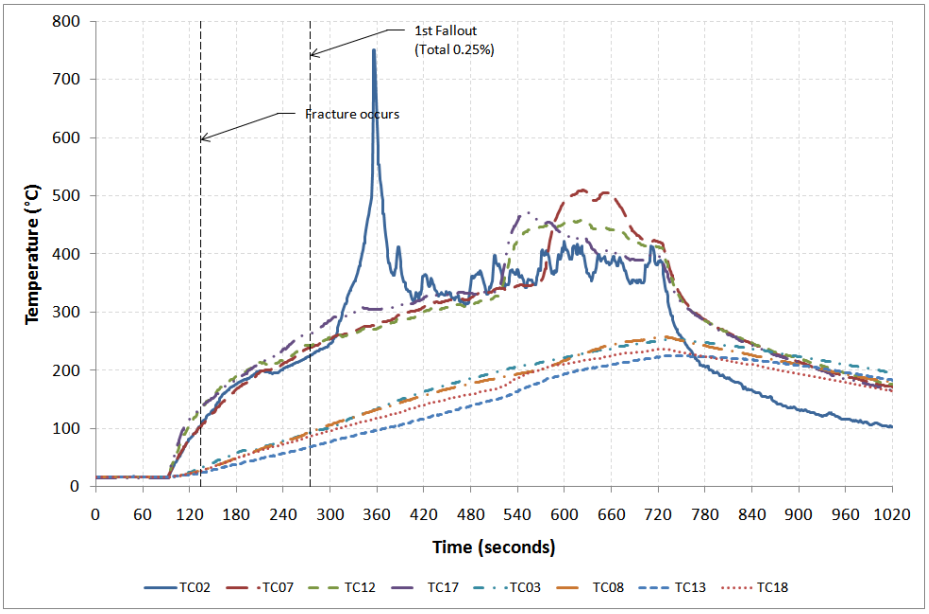

Figure C-113: Glass temperature profiles on exposed side for experiment 6 Test 6

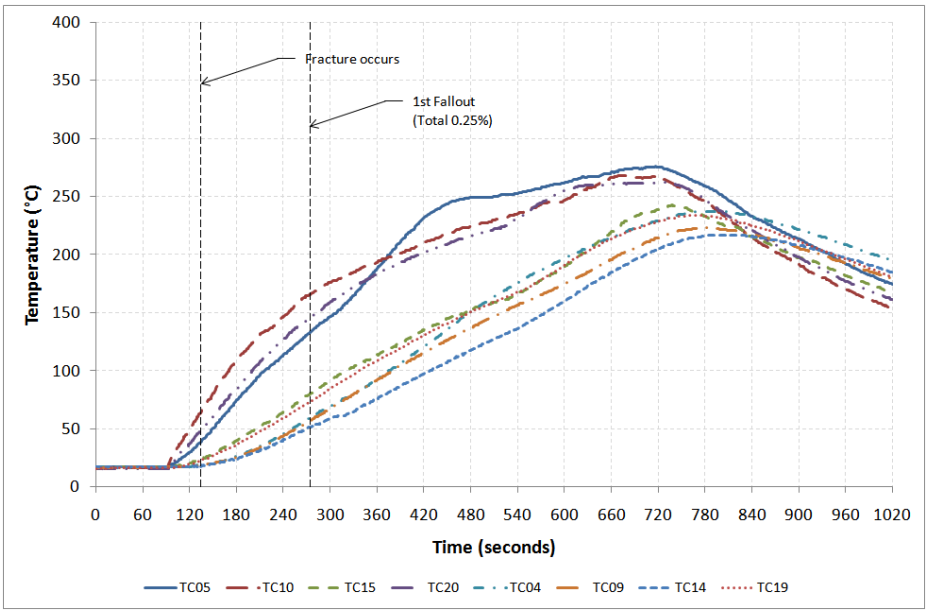

Figure C-114: Glass temperature profiles on unexposed side for experiment 6 Test 6

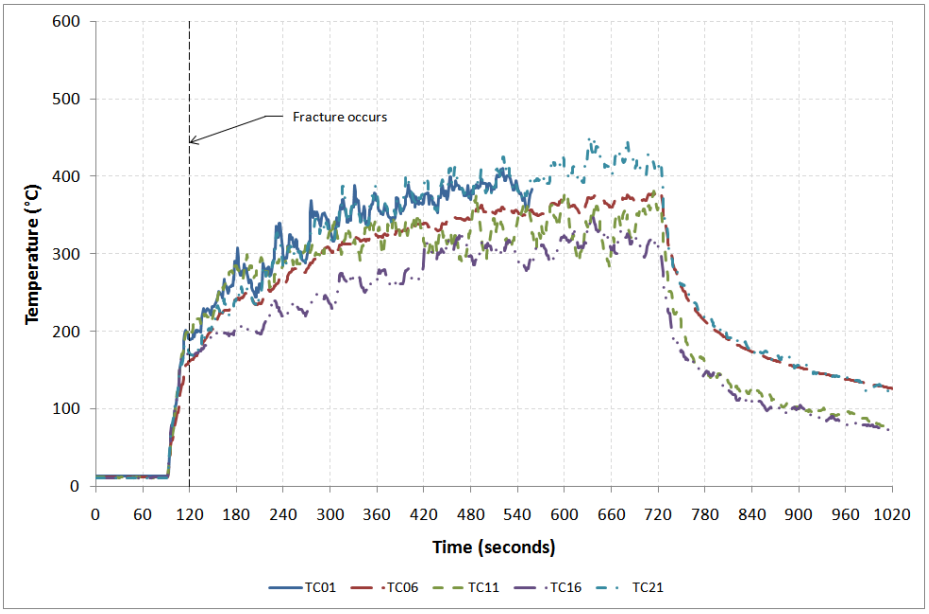

Figure C-115: Gas temperature profiles for experiment 6 Test 7

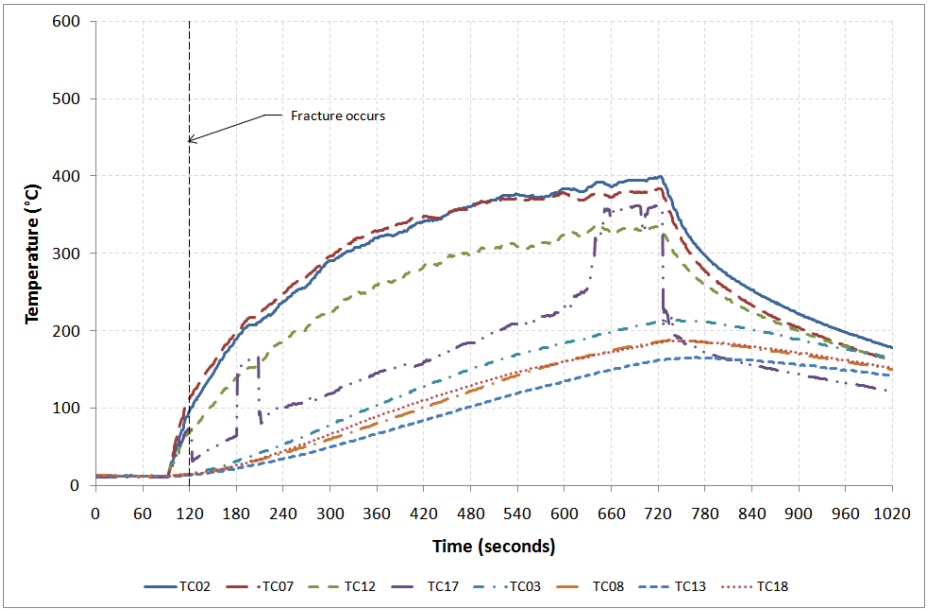

Figure C-116: Glass temperature profiles on exposed side for experiment 6 Test 7

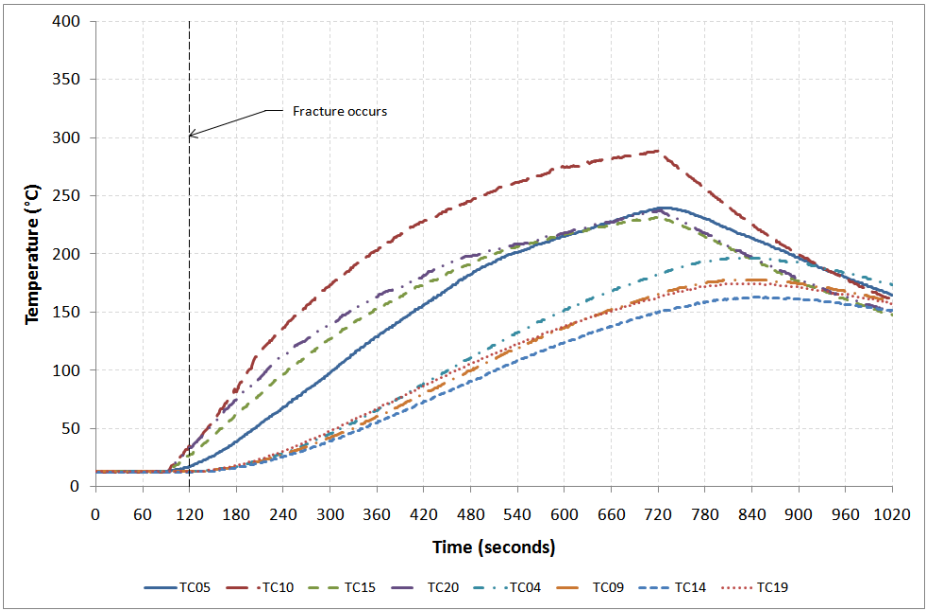

Figure C-117: Glass temperature profiles on unexposed side for experiment 6 Test 7

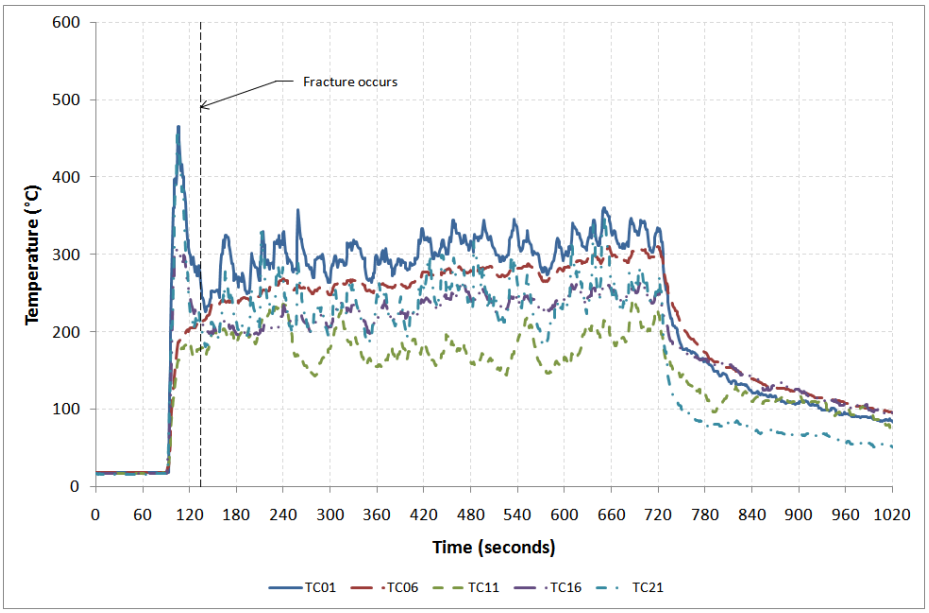

Figure C-118: Gas temperature profiles for experiment 6 Test 8

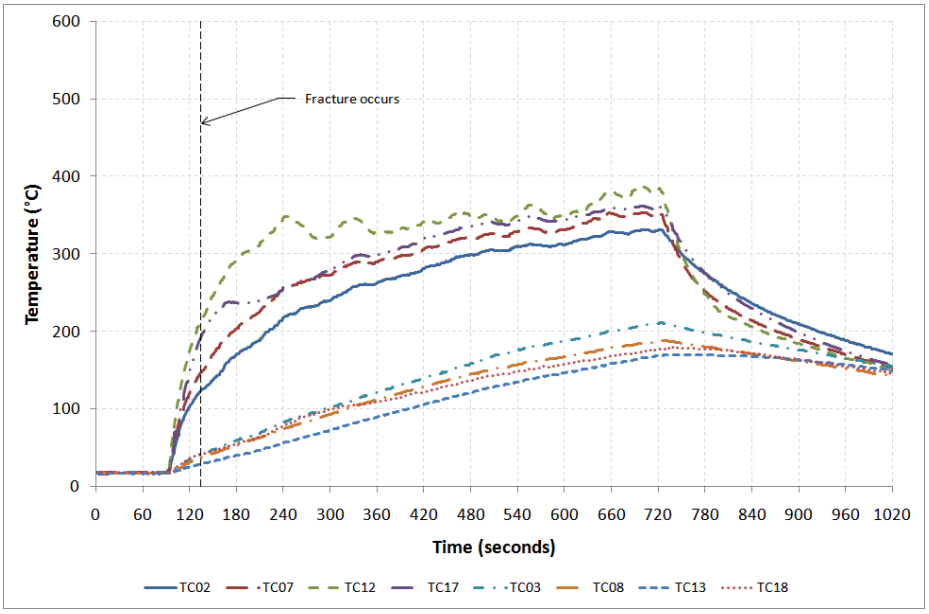

Figure C-119: Glass temperature profiles on exposed side for experiment 6 Test 8

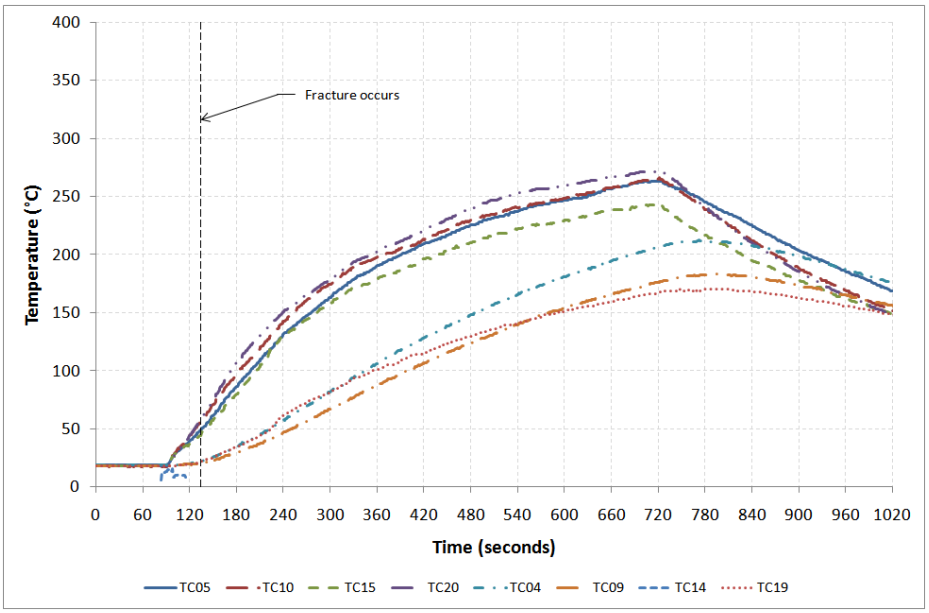

Figure C-120: Glass temperature profiles on unexposed side for experiment 6 Test 8

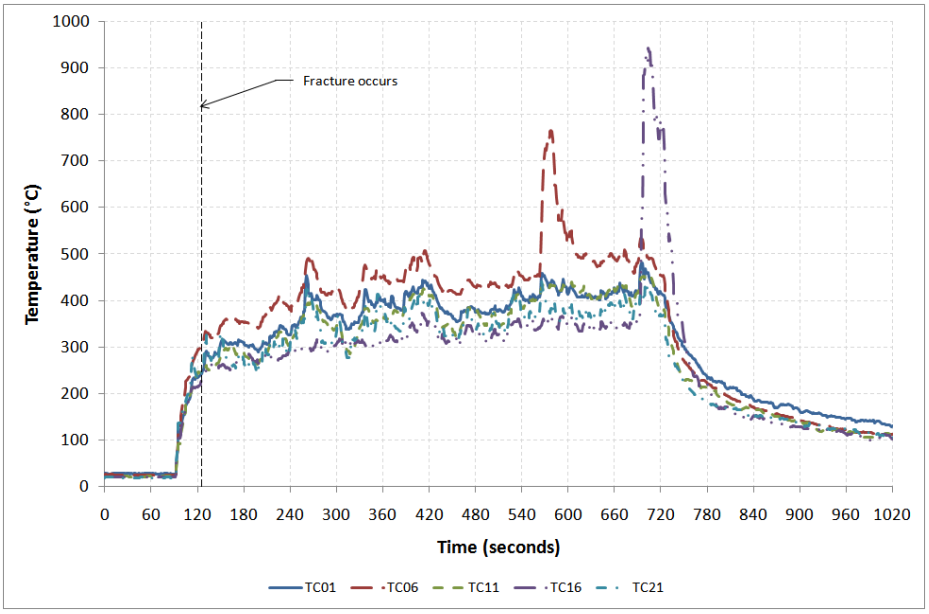

Figure C-121: Gas temperature profiles for experiment 6 Test 9

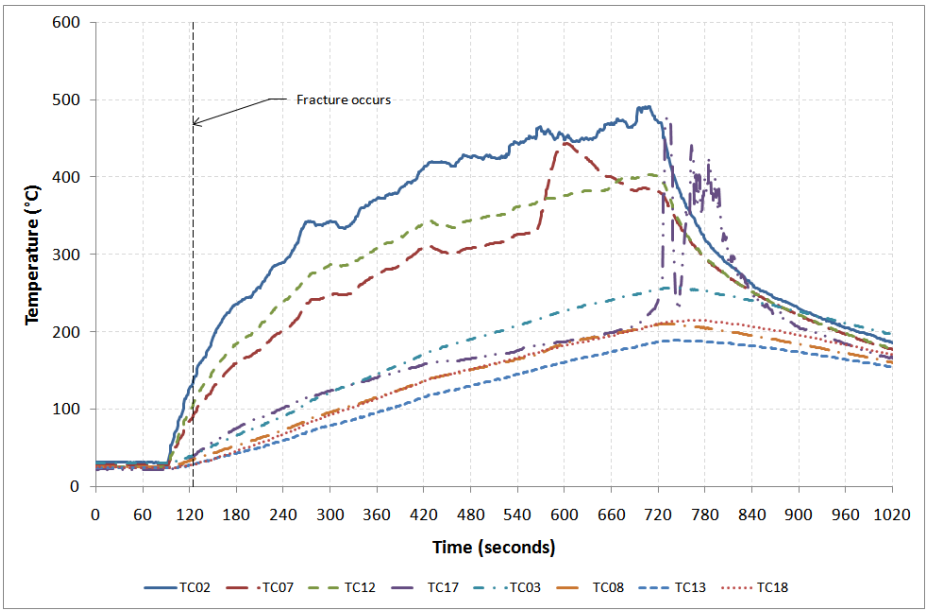

Figure C-122: Glass temperature profiles on exposed side for experiment 6 Test 9

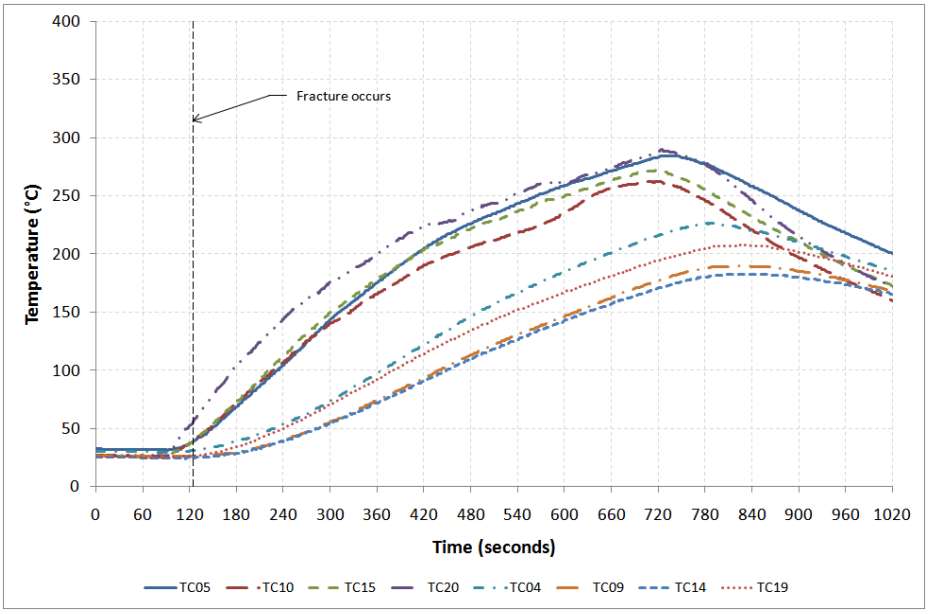

Figure C-123: Glass temperature profiles on unexposed side for experiment 6 Test 9

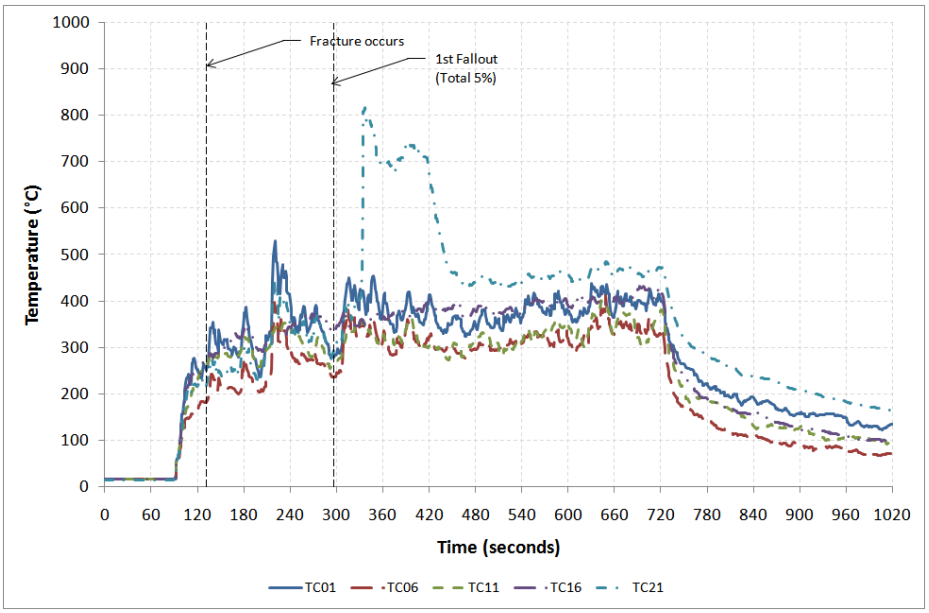

Figure C-124: Gas temperature profiles for experiment 6 Test 10

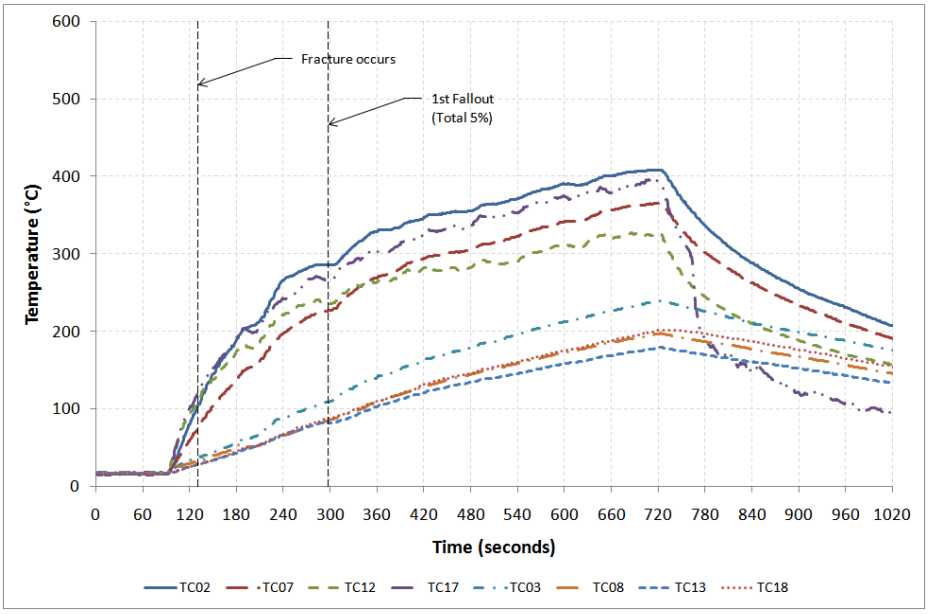

Figure C-125: Glass temperature profiles on exposed side for experiment 6 Test 10

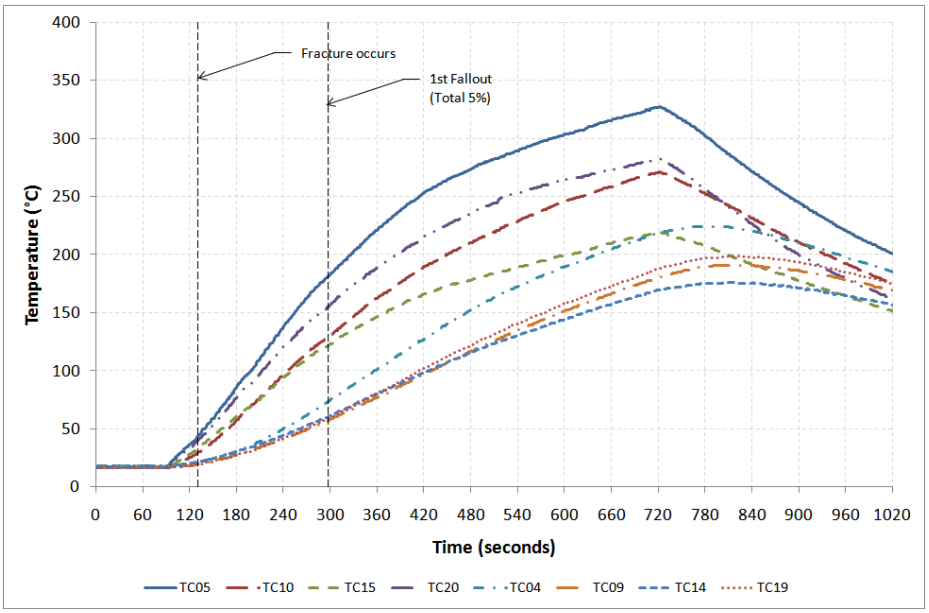

Figure C-126: Glass temperature profiles on unexposed side for experiment 6 Test 10

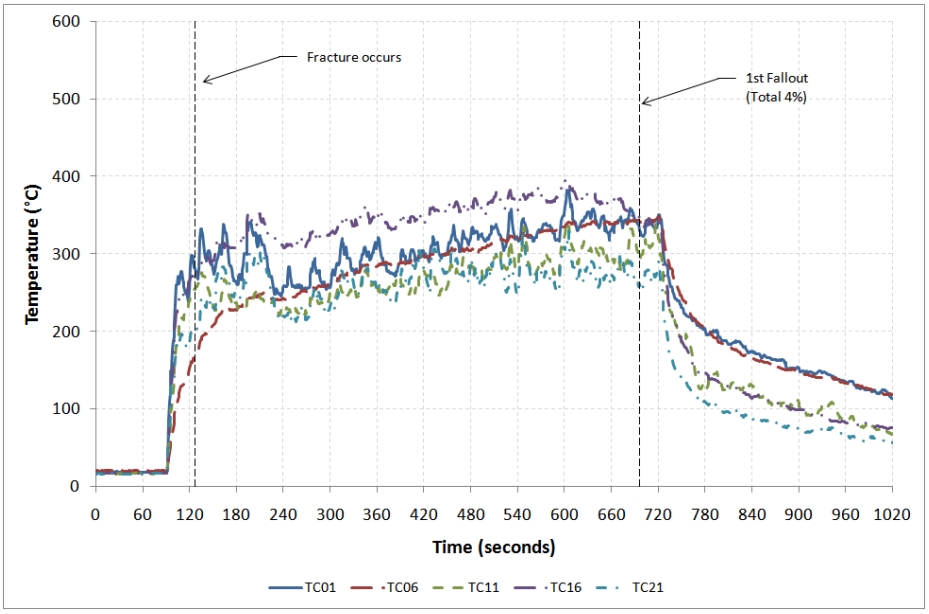

Figure C-127: Gas temperature profiles for experiment 6 Test 11

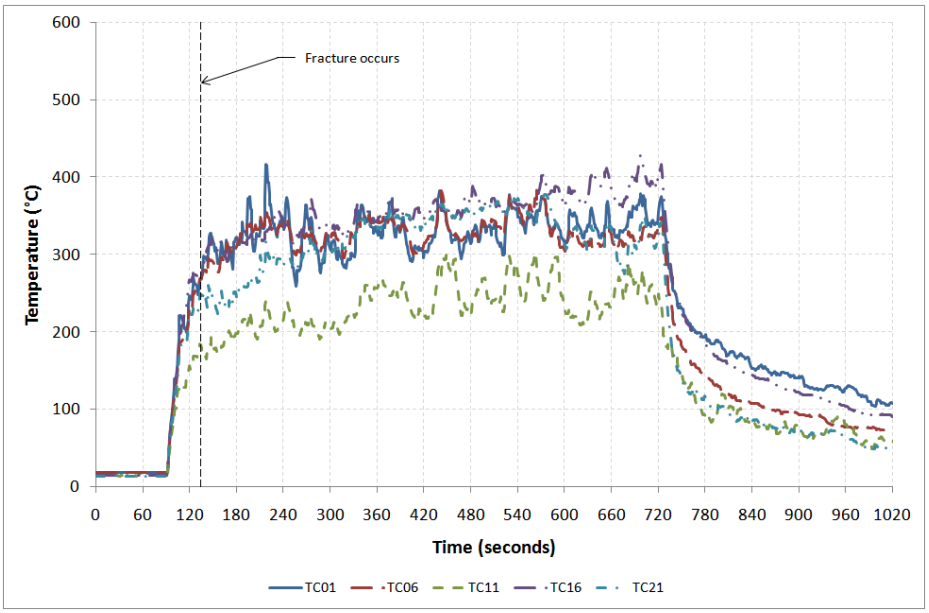

Figure C-128: Gas temperature profiles for experiment 6 Test 12

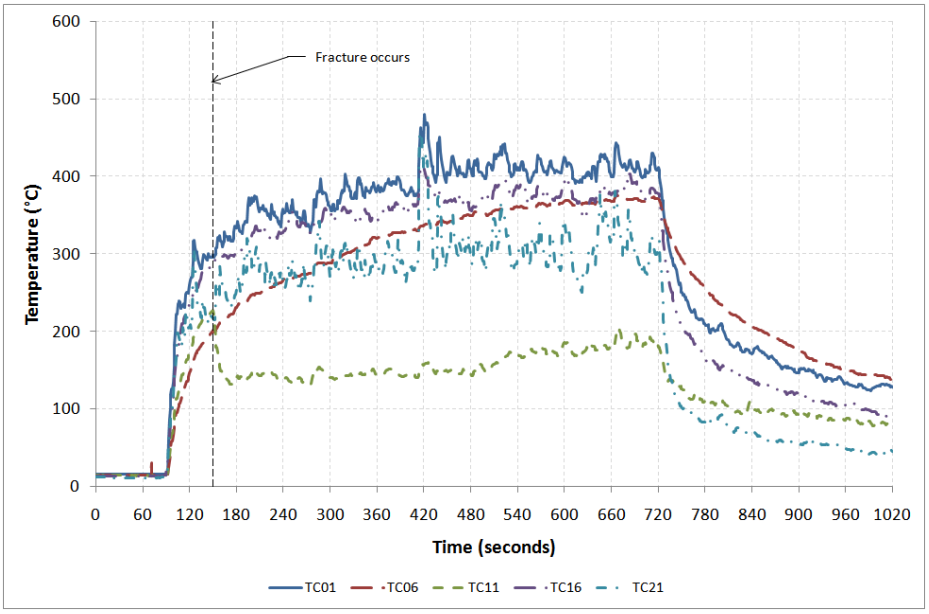

Figure C-129: Gas temperature profiles for experiment 6 Test 13

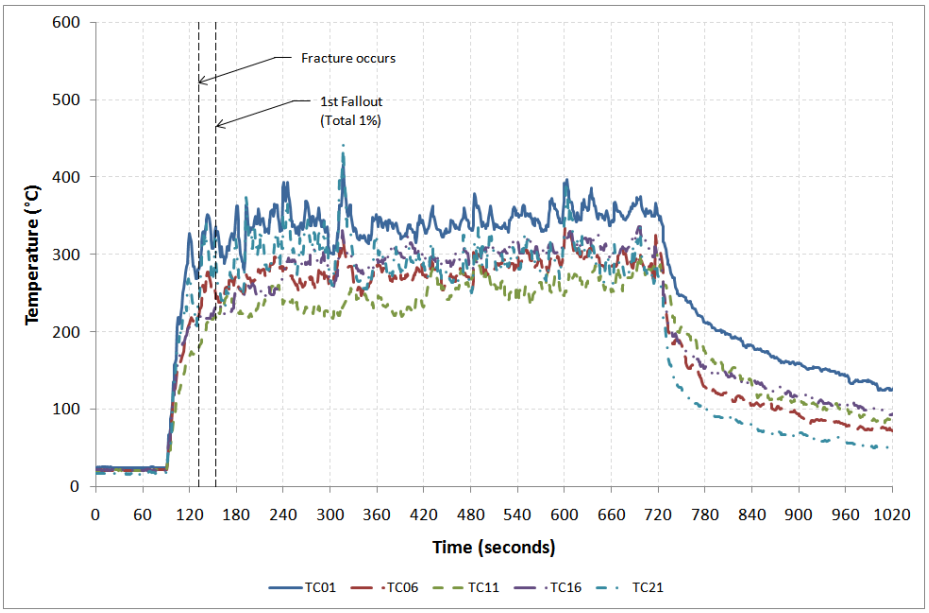

Figure C-130: Gas temperature profiles for experiment 6 Test 14

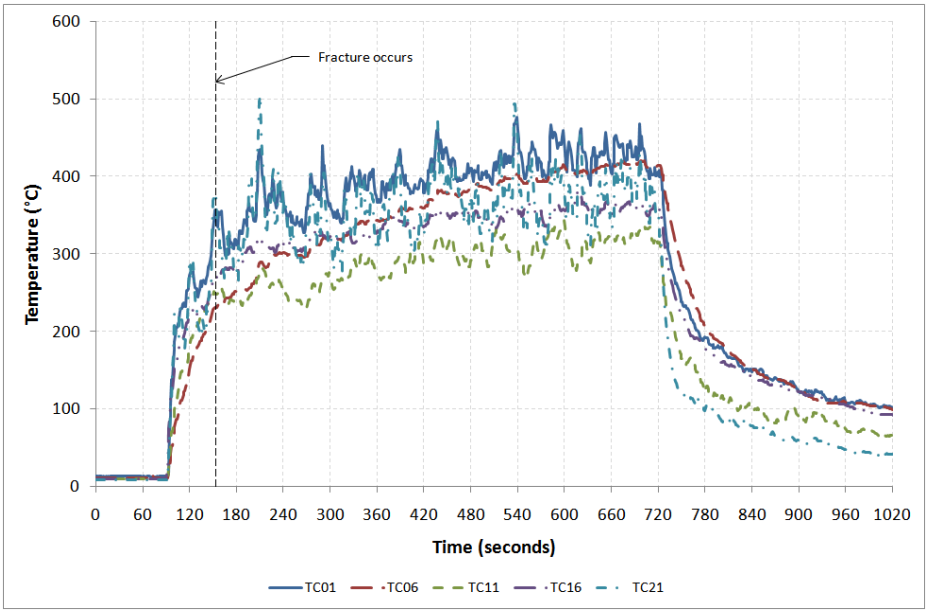

Figure C-131: Gas temperature profiles for experiment 6 Test 15

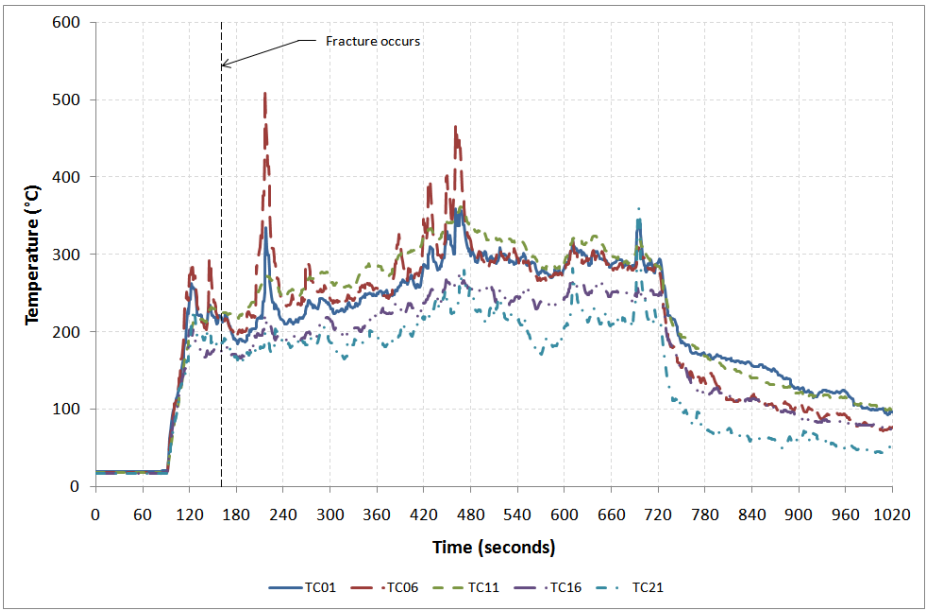

Figure C-132: Gas temperature profiles for experiment 6 Test 16

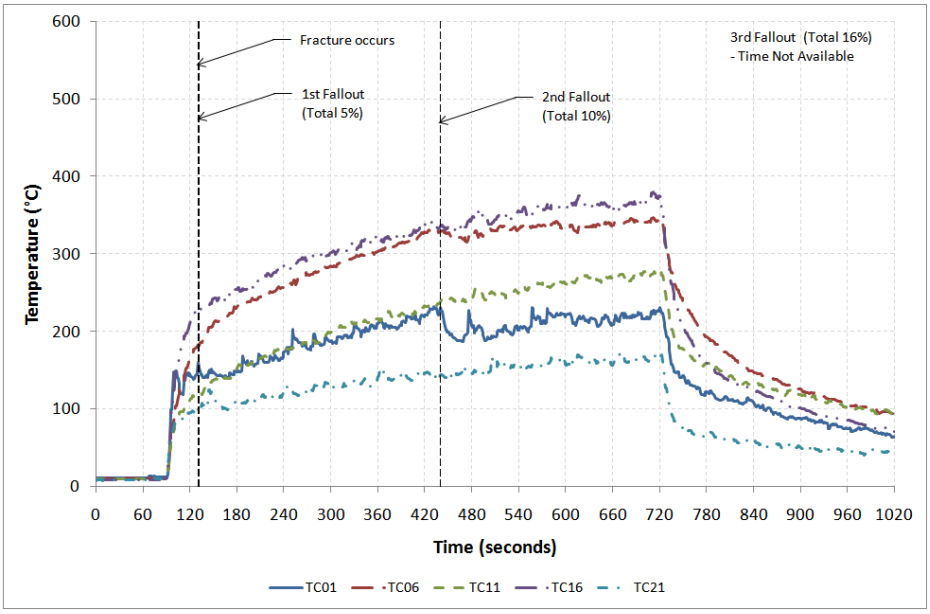

Figure C-133: Gas temperature profiles for experiment 6 Test 17

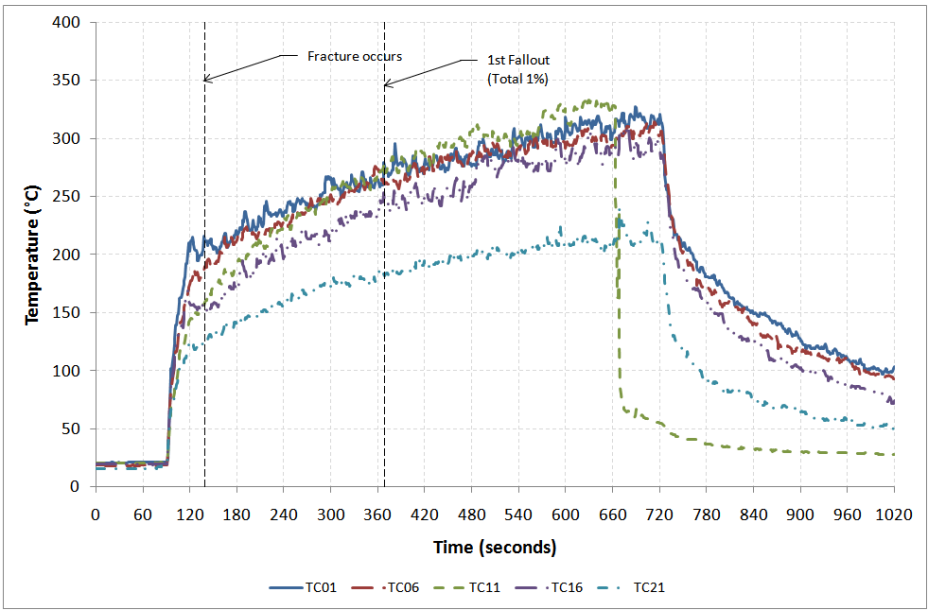

Figure C-134: Gas temperature profiles for experiment 6 Test 18

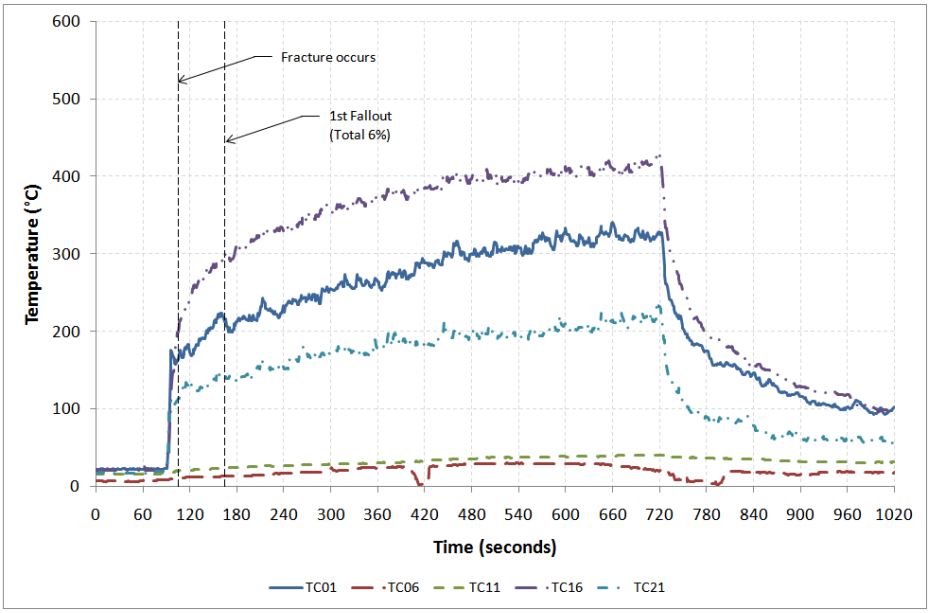

Figure C-135: Gas temperature profiles for experiment 6 Test 19

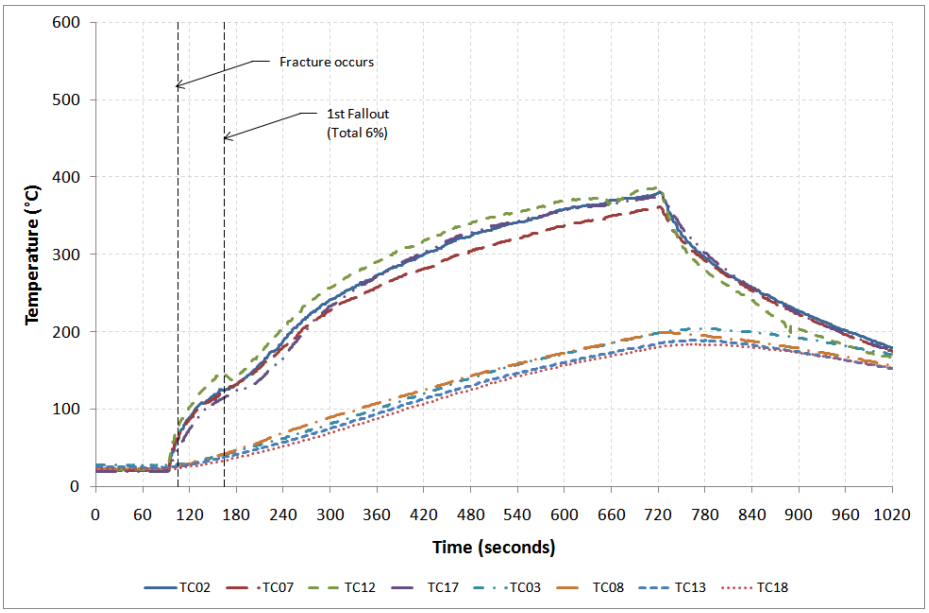

Figure C-136: Glass temperature profiles on exposed side for experiment 6 Test 19

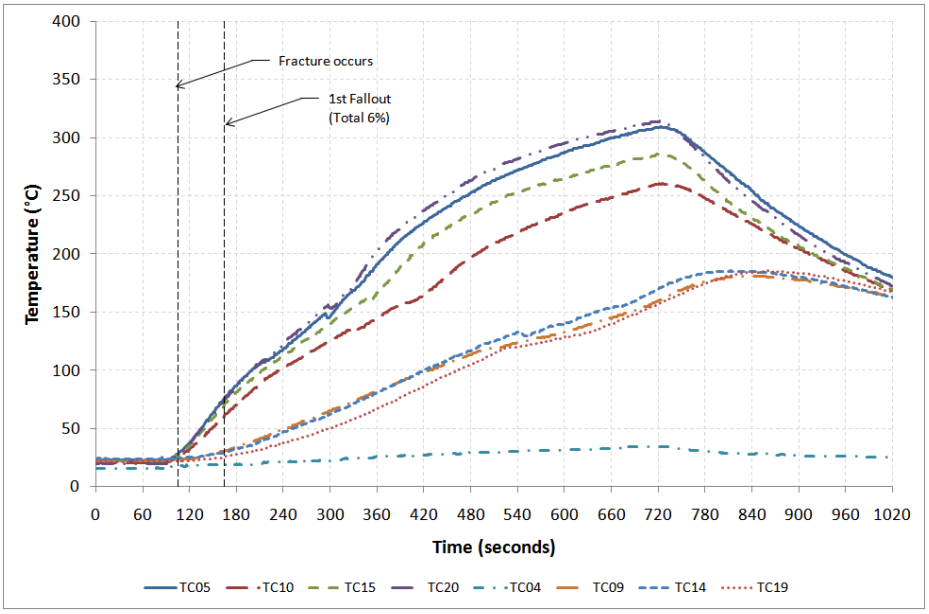

Figure C-137: Glass temperature profiles on unexposed side for experiment 6 Test 19

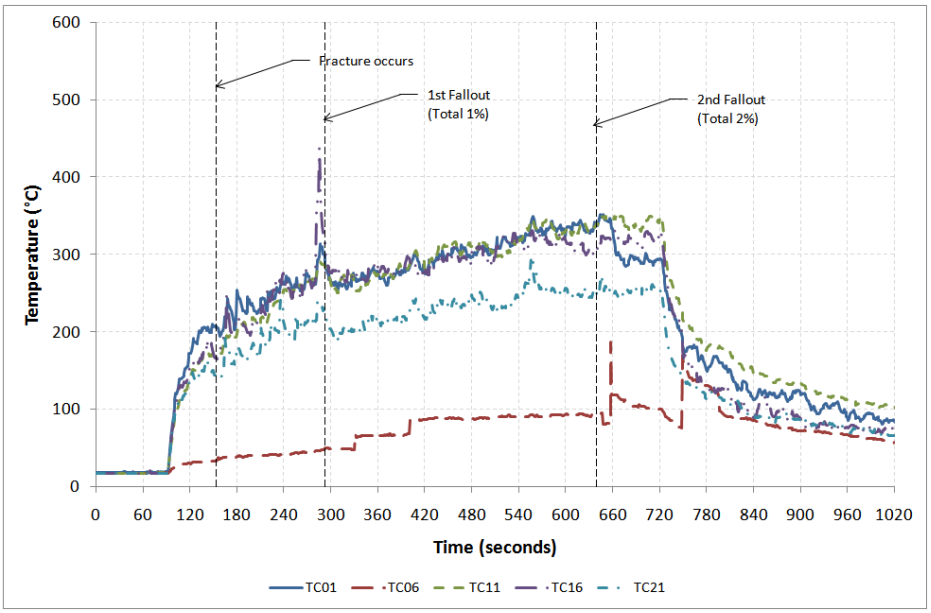

Figure C-138: Gas temperature profiles for experiment 6 Test 20

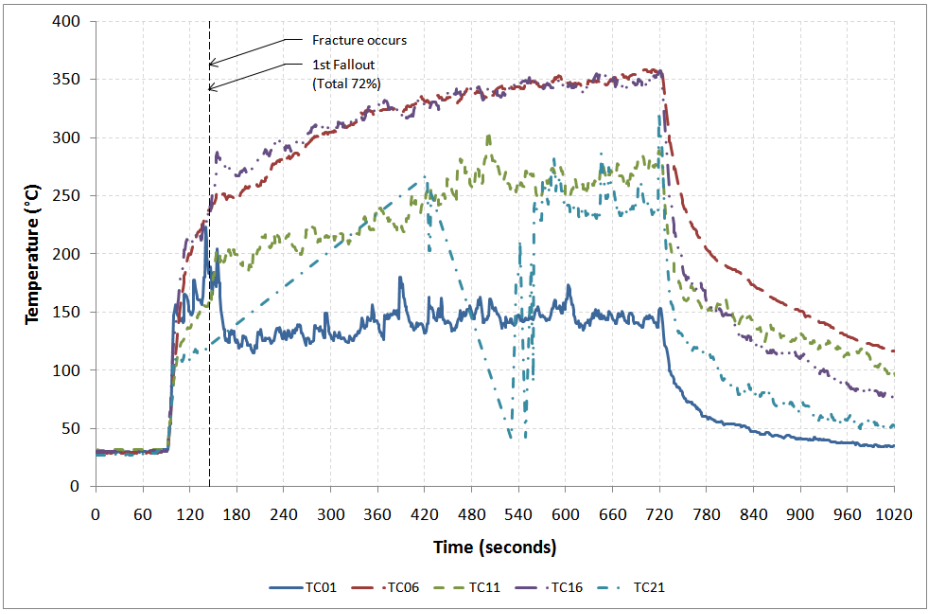

Figure C-139: Gas temperature profiles for experiment 6 Test 21

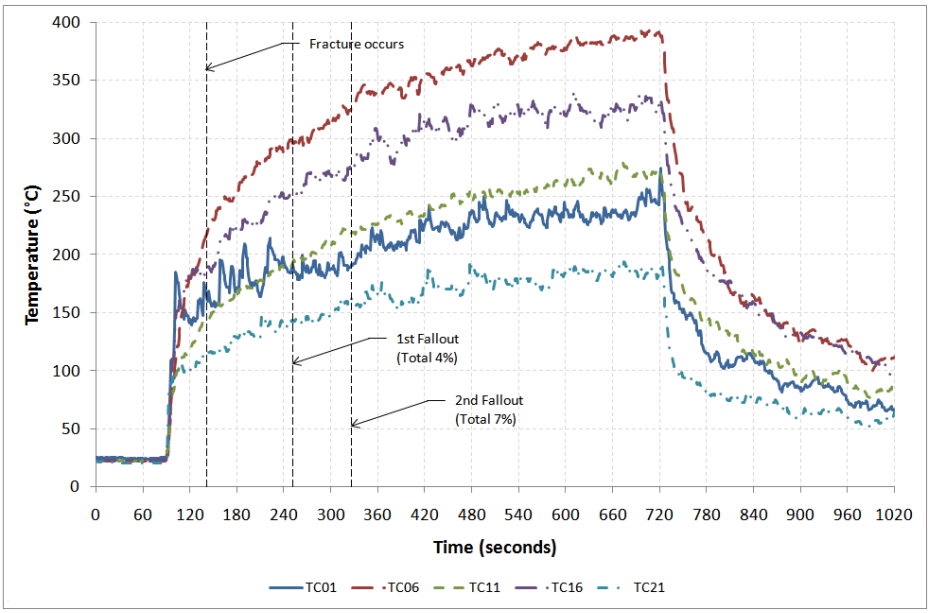

Figure C-140: Gas temperature profiles for experiment 6 Test 22

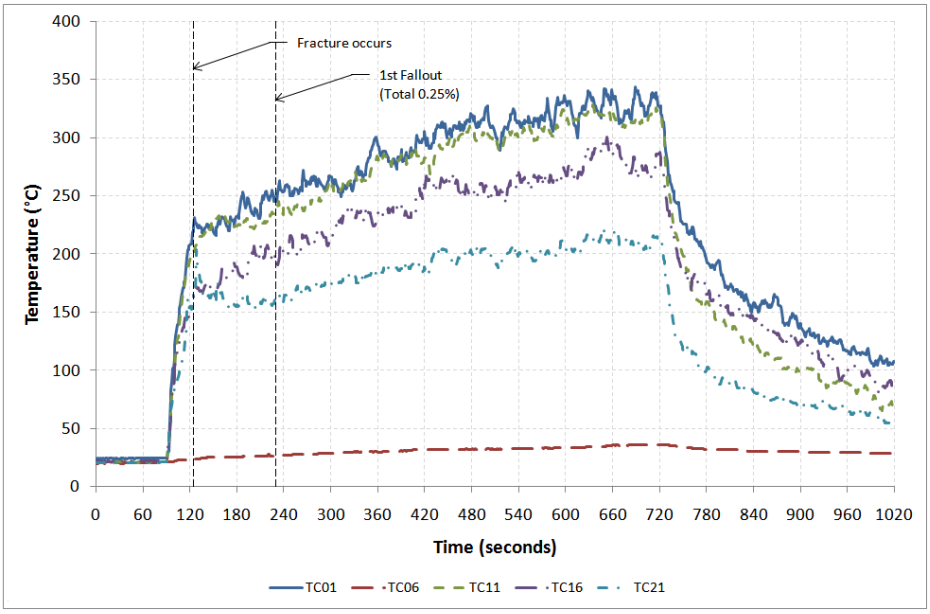

Figure C-141: Gas temperature profiles for experiment 6 Test 23

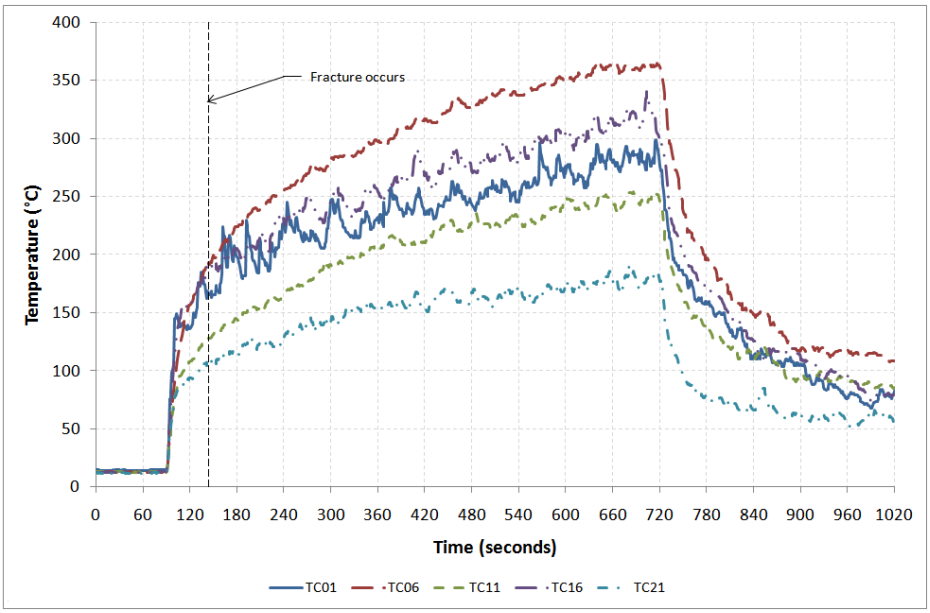

Figure C-142: Gas temperature profiles for experiment 6 Test 24

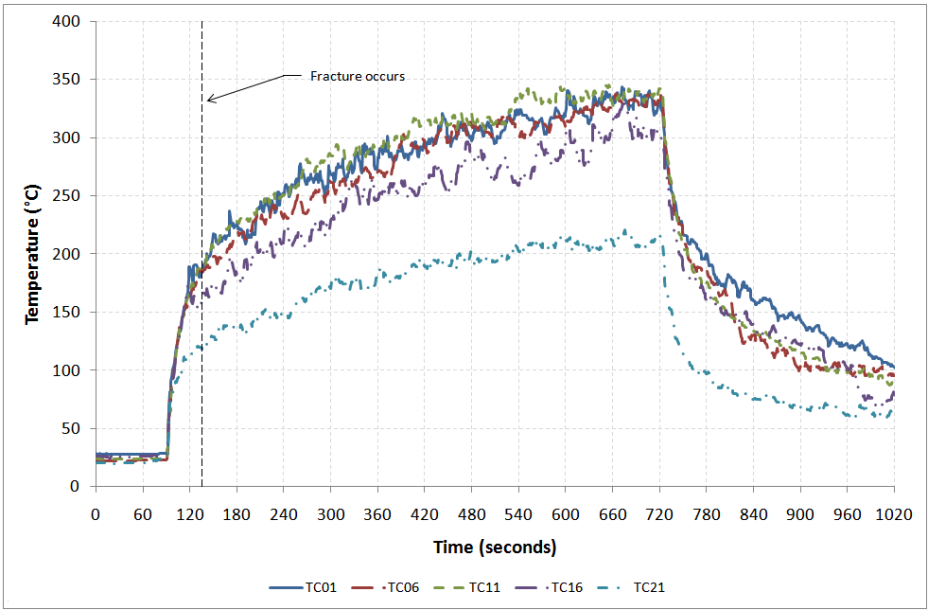

Figure C-143: Gas temperature profiles for experiment 6 Test 25

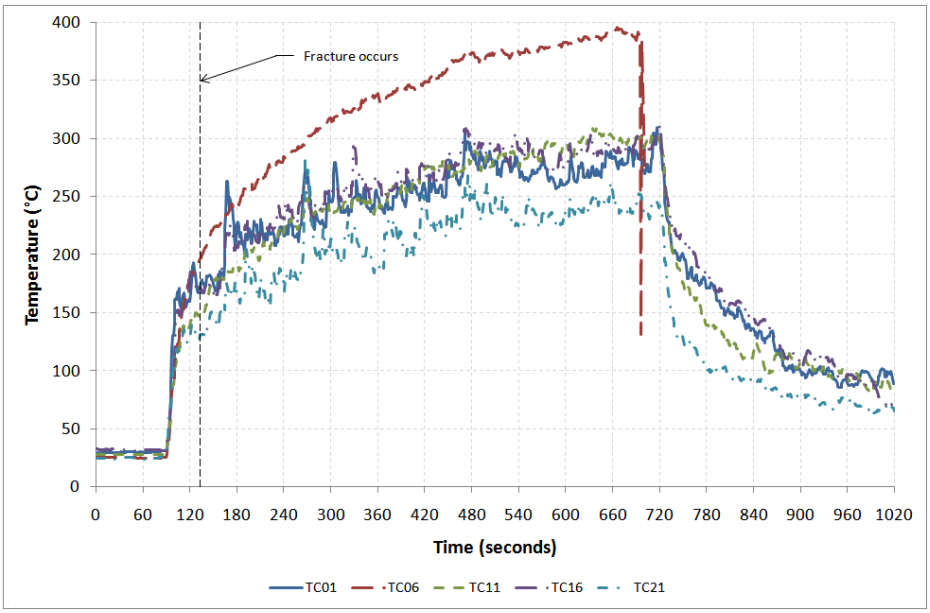

Figure C-144: Gas temperature profiles for experiment 6 Test 26

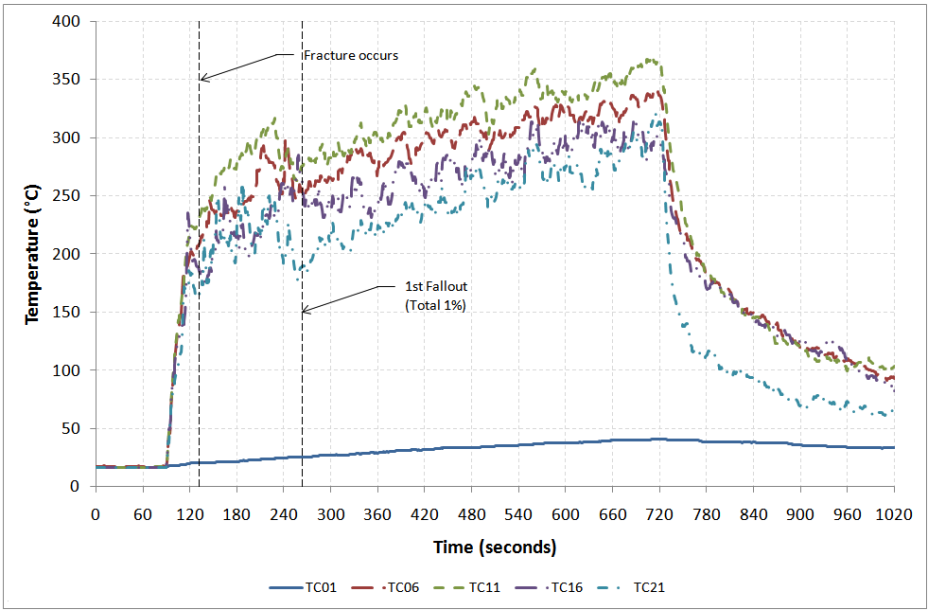

Figure C-145: Gas temperature profiles for experiment 6 Test 27

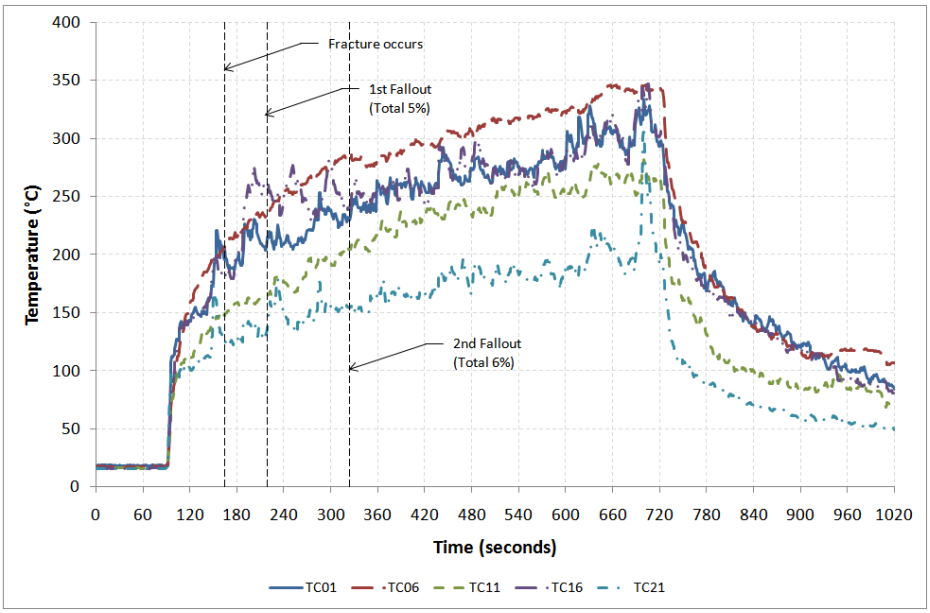

Figure C-146: Gas temperature profiles for experiment 6 Test 28

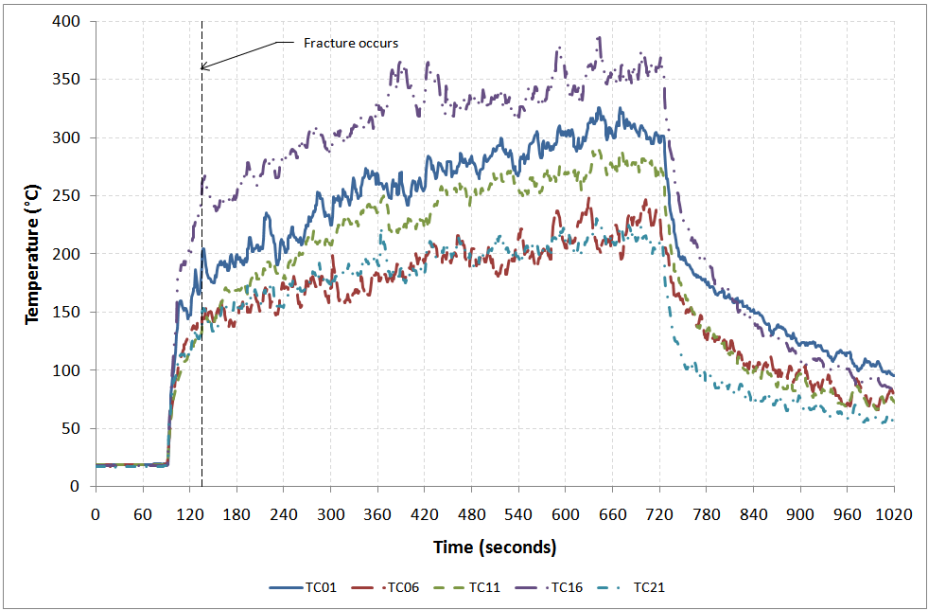

Figure C-147: Gas temperature profiles for experiment 6 Test 29

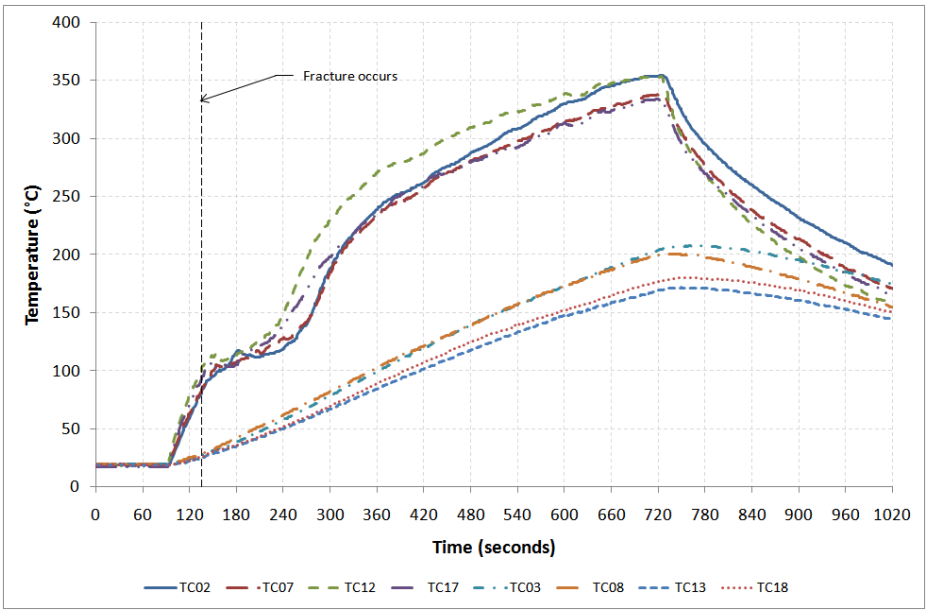

Figure C-148: Glass temperature profiles on exposed side for experiment 6 Test 29

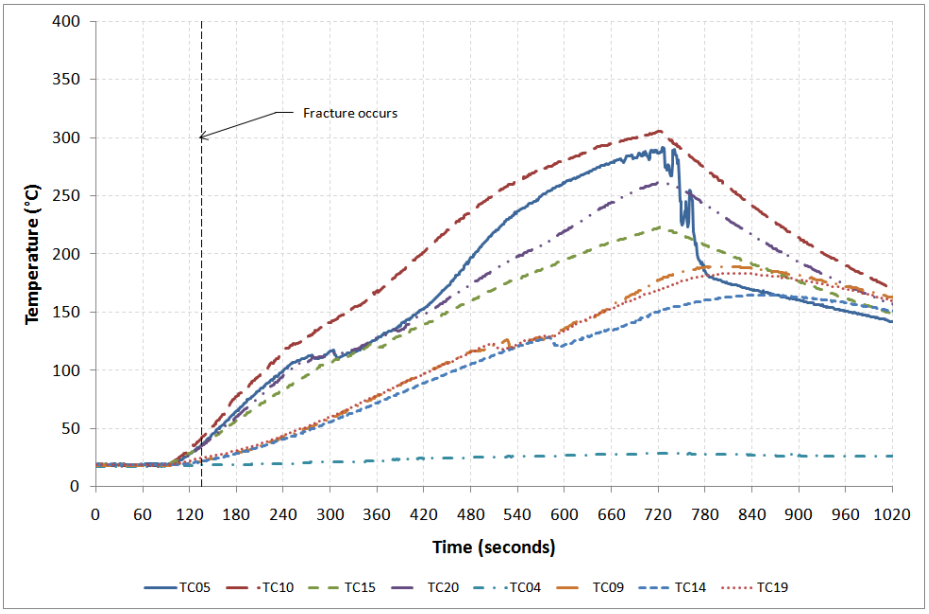

Figure C-149: Glass temperature profiles on unexposed side for experiment 6 Test 29

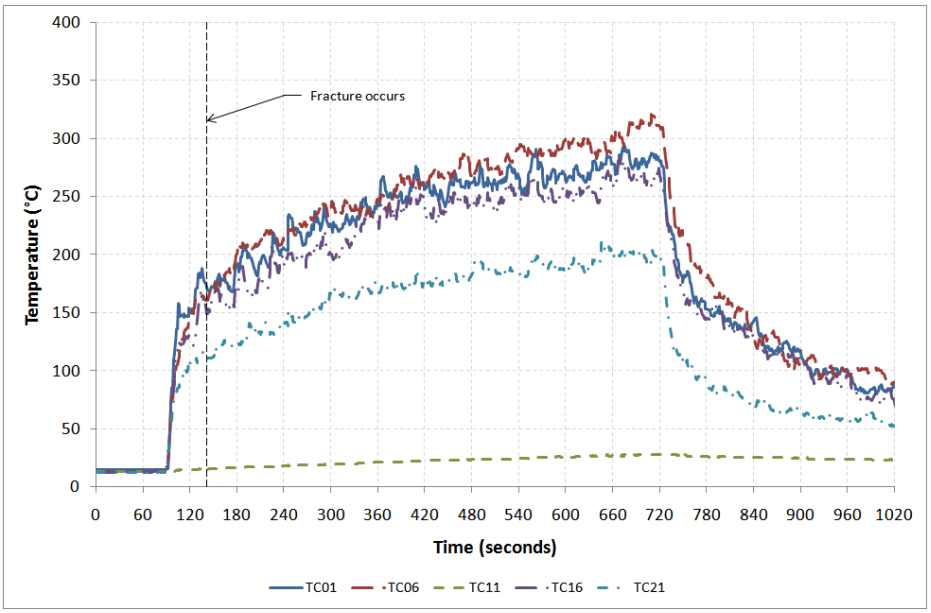

Figure C-150: Gas temperature profiles for experiment 6 Test 30

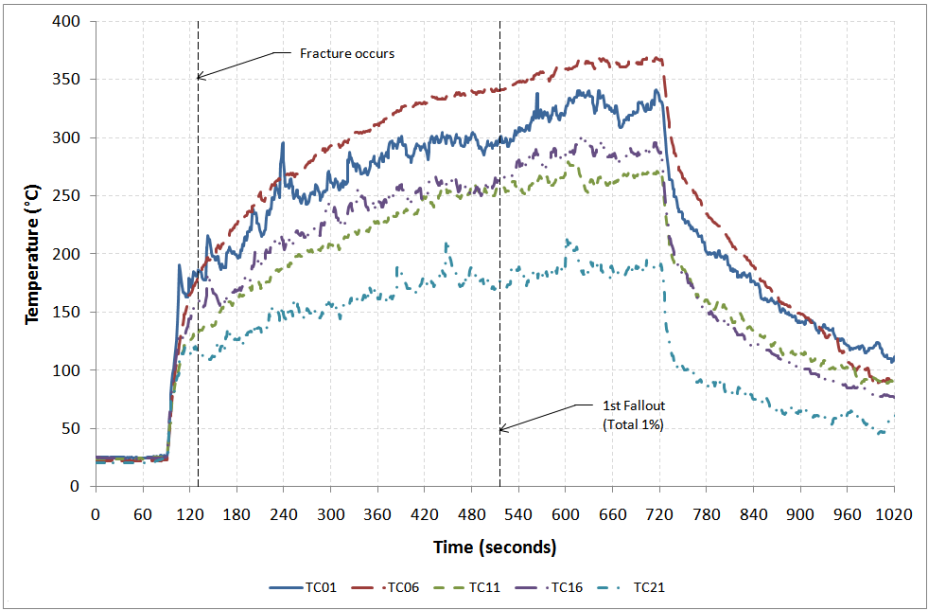

Figure C-151: Gas temperature profiles for experiment 6 Test 31

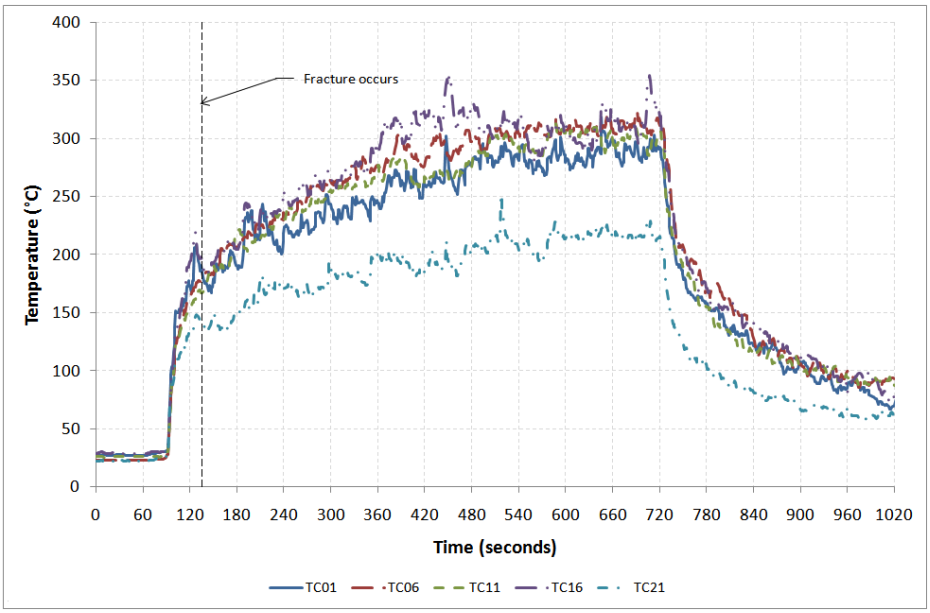

Figure C-152: Gas temperature profiles for experiment 6 Test 32

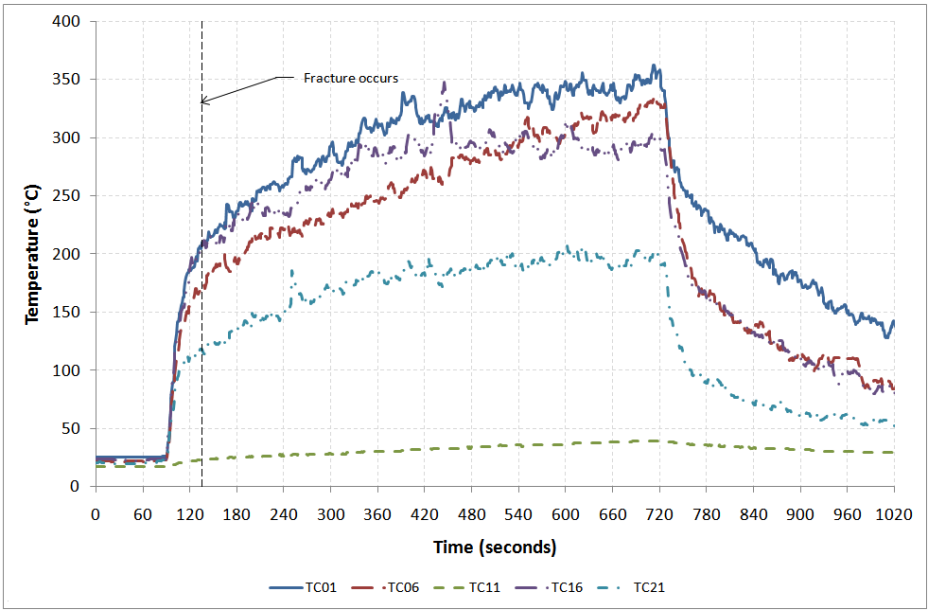

Figure C-153: Gas temperature profiles for experiment 6 Test 34

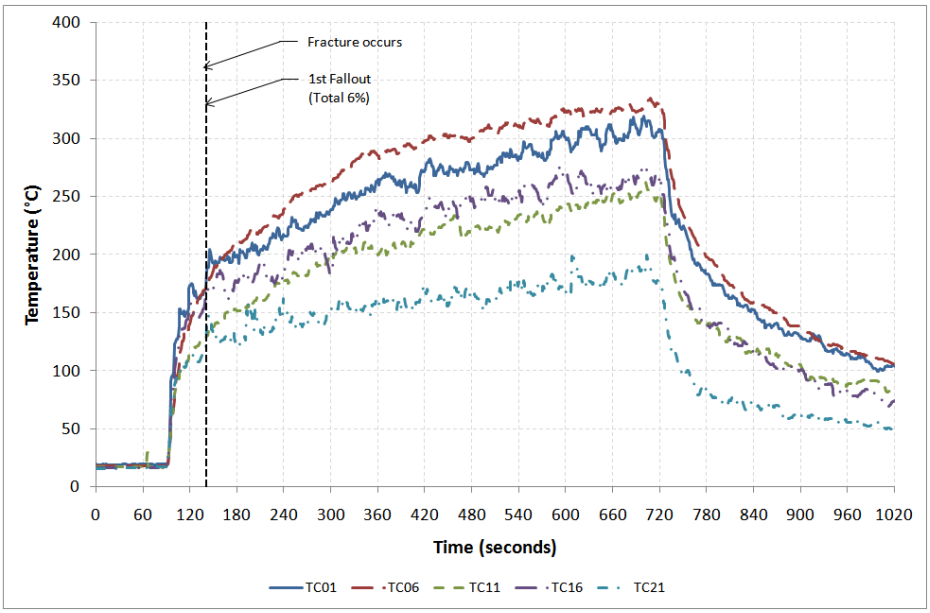

Figure C-154: Gas temperature profiles for experiment 6 Test 35

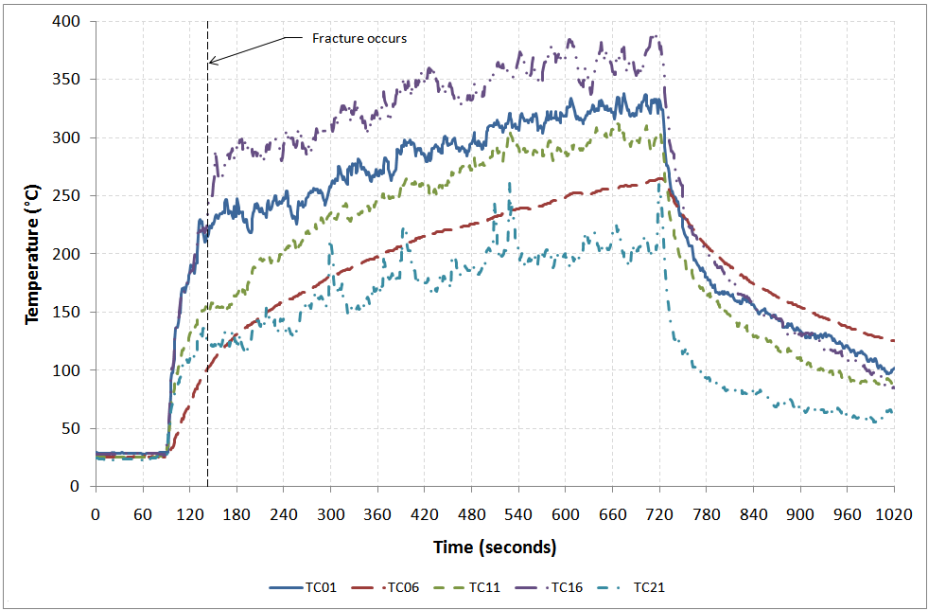

Figure C-155: Gas temperature profiles for experiment 6 Test 36

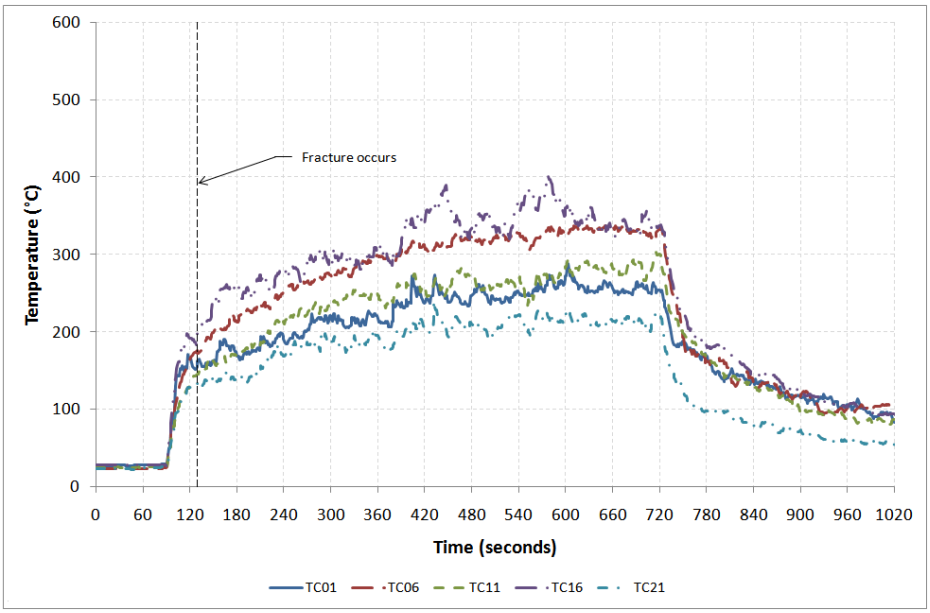

Figure C-156: Gas temperature profiles for experiment 6 Test 37

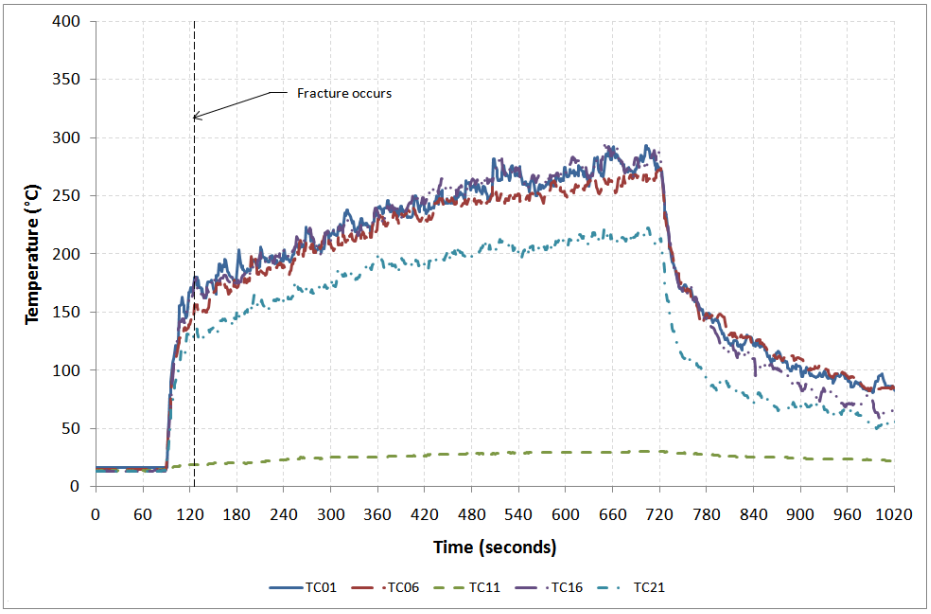

Figure C-157: Gas temperature profiles for experiment 6 Test 38

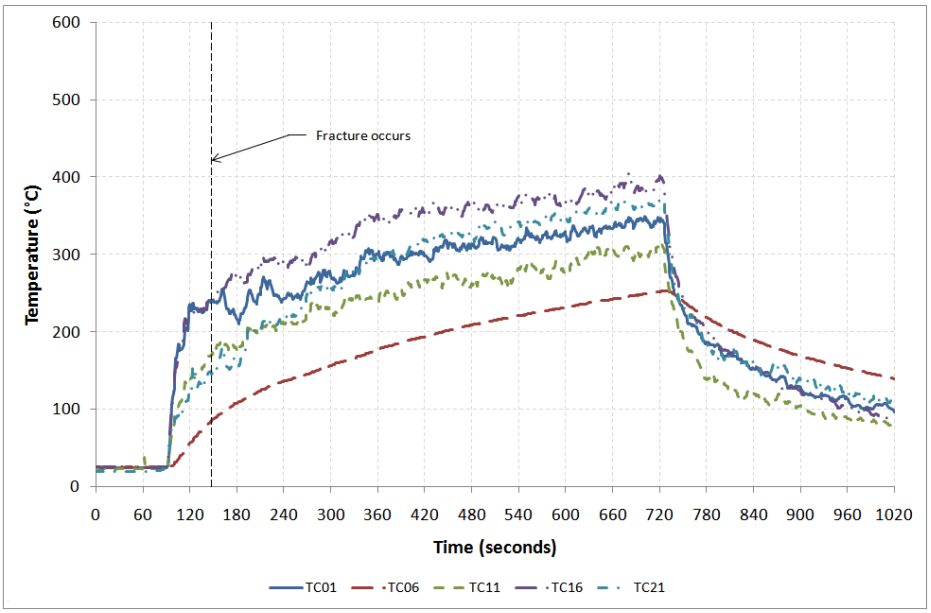

Figure C-158: Gas temperature profiles for experiment 6 Test 39

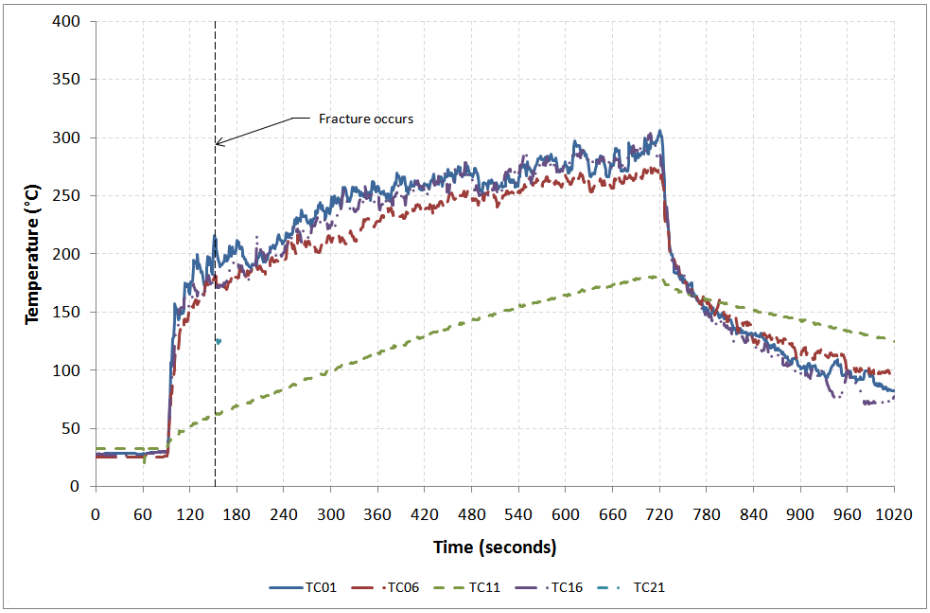

Figure C-159: Gas temperature profiles for experiment 6 Test 40

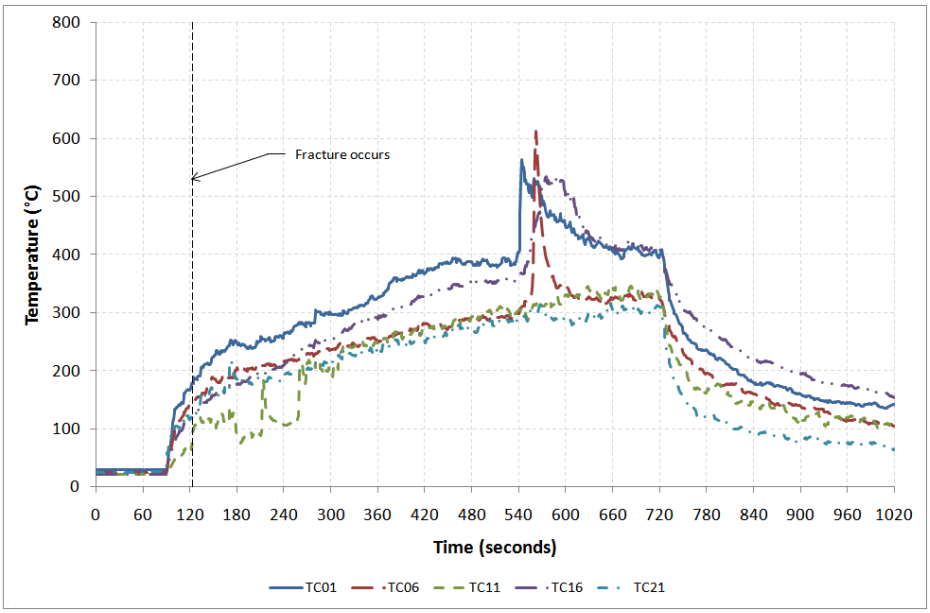

Figure C-160: Gas temperature profiles for experiment 6 Test 41

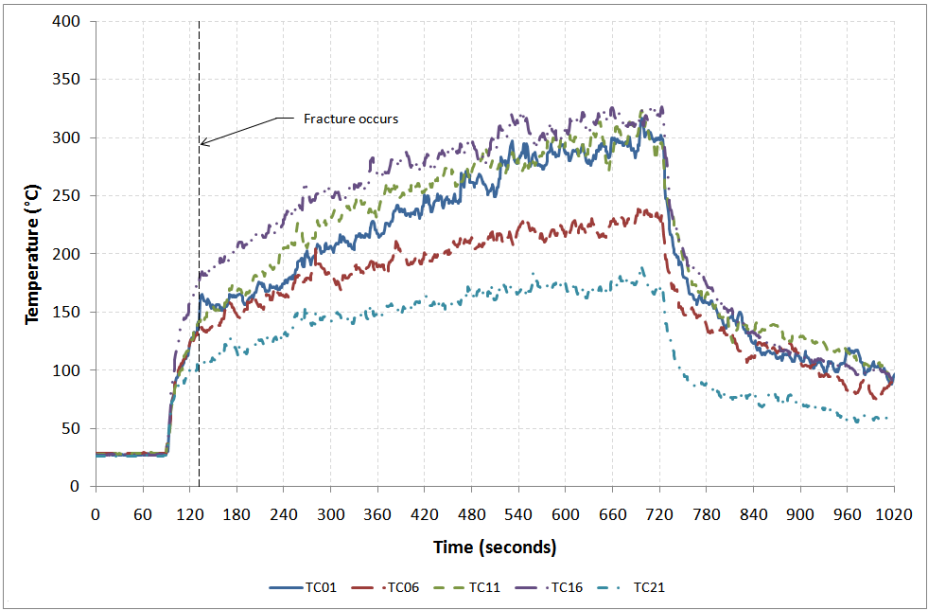

Figure C-161: Gas temperature profiles for experiment 6 Test 42

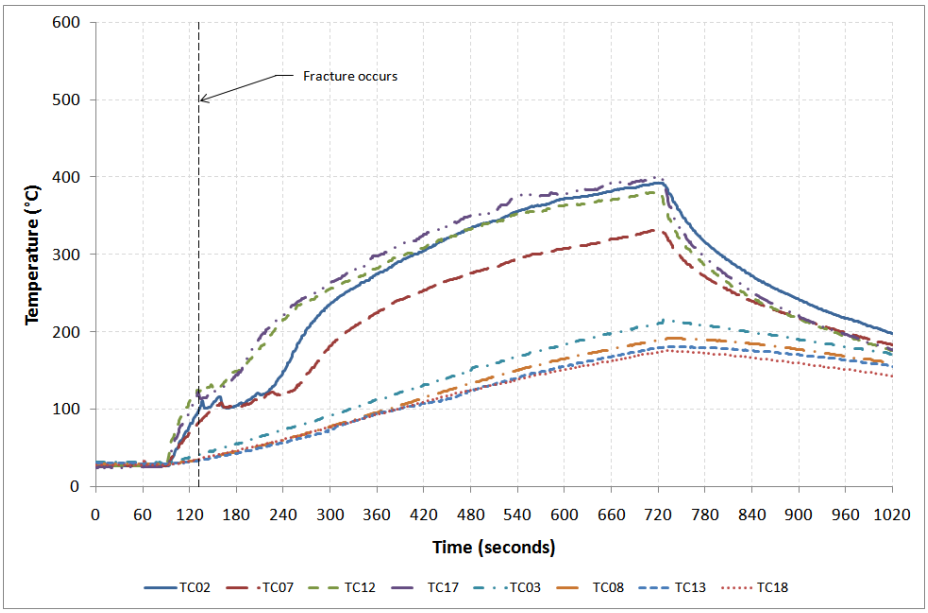

Figure C-162: Glass temperature profiles on exposed side for experiment 6 Test 42

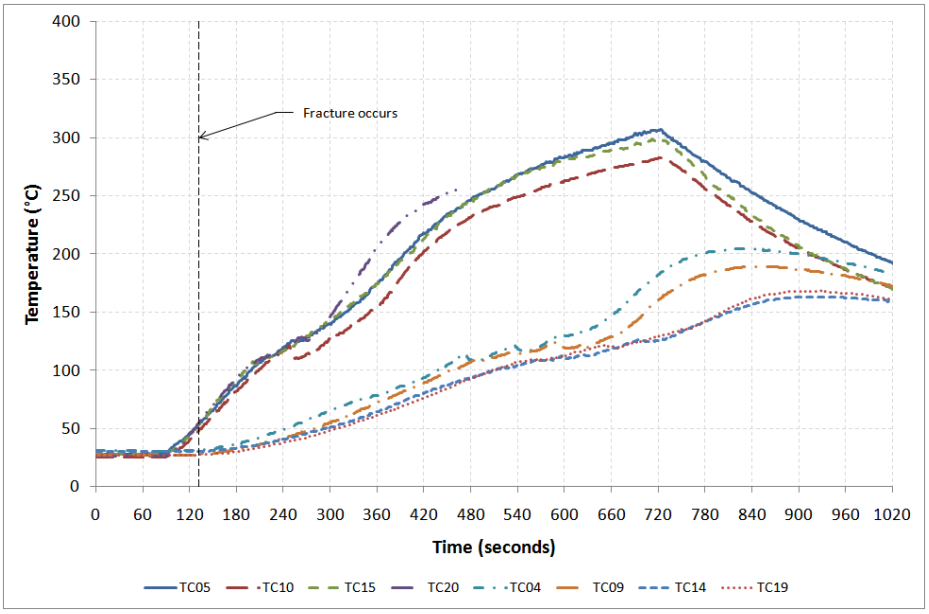

Figure C-163: Glass temperature profiles on unexposed side for experiment 6 Test 42

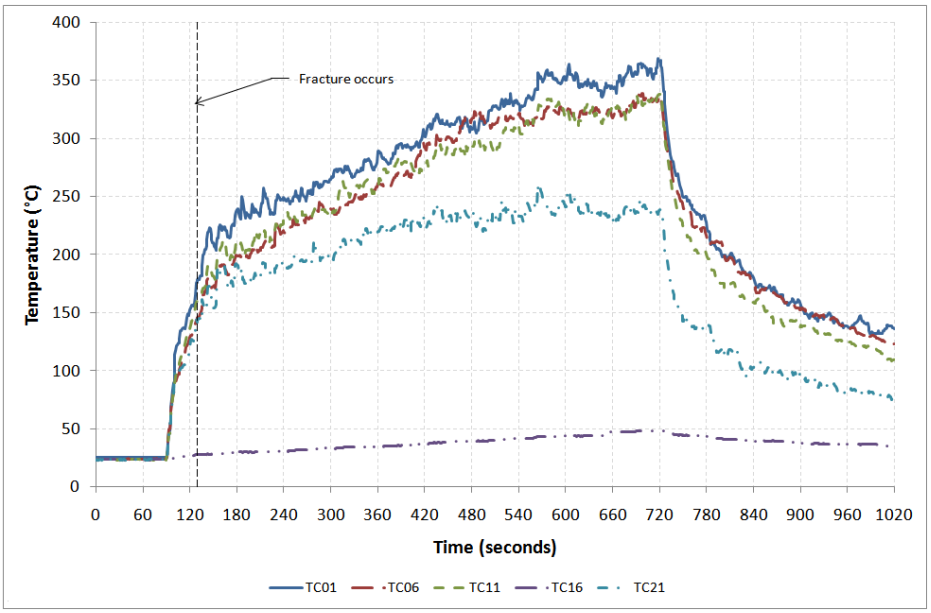

Figure C-164: Gas temperature profiles for experiment 6 Test 43

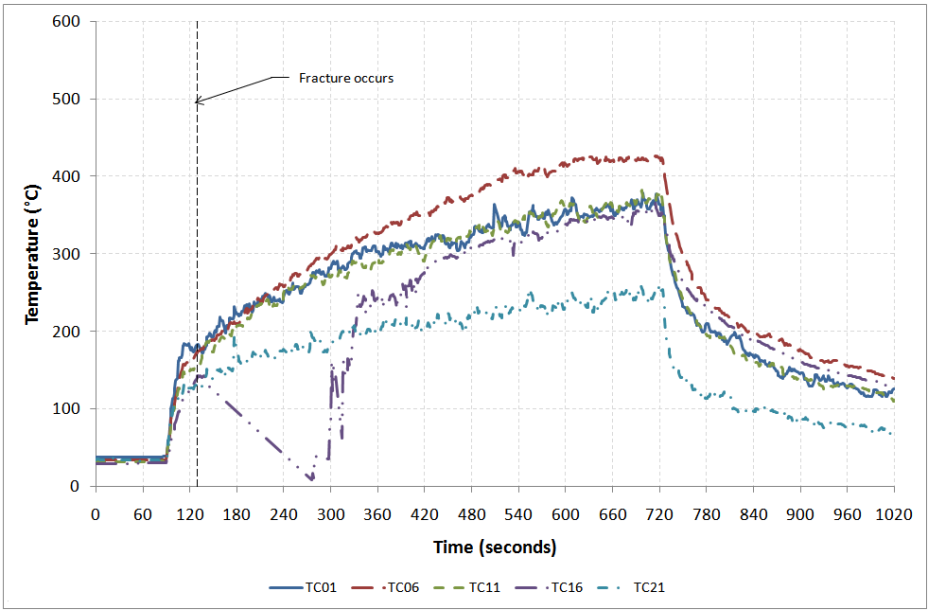

Figure C-165: Gas temperature profiles for experiment 6 Test 44

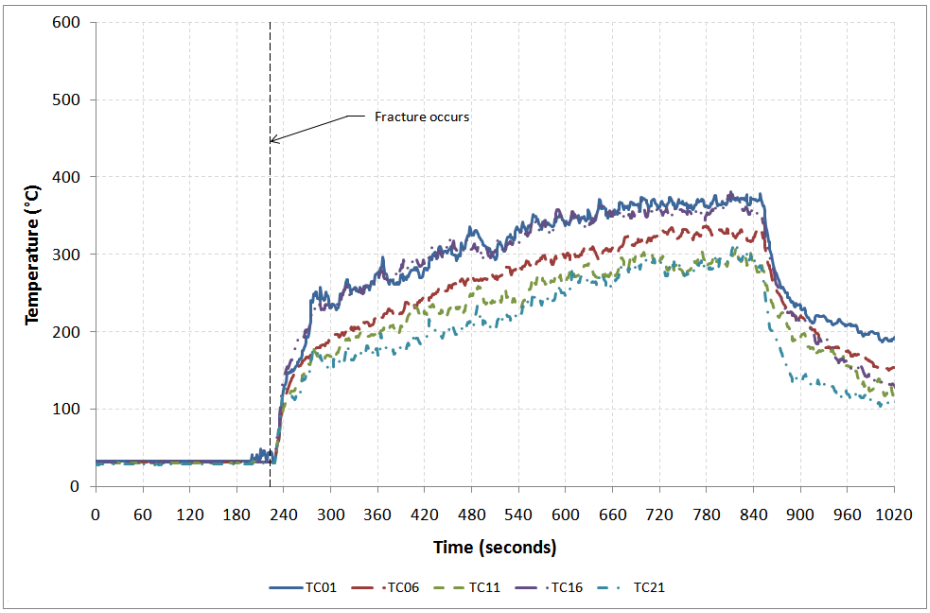

Figure C-166: Gas temperature profiles for experiment 6 Test 45

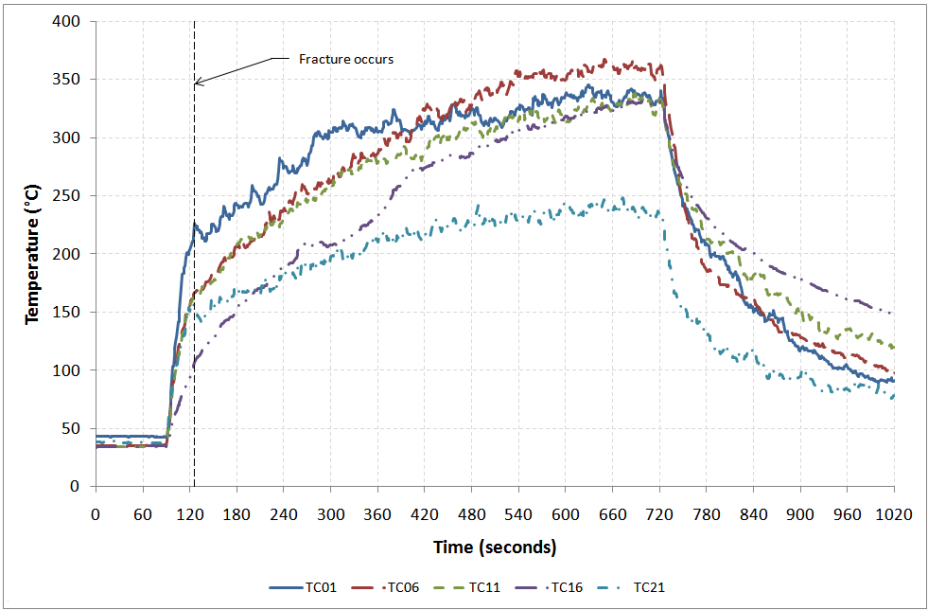

Figure C-167: Gas temperature profiles for experiment 6 Test 46

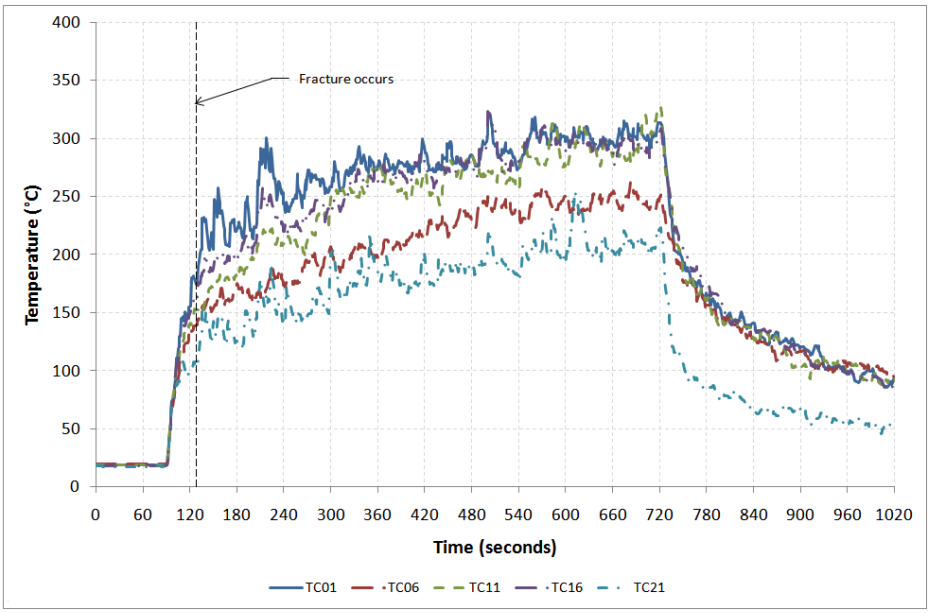

Figure C-168: Gas temperature profiles for experiment 6 Test 47

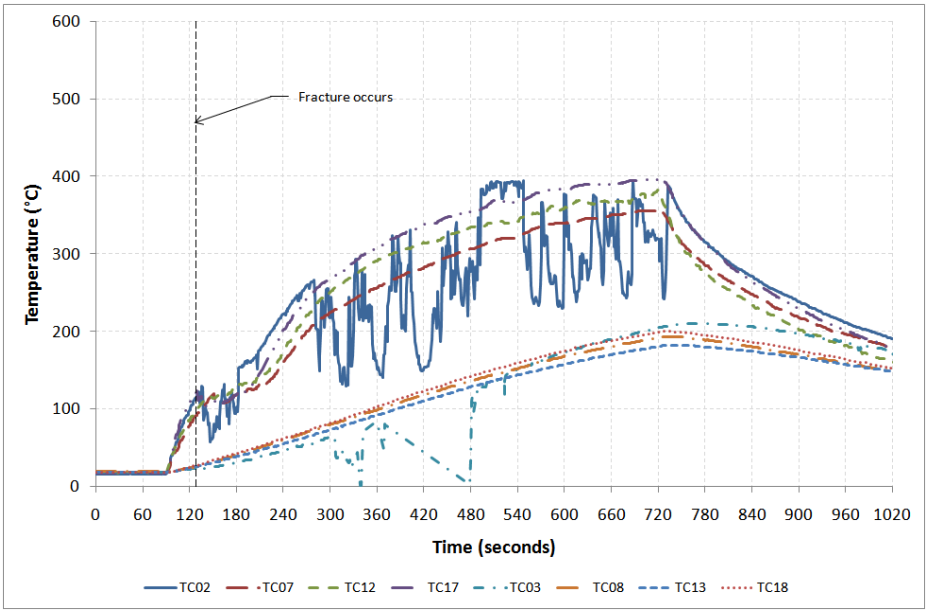

Figure C-169: Glass temperature profiles on exposed side for experiment 6 Test 47

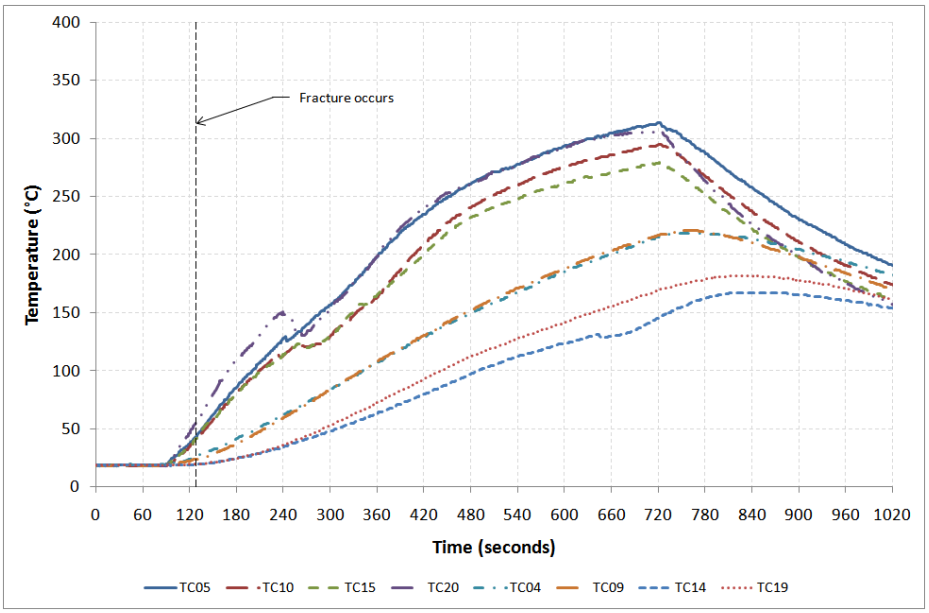

Figure C-170: Glass temperature profiles on unexposed side for experiment 6 Test 47

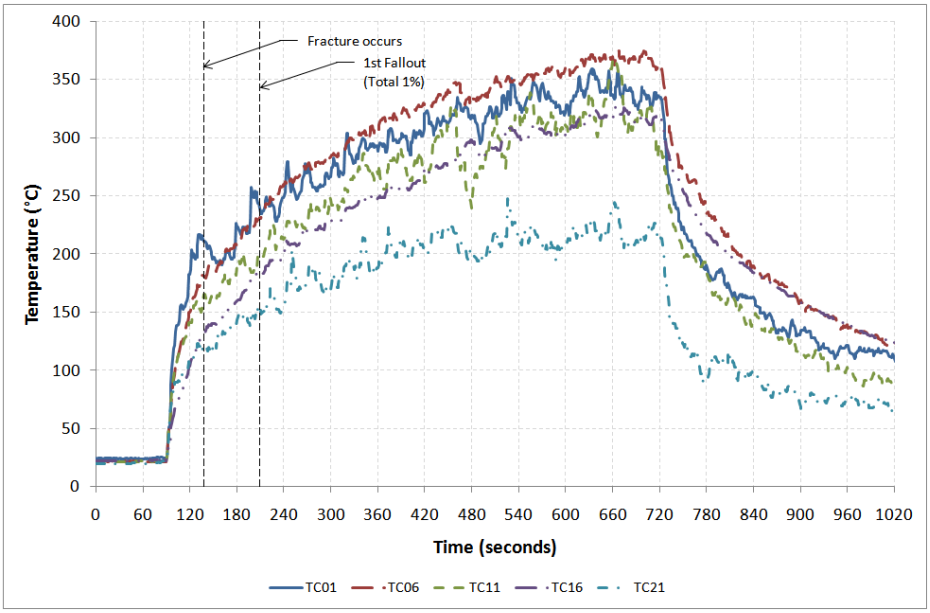

Figure C-171: Gas temperature profiles for experiment 6 Test 48

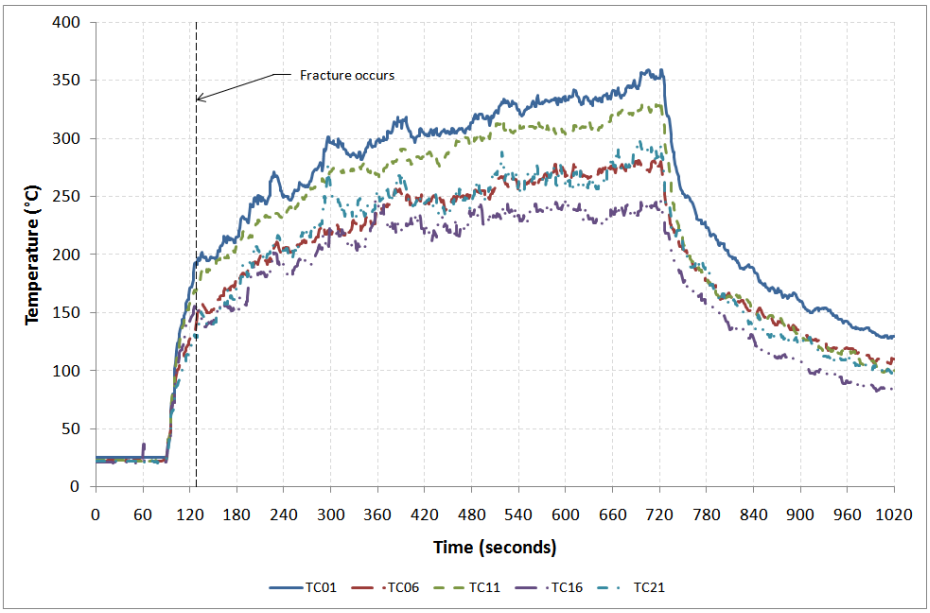

Figure C-172: Gas temperature profiles for experiment 6 Test 49

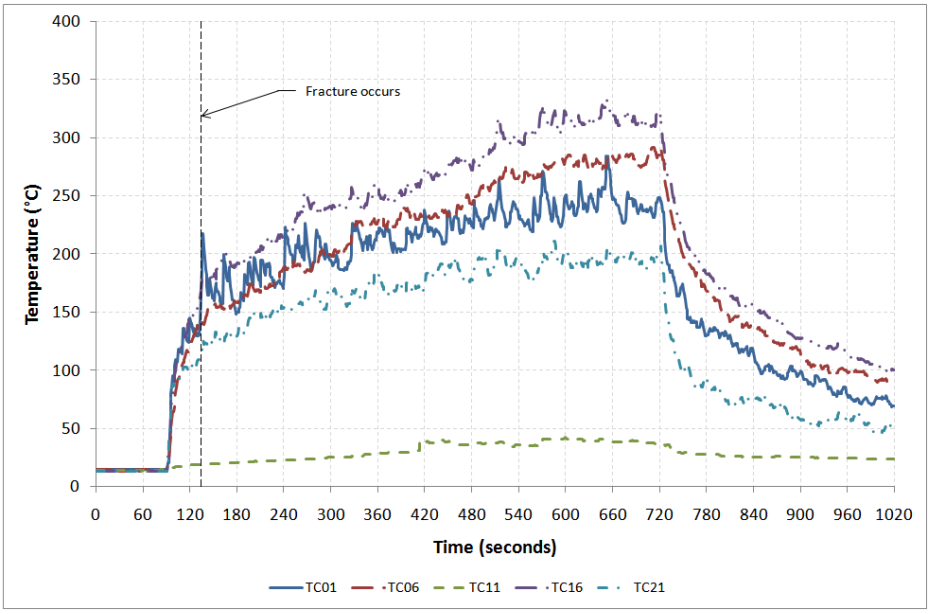

Figure C-173: Gas temperature profiles for experiment 6 Test 50

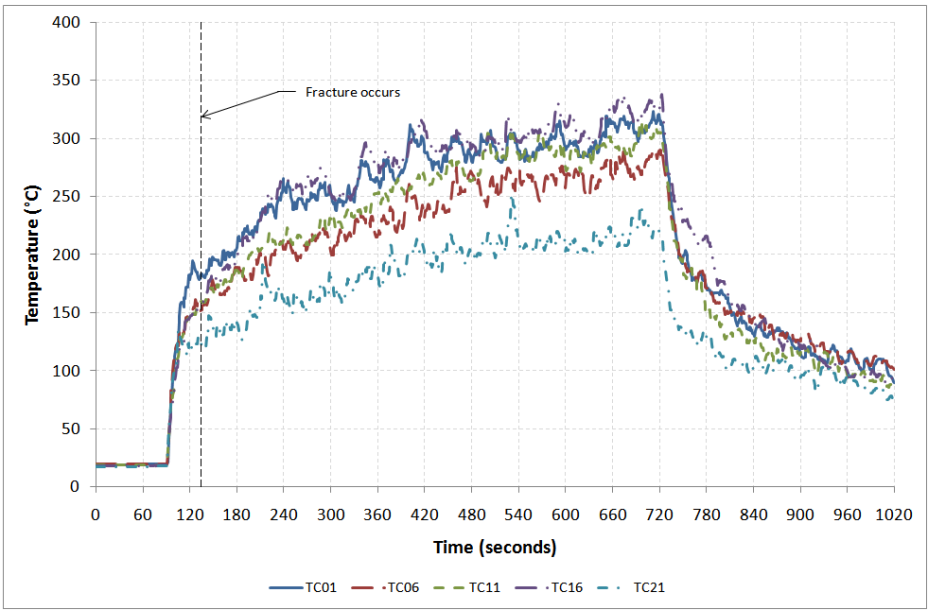

Figure C-174: Gas temperature profiles for experiment 6 Test 51

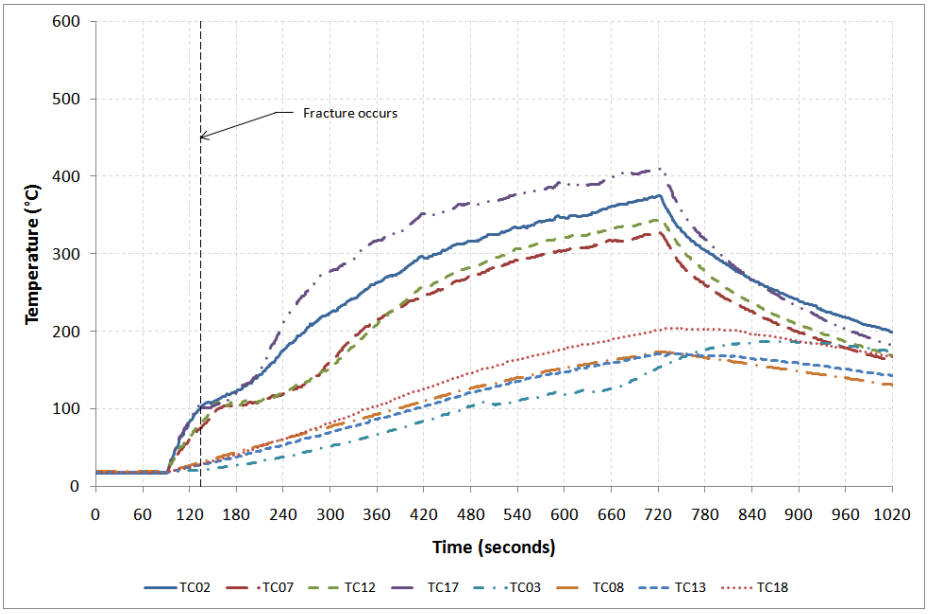

Figure C-175: Glass temperature profiles on exposed side for experiment 6 Test 51

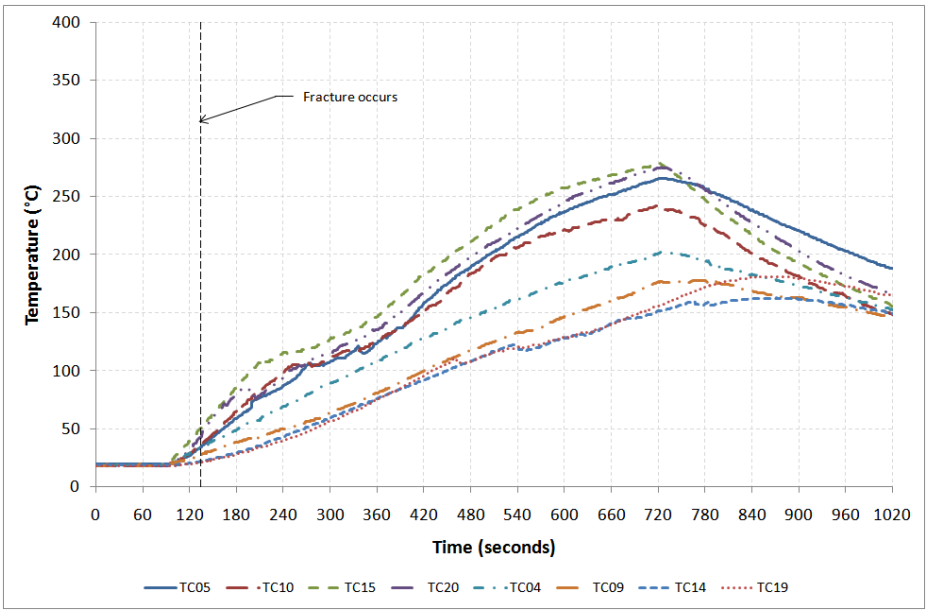

Figure C-176: Glass temperature profiles on unexposed side for experiment 6 Test 51

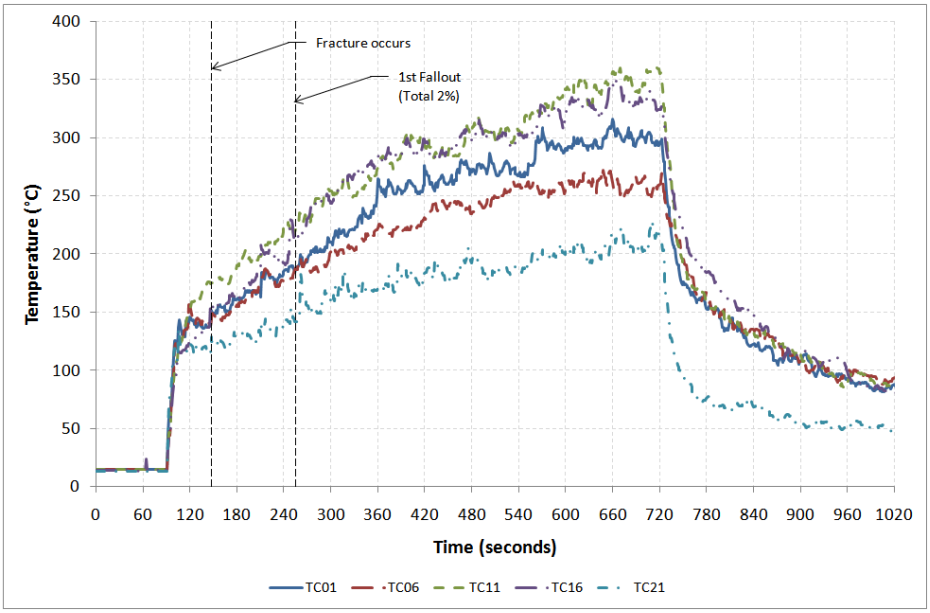

Figure C-177: Gas temperature profiles for experiment 6 Test 52

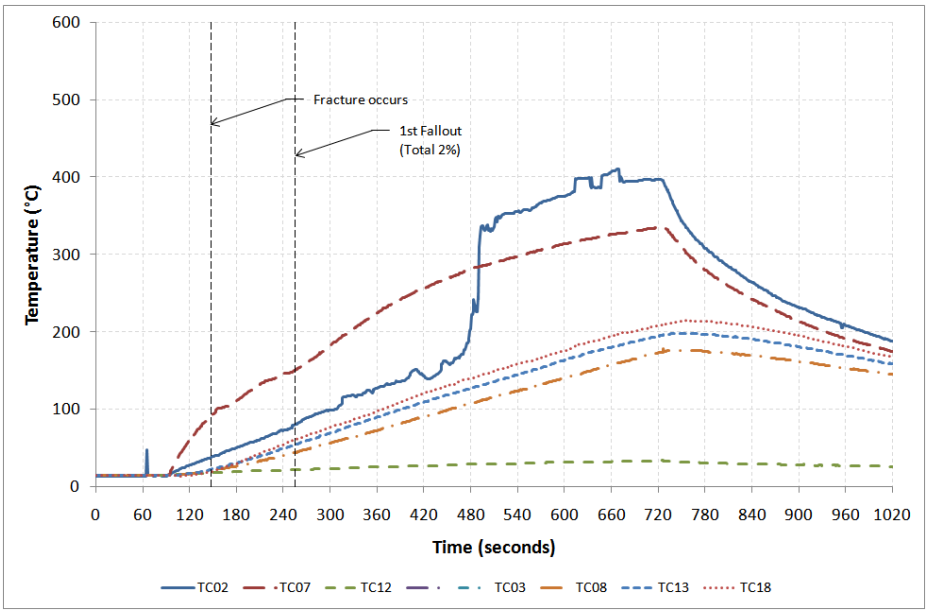

Figure C-178: Glass temperature profiles on exposed side for experiment 6 Test 52 (TC17 reading not available)

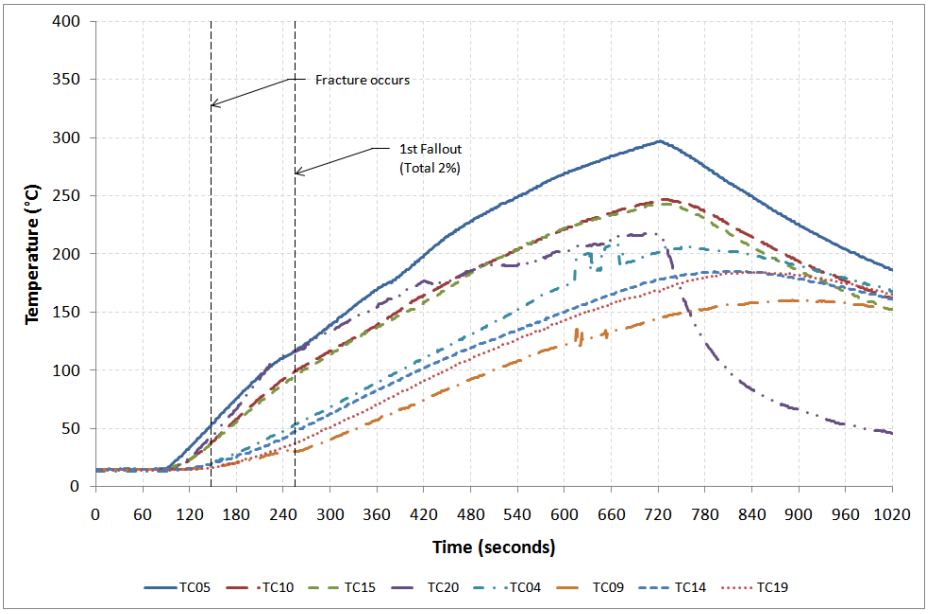

Figure C-179: Glass temperature profiles on unexposed side for experiment 6 Test 52

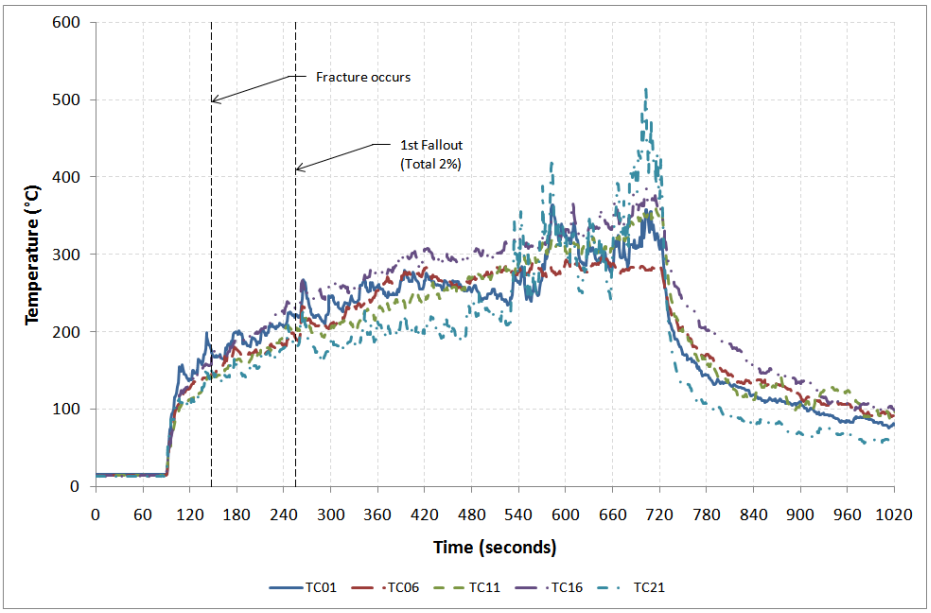

Figure C-180: Gas temperature profiles for experiment 6 Test 53

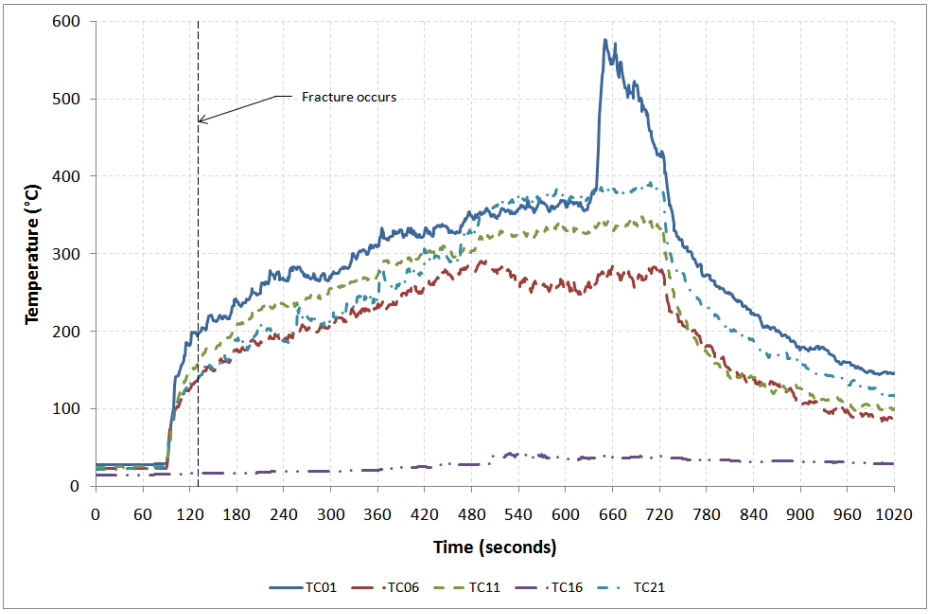

Figure C-181: Gas temperature profiles for experiment 6 Test 54

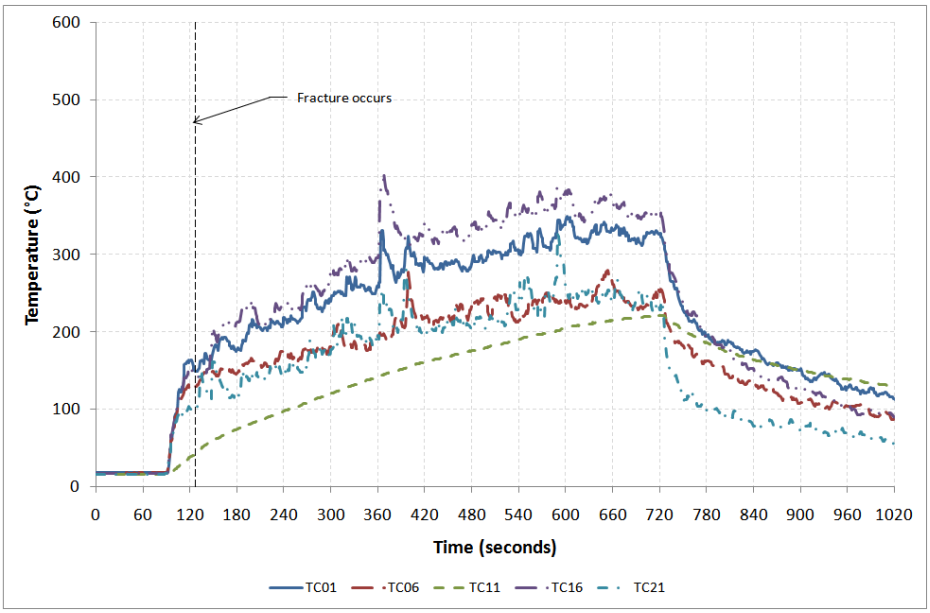

Figure C-182: Gas temperature profiles for experiment 6 Test 55

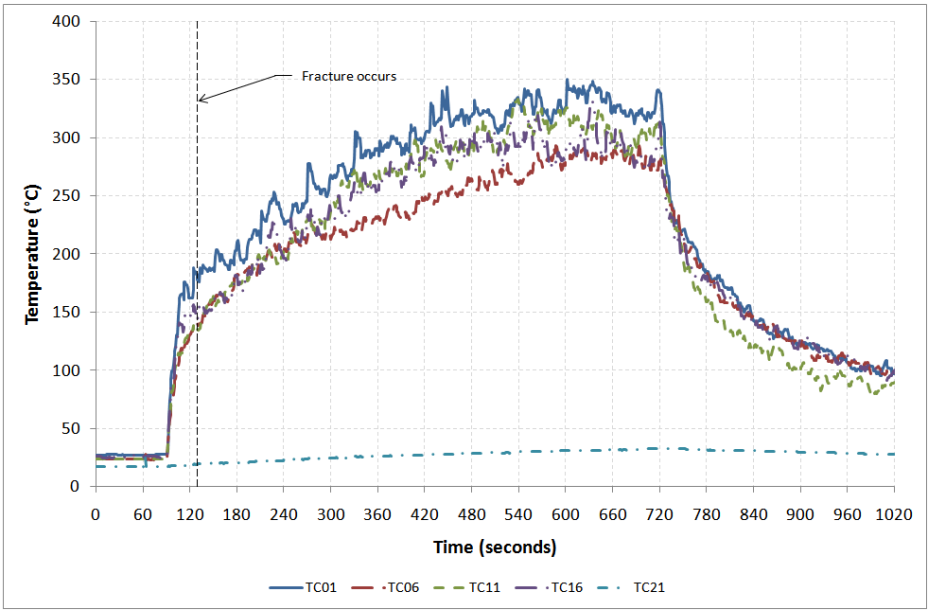

Figure C-183: Gas temperature profiles for experiment 6 Test 56

APPENDIX D - THERMAL STRAIN PROFILES

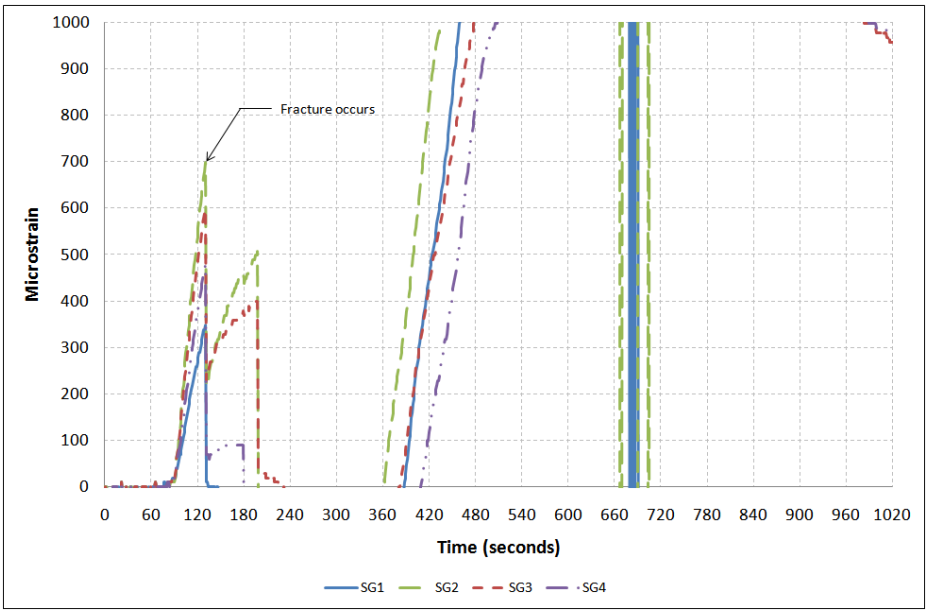

Figure D-1: Thermally induced strain profiles for experiment with sample 4 Test 61

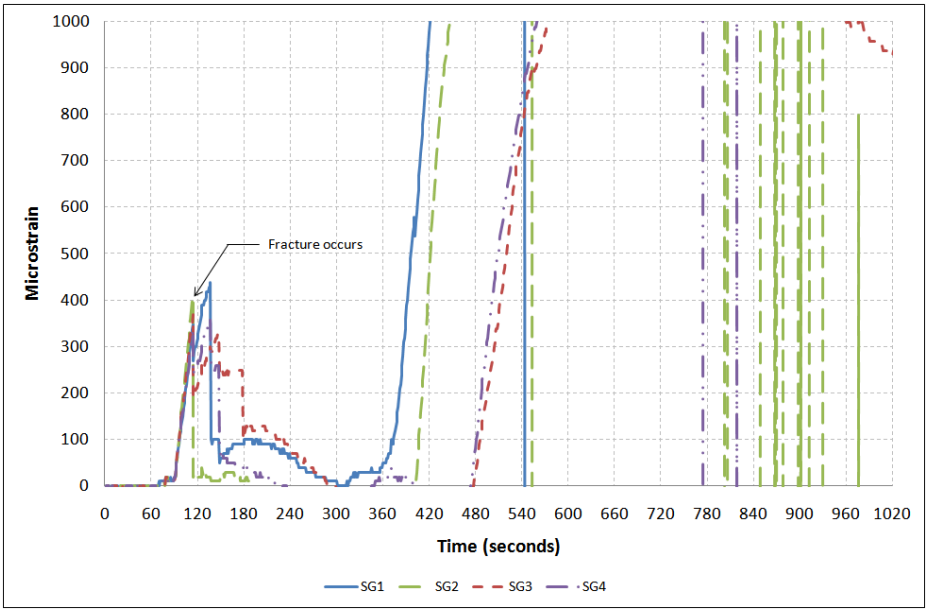

Figure D-2: Thermally induced strain profiles for experiment with sample 4 Test 62

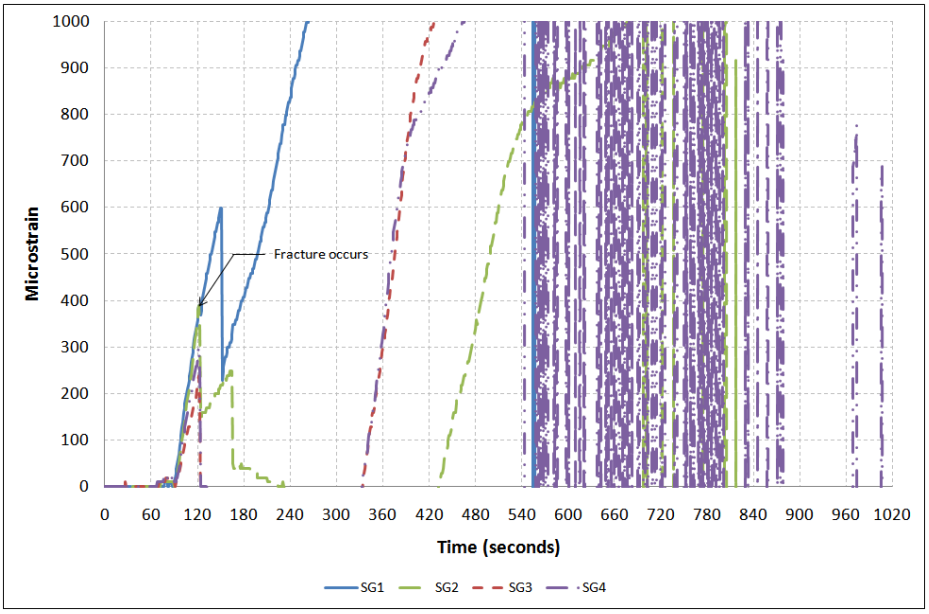

Figure D-3: Thermally induced strain profiles for experiment with sample 4 Test 63

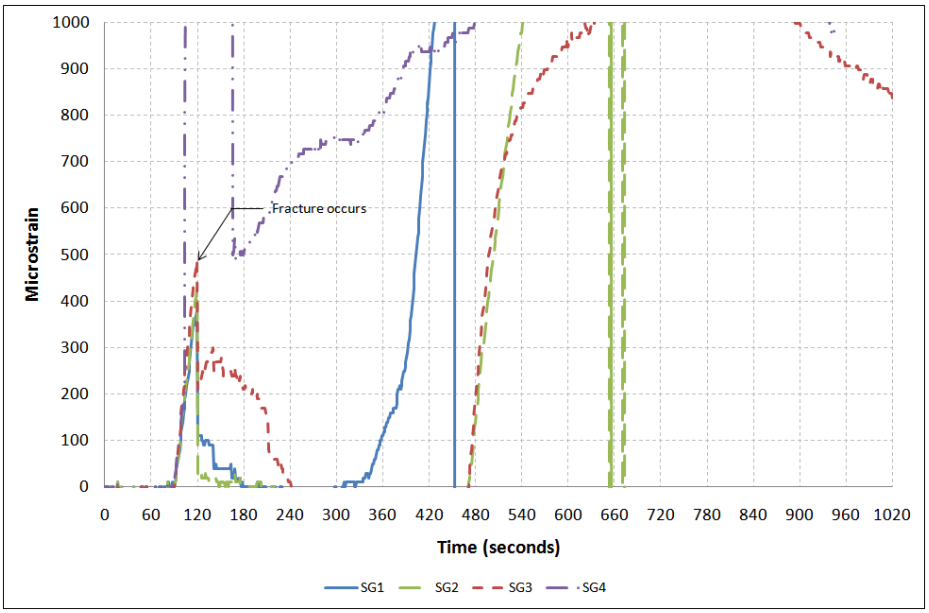

Figure D-4: Thermally induced strain profiles for experiment with sample 4 Test 64

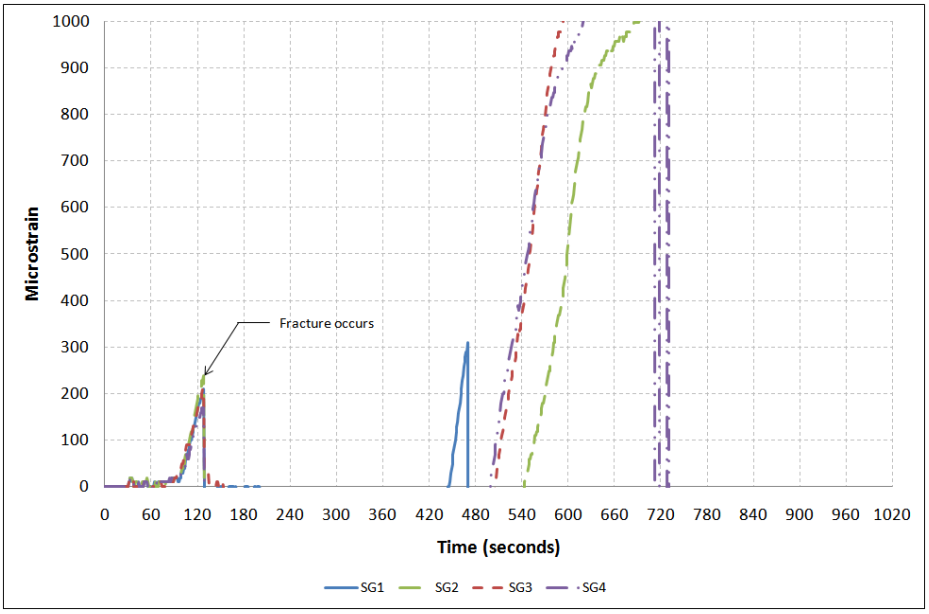

Figure D-5: Thermally induced strain profiles for experiment with sample 6 Test 47

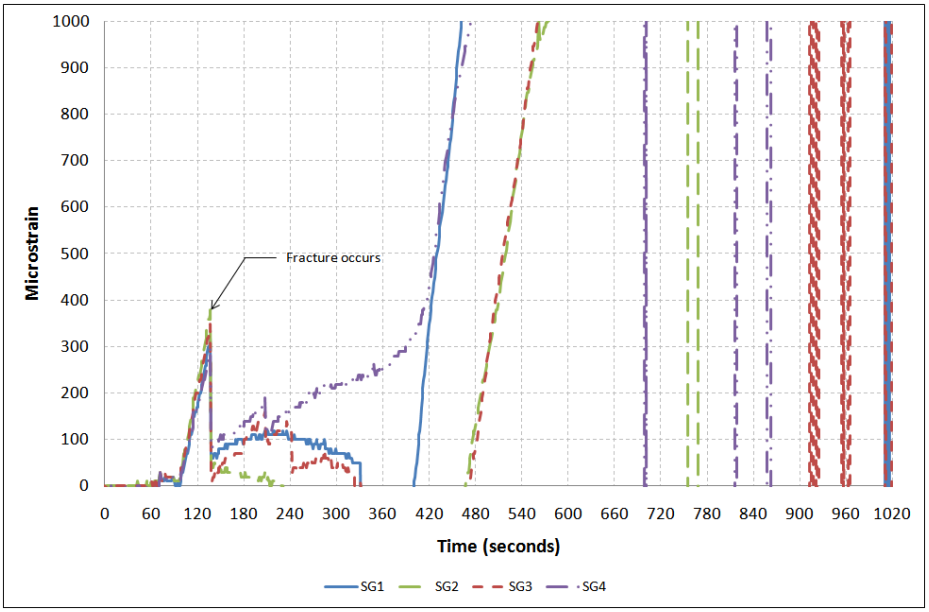

Figure D-6: Thermally induced strain profiles for experiment with sample 6 Test 48

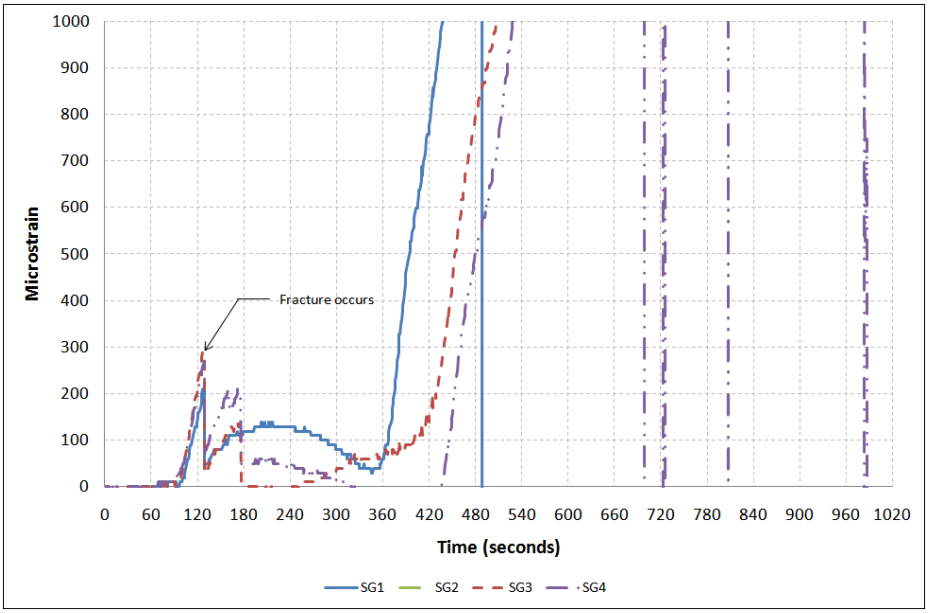

Figure D-7: Thermally induced strain profiles for experiment with sample 6 Test 49

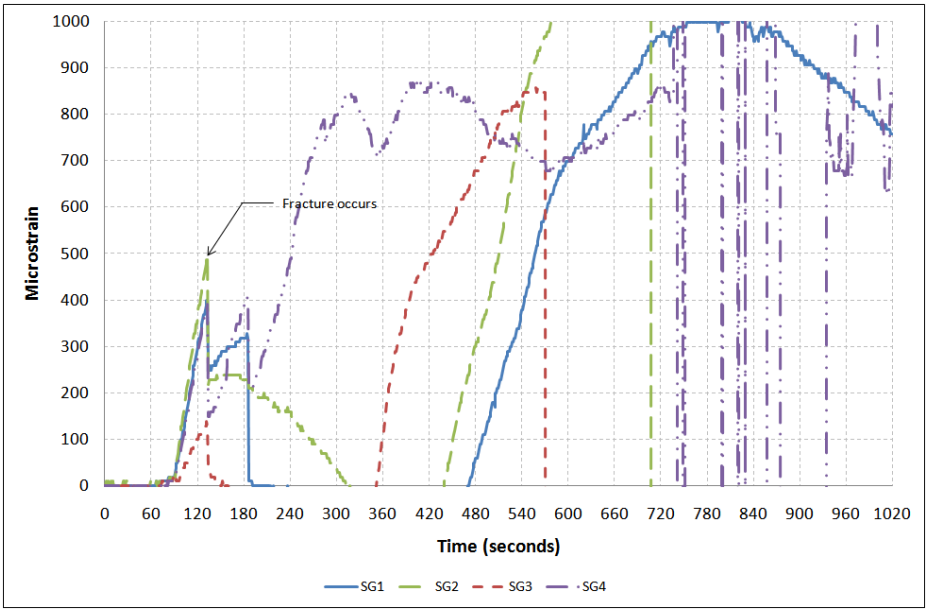

Figure D-8: Thermally induced strain profiles for experiment with sample 6 Test 50

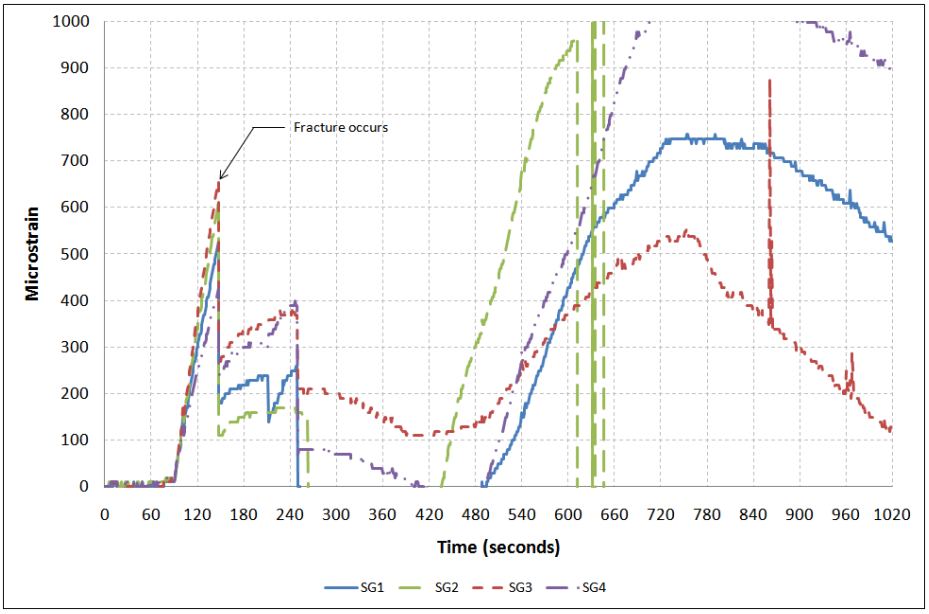

Figure D-9: Thermally induced strain profiles for experiment with sample 6 Test 52

APPENDIX E - EXPERIMENTAL RESULTS

Table E-1: Summary of experimental results for glass samples with rubber beading and thermocouples attached

Experiment Sample	Actual Heat Flux (kW/m^2)	Time to Fracture (seconds)		Crack Position	ΔT1 at Fracture (°C)	ΔT2 at Fracture (°C)	ΔT3 at Fracture (°C)	% Glass Fallout	ΔT1 at Fallout (°C)	ΔT2 at Fallout (°C)	ΔT3 at Fallout (°C)
		Incl. Baseline	Excl. Baseline								
4 Test 1	34.6	117	27	-	90	114	99	0	-	-	-
4 Test 2	21.9	130	40	-	159	N/A	145	13 (@131s)	162	168	148
4 Test 3	26.9	123	33	-	118	85	135	0	-	-	-
4 Test 5	35.7	126	36	-	154	169	137	0	-	-	-
4 Test 6	26.3	129	39	-	123	118	141	0	-	-	-
4 Test 7	25.1	123	33	-	91	98	94	2 (@465s)	437	272	436
4 Test 52	46.4	127	37	-	82	83	91	0	-	-	-

Table E-1 **(con't)**

Experiment Sample	Actual Heat Flux (kW/m^2)	Time to Fracture (seconds)		Crack Position	ΔT1 at Fracture (°C)	ΔT2 at Fracture (°C)	ΔT3 at Fracture (°C)	% Glass Fallout	ΔT1 at Fallout (°C)	ΔT2 at Fallout (°C)	ΔT3 at Fallout (°C)
		Incl. Baseline	Excl. Baseline								
4 Test 57	46.5	119	29	-	65	67	78	4 (N/A)	-	-	-
4 Test 64	44.7	119	29	SG3	64	80	77	0	-	-	-
6 Test 1	27.7	113	23	-	84	95	90	0.25 (@162s)	145	173	161
6 Test 3	36.1	147	57	-	119	148	119	0	-	-	-
6 Test 4	34.7	119	29	-	159	113	133	0	-	-	-
6 Test 5	28.4	112	22	-	104	82	77	0.5 (@245s)	256	262	250
6 Test 6	30.1	134	44	-	109	145	112	0.25 (@275s)	176	239	189
6 Test 7	24.1	120	30	-	98	94	63	0	-	-	-

Table E-1 **(con't)**

Experiment Sample	Actual Heat Flux (kW/m^2)	Time to Fracture (seconds)		Crack Position	ΔT1 at Fracture (°C)	ΔT2 at Fracture (°C)	ΔT3 at Fracture (°C)	% Glass Fallout	ΔT1 at Fallout (°C)	ΔT2 at Fallout (°C)	ΔT3 at Fallout (°C)
		Incl. Baseline	Excl. Baseline								
6 Test 42	46.0	132	42	-	88	76	99	0	-	-	-
6 Test 52	36.5	148	58	SG3	70	127	46	2 (@255s)	106	223	88

Table E-2: Summary of experimental results for glass samples with rubber beading and no thermocouples attached

Experiment Sample	Actual Heat Flux (kW/m^2)	Time to Fracture (seconds)		Crack Position	% Glass Fallout
		Incl. Baseline	Excl. Baseline		
4 Test 44	48.3	120	30	-	2 (@158s) 3 (@191s) 4 (@226s) 5 (@436s) 7 (@459s)
4 Test 45	42.2	124	34	-	20 (@708s)
4 Test 46	43.7	122	32	-	2 (@353s) 11 (@356s) 14 (@376s)
4 Test 47	44.0	124	34	-	2 (@280s) 5 (@318s)

Table E-2 **(con't)**

Experiment Sample	Actual Heat Flux (kW/m^2)	Time to Fracture (seconds)		Crack Position	% Glass Fallout
		Incl. Baseline	Excl. Baseline		
4 Test 48	45.3	120	30	-	1 (@359s) 3 (@396s) 9 (@500s) 14 (@587s)
4 Test 49	48.3	129	39	-	0.25 (@161s)
4 Test 50	47.0	129	39	-	1.5 (@300s) 7.5 (@312s) 15.5 (@336s) 24.5 (@342s) 25.5 (@357s) 31.5 (@361s) 32 (@577s)
4 Test 51	47.4	130	40	-	0
4 Test 53	45.4	113	23	-	1 (@281s)

Table E-2 **(con't)**

Experiment Sample	Actual Heat Flux (kW/m^2)	Time to Fracture (seconds)		Crack Position	% Glass Fallout
		Incl. Baseline	Excl. Baseline		
4 Test 54	48.4	117	27	-	0
4 Test 55	48.7	121	31	-	1 (@553s) 3 (@606s)
4 Test 56	45.9	123	33	-	0
4 Test 58	45.7	128	38	-	47 (@357s)
4 Test 59	44.5	125	35	-	55 (@247s) 59 (@353s) 64 (@360s) 75 (@620s)
4 Test 62	43.2	114	24	SG2	2 (@657s)
6 Test 41	46.6	123	33	-	0
6 Test 43	45.7	129	39	-	0
6 Test 44	49.8	129	39	-	0
6 Test 45*	47.6	222	60	-	0

Table E-2 **(con't)**

Experiment Sample	Actual Heat Flux (kW/m^2)	Time to Fracture (seconds)		Crack Position	% Glass Fallout
		Incl. Baseline	Excl. Baseline		
6 Test 46	57.7	126	36	-	0
6 Test 50	41.1	134	44	SG2	0
6 Test 53	38.6	140	50	-	9 (@467s) 10 (@524s) 11 (@558s)
6 Test 54	42.1	131	41	-	0
6 Test 55	41.3	127	37	-	0
6 Test 56	43.8	130	40	-	0

Table E-3: Summary of experimental results for glass samples with kaowool beading and thermocouples attached

Experiment Sample	Actual Heat Flux (kW/m^2)	Time to Fracture (seconds)		Crack Position	ΔT1 at Fracture (°C)	ΔT2 at Fracture (°C)	ΔT3 at Fracture (°C)	% Glass Fallout	ΔT1 at Fallout (°C)	ΔT2 at Fallout (°C)	ΔT3 at Fallout (°C)
		Incl. Baseline	Excl. Baseline								
4 Test 8	30.6	128	38	-	154	74	103	2 (@128s)	154	74	103
4 Test 9	49.1	116	26	-	43	31	39	1 (@438s) 5 (@442s)	346 361	378 379	274 275
4 Test 10	32.1	137	47	-	110	101	126	0	-	-	-
4 Test 11	34.7	115	25	-	19	15	16	0	-	-	-
4 Test 12	43.9	121	31	-	179	16	96	2 (@246s)	216	110	139
4 Test 13	41.6	123	33	-	52	17	47	0	-	-	-
4 Test 18	38.7	128	38	-	44	47	51	2 (@185s) 9 (@315s)	63 114	66 169	74 127
4 Test 21	12.8	127	37	-	102	119	125	0	-	-	-
4 Test 26	45.6	132	42	-	160	100	135	8 (@190s)	185	125	236
4 Test 28	44.4	122	32	-	66	53	70	9 (N/A)	-	-	-

Table E-3 **(con't)**

Experiment Sample	Actual Heat Flux (kW/m^2)	Time to Fracture (seconds)		Crack Position	ΔT1 at Fracture (°C)	ΔT2 at Fracture (°C)	ΔT3 at Fracture (°C)	% Glass Fallout	ΔT1 at Fallout (°C)	ΔT2 at Fallout (°C)	ΔT3 at Fallout (°C)
		Incl. Baseline	Excl. Baseline								
4 Test 37	40.3	141	51	-	95	121	84	67 (@193s)	-	-	-
4 Test 61	44.1	130	40	SG2	88	67	64	3 (@179s)	110	76	96
6 Test 8	28.1	134	44	-	184	179	93	0	-	-	-
6 Test 9	33.1	125	35	-	96	79	85	0	-	-	-
6 Test 10	34.1	131	41	-	91	85	88	5 (@297s)	176	242	182
6 Test 19	43.5	105	15	-	49	30	50	6 (@165s)	109	71	130
6 Test 29	42.6	135	45	-	75	110	81	0	-	-	-
6 Test 33	44.6	164	74	-	87	78	111	1 (@165s) 5 (@225s)	88 125	77 100	113 163
6 Test 47	44.9	128	38	SG2	94	65	83	0	-	-	-

Table E-4: Summary of experimental results for glass samples with kaowool beading and no thermocouples attached

Experiment Sample	Actual Heat Flux (kW/m^2)	Time to Fracture (seconds)		Crack Position	% Glass Fallout
		Incl. Baseline	Excl. Baseline		
4 Test 14	33.4	139	49	-	87 (@219s)
4 Test 15	31.8	128	38	-	0
4 Test 16	30.9	127	37	-	1 (@180s)
4 Test 17	35.0	128	38	-	42 (@129s)
4 Test 19	37.2	133	43	-	2 (@671s)
4 Test 20	27.5	140	50	-	6 (@140s)
4 Test 22	N/A	133	43	-	1 (@254s)
4 Test 23	N/A	133	43	-	6 (@468s)
4 Test 24	43.4	137	47	-	11 (@225s)
4 Test 25	46.9	118	28	-	9 (@180s) 15 (@284s)
4 Test 27	44.5	142	52	-	52 (@197s)

APPENDIX E

Experiment Sample	Actual Heat Flux (kW/m^2)	Time to Fracture (seconds)		Crack Position	% Glass Fallout
		Incl. Baseline	Excl. Baseline		
4 Test 29	43.7	122	32	-	5 (@188s) 39 (@283s)
4 Test 30	45.9	136	46	-	1 (@226s)
4 Test 31	44.4	140	50	-	5 (@140s) 10 (@311s)
4 Test 32	43.6	128	38	-	4 (N/A)
4 Test 33	44.8	140	50	-	73 (@141s)
4 Test 34	44.2	141	51	-	5 (@142s) 22 (@398s)
4 Test 35	38.7	132	42	-	8 (@133s) 16 (@330s)
4 Test 36	38.9	127	37	-	8 (@167s) 18 (@332s)
4 Test 38	39.0	136	46	-	1 (@231s)

APPENDIX E

Experiment Sample	Actual Heat Flux (kW/m^2)	Time to Fracture (seconds)		Crack Position	% Glass Fallout
		Incl. Baseline	Excl. Baseline		
4 Test 39	39.4	130	40	-	4 (@206s) 6 (@332s) 11 (@350s)
4 Test 40	39.7	127	37	-	0
4 Test 41	39.7	139	59	-	16 (@139s) 24 (@446s)
4 Test 42	34.2	137	47	-	2 (@138s) 95 (@282s)
4 Test 43	42.2	142	52	-	7 (@142s) 15 (@535s)
4 Test 60	42.5	127	37	SG2	1 (@127s) 5 (@246s)
4 Test 63	41.7	123	33	SG2	7 (@123s)
6 Test 11	40.8	127	37	-	4 (@696s)
6 Test 12	32.3	134	44	-	0

Table E-4 (**con't)**

Experiment Sample	Actual Heat Flux (kW/m^2)	Time to Fracture (seconds)		Crack Position	% Glass Fallout
		Incl. Baseline	Excl. Baseline		
6 Test 13	36.9	150	60	-	0
6 Test 14	35.6	132	42	-	1 (@154s)
6 Test 15	27.5	154	64	-	0
6 Test 16	13.1	161	71	-	0
6 Test 17	40.4	131	41	-	5 (@132s) 10 (@440s) 16 (N/A)
6 Test 18	43.4	139	49	-	1 (@369s)
6 Test 20	42.4	154	64	-	1 (@292s) 2 (@639s)
6 Test 21	43.9	145	55	-	72 (@145s)
6 Test 22	45.5	141	51	-	4 (@251s) 7 (@327s)

Table E-4 **(con't)**

Experiment Sample	Actual Heat Flux (kW/m^2)	Time to Fracture (seconds)		Crack Position	% Glass Fallout
		Incl. Baseline	Excl. Baseline		
6 Test 23	42.8	125	35	-	0.25 (@230s)
6 Test 24	41.0	144	54	-	0
6 Test 25	44.9	136	46	-	0
6 Test 26	44.9	133	43	-	0
6 Test 27	38.8	132	42	-	1 (@263s)
6 Test 28	43.5	165	75	-	5 (@219s) 6 (@324s)
6 Test 30	43.8	142	52	-	0
6 Test 31	43.4	131	41	-	1 (@516s)
6 Test 32	45.8	135	45	-	0
6 Test 34	44.4	135	45	-	0
6 Test 35	42.5	140	50	-	6 (@141s)
6 Test 36	44.5	143	53	-	0

APPENDIX E

Experiment Sample	Actual Heat Flux (kW/m^2)	Time to Fracture (seconds)		Crack Position	% Glass Fallout
		Incl. Baseline	Excl. Baseline		
6 Test 37	45.5	130	40	-	0
6 Test 38	46.7	126	36	-	0
6 Test 39	45.7	147	57	-	0
6 Test 40	47.7	152	62	-	0
6 Test 48	45.0	138	48	SG2	1 (@209s)
6 Test 49	44.6	128	38	SG3	0

Notes:

N/A – Not available

* 162 seconds baseline

APPENDIX F - TEMPERATURE DIFFERENCES AT GLASS FRACTURE FOR SAMPLES WITH STRAIN GAUGES

Table F-1: Summary of temperature differences at glass fracture for experiment samples with strain gauges

Experimental Sample	ΔT1 at Fracture (°C)					ΔT2 at Fracture (°C)					ΔT3 at Fracture (°C)				
	Top (SG1)	Right (SG2)	Left (SG4)	Bottom (SG3)	Max	Top (SG1)	Right (SG2)	Left (SG4)	Bottom (SG3)	Max	Top (SG1)	Right (SG2)	Left (SG4)	Bottom (SG3)	Max
4 Test 61	N/A	88	68	N/A	N/A	67	64	67	66	67	N/A	64	46	N/A	N/A
4 Test 64	18	50	39	64	64	79	76	78	80	80	19	33	25	77	77
6 Test 47	N/A	94	65	72	N/A	N/A	62	63	64	N/A	N/A	65	41	83	N/A
6 Test 52	N/A	N/A	70	N/A	N/A	N/A	127	126	125	N/A	N/A	N/A	46	N/A	N/A

Note:

N/A – Not available

APPENDIX G - POST-FRACTURE PATTERN

Due to a technical difficulty with the digital camera, there were no photos for experiment samples 4 Test 8, 4 Test 35 to 4 Test 43, 6 Test 9 and 6 Test 17 to 6 Test 30. Post-fracture pattern sketches were produced for some experiment samples only due to the time constraint imposed on the research. It should be noted that the photos were taken after the cooling stage so some photos will indicate glass fallout but the fallout did not occur during the heating stage. All fallouts reported occurred during the heating stage of the experiments unless notified otherwise.

(a) Photo

(b) Sketch

Figure G-1: Post-fracture pattern for experimental sample 4 Test 1

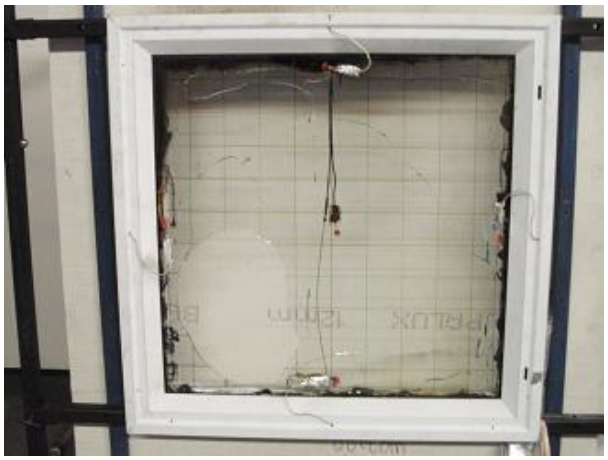

(a) Photo

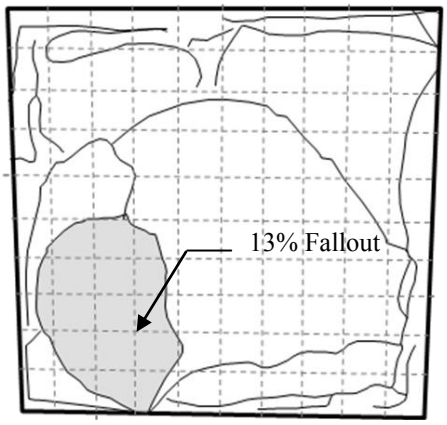

(b) Sketch

Figure G-2: Post-fracture pattern for experimental sample 4 Test 2

(a) Photo

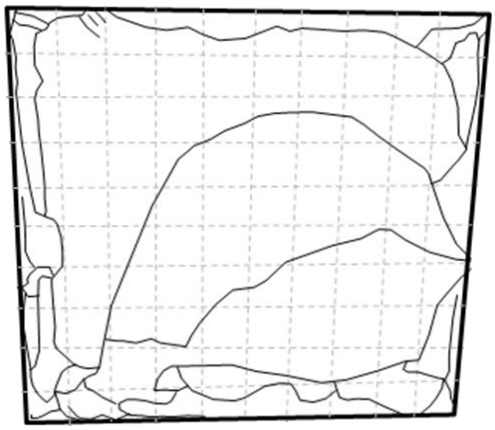

(b) Sketch

Figure G-3: Post-fracture pattern for experimental sample 4 Test 3

	Sketch not produced
(a) Photo	(b) Sketch

Figure G-4: Post-fracture pattern for experimental sample 4 Test 4

	Sketch not produced
(a) Photo	(b) Sketch

Figure G-5: Post-fracture pattern for experimental sample 4 Test 5

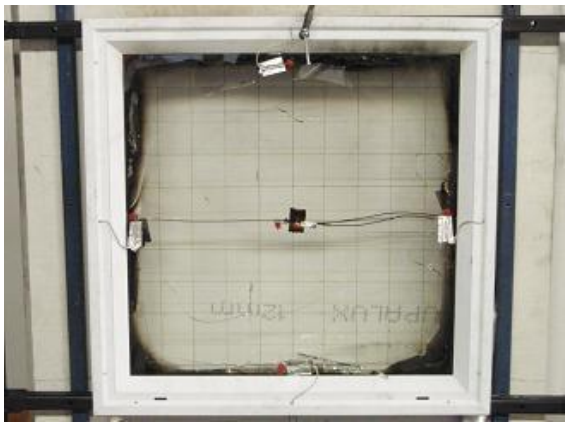

(a) Photo

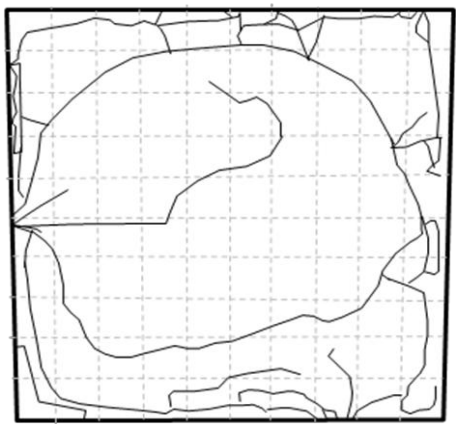

(b) Sketch

Figure G-6: Post-fracture pattern for experimental sample 4 Test 6

(a) Photo

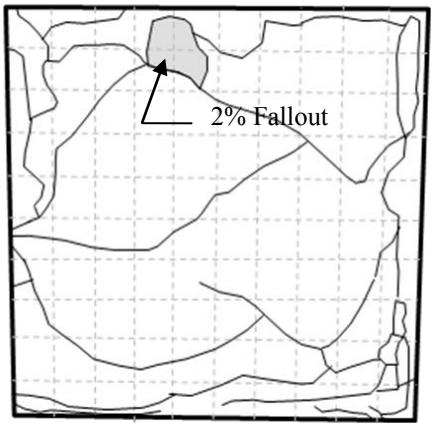

(b) Sketch

Figure G-7: Post-fracture pattern for experimental sample 4 Test 7

(a) Photo

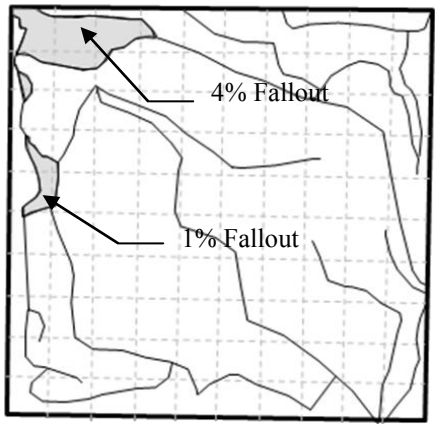

(b) Sketch

Figure G-8: Post-fracture pattern for experimental sample 4 Test 9

(a) Photo

Sketch not produced

(b) Sketch

Figure G-9: Post-fracture pattern for experimental sample 4 Test 10

(a) Photo

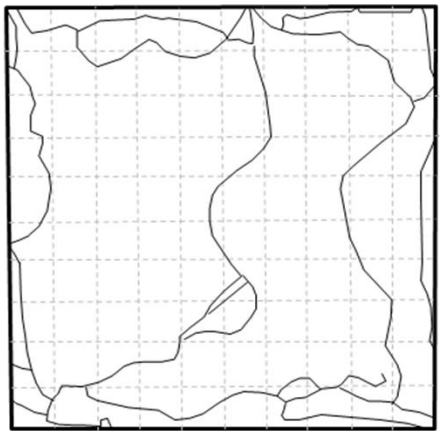

(b) Sketch

Figure G-10: Post-fracture pattern for experimental sample 4 Test 11

(a) Photo

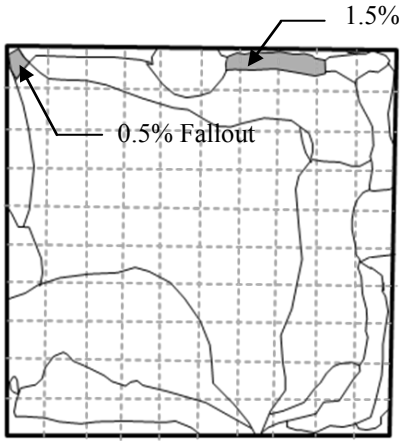

(b) Sketch

Figure G-11: Post-fracture pattern for experimental sample 4 Test 12

(a) Photo

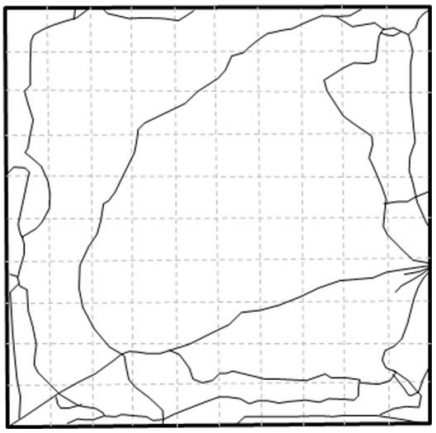

(b) Sketch

Figure G-12: Post-fracture pattern for experimental sample 4 Test 13

(a) Photo

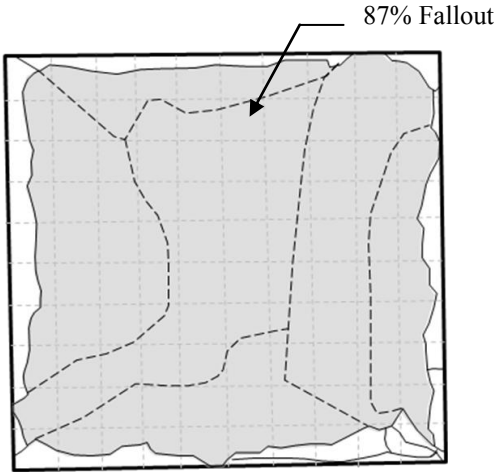

(b) Sketch

Figure G-13: Post-fracture pattern for experimental sample 4 Test 14

(a) Photo

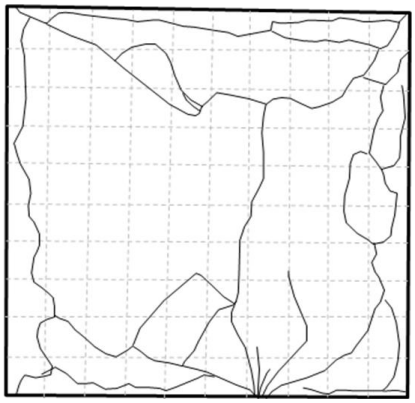

(b) Sketch

Figure G-14: Post-fracture pattern for experimental sample 4 Test 15

(a) Photo

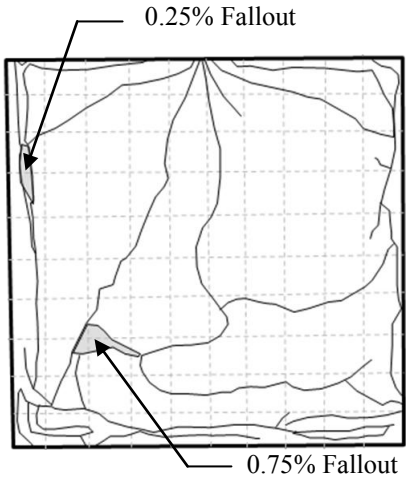

(b) Sketch

Figure G-15: Post-fracture pattern for experimental sample 4 Test 16

(a) Photo

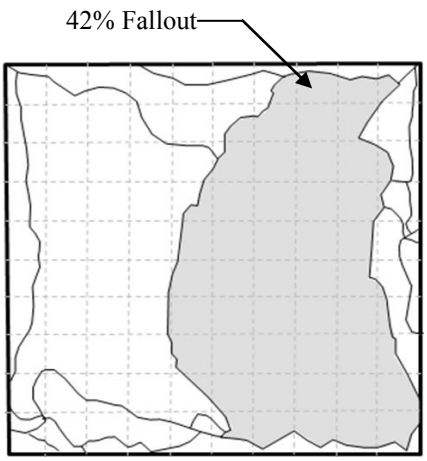

(b) Sketch

Figure G-16: Post-fracture pattern for experimental sample 4 Test 17

(a) Photo

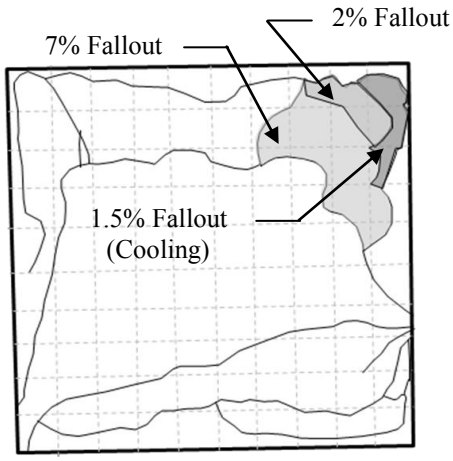

(b) Sketch

Figure G-17: Post-fracture pattern for experimental sample 4 Test 18

	Sketch not produced
(a) Photo	(b) Sketch

Figure G-18: Post-fracture pattern for experimental sample 4 Test 19

	Sketch not produced
(a) Photo	(b) Sketch

Figure G-19: Post-fracture pattern for experimental sample 4 Test 20

(a) Photo

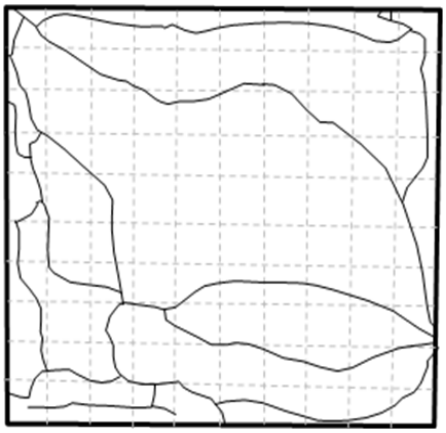

(b) Sketch

Figure G-20: Post-fracture pattern for experimental sample 4 Test 21

(a) Photo

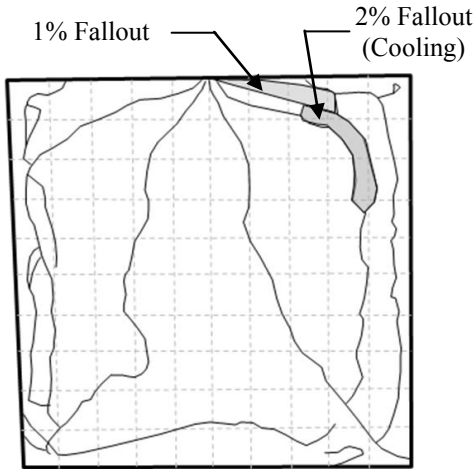

(b) Sketch

Figure G-21: Post-fracture pattern for experimental sample 4 Test 22

(a) Photo

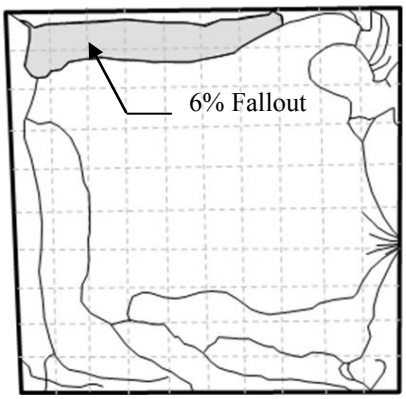

(b) Sketch

Figure G-22: Post-fracture pattern for experimental sample 4 Test 23

(a) Photo

Sketch not produced

(b) Sketch

Figure G-23: Post-fracture pattern for experimental sample 4 Test 24

	Sketch not produced
(a) Photo	(b) Sketch

Figure G-24: Post-fracture pattern for experimental sample 4 Test 25

	Sketch not produced
(a) Photo	(b) Sketch

Figure G-25: Post-fracture pattern for experimental sample 4 Test 26

	Sketch not produced
(a) Photo	(b) Sketch

Figure G-26: Post-fracture pattern for experimental sample 4 Test 27

	Sketch not produced
(a) Photo	(b) Sketch

Figure G-27: Post-fracture pattern for experimental sample 4 Test 28

	Sketch not produced
(a) Photo	(b) Sketch

Figure G-28: Post-fracture pattern for experimental sample 4 Test 29

	Sketch not produced
(a) Photo	(b) Sketch

Figure G-29: Post-fracture pattern for experimental sample 4 Test 30

(a) Photo

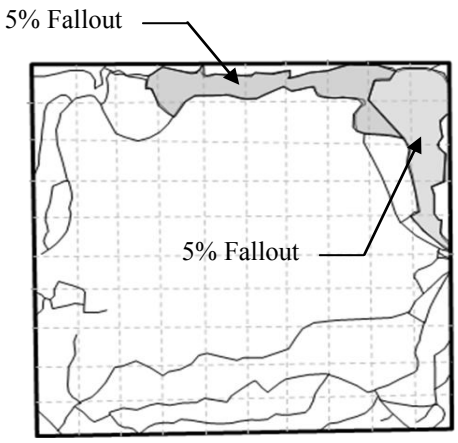

(b) Sketch

Figure G-30: Post-fracture pattern for experimental sample 4 Test 31

(a) Photo

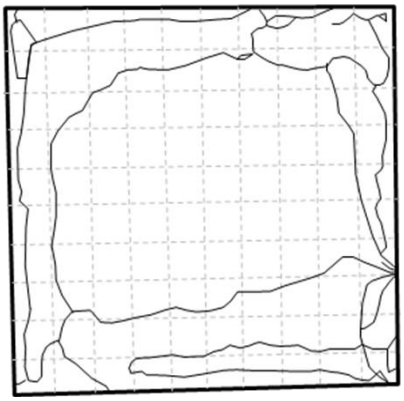

(b) Sketch

Figure G-31: Post-fracture pattern for experimental sample 4 Test 32

(a) Photo

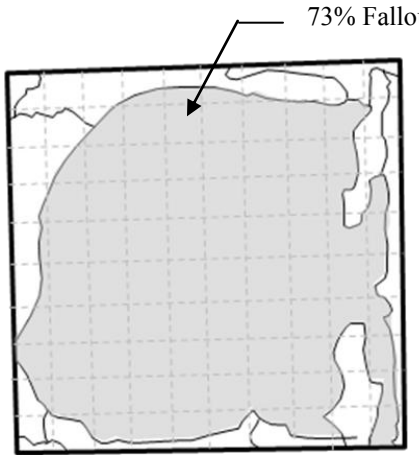

(b) Sketch

Figure G-32: Post-fracture pattern for experimental sample 4 Test 33

(a) Photo

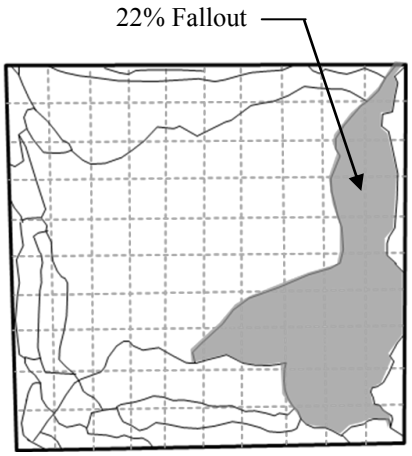

(b) Sketch

(Progressive fallout history not available)

Figure G-33: Post-fracture pattern for experimental sample 4 Test 34

	Sketch not produced
(a) Photo	(b) Sketch

Figure G-34: Post-fracture pattern for experimental sample 4 Test 44

	Sketch not produced
(a) Photo	(b) Sketch

Figure G-35: Post-fracture pattern for experimental sample 4 Test 45

	Sketch not produced
(a) Photo	(b) Sketch

Figure G-36: Post-fracture pattern for experimental sample 4 Test 46

	Sketch not produced
(a) Photo	(b) Sketch

Figure G-37: Post-fracture pattern for experimental sample 4 Test 47

	Sketch not produced
(a) Photo	(b) Sketch

Figure G-38: Post-fracture pattern for experimental sample 4 Test 48

	Sketch not produced
(a) Photo	(b) Sketch

Figure G-39: Post-fracture pattern for experimental sample 4 Test 49

	Sketch not produced
(a) Photo	(b) Sketch

Figure G-40: Post-fracture pattern for experimental sample 4 Test 50

	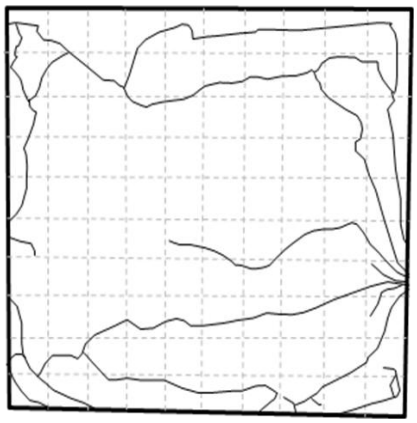
(a) Photo	(b) Sketch

Figure G-41: Post-fracture pattern for experimental sample 4 Test 51

Sketch not produced

(a) Photo

(b) Sketch

Figure G-42: Post-fracture pattern for experimental sample 4 Test 52

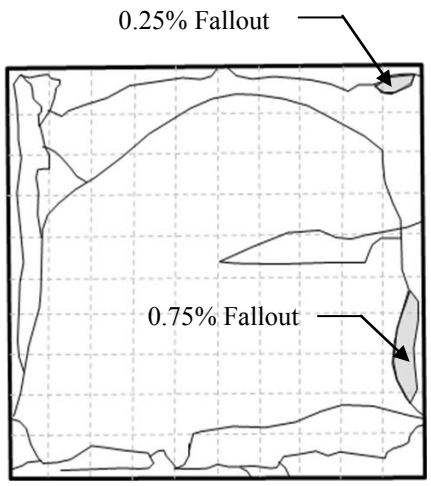

(a) Photo

(b) Sketch

Figure G-43: Post-fracture pattern for experimental sample 4 Test 53

(a) Photo

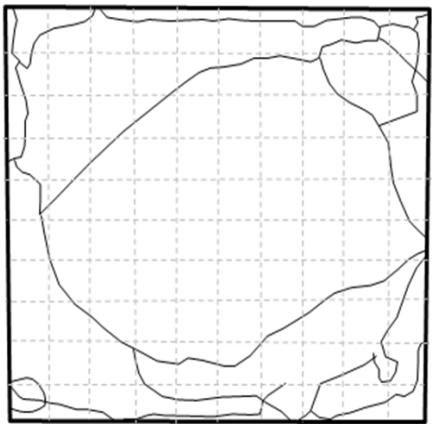

(b) Sketch

Figure G-44: Post-fracture pattern for experimental sample 4 Test 54

(a) Photo

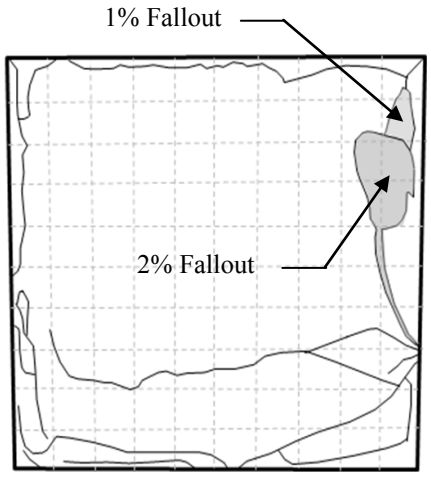

(b) Sketch

Figure G-45: Post-fracture pattern for experimental sample 4 Test 55

(a) Photo

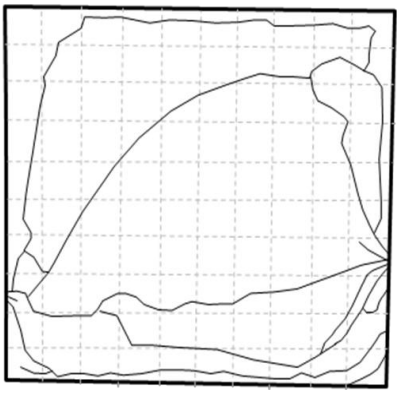

(b) Sketch

Figure G-46: Post-fracture pattern for experimental sample 4 Test 56

(a) Photo

Sketch not produced

(b) Sketch

Figure G-47: Post-fracture pattern for experimental sample 4 Test 57

	Sketch not produced
(a) Photo	(b) Sketch

Figure G-48: Post-fracture pattern for experimental sample 4 Test 58

	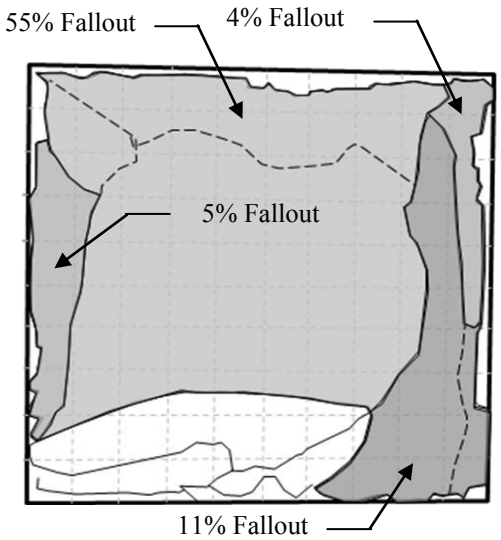
(a) Photo	(b) Sketch

Figure G-49: Post-fracture pattern for experimental sample 4 Test 59

(a) Photo

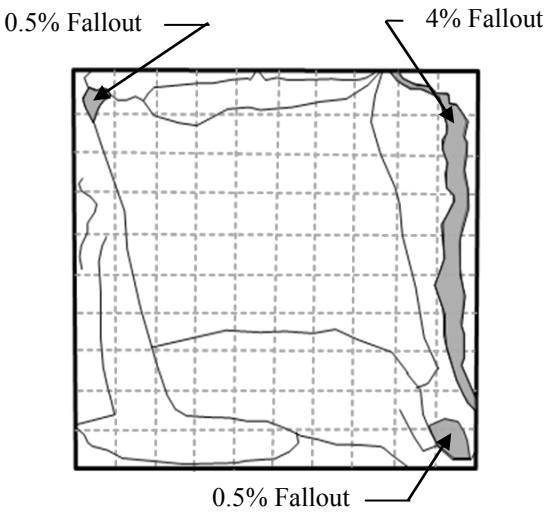

(b) Sketch

Figure G-50: Post-fracture pattern for experimental sample 4 Test 60

(a) Photo

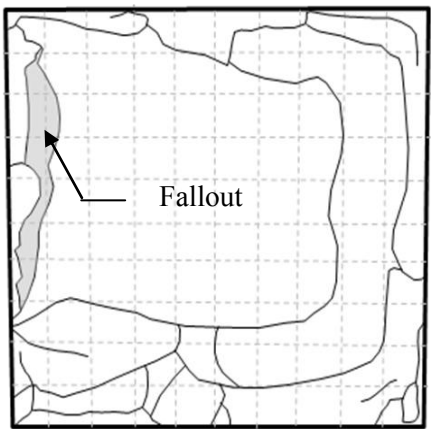

(b) Sketch

Figure G-51: Post-fracture pattern for experimental sample 4 Test 61

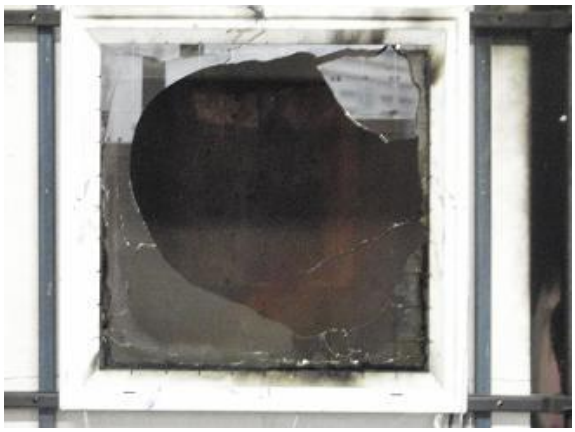

(a) Photo

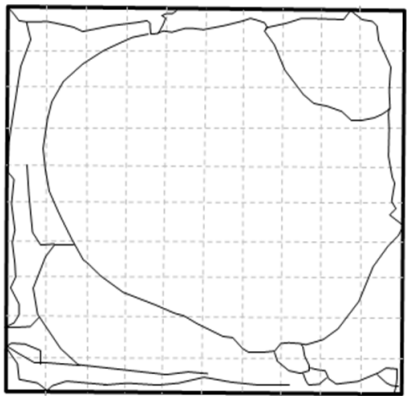

(b) Sketch

Figure G-52: Post-fracture pattern for experimental sample 4 Test 62

(a) Photo

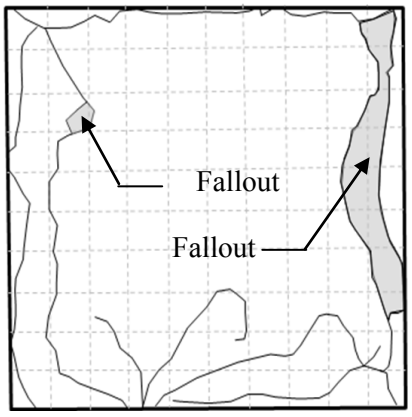

(b) Sketch

Figure G-53: Post-fracture pattern for experimental sample 4 Test 63

(a) Photo

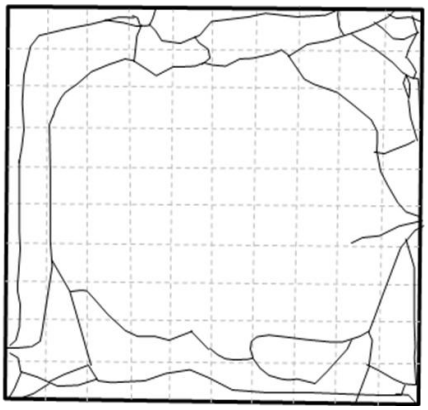

(b) Sketch

Figure G-54: Post-fracture pattern for experimental sample 4 Test 64

(a) Photo

Sketch not produced

(b) Sketch

Figure G-55: Post-fracture pattern for experimental sample 6 Test 1

	Sketch not produced
(a) Photo	(b) Sketch

Figure G-56: Post-fracture pattern for experimental sample 6 Test 2

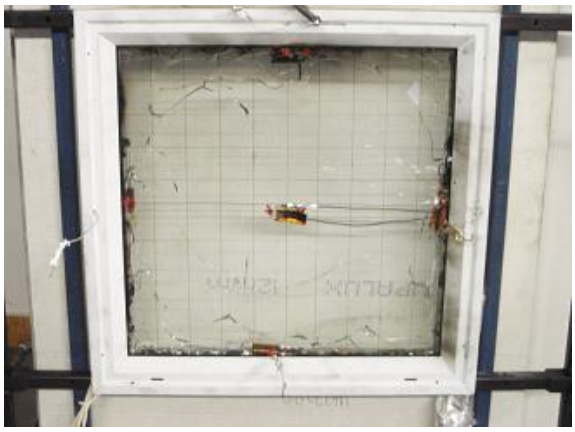	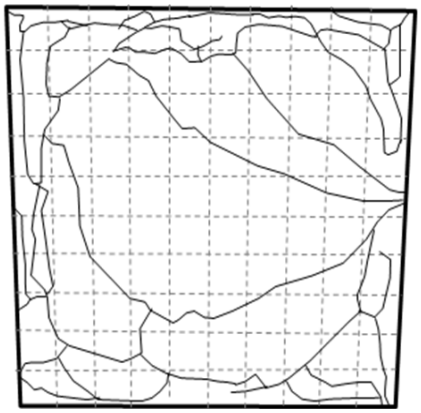
(a) Photo	(b) Sketch

Figure G-57: Post-fracture pattern for experimental sample 6 Test 3

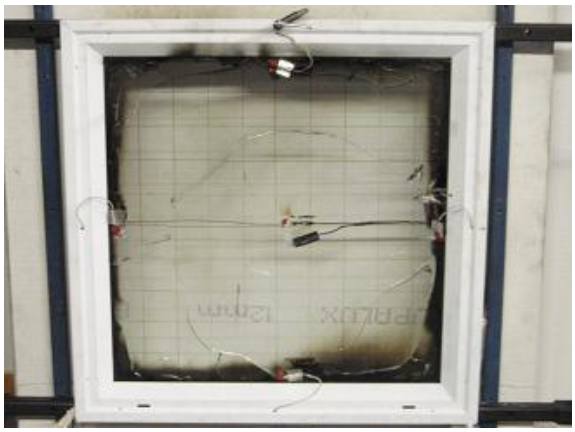	Sketch not produced
(a) Photo	(b) Sketch

Figure G-58: Post-fracture pattern for experimental sample 6 Test 4

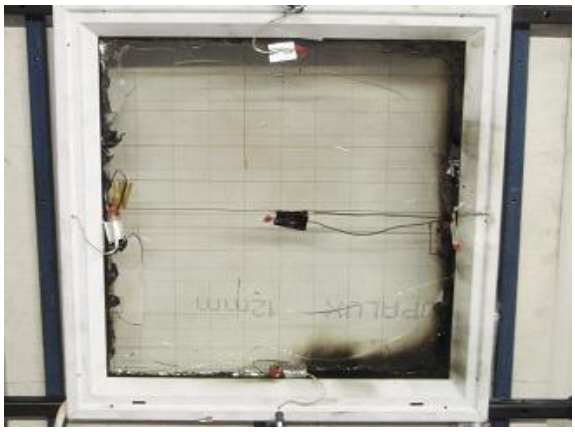	Sketch not produced
(a) Photo	(b) Sketch

Figure G-59: Post-fracture pattern for experimental sample 6 Test 5

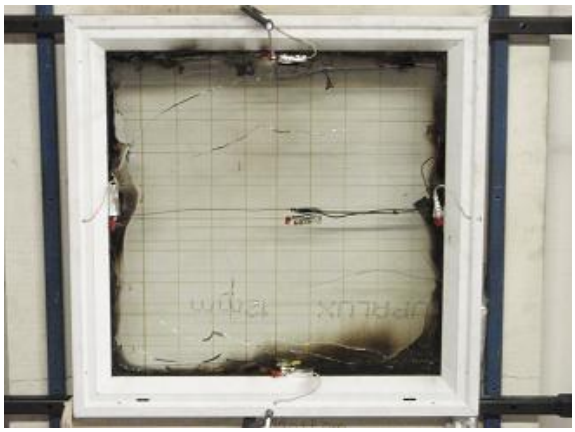

(a) Photo

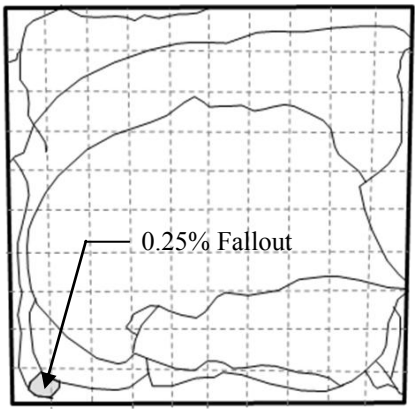

(b) Sketch

Figure G-60: Post-fracture pattern for experimental sample 6 Test 6

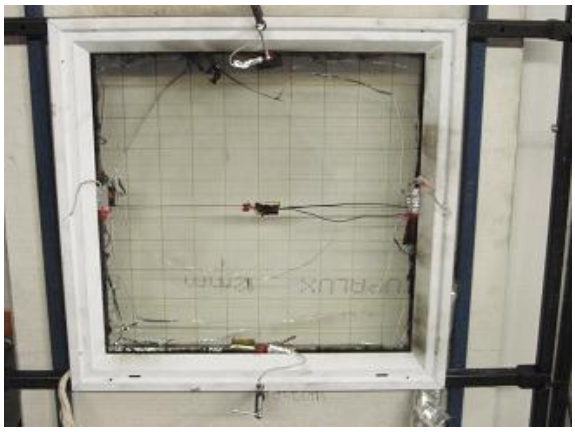

(a) Photo

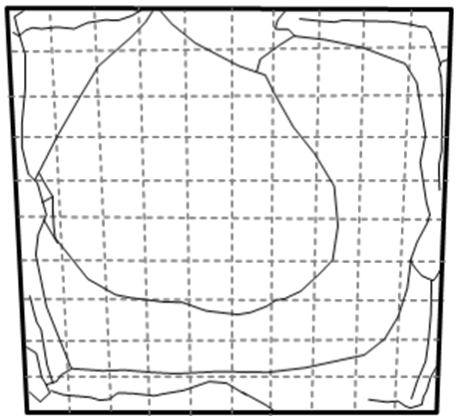

(b) Sketch

Figure G-61: Post-fracture pattern for experimental sample 6 Test 7

(a) Photo

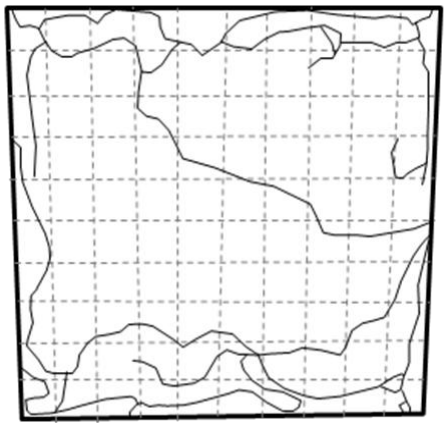

(b) Sketch

Figure G-62: 8 Post-fracture pattern for experimental sample 6 Test 8

(a) Photo

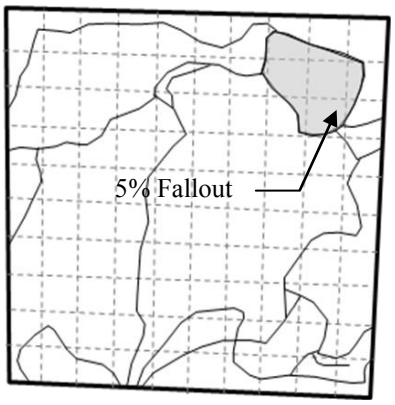

(b) Sketch

Figure G-63: Post-fracture pattern for experimental sample 6 Test 10

(a) Photo

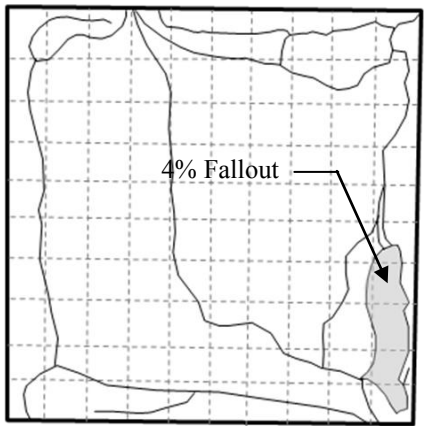

(b) Sketch

Figure G-64: Post-fracture pattern for experimental sample 6 Test 11

(a) Photo

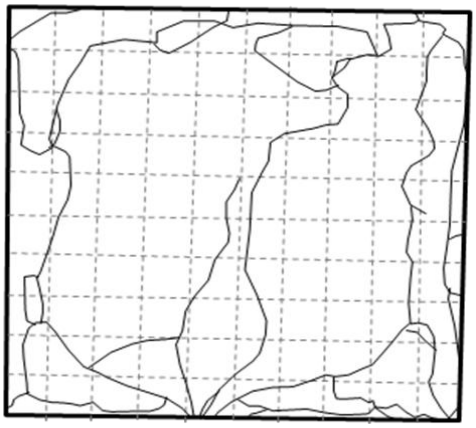

(b) Sketch

Figure G-65: Post-fracture pattern for experimental sample 6 Test 12

(a) Photo

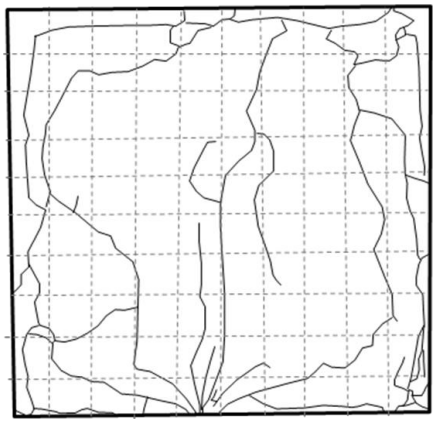

(b) Sketch

Figure G-66: Post-fracture pattern for experimental sample 6 Test 13

(a) Photo

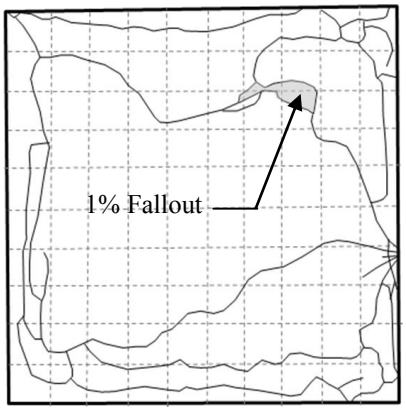

(b) Sketch

Figure G-67: Post-fracture pattern for experimental sample 6 Test 14

(a) Photo

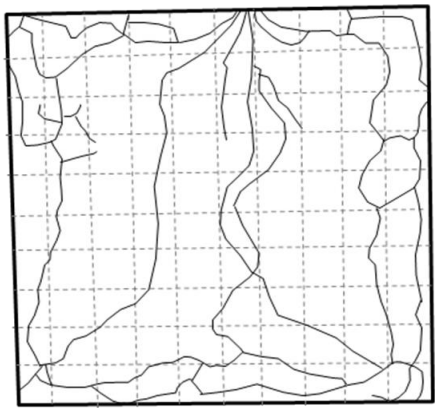

(b) Sketch

Figure G-68: Post-fracture pattern for experimental sample 6 Test 15

(a) Photo

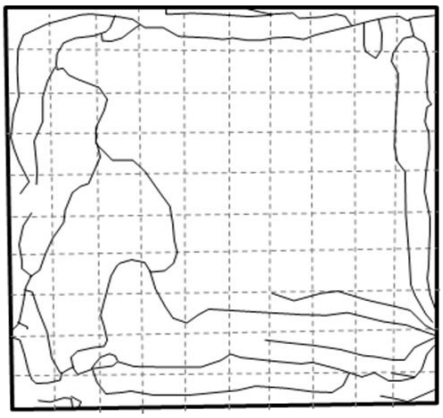

(b) Sketch

Figure G-69: Post-fracture pattern for experimental sample 6 Test 16

	Sketch not produced
(a) Photo	(b) Sketch

Figure G-70: Post-fracture pattern for experimental sample 6 Test 28

	Sketch not produced
(a) Photo	(b) Sketch

Figure G-71: Post-fracture pattern for experimental sample 6 Test 29

	Sketch not produced
(a) Photo	(b) Sketch

Figure G-72: Post-fracture pattern for experimental sample 6 Test 30

	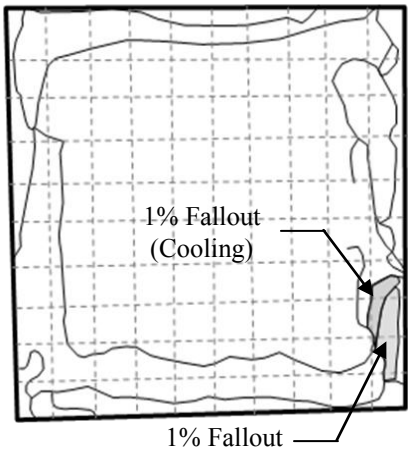
(a) Photo	(b) Sketch

Figure G-73: Post-fracture pattern for experimental sample 6 Test 31

(a) Photo

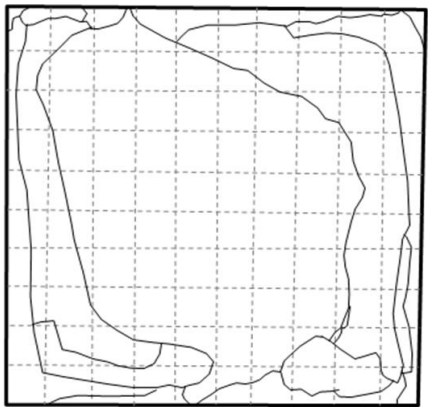

(b) Sketch

Figure G-74: Post-fracture pattern for experimental sample 6 Test 32

(a) Photo

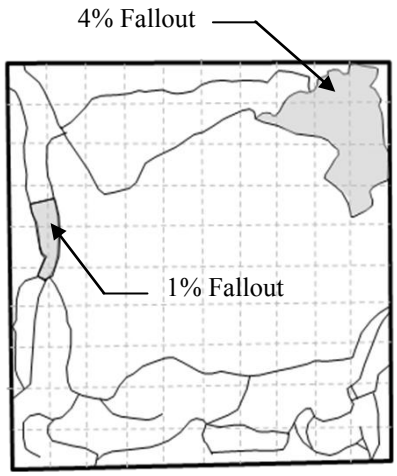

(b) Sketch

Figure G-75: Post-fracture pattern for experimental sample 6 Test 33

(a) Photo

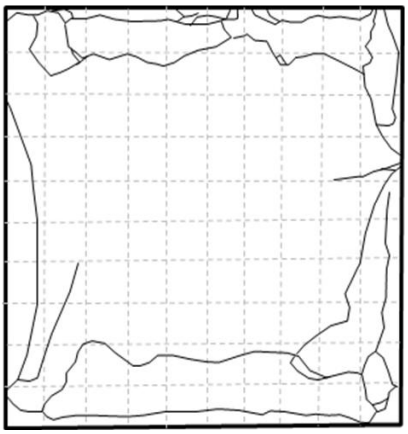

(b) Sketch

Figure G-76: Post-fracture pattern for experimental sample 6 Test 34

(a) Photo

Sketch not produced

(b) Sketch

Figure G-77: Post-fracture pattern for experimental sample 6 Test 35

	Sketch not produced
(a) Photo	(b) Sketch

Figure G-78: Post-fracture pattern for experimental sample 6 Test 36

	Sketch not produced
(a) Photo	(b) Sketch

Figure G-79: Post-fracture pattern for experimental sample 6 Test 37

	Sketch not produced
(a) Photo	(b) Sketch

Figure G-80: Post-fracture pattern for experimental sample 6 Test 38

	Sketch not produced
(a) Photo	(b) Sketch

Figure G-81: Post-fracture pattern for experimental sample 6 Test 39

	Sketch not produced
(a) Photo	(b) Sketch

Figure G-82: Post-fracture pattern for experimental sample 6 Test 40

	
(a) Photo	(b) Sketch

Figure G-83: Post-fracture pattern for experimental sample 6 Test 41

(a) Photo

(b) Sketch

Figure G-84: Post-fracture pattern for experimental sample 6 Test 42

(a) Photo

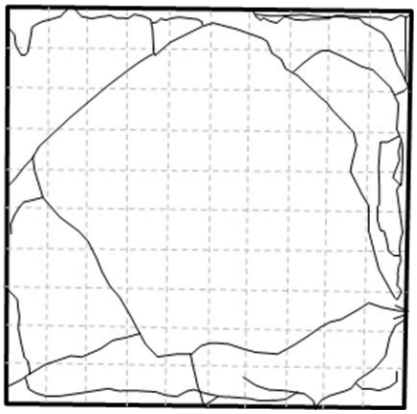

(b) Sketch

Figure G-85: Post-fracture pattern for experimental sample 6 Test 43

(a) Photo

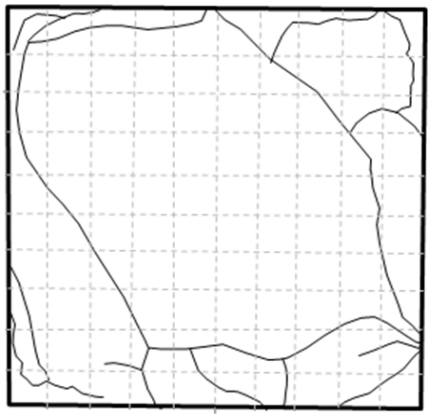

(b) Sketch

Figure G-86: Post-fracture pattern for experimental sample 6 Test 44

(a) Photo

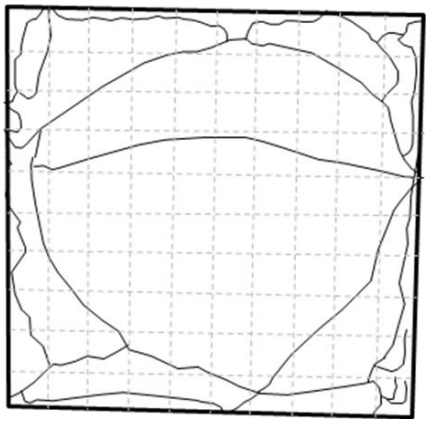

(b) Sketch

Figure G-87: Post-fracture pattern for experimental sample 6 Test 45

	Sketch not produced
(a) Photo	(b) Sketch

Figure G-88: Post-fracture pattern for experimental sample 6 Test 46

	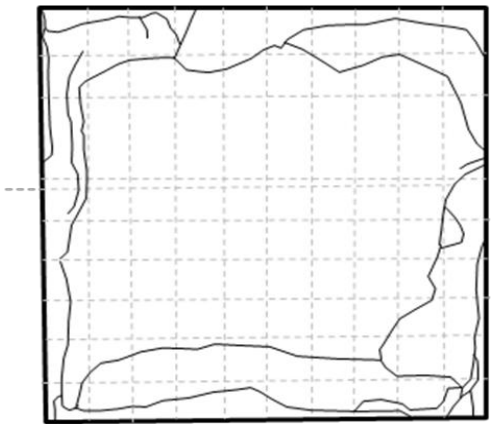
(a) Photo	(b) Sketch

Figure G-89: Post-fracture pattern for experimental sample 6 Test 47

(a) Photo

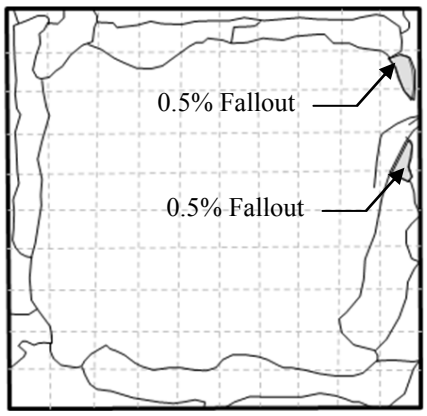

(b) Sketch

Figure G-90: Post-fracture pattern for experimental sample 6 Test 48

(a) Photo

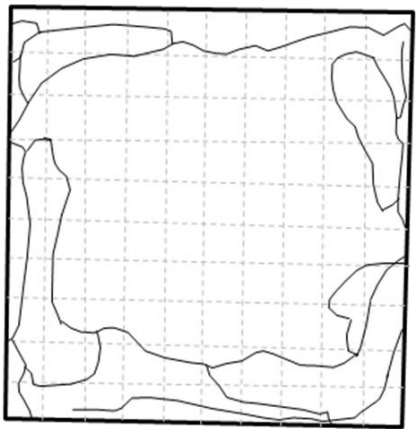

(b) Sketch

Figure G-91: Post-fracture pattern for experimental sample 6 Test 49

(a) Photo

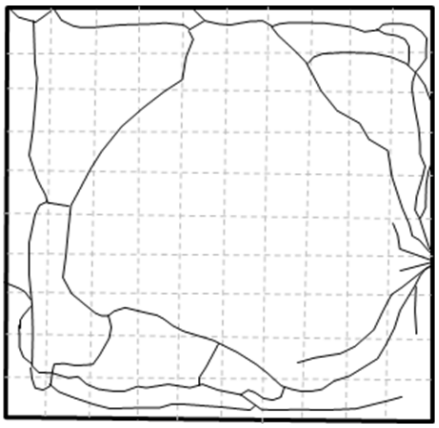

(b) Sketch

Figure G-92: Post-fracture pattern for experimental sample 6 Test 50

(a) Photo

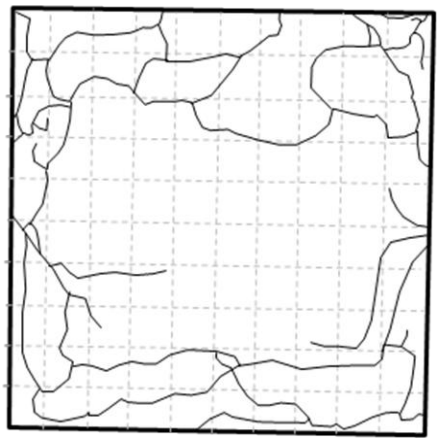

(b) Sketch

Figure G-93: Post-fracture pattern for experimental sample 6 Test 51

(a) Photo

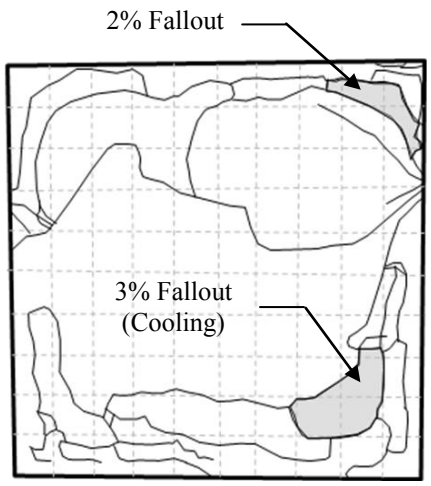

(b) Sketch

Figure G-94: Post-fracture pattern for experimental sample 6 Test 52

(a) Photo

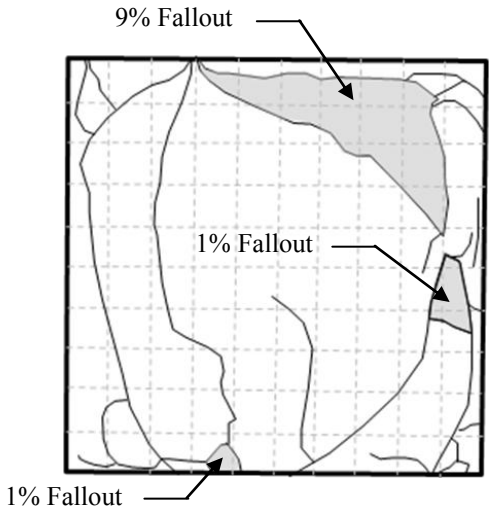

(b) Sketch

Figure G-95: Post-fracture pattern for experimental sample 6 Test 53

(a) Photo

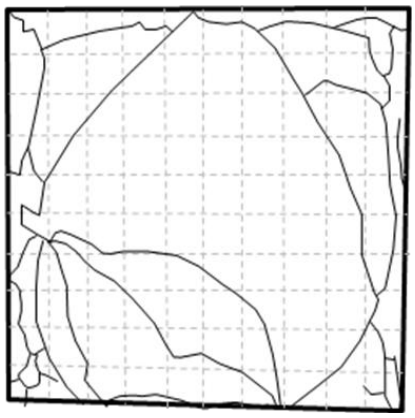

(b) Sketch

Figure G-96: Post-fracture pattern for experimental sample 6 Test 54

(a) Photo

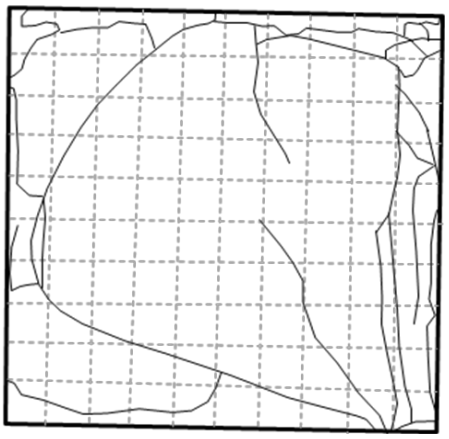

(b) Sketch

Figure G-97: Post-fracture pattern for experimental sample 6 Test 55

(a) Photo

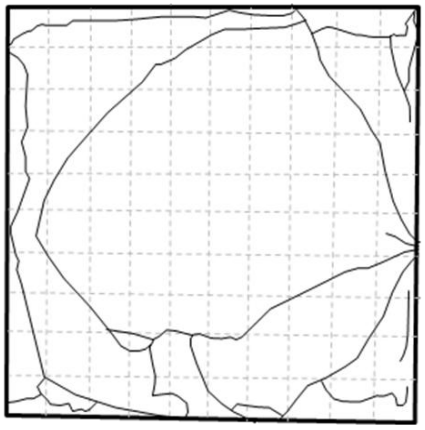

(b) Sketch

Figure G-98: Post-fracture pattern for experimental sample 6 Test 56

APPENDIX H - LOAD-DEFLECTION CURVES FROM FOUR-POINT TEST

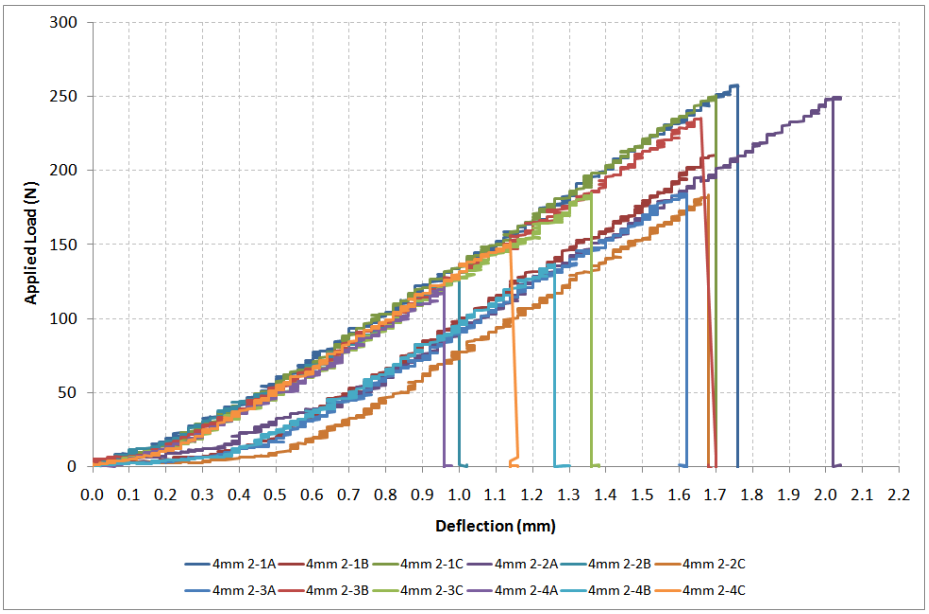

Figure H-1: Load - deflection plots for 4 mm thick glass samples

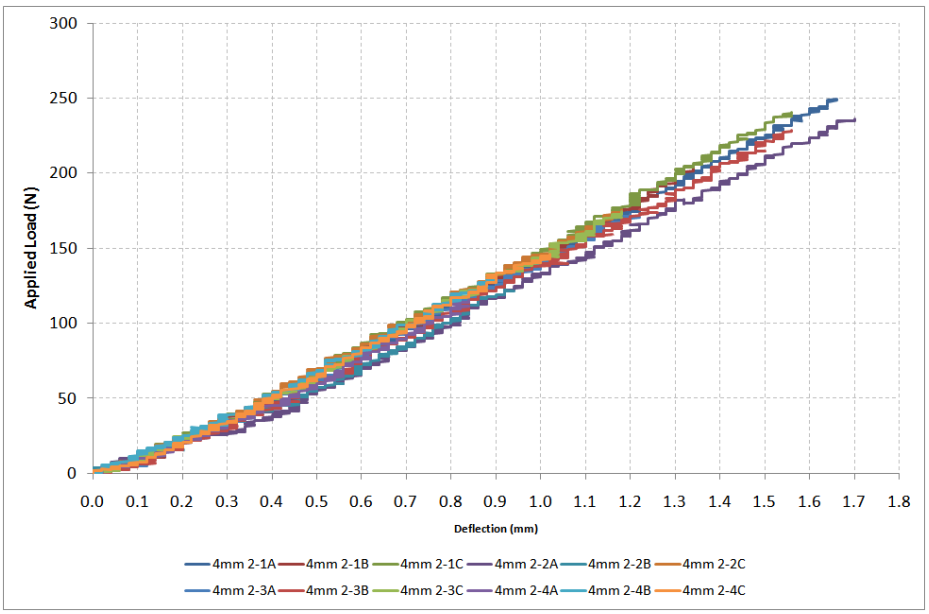

Figure H-2: Corrected load – deflection plots for 4 mm thick glass samples

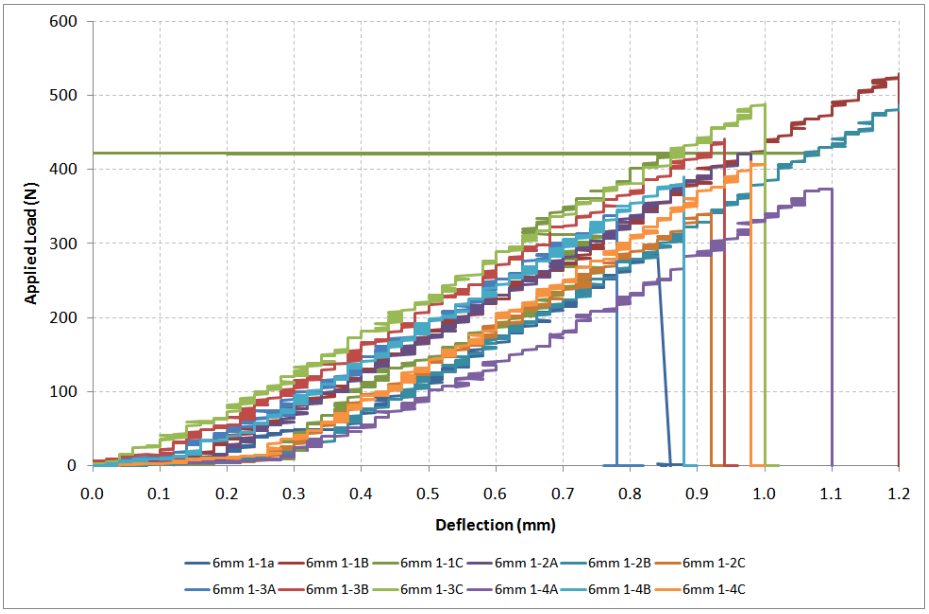

Figure H-3: Load – deflection plots for 6 mm thick glass samples

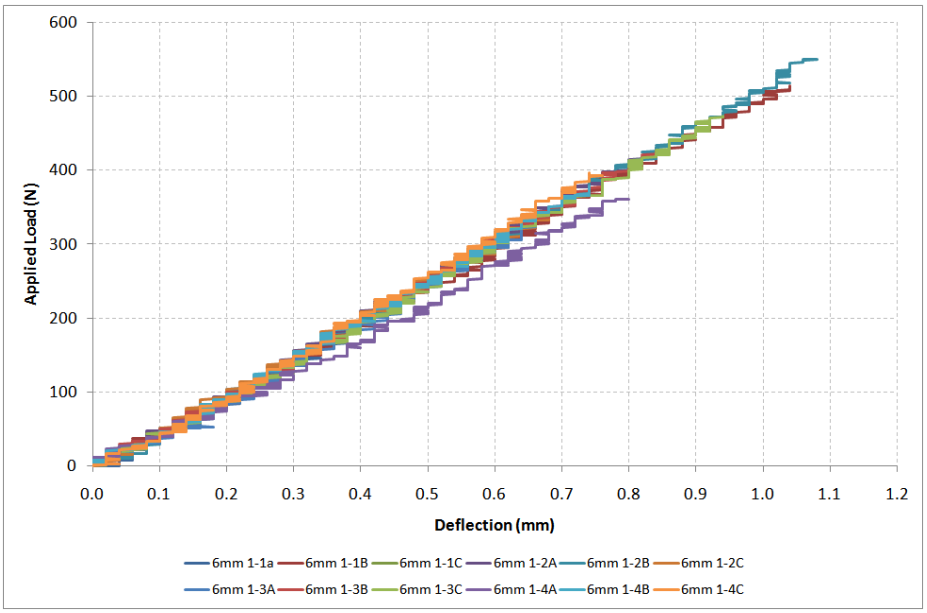

Figure H-4: Corrected load – deflection plots for 6 mm thick glass samples

APPENDIX I - DATA AND RESULTS FROM FOUR-POINT BENDING TEST RESULTS

Table I-1: Summary of Four-Point Bending Test Results

Test Specimen	Dimension of Test Specimen		Second Moment of Inertia	Breaking Load	Maximum Deflection	Fracture Strength	Modulus of Elasticity
	Width (mm)	Thickness (mm)	(mm^4)	(N)	(mm)	(MPa)	(GPa)
1-1a	31.28	5.92	540.8	240.0	0.50	36.1	70.7
1-1b	30.72	5.93	533.8	513.7	1.04	78.5	73.8
1-1c	30.65	5.90	524.6	420.0	N/A	64.9	N/A
1-2a	30.82	5.94	538.3	415.4	0.82	63.0	75.0
1-2b	30.95	5.92	535.1	549.7	1.06	83.6	77.3
1-2c	30.33	5.93	527.1	335.4	0.68	51.9	74.6
1-3a	30.55	5.93	530.9	323.4	0.66	49.7	73.6
1-3b	30.24	5.87	509.7	425.7	0.84	67.4	79.3
1-3c	30.66	5.90	524.7	473.1	0.94	73.1	76.5
1-4a	29.81	5.94	520.6	361.2	0.80	56.7	69.1
1-4b	29.84	5.98	531.8	378.2	0.74	58.5	76.6
1-4c	31.47	5.92	544.1	396.5	0.74	59.3	78.5
2-1a	30.77	3.84	145.2	249.1	1.66	90.6	82.4
2-1b	31.08	3.90	153.6	203.4	1.34	71.0	78.8
2-1c	31.45	3.91	156.7	240.5	1.56	82.5	78.5
2-2a	30.00	3.82	139.4	236.0	1.70	89.0	79.4
2-2b	29.85	3.86	143.1	124.5	0.92	46.2	75.4
2-2c	31.28	3.85	148.8	175.4	1.18	62.4	79.7
2-3a	30.13	3.86	144.4	172.6	1.20	63.4	79.4

Table I-1 **(con't)**

Test Specimen	Dimension of Test Specimen		Second Moment of Inertia	Breaking Load	Maximum Deflection	Fracture Strength	Modulus of Elasticity
	Width (mm)	Thickness (mm)	(mm^4)	(N)	(mm)	(MPa)	(GPa)
2-3b	29.87	3.87	144.3	228.6	1.56	84.3	81.0
2-3c	30.72	3.90	151.9	174.2	1.18	61.5	77.5
2-4a	30.42	3.88	148.1	116.0	0.84	41.8	74.4
2-4b	29.86	3.88	145.3	129.7	0.90	47.6	79.0
2-4c	30.73	3.89	150.7	146.3	1.02	51.9	75.9

N/A – Not Available

APPENDIX J - STRESS FORMULA FOR FOUR-POINT BENDING TEST

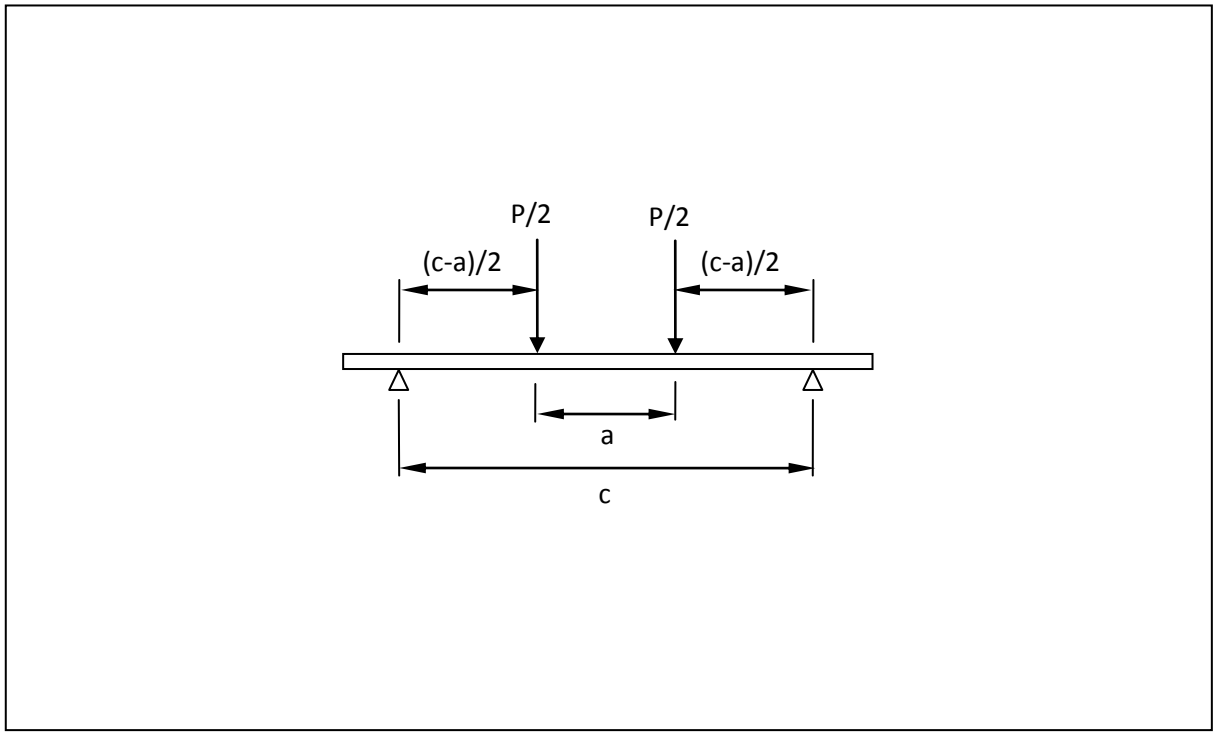

Figure J-1: Diagram showing four-point loading arrangement

In basic solid mechanics, stress is defined as,

$$\sigma = \frac{M}{Z} \tag{J1}$$

and based on the load arrangement in Figure I-1,

$$M = \frac{P}{2}\frac{(c-a)}{2} = \frac{P(c-a)}{4} \tag{J2}$$

$$Z = \frac{b\delta^2}{6} \text{ for a thin rectangular section} \tag{J3}$$

Substitute Equations (J2) and (J3) into Equation (J1),

$$\sigma = \frac{P(c-a)}{4}\frac{6}{b\delta^2} = \frac{3P(c-a)}{2b\delta^2} \tag{J4}$$

APPENDIX K - LUMPED MASS MODEL EQUATION TO PREDICT TIME TO GLASS FRACTURE

The derivation of the lumped mass model equation is based on the Shields et al. (2001) which involves rearranging the energy balance relationship given in (K1)

$$mc_p \frac{dT_{glass}}{dt} + hA\left(T_{glass} - T_\infty\right) = \dot{q}'' A \qquad \text{(K1)}$$

Let $\theta = T_{glass} - T_\infty$ and $m = A\delta\rho$

$$\frac{d\theta}{dt} + \frac{h\theta}{\delta\rho c_p} = \frac{\dot{q}''}{\delta\rho c_p}$$

This can be solved using the integrating factor

So $\theta e^{\int \frac{hdt}{\delta\rho c_p}} = \int \frac{\dot{q}''}{\delta\rho c_p} e^{\int \frac{hdt}{\delta\rho c_p} dt} = \frac{\dot{q}''}{h} e^{\frac{ht}{\delta\rho c_p}} + c$

When t = 0, θ = 0, so c = $\frac{\dot{q}''}{h}$

So $\theta = \frac{\dot{q}''}{h}\left[1 - e^{\frac{-ht}{\delta\rho c_p}}\right]$ and then $e^{\frac{ht}{\delta\rho c_p}} = \left[\frac{\dot{q}''}{\dot{q}'' - h\theta}\right]$

So, $t = \frac{\delta\rho c_p}{h} \ln\left[\frac{\dot{q}''}{\dot{q}'' - h\left(T_g - T_\infty\right)}\right]$ and let $\dot{q}''_{crit} = h\left(T_{glass} - T_\infty\right)$

So, $t = \frac{\delta\rho c_p}{h} \ln\left[\frac{\dot{q}''}{\dot{q}'' - \dot{q}''_{crit}}\right]$ (K2)